

Isolation of Reactive Main Group Species by Anionic *N*-Heterocyclic Olefins and Terphenyl
Ligands

by

Samuel R. Baird

A thesis submitted in partial fulfillment of the requirements for the degree of

Doctor of Philosophy

Department of Chemistry

University of Alberta

© Samuel R. Baird, 2024

Abstract

The work in this Thesis describes the preparation of a new vinyl lithium reagent, $[(^{\text{Me}}\text{IPrCH})\text{Li}]_2$ ($^{\text{Me}}\text{IPr} = (\text{MeCNDipp})_2\text{C};$; $\text{Dipp} = 2,6\text{-}^i\text{Pr}_2\text{C}_6\text{H}_3$), which was utilized as a general source for the anionic *N*-heterocyclic olefin (aNHO) $[(^{\text{Me}}\text{IPrCH})]^-$, a potential 2σ , 2π -electron donor. Utilizing $[(^{\text{Me}}\text{IPrCH})\text{Li}]_2$, a complete acyclic divinyltetrelene series $(^{\text{Me}}\text{IPrCH})_2\text{E}$: ($\text{E} = \text{Si} - \text{Pb}$) was prepared with $(^{\text{Me}}\text{IPrCH})_2\text{Si}$: being the first example of a stable two-coordinate acyclic diorganosilylene. Notably, $(^{\text{Me}}\text{IPrCH})_2\text{Si}$: exhibits dual nucleophilic and electrophilic character at the Si(II) center.

The efficacy of $[(^{\text{Me}}\text{IPrCH})\text{Li}]_2$ to stabilize low-valent main group elements was extended to the Group 13 elements, with a tetrahedron-shaped indium(I) tetramer, $[(^{\text{Me}}\text{IPrCH})\text{In}]_4$, supported by aNHOs being described. Scission of the indium(I) tetramer was possible upon the addition of a strong Lewis base affording monomeric units that exhibit both electrophilic and nucleophilic characteristics. This indium(I) tetramer was also found to be highly reactive with the activation of strong H–B bonds in boranes by the In(I) centers, while the steric profile of the aNHO allowed for the isolation of a rare neutral indium-imide, RInNR' . The synthesis of a related aNHO synthon, $[(\text{SIPrCH})\text{Li}]_2$ ($\text{SIPr} = (\text{H}_2\text{CNDipp})_2\text{C};$), is also described.

Next, the preparation of a diborene ($\text{RB}=\text{BR}$) stabilized by aNHOs was explored. The precursor $(\text{SIPrCH})\text{ClB-BCl}(\text{CHSIPr})$ was prepared in high yield by combining $[(\text{SIPrCH})\text{Li}]_2$ with $\text{Me}_2\text{S}\cdot\text{Cl}_2\text{B-BCl}_2\cdot\text{SMe}_2$. Unfortunately, attempts to reduce $(\text{SIPrCH})\text{ClB-BCl}(\text{CHSIPr})$ gave exclusively decomposition/hydrolysis and, in one instance, a C–N ligand activation product which may have been formed by a transient diborene. Computationally, it was found

that the theoretical diborene, $(^{\text{Me}}\text{IPrCH})\text{B}=\text{B}(\text{CH}^{\text{Me}}\text{IPr})$ will likely exist in a triplet ground state.

The synthesis of an aminoborane supported by a sterically demanding terphenyl ligand (an inorganic analogue to styrene), $\text{Ar}^{\text{Dipp}}\text{B}(\text{H})=\text{NH}_2$ ($\text{Ar}^{\text{Dipp}} = 2,6\text{-Dipp}_2\text{C}_6\text{H}_3$), was investigated. First, the terphenyl-supported amine-borane adduct $\text{Ar}^{\text{Dipp}}\text{BH}_2\cdot\text{NH}_3$, was prepared in high yield in an efficient one-pot synthesis by combining $\text{Ar}^{\text{Dipp}}\text{Li}$ and $\text{Me}_2\text{S}\cdot\text{BH}_3$, followed by the addition of excess $[\text{NH}_4]\text{Cl}$, liberating H_2 , LiCl and SMe_2 as by-products. $\text{Ar}^{\text{Dipp}}\text{BH}_2\cdot\text{NH}_3$ could be dehydrogenated further to give the target species $\text{Ar}^{\text{Dipp}}\text{B}(\text{H})=\text{NH}_2$ by using a catalytic amount of $[\text{Rh}(\text{COD})\text{Cl}]_2$ ($\text{COD} = 1,5\text{-cyclooctadiene}$). Unfortunately, attempts to dehydrogenate $\text{Ar}^{\text{Dipp}}\text{B}(\text{H})=\text{NH}_2$ further were unsuccessful, possibly due to the low hydridic character within the boron-bound hydrides.

Lastly, the bulky *N*-heterocyclic carbene (NHC) $^{\text{Me}}\text{ITr}$ ($^{\text{Me}}\text{ITr} = (\text{MeCNCPh}_3)_2\text{C}:$) was prepared by incorporating methyl groups in the backbone of the heterocyclic ring forcing the nitrogen-bound trityl groups forward to further protect the coordination pocket of the carbene. This arrangement raises the percent buried volume ($\%V_{\text{Bur}}$) to an astounding 72.6 %, making $^{\text{Me}}\text{ITr}$ the world's bulkiest NHC to date.

Preface

A portion of the work presented in this Thesis has been done in collaboration with other researchers and support staff within the Department of Chemistry at the University of Alberta and with researchers external to the University of Alberta.

All single-crystal X-ray crystallographic studies described herein were performed by Dr. Michael J. Ferguson or Dr. Yuqiao Zhou at the University of Alberta, including the mounting of crystals, diffractometer operation, structure refinement, and the preparation of the crystallographic data tables. Element analyses were performed by Dr. Wayne Moffat and Jennifer Jones at the Analytical Instrument Laboratory at the University of Alberta. Computational studies were performed with the essential help of the Shared Hierarchical Academic Computing Network (SHARCNET: www.computecanada.ca), WestGrid (www.westgrid.ca), and Digital Research Alliance of Canada (www.computecanada.ca). The work in Thesis was supported by the Canadian Foundation for Innovation, the Faculty of Science at the University of Alberta, the Natural Sciences and Engineering Research Council of Canada, and the University of Alberta Doctoral Recruitment Scholarship programs.

In Chapter 1, all writing was completed by Samuel R. Baird, with feedback from Prof. Eric Rivard between Thesis drafts. In Chapter 2, the synthesis and characterization of $^{\text{Me}}\text{IPrCH}(\text{I})$ and $[(^{\text{Me}}\text{IPrCH})\text{Li}]_2$ was done in collaboration with Dr. Matthew M. D. Roy, a former graduate student in the Rivard group. The synthesis and characterization of $(^{\text{Me}}\text{IPrCH})_2\text{Si}$ was first conducted by Dr. Matthew M. D. Roy. $^{207}\text{Pb}\{^1\text{H}\}$ NMR spectra were collected by Mark Miskolzie. In Chapter 3, Diffusion-Ordered spectroscopy (DOSY) experiments were performed by Mark Miskolzie. Atoms-In-Molecules (AIM) computations and the interpretation of the Natural Bonding Order (NBO) analyses of $(^{\text{Me}}\text{IPrCH})\text{InNAr}^{\text{Dipp}}$

and related indium-imides were done in collaboration with Dr. Emanuel Hupf (Universität Bremen). The synthesis and characterization of $[(\text{SIPrCH})\text{Li}]_2$ was done in collaboration with Dr. Ian C. Watson, a former graduate student in the Rivard group. In Chapter 5, the initial synthetic routes to $\text{Ar}^{\text{Dipp}}\text{B}(\text{H})=\text{NH}_2$ were developed by Dr. Eike Dornsiepen (University of Alberta). The synthesis and characterization of $[\text{Ar}^{\text{Dipp}}\text{BH}_2\cdot\text{NH}_2\text{Li}]_2$, as well as attempts to prepare $\text{Ar}^{\text{Dipp}}\text{B}(\text{H})=\text{NH}_2$, were performed by a previous Rivard group undergraduate Evangeline Dugbenu. In Chapter 5, the crystals of $^{\text{M}}\text{eITr}$ suitable for X-ray crystallographic studies were grown by a former graduate student, who has since left the Rivard group, Saro Birgani.

According to the Thesis policy within our research group, each Chapter of this Thesis is essentially self-contained, and prepared in the form of a paper that is intended to for publication in peer-reviewed journals.

A portion of this Thesis has been previously published and the publications are listed below:

Chapter 2:

M. M. D. Roy, S. R. Baird, E. Dornsiepen, L. A. Paul, L. Miao, M. J. Ferguson, Y. Zhou, I. Siewert, E. Rivard, *Chem. Eur. J.* **2021**, *27*, 8572–8579.

Chapter 3:

S. R. Baird, E. Hupf, I. C. Watson, M. J. Ferguson, E. Rivard, *Chem. Commun.* **2023**, *59*, 2903–2906.

Dedicated to my family, especially my parents, Ian Douglas Baird, and Katherine Anne Barber, for their endless love, for teaching me never to give up and to admit to failures

Acknowledgements

First of all, I would like to thank my family. My parents, Ian Baird and Katherine Barber, for supporting my curiosity, and passions from a young age and all through my time at Mount Allison University (Mt.A) and University of Alberta (UofA). I would like to thank my younger brother, William Baird, for all of the laughs and thought-provoking conversations. To my grandparents Ian and Maureen Barber, Shelia Baird, Doug and Pam Baird, thank you for the financial support throughout my post-secondary education, words of advice, and bottomless love. Ashlyn, thank you for your endless kindness and love. You've given me so much support, putting up with my shenanigans, for all of the ski trips, much needed hugs, and lots of laughs. Thank you, Socks, and Luffy for insisting on "editing" my work.

To my friends from Mt.A and Dalhousie, Hailie Tattrie, Sarah Martell, Marcus Kindervater, Akarsh Pi, Joe Bedard, Courtney Law, Zachary "Wig Boy 1" LeBlanc, Michael "Wig Boy 2" Anghel, Vanessa Chiasson, Dana "Big D" Bidgood, Sam and Robyn Donaldson. I know we do not see each other as much as we used to, but you guys have helped me so much during my time in Alberta, especially during difficult times such as the COVID-19 pandemic. I love visiting you when I come back to the Maritimes for vacation; you truly are part of my family.

I would like to thank my family away from home, Cheryl, Patrick, Iain, and Declan Flemming for welcoming me into your home. You've made Edmonton feel like a second home to me and I don't know what my time in Edmonton would've looked like without you. And of course, thank you to Pepper for always being the one who was the most excited to see me, you'll get many more belly rubs before I leave.

To all of the Rivardians, past and present, thank you creating a great environment to work in. The jokes and general mischief make the lab such an enjoyable environment. Special thanks to previous members: Dr. Emanuel Hupf, Dr. Matthew Roy, Dr. Sarah Parke, Dr. Chrissy Braun, Dr. Bruno Lupi, Dr. Ian Watson, Dr. Jocelyn Sinclair, Dr. Eike Dornsiepen, Dr. Tanja Kunz, and Janelle Bykowski.

Dr. Alvaro Omaña, I want to give you a special thank you for my being my best friend in the Rivard group, but also here at the UofA. You always offered kind words of advice, lots of laughs, and crazy nights as Sherlocks.

I would like to also thank all of current members of the Rivard group: Brandon Fernette, William Medora, Abhishek “Abhi” Muralidharan, Mamak Bakhtiari, Qiannan (Nancy) Wu, Aislinn Cassie-Morfoot, Eric Butler, Haochen (Andrew) Tan, Dr. Natsuki Kato, and Dr. Ludwig Zapf. We’ll have to out for a breakfast sometime soon, hopefully I don’t sleep in, and have the “airport special” (coffee and beer).

I am very grateful for the new friends I have made during my time at the University of Alberta. Thank you for all the fun times and chaotic adventures. A special thank you to: Dr. Kevin “Ktown” O’Connor, Riley Hooper, Dr. Sarah Milliken, Dr. Chris “Cruising for a Boozing” Cooze, Wesley “Weston” McNutt, Dr. Arsh Hazrah, Dr. Kelli McCord, Nicholas Kiassoon, Jake Blackner, Dominic “DL” Laverne, Abbie Rublitz, Zachary Shroeder, Cole Butler, and Christina Zafeiridou.

It is said it takes a village to make chemistry work and I truly believe that. The Chemistry Department has the best staff on campus. You’ve made navigating the trials of graduate school just a little bit easier and I am so thankful to you. A massive thank you to the

Machine Shop powerhouses Dirk Kelm and Paul Crothers, Dr. Jason Cooke, Dr. Mike Ferugson (sorry for all of the terrible crystal I brought down to you), Dr. Yuqiao Zhou, Dr. Wayne Moffat, Jennifer Jones, Andrew Yeung, Ryan Lewis, Mike “Stores Mike” Bartowski, and Mark “NMark” Miskolzie.

To my supervisor Prof. Eric Rivard, thank you for taking me on as a student. I strongly believe that you were the supervisor I needed after my undergraduate degree. You’ve helped me by building up my strengths and helping me overcome my short comings, both professionally and as a chemist. I am incredibly thankful for the opportunities you have given me. Thank you so much.

Finally, I would like to thank my late undergraduate mentor Dr. Stephen “Old Man” Westcott. Thank you for all of the support, advice that you kindly gave, and for sending me to Alberta to work with Eric. I am sorry that we will not be able to have a beer for a while but hopefully when we finally do, I can share some of my adventures with you over a long overdue cold one.

Table of Contents

Chapter 1 – Introduction	1
1.1 Main Group Element Compounds: From Structural Curiosities to Applications	1
1.2 Kinetic Stabilization of Low Valent Main Group Elements	3
1.2.1 Kinetic Stabilization of Low-Valent Group 13 Elements	4
1.2.2 Kinetic Stabilization of Low-Valent Group 14 Elements	11
1.2.3 Kinetic Stabilization of Group 13–Nitrogen Multiply-Bonded Species	17
1.3 <i>N</i> -Heterocyclic Carbenes	19
1.3.1 Properties of <i>N</i> -Heterocyclic Carbenes and Coordination Chemistry Highlights	20
1.4 <i>N</i> -Heterocyclic Olefins: An Unassuming Beginning	24
1.4.1 Synthesis of <i>N</i> -Heterocyclic Olefins	25
1.4.2 Properties of <i>N</i> -Heterocyclic Olefins	30
1.4.3 Neutral <i>N</i> -Heterocyclic Olefins as Ligands	33
1.4.4 Anionic <i>N</i> -Heterocyclic Olefins as Ligands	35
1.5 Thesis Objectives	39
1.6 References	40
Chapter 2 – A Stable Homoleptic Tetrelene Series	49
2.1 Introduction	49

2.2 Results and Discussion	50
2.3 Conclusions	58
2.4 Experimental Details	59
2.4.1 General Considerations	59
2.4.2 Synthetic Procedures	60
2.4.3 X-Ray Crystallography	67
2.5 References	72
Chapter 3 – An Indium(I) Tetramer Bound by Anionic <i>N</i> -Heterocyclic Olefins: Ambiphilic Reactivity, Transmetallation and a Rare Indium-Imide	77
3.1 Introduction	77
3.2 Results and Discussion	78
3.3 Conclusions	94
3.4 Experimental Details	95
3.4.1 General Considerations	95
3.4.2 Synthetic Procedures	96
3.4.3 X-Ray Crystallography	104
3.4.4 Density Functional Theory (DFT) Computations and UV-vis Data	116
3.5 References	117

Chapter 4 – C-N Activation by a Possible Transient Diborene Supported by an Anionic <i>N</i> -Heterocyclic Olefin	123
4.1 Introduction	123
4.2 Results and Discussion	125
4.3 Conclusions	139
4.4 Experimental Details	140
4.4.1 General Considerations	140
4.4.2 Synthetic Procedures	141
4.4.3 X-Ray Crystallography	147
4.4.4 Density Functional (DFT) Computations	159
4.5 References	160
Chapter 5 – The Synthesis of a Terphenyl-Supported Aminoborane an Inorganic Analogue to Styrene	165
5.1 Introduction	165
5.2 Results and Discussion	166
5.3 Conclusions	184
5.4 Experimental Details	184
5.4.1 General Considerations	184
5.4.2 Synthetic Procedures	185

5.4.3 X-Ray Crystallography	191
5.4.4 Density Functional Theory (DFT) Computations	200
5.5 References	201
Chapter 6 – The Synthesis of The World’s Bulkiest <i>N</i> -Heterocyclic Carbene	205
6.1 Introduction	205
6.2 Results and Discussion	206
6.3 Conclusions	214
6.4 Experimental Details	214
6.4.1 General Considerations	214
6.4.2 Synthetic Procedures	215
6.4.3 X-Ray Crystallography	217
6.4.4 Density Functional Theory (DFT) Computations	222
6.5 References	222
Chapter 7 – Summary and Future Directions	226
7.1 References	234
Complete Bibliography	237

List of Figures

- Figure 1.1.** Molecular orbital (MO) depiction of linear ($D_{\infty h}$) and trans-bent (C_{2h}) heavy Group 13 element dimetallenes with Power and coworkers' *trans*-bent dimetallenes $Ar^{Dipp}MMAr^{Dipp}$ ($M = Ga$ (**6**), In (**7**), Tl (**8**)). 7
- Figure 1.2.** Resonance structures of $\{(Me_3Si)_2HC\}_2SnSn\{(CH(SiMe_3)_2\}_2$ (**17**), the reversible homolytic cleavage of the Sn–Sn bond of **17** (top) and an illustration of the *trans*-bending in **17** in the solid state (bottom). 12
- Figure 1.3.** The heavy Group 14 alkyne analogues **18–21** with their respective L–E–E bond angles (L = ligand; E = Si–Pb) illustrating a reduction in the multiple bond character descending the Group 14. 14
- Figure 1.4.** Frontier molecular orbitals (FMOs) of $\{(Me_3Si)_2N\}_2Ge$: illustrating σ -withdrawal and π -donation by flanking nitrogen atoms. 15
- Figure 1.5.** Diagram depicting the σ -donating and π -accepting interactions for *N*-heterocyclic carbenes (NHCs) and cyclic(alkyl)amino carbenes (CAAC). 21
- Figure 1.6.** Graphical illustration of percent buried volume ($\%V_{Bur}$) and the calculated $\%V_{Bur}$ for IPr and Im^iPr_2 when the NHC–Au distance is set to 2.0 Å. 22
- Figure 1.7.** Resonance forms of *N*-heterocyclic olefins (NHOs) and the methylene phosphorane Ph_3CH_2 and the general structure of a Breslow intermediate. 25
- Figure 1.8.** NHO and mNHO Rh-complexes (top) and competitive binding experiment between NHOs and mNHOs (bottom). 32
- Figure 1.9.** Early examples of NHO transition metal complexes. 33
- Figure 1.10.** Examples of NHOs coordinating to main group halides and hydrides. 34
- Figure 2.1.** Alkyl- and aryl-substituted tetrelenes (Trip = 2,4,6- i -Pr₃C₆H₂). 50

- Figure 2.2.** Molecular structure of $^{\text{Me}}\text{IPrCH}(\text{I})$ (**1**) with thermal ellipsoids plotted at 50 % probability. 52
- Figure 2.3.** $^{207}\text{Pb}\{^1\text{H}\}$ NMR spectrum of $(^{\text{Me}}\text{IPrCH})_2\text{Pb}$: (**7**) in $[\text{d}_8]\text{toluene}$. 55
- Figure 2.4.** Molecular structure of $(^{\text{Me}}\text{IPrCH})_2\text{Si}(\text{dba})$ (**8**) with thermal ellipsoids plotted at 50 % probability. 58
- Figure 3.1.** Major resonance forms of the anionic *N*-heterocyclic olefin (aNHO) $^{\text{Me}}\text{IPrCH}^-$ (left) and structure of $(^{\text{Me}}\text{IPrCH})_2\text{Si}$: (right). 78
- Figure 3.2.** Molecular structure of $[(^{\text{Me}}\text{IPrCH})\text{In}]_4$ (**1**) with thermal ellipsoids plotted at 50 % probability. 80
- Figure 3.3.** Experimentally determined UV-vis spectrum of $[(^{\text{Me}}\text{IPrCH})\text{In}]_4$ (**1**) in hexanes with computed UV-vis spectra overlay with corresponding oscillator strengths for $[(^{\text{Me}}\text{PhCH})\text{In}]_4$ (**1^M**). Computed at B3LYP/cc-pVDZ(-PP) level of theory. 81
- Figure 3.4.** Molecular structure of $[(\text{SIPrCH})\text{Li}]$ (**2**) with thermal ellipsoids plotted at 50 % probability. 82
- Figure 3.5.** Molecular structure of $(^{\text{Me}}\text{IPrCH})\text{In}(\text{THF})\cdot\text{B}(\text{C}_6\text{F}_5)_3$ (**4**) with thermal ellipsoids plotted at 50 % probability. 84
- Figure 3.6.** Molecular structure of $(^{\text{Me}}\text{IPrCH})\text{Bpin}$ (**5**) with thermal ellipsoids plotted at 50 % probability. 87
- Figure 3.7.** Possible reaction mechanism of the reaction of monomeric **1^M** with HBpin. $(^{\text{Me}}\text{IPrCH})\text{BH}(\text{In})\text{pin}$ represents a transition state, all other geometries are minima on the potential energy surface. 88
- Figure 3.8.** Molecular structure of $(^{\text{Me}}\text{IPrCH})\text{InNAr}^{\text{Dipp}}$ (**6**) with thermal ellipsoids plotted at 50 % probability. 90

- Figure 3.9.** HOMO-1 (left), HOMO (middle), and LUMO (right) of $(^{\text{Me}}\text{IPrCH})\text{InNAr}^{\text{Dipp}}$ (**6**) computed at the B3LYP/cc-pVDZ(-PP) level of theory with the orbitals plotted with an *iso*-value of ± 0.02 . 91
- Figure 3.10.** Highest occupied molecular orbitals of modeled imides and $(^{\text{Me}}\text{IPrCH})\text{InNAr}^{\text{Dipp}}$ (**6**) at *iso*-values of ± 0.02 (top) and ± 0.04 (bottom). 92
- Figure 3.11.** Experimentally determined UV-vis spectrum of $(^{\text{Me}}\text{IPrCH})\text{InNAr}^{\text{Dipp}}$ (**6**) in hexanes with computed UV-vis spectra overlay with corresponding oscillator strengths. Computed at B3LYP/cc-pVDZ(-PP) level of theory. 93
- Figure 3.12.** Molecular structure of $[(^{\text{Me}}\text{IPrCH})_6\text{In}_6\text{P}_8]$ (**7**) with thermal ellipsoids plotted at 50 % probability. 94
- Figure 4.1.** The first diborane(4) isolated, $[\text{Mes}_2\text{B}=\text{BMes}(\text{Ph})]^{2-}$, and a parent diborene stabilized by *N*-heterocyclic carbene ligands. 124
- Figure 4.2.** Molecular structure of $^{\text{Me}}\text{IPrCH}_2 \cdot \text{BCl}_3$ (**1**) plotted with thermal ellipsoids at 50 % probability. 126
- Figure 4.3.** Molecular structure $^{\text{Me}}\text{IPrCH}(\text{Br})$ (**3**) with thermal ellipsoids plotted at 50 % probability. 128
- Figure 4.4.** Molecular structure of $^{\text{Me}}\text{IPrCH}_2 \cdot \text{Br}_2\text{B}-\text{BBr}_2 \cdot \text{CH}_2^{\text{Me}}\text{IPr}$ (**2**) with thermal ellipsoids plotted at 50 % probability. 131
- Figure 4.5.** Molecular structure of $(^{\text{Me}}\text{IPrCH})\text{BMes}_2$ (**4**) with thermal ellipsoids plotted at 50 % probability. 133
- Figure 4.6.** Molecular structure of $(\text{SIPrCH})\text{ClB}-\text{BCl}(\text{CHSIPr})$ (**6**) with thermal ellipsoids plotted at 50 % probability. 135

- Figure 4.7.** Molecular structure of $[(\{HN(H_2C)_2N(Dipp)\}C=CH)B(Dipp)]_2$ (**8**) with thermal ellipsoids plotted at 50 % probability. 138
- Figure 4.8.** Computed SOMOs of $(^{Me}IPrCH)B=B(CH^{Me}IPr)$ (**9**) at the B3LYP/cc-pVDZ level of theory. 139
- Figure 5.1.** Iminoboranes stabilized kinetically and by inter/intramolecular FLPs. 166
- Figure 5.2.** Molecular structure of $[Ar^{Dipp}BH_3]Li(THF)_3$ (**2**) with thermal ellipsoids plotted at 50 % probability. 168
- Figure 5.3.** Molecular structure of $Ar^{Dipp}BH_2 \cdot NH_3$ (**3**) with thermal ellipsoids plotted at 50 % probability. 170
- Figure 5.4.** Molecular structure of $[Ar^{Dipp}BH_2 \cdot NH_2Li]_2$ (**4**) with thermal ellipsoids plotted at 50 % probability. 172
- Figure 5.5.** Computed (black trace; M06-2X/cc-pVTZ) and measured (red trace) IR spectra (drop-cast from benzene, KBr plate) of $Ar^{Dipp}B(H)=NH_2$ (**5**). 174
- Figure 5.6.** Molecular structure of $Ar^{Dipp}B(C_8H_{14})$ (**6**) with thermal ellipsoids plotted at 50 % probability. 176
- Figure 5.7.** 2H NMR spectrum of $Ar^{Dipp}BH_2 \cdot ND_3$ (**6**) in C_6H_6 . 177
- Figure 5.8.** Excerpt from the 2H NMR spectrum of $Ar^{Dipp}B(H)=ND_2$ (**8**) in C_6H_6 showing two magnetically-inequivalent ND resonances. 178
- Figure 5.9.** Computed HOMO-9 of $Ar^{Dipp}B(H)=NH_2$ (**5**) at the M06-2X/cc-pVTZ level of theory. 179

- Figure 5.10.** NBOs of $\text{Ar}^{\text{Dipp}}\text{B}(\text{H})=\text{NH}_2$ (**5**) depicting (with e^- occupancy): the lone pair of N [$1.7 e^-$] (left); the B–N σ orbital [$2.0 e^-$] (middle); the partially-occupied p-orbital of B [$0.3 e^-$] (right). Computed at the M06-2X/cc-pVTZ level of theory. 179
- Figure 5.11.** Optimized gas phase geometry of $\text{Ar}^{\text{Dipp}}\text{B}(\text{H})=\text{NH}_2$ (**5**) computed at the M06-2X/cc-pVTZ level of theory with a) calculated bond lengths [\AA], and b) Wiberg bond indices (WBI) and natural charges (Q_{NPA}). 181
- Figure 5.12.** Computed HOMO (left) and LUMO (right) of $\text{Ar}^{\text{Dipp}}\text{N}(\text{H})=\text{BH}_2$ (**13**) at the M06-2X/cc-pVTZ level of theory. 182
- Figure 6.1.** Bertrand's phosphinocarbene and select sterically demanding NHCs. 206
- Figure 6.2.** Molecular structure of $[\text{Me}^e\text{ITrH}]\text{OTf}$ (**2**) plotted with thermal ellipsoids at 50 % probability. 208
- Figure 6.3.** Molecular structure of Me^eITr (**3**) plotted with thermal ellipsoids at 50 % probability. 210
- Figure 6.4.** Computed steric map generated during the $\%V_{\text{Bur}}$ calculation and space filling model of Me^eITr (**3**) extracted from X-ray crystallographic data. 211
- Figure 6.5.** Computed HOMO (right) and LUMO (left) of Me^eITr (**3**) at the B3LYP/def2-TZVP level of theory. 211
- Figure 6.6.** Computed structure of $\text{Me}^e\text{ITr}\cdot\text{Pd}$ at the B3LYP/def2-TZVP level of theory. 213

List of Schemes

- Scheme 1.1.** a) Reduction of Cl_2SiMe_2 with sodium metal giving polymethylsilane; b) Reduction of Cl_2SiPh_2 with sodium metal by Kipping; c) West and coworkers' preparation of a kinetically-stabilized disilene $\text{Mes}_2\text{Si}=\text{SiMes}_2$ (**1**) *via* photolysis. 4
- Scheme 1.2.** a) Synthesis of $\text{Ar}^{\text{Trip}}\text{In}$: (**2**) and $\text{Ar}^{\text{Trip}}\text{Tl}$: (**3**); b) Preparation of $\text{Ar}^{i\text{Pr}8}\text{Ga}$: (**4**); c) Synthesis of $\text{Ar}^{i\text{Pr}8}\text{Al}$: (**5**). 5
- Scheme 1.3.** a) Synthesis of $\text{Ar}^{\text{Dipp}}\text{In}\cdot\text{B}(\text{C}_6\text{F}_5)_3$ (**9**); b) Preparation of $[\text{Ar}^{\text{Dipp}}\text{GaH}(\mu\text{-H})]_2$ (**10**) and $[\text{Ar}^{\text{Dipp}}\text{GaH}(\mu\text{-NH}_2)]_2$ (**11**) from H_2 and NH_3 gas, respectively. 8
- Scheme 1.4.** Preparation of the dialumene-arene adducts $\text{Ar}^{\text{Dipp}}\text{Al}(\text{C}_6\text{H}_5\text{Me})\text{AlAr}^{\text{Dipp}}$ (**12**) and $\text{BbpAl}(\text{C}_6\text{H}_6)\text{AlBbp}$ (**13**). 9
- Scheme 1.5.** a) Synthesis of $[\text{B}(\text{tBu})]_4$ (**14**); b) Preparation of $[\text{B}(\text{TMP})]_4$ (**15**) and *cyclo*- $[\text{B}(\text{N}^i\text{Pr}_2)]_4$ (**16**). 10
- Scheme 1.6.** Representative ligand activation product by a possible transient borylene isolated by Power and Grigsby upon reduction of $\text{Ar}^{\text{Mes}}\text{BBr}_2$. 11
- Scheme 1.7.** a) Synthesis of Cp^*_2Si : (**22**); b) Preparation of $(\text{HCN}^t\text{Bu})_2\text{Si}$: (**23**); c) Synthesis of $(\text{H}_2\text{CC}(\text{SiMe}_3)_2)_2\text{Si}$: (**24**) and subsequent ligand decomposition *via* 1,2-migration $(\text{H}_2\text{C})_2\text{C}(\text{SiMe}_3)_2(\text{Me}_3\text{Si})\text{C}=\text{SiSiMe}_3$ (**25**). 16
- Scheme 1.8.** Synthesis of the iminoborane ${}^t\text{BuB}\equiv\text{N}^t\text{Bu}$ (**26**) and its subsequent dimerization to the aminoborane $[{}^t\text{BuBN}^t\text{Bu}]_2$ (**28**). 18
- Scheme 1.9.** Synthesis of $\text{Ar}^{\text{Dipp}}\text{MNAr}^{\text{Xyl-}t\text{Bu}}$ ($\text{M} = \text{Ga}$ (**29**), In (**30**)). 18

Scheme 1.10. a) Synthesis the NHC stabilized-diborene $\text{IPr}\cdot\text{HB}=\text{BH}\cdot\text{IPr}$ (32); b) Synthesis of a NHC-stabilized boron-boron triple bond $\text{IPr}\cdot\text{B}\equiv\text{B}\cdot\text{IPr}$ (33); c) Synthesis of a NHC -tabilized silylene $\text{IPr}\cdot\text{SiBr}_2$ (34).	23
Scheme 1.11. Early reports on the synthesis of sterically unencumbered NHOs.	27
Scheme 1.12. General synthetic routes to NHOs.	28
Scheme 1.13. Synthesis of mesoionic NHOs (mNHOs) derived from: a) triazoles, b) abnormal carbenes as described by Hansmann, and c) the salient canonical resonance forms of mNHOs.	29
Scheme 1.14. Synthesis of triazole-derived NHOs.	30
Scheme 1.15. Solvent and ligand activation of NHO-borane adducts.	35
Scheme 1.16. Synthesis of $(\text{ImMe}_4\text{CH})\text{SiMe}_3$ (60) and the resonance forms of aNHOs.	36
Scheme 1.17. a) Synthesis of the divinylgermylene $(^{\text{Me}}\text{IPrCH})_2\text{Ge}$: (62); b) Preparation of the vinyl silylsilylene $(^{\text{Me}}\text{IPrCH})\text{Si}\{\text{Si}(\text{SiMe}_3)_3\}$ (64).	37
Scheme 1.18. a) Synthesis of divinylidiphosphene $(\text{IPrCHPh})\text{P}=\text{P}(\text{CPhIPr})$ (66); b) Preparation of divinylidiphosphines $(\text{CAAC}^{\text{Et}})\text{C}(\text{R})\text{P}=\text{P}\text{C}(\text{R})(\text{CAAC}^{\text{Et}})$ ($\text{R} = \text{'Bu}$ (67), Ad (68)).	38
Scheme 2.1. One-pot synthesis of $^{\text{Me}}\text{IPrCH}(\text{I})$ (1).	51
Scheme 2.2. Synthesis of $[\text{ImMe}_2^i\text{Pr}_2\text{CH}_3]\text{I}$ (4) and $\text{ImMe}_2^i\text{Pr}_2\text{CH}_2$ (3).	54
Scheme 2.3. a) Synthesis of the divinylsilyene $(^{\text{Me}}\text{IPrCH})_2\text{Si}$: (7); b) Attempted synthesis of silylene d^{10} complexes.	56
Scheme 2.4. The synthesis of $(^{\text{Me}}\text{IPrCH})_2\text{Si}(\text{dba})$ (8).	57
Scheme 3.1. Synthetic route to $[(^{\text{Me}}\text{IPrCH})\text{In}]_4$ (1).	79
Scheme 3.2. One-pot synthesis of $[(\text{SIPrCH})\text{Li}]_2$ (2).	82

Scheme 3.3.	Synthesis of $(^{\text{Me}}\text{IPrCH})\text{In}\cdot\text{B}(\text{C}_6\text{F}_5)_3$ (4') and $(^{\text{Me}}\text{IPrCH})\text{In}(\text{THF})\cdot\text{B}(\text{C}_6\text{F}_5)_3$ (4).	85
Scheme 3.4.	Synthesis of $(^{\text{Me}}\text{IPrCH})\text{B}(\text{H})\text{Trip}$ and $(^{\text{Me}}\text{IPrCH})\text{Bpin}$ (5).	86
Scheme 3.5.	Synthetic route to $(^{\text{Me}}\text{IPrCH})\text{InNAr}^{\text{Dipp}}$ (6) and its major resonance forms (left) and the structure of Power's imide $\text{Ar}^{\text{Dipp}}\text{InNAr}^{\text{Xyl-}t\text{Bu}}$ (right).	89
Scheme 4.1.	Synthesis of $^{\text{Me}}\text{IPrCH}_2\cdot\text{BCl}_3$ (1).	125
Scheme 4.2.	Synthesis of $^{\text{Me}}\text{IPrCH}(\text{Br})$ (3) (top) and proposed mechanism of formation of $^{\text{Me}}\text{IPrCH}(\text{Br})$ (3) (bottom).	128
Scheme 4.3.	Synthesis of $[(\{\text{HN}(\text{H}_2\text{C})_2\text{N}(\text{Dipp})\}\text{C}=\text{CH})\text{B}(\text{Dipp})]_2$ (8).	137
Scheme 5.1.	Synthetic routes to $\text{Ar}^{\text{Dipp}}\text{B}(\text{OMe})_2$ (1) and $[\text{Ar}^{\text{Dipp}}\text{BH}_3]\text{Li}(\text{THF})_3$ (2).	167
Scheme 5.2.	Synthetic routes to $\text{Ar}^{\text{Dipp}}\text{BH}_2\cdot\text{NH}_3$ (3).	169
Scheme 5.3.	Proposed synthetic route to $\text{Ar}^{\text{Dipp}}\text{B}(\text{C}_8\text{H}_{14})$.	175
Scheme 5.4.	Attempted synthesis of $\text{Ar}^{\text{Dipp}}\text{N}(\text{H})=\text{BH}_2$ (13).	182
Scheme 6.1.	The synthesis of 2-trityl-4,5-dimethylimidazole (1) and $[\text{MeITrH}]\text{OTf}$ (2).	207
Scheme 7.1.	a) Proposed synthetic route to the dianionic NHO synthon $[(^{\text{Me}}\text{IPrC})\text{Li}]_2$; b) Proposed synthetic route to the silylated aNHO $[(^{\text{Me}}\text{IPrC}(\text{SiMe}_3)\text{Li}]$; c) Resonance forms of a dianionic NHO.	227
Scheme 7.2.	Proposed synthesis of cyclic divinyliditetrelenes and cyclic Group 14 diradicaloids.	227
Scheme 7.3.	a) Proposed synthetic route to the Al(I) tetramer $[(^{\text{Me}}\text{IPrCH})\text{Al}]_4$; b) Proposed synthesis of the aluminum-imide $(^{\text{Me}}\text{IPrCH})\text{AlNAr}^{\text{Dipp}}$ and Power's aluminum-imide $\text{Ar}^{\text{iPr}_8}\text{AlNAr}^{\text{Mes}}$.	229

Scheme 7.4. a) Proposed synthetic route to $[(^{\text{Me}}\text{IPrC}(\text{Trip})\text{Li}]$ and the possibly *trans*-bent diborene $(^{\text{Me}}\text{IPrCTrip})\text{B}=\text{B}(\text{CTrip}^{\text{Me}}\text{IPr})$; b) Postulated synthetic pathway to the dialumene $(^{\text{Me}}\text{IPrCTrip})\text{Al}=\text{Al}(\text{CTrip}^{\text{Me}}\text{IPr})$. 231

Scheme 7.5. Proposed dehydrogenation of $\text{Ar}^{\text{Dipp}}\text{B}(\text{H})=\text{NH}_2$ with an iridium catalyst to give $[\text{Ar}^{\text{Dipp}}\text{BNH}]_2$ (top) and dehydrogenation of $\text{PB}\{\text{HBNH}\}$ to give $\text{PB}\{\text{BN}\}_2\text{PB}$ and its subsequent deposition of $(\text{BN})_x$. 232

Scheme 7.6. Proposed synthetic routes to $^{\text{Me}}\text{ITr}\cdot\text{InH}$, a monocoordinated In(I)-hydride. 233

List of Tables

Table 2.1.	X-ray crystallographic data details for $^{\text{Me}}\text{IPrCH}(\text{I})$ (1).	68
Table 2.2.	X-ray crystallographic data details for $(^{\text{Me}}\text{IPrCH})_2\text{Si}(\text{dba})$ (8).	70
Table 3.1.	X-ray crystallographic data details for $[(^{\text{Me}}\text{IPrCH})\text{In}]_4$ (1)•2 toluene.	105
Table 3.2.	X-ray crystallographic data details for $[(\text{SIPrCH})\text{Li}]_2$ (2)•toluene.	107
Table 3.3.	X-ray crystallographic data details for $(^{\text{Me}}\text{IPrCH})\text{In}(\text{THF})\cdot\text{B}(\text{C}_6\text{F}_5)_3$ (4)•pentane.	109
Table 3.4.	X-ray crystallographic details for $(^{\text{Me}}\text{IPrCH})\text{Bpin}$ (5).	111
Table 3.5.	X-ray crystallographic details for $(^{\text{Me}}\text{IPrCH})\text{InNAr}^{\text{Dipp}}$ (6)•toluene.	113
Table 3.6.	X-ray crystallographic details for $[(^{\text{Me}}\text{IPrCH})_6\text{In}_6\text{P}_8]$ (7).	115
Table 4.1.	X-ray crystallographic details for $^{\text{Me}}\text{IPrCH}_2\cdot\text{BCl}_3$ (1)•0.5 hexane.	148
Table 4.2.	X-ray crystallographic details for $(^{\text{Me}}\text{IPrCH}_2)\text{Br}_2\text{B}\cdot\text{BBr}_2(\text{CH}_2^{\text{Me}}\text{IPr})$ (2).	150
Table 4.3.	X-ray crystallographic details for $^{\text{Me}}\text{IPrCH}(\text{Br})$ (3).	152
Table 4.4.	X-ray crystallographic details for $(^{\text{Me}}\text{IPrCH})\text{BMes}_2$ (4).	154
Table 4.5.	X-ray crystallographic details for $(\text{SIPrCH})\text{ClB}\cdot\text{BCl}(\text{CHSIPr})$ (6).	156
Table 4.6.	X-ray crystallographic details for $[(\{\text{HN}(\text{H}_2\text{C})_2\text{N}(\text{Dipp})\}\text{C}=\text{CH})\text{B}(\text{Dipp})]_2$ (8).	158
Table 5.1.	X-ray crystallographic data details for $[\text{Ar}^{\text{Dipp}}\text{BH}_3]\text{Li}(\text{THF})_3$ (2).	193
Table 5.2.	X-ray crystallographic data details for $\text{Ar}^{\text{Dipp}}\text{BH}_2\cdot\text{NH}_3$ (3).	195
Table 5.3.	X-ray crystallographic data details for $[\text{Ar}^{\text{Dipp}}\text{BH}_2\cdot\text{NH}_2\text{Li}]_2$ (4) and $\sim 2\%$ $\text{Ar}^{\text{Dipp}}\text{I}$.	197
Table 5.4.	X-ray crystallographic data details for $\text{Ar}^{\text{Dipp}}\text{B}(\text{C}_8\text{H}_{14})$ (4).	199
Table 6.1.	X-ray crystallographic details for $[\text{MeITrH}]\text{OTf}$ (2)•1.5 PhF.	218

Table 6.2. X-ray crystallographic details for ^{Me}ITr (**3**)•THF.

220

List of Symbols and Abbreviations

Å	Ångstrom
Ad	Adamantyl
ADP	Anisotropic Displacement Parameters
AIM	Atoms-In-Molecules
aNHO	Anionic <i>N</i> -Heterocyclic Olefin
Ar	Aryl
Ar ^{Dipp}	2,6-Dipp ₂ C ₆ H ₃
Ar ^F	2,4,6-(F ₃ C) ₃ C ₆ H ₂
Ar ^{Mes}	2,6-Mes ₂ C ₆ H ₃
Ar ^{Trip}	2,6-Trip ₂ C ₆ H ₃
Ar ^{<i>i</i>Pr⁸}	2,6-Trip-3,5- <i>i</i> Pr ₂ C ₆ H
Ar ^{Xyl-<i>t</i>Bu}	2,6-(Xyl-4- <i>t</i> Bu) ₂ C ₆ H ₃
Avg.	Average
B3LYP	Becke, 3-Parameter, Lee–Yang–Parr
Bbp	2,6-(CH(SiMe ₃) ₂) ₂ C ₆ H ₃
Bcat	B(OC ₆ H ₄ O)
bcp	Bond critical points
ⁿ Bu	Normal Butyl
^s Bu	Secondary Butyl
^t Bu	Tertiary Butyl
<i>ca.</i>	<i>circa</i> , Latin for, Approximately
CAAC	Cyclic(alkyl)amino Carbene
CAAC ^{Et}	[(Et ₂ C)H ₂ C(Me ₂ C)NDipp]C:
CAAO	Cyclic(alkyl)amino olefin
C ₆ D ₆	Benzene-d ₆
CDCl ₃	Chloroform-d

CD ₂ Cl ₂	Dichloromethane-d ₂
CD ₃ CN	Acetonitrile-d ₃
^{Cl} Mes	(ClCNMe) ₂ C:
COD	1,5-Cyclooctadiene
Cp	Cyclopentadienyl, C ₅ H ₅
Cp*	Pentamethylcyclopentadienyl, C ₅ Me ₅
CPh ₃	Trityl
Cy	Cyclohexyl
°C	Degree Celsius
δ	Chemical Shift
δ+/δ-	Partial Positive/Negative Charges
DABCO	1,4-Diazabicyclo[2.2.2]octane
dba	Dibenzylideneacetone
DFT	Density Functional Theory
dcpBiph	2-(dicyclohexylphosphino)-biphenyl
Dipp	2,6- ⁱ Pr ₂ C ₆ H ₃
DOSY	Diffusion-Ordered Spectroscopy
Et ₂ O	Diethyl Ether
η ⁿ	Indicates Hapticity (<i>n</i>)
FT	Fourier Transform
FLP	Frustrated Lewis Pair
FMOs	Frontier Molecular Orbitals
g	Gram
HBpin	Pinacolborane
HOMO	Highest Occupied Orbital
HSQC	Heteronuclear Single Quantum Coherence
Hz	Hertz
IAd	(HCNAd) ₂ C:

ImMe ₂	(HCNMe) ₂ C:
ImMe ₄	(MeCNMe) ₂ C:
Im ⁱ Pr ₂	(HCN ⁱ Pr ₂) ₂ C:
ITr	(HCNPh ₃) ₂ C:
IR	Infrared
K	Kelvin
kcal	Kilocalorie
kJ	Kilojoule
L	General Neutral Ligand
LA	Lewis Acid
LB	Lewis Base
LUMO	Lowest Occupied Orbital
M	Variable Metal
M06	Minnesota 06 Functional
Me	Methyl
Me ^c IPr	(MeCNDipp) ₂ C:
Me ^c IPh	(MeCNPh) ₂ C:
Me ^c ITr	(MeCNCPh ₃) ₂ C:
Mes	2,4,6-Me ₃ C ₆ H ₂
Mes*	2,4,6- ^t Bu ₃ C ₆ H ₂
MHz	Megahertz
mNHO	Mesoionic <i>N</i> -Heterocyclic Olefin
MO	Molecular Orbital
mol	Mole
mmol	Millimole
MMA	Methyl Methacrylate
M.p.	Melting Point
Nacnac	General β-Diketimine Ligand

NBO	Natural Bond Order
NCI	Non-Covalent Interactions
NHC	<i>N</i> -Heterocyclic Carbene
NHO	<i>N</i> -Heterocyclic Olefin
NMR	Nuclear Magnetic Resonance
OTf ⁻	Triflate Anion; O ₃ SCF ₃ ⁻
PB	ⁱ Pr ₂ P(C ₆ H ₄)BCy ₂
pin	Pinacolato
Ph	Phenyl
ppm	Parts per Million
ⁱ Pr	<i>iso</i> -Propyl
ⁿ Pr	Normal propyl
IPr	(HCNDipp) ₂ C:
SIPr	(H ₂ CNDipp) ₂ C:
SImMe ₂	(H ₂ CNMe) ₂ C:
SIMes	(H ₂ CNMes) ₂ C:
SOMO	Singly Occupied Molecular Orbital
TD-DFT	Time-Dependant Density Functional Theory
TEPs	Tolman Electronic Parameters
THF	Tetrahydrofuran
TMEDA	Tetramethylethylenediamine
TMP	2,2,6,6-Tetramethylpiperidide
Trip	2,4,6- ⁱ Pr ₃ C ₆ H ₂
ⁿ J _{AB}	n-Bond Coupling Constant Between A and B
UV-vis	Ultraviolet-Visible Spectroscopy
<i>Vide supra</i>	Latin for, See above
<i>Vide infra</i>	Latin for, See below
<i>Via</i>	Latin for, by way of

WBI	Wiberg Bond Index
$\%V_{\text{Bur}}$	Percent Buried Volume
VMD	Visual Molecular Dynamics
$\{^n\text{X}\}$	Decoupled to ^nX Nucleus
X	Variable Halide
Xyl	2,6-Me ₂ C ₆ H ₃

Chapter 1 – Introduction

1.1 Main Group Element Compounds: From Structural Curiosities to Applications

The field of organometallic chemistry has a long history, dating as far back as 1831 with the discovery of Zeise's salt, $(K[PtCl_3(C_2H_4)] \cdot H_2O)$,¹ in which the bonding of the ethylene ligand confused chemists for the better part of a century.² Perhaps the most important discovery in the field of organometallics is that of ferrocene, Cp_2Fe ($Cp = \eta^5-C_5H_5$), first reported in 1951,³ which led to an explosion in interest transition metal coordination chemistry and organometallics due to its unusual bonding and structure. The fundamental investigations that followed gave rise to seminal discoveries in transition metal homogenous catalysis, including the catalytic hydrogenation of olefins with Wilkinson's catalyst, $[RhCl(PPh_3)_3]$,⁴ the reversible activation of H_2 by Vaska's complex, $[IrCl(CO)(PPh_3)_3]$,⁵ and the activation of C-H bonds by iridium(I) complexes.⁶ These reports catapulted the field to even greater heights leading to the development of a vast library of homogenous transition metal catalysts moving transition metal coordination chemistry out of the realm of structural curiosities to being indispensable tools in homogenous catalysis.

In contrast to the breakneck pace in the development of transition metal chemistry after 1951, the study of main group elements proceeded rather slowly. It is notable that main group species containing element-element single bonds (E-E) appeared early in the study of organometallic chemistry with the synthesis of cacodyl ($Me_2As-AsMe_2$) in the late 18th century.⁷ Another early example of a homonuclear main group E-E single bond can be found in Cl_2B-BCl_2 , first reported in 1925 by Stock and coworkers.⁸ These two examples proved

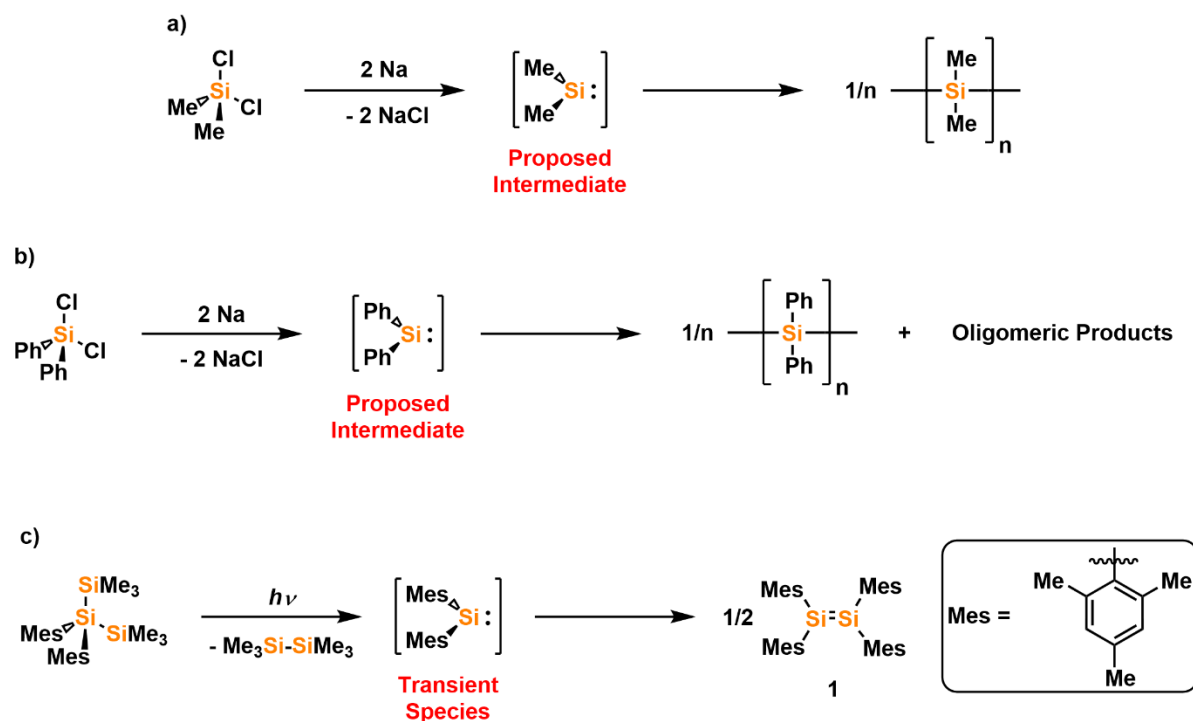
that electropositive elements could indeed form electron-precise single bonds, which up to that point was not considered possible. However, general interest in the study of main group element-containing compounds was rather limited. This was primarily due to the belief that elements of principal quantum numbers greater than two ($n > 2$) could not form element-element double bonds (E=E), with themselves or other elements, commonly known as the “Double Bond Rule”.⁹ Compounding this belief was that compounds of the main group elements often have frontier (HOMO–LUMO) orbitals separated by large energy gaps with *d*-orbitals that are not energetically accessible;¹⁰ as such, it was believed that main group elements could not participate in reactions typically mediated by transition metals, such as H₂ activation.

The “Double Bond Rule” was broken by Lappert and coworkers in the 1970s and 1980s when they reported the isolation of acyclic two-coordinate dialkyl tetrelene dimers in the solid state, $\{(Me_3Si)_2HC\}_2E=E\{(CH(SiMe_3)_2\}_2$, (E = Ge, Sn, Pb); notably, these species exists as discrete monomers in solution $((Me_3Si)_2HC)_2E$.¹¹ West and coworkers reported the first kinetically-stabilized disilene $Mes_2Si=SiMes_2$ (Mes = 2,4,6-Me₃C₆H₂) in 1981.¹² Yoshifuji and coworkers would in the same year report the isolation of a stable diphosphene $Mes^*P=PMes^*$ (Mes* = 2,4,6-*t*Bu₃C₆H₂).¹³ These examples would help put the “Double Bond Rule” to rest. In 2005, Power and coworkers demonstrated that H₂ activation by low-valent main group elements was possible when they combined $Ar^{Dipp}GeGeAr^{Dipp}$ (Ar^{Dipp} = 2,6-Dipp₂C₆H₃; Dipp = 2,6-*i*Pr₂C₆H₃), a heavy Group 14 element analogue to acetylene (HC≡CH), with H₂ gas affording various germanium-hydride species.¹⁴ Stephan and coworkers would later demonstrate that frustrated Lewis pairs (FLPs) devoid of transition metal elements could reversibly activate H₂, mimicking the reactivity of transition metals.¹⁵ These examples of main

group elements defying prevailing beliefs has allowed for the emergence of a field of fervent study that is continuously pushing the boundaries of known reactivity of main group species.

1.2 Kinetic Stabilization of Low-Valent Main Group Elements

“Kinetic stabilization” refers to the use of sterically hindered substituents, typically organic groups, to prevent uncontrolled ligand activation, oligomerization/polymerization and/or unwanted redox reactions from transpiring.¹⁶ For example, reduction of Me_2SiCl_2 with sodium metal (Wurtz coupling) affords the dimethylsilane polymer $[\text{SiMe}_2]_n$, possibly through the Si(II) intermediate $\text{Me}_2\text{Si}:$ (Scheme 1.1a).¹⁷ Reduction of the related chlorosilane Ph_2SiCl_2 by Kipping with sodium affords similar oligomeric diphenylsilane products, which possibly contains some polymeric $[\text{SiPh}_2]_n$ (Scheme 1.1b).¹⁸ The postulated intermediate in the above mentioned reaction, $\text{Me}_2\text{Si}:$, has been observed in frozen argon matrix conditions (10 K),¹⁹ and both $\text{Me}_2\text{Si}:$ and $\text{Ph}_2\text{Si}:$ have been generated/detected as transient species in solution by UV-vis spectroscopy *via* laser flash photolysis studies involving $[\text{SiMe}_2]_6$ and $(\text{H}_2\text{C}(\text{H}_2\text{C})(\text{SiMe}_3))_2\text{SiPh}_2$ as precursors; these species have exceedingly short lifetimes on the scale of 0.6–1.5 μs and 250–600 μs , respectively.²⁰ West and coworkers were able to overcome the tendency of low-valent Si(II) species to oligomerize by the incorporation of more sterically-demanding Mes substituents in the disilene dimer $\text{Mes}_2\text{Si}=\text{SiMes}_2$ (**1**), which was prepared by photolysis of $\text{Mes}_2\text{Si}(\text{SiMe}_3)_2$ (Scheme 1.1c).¹²

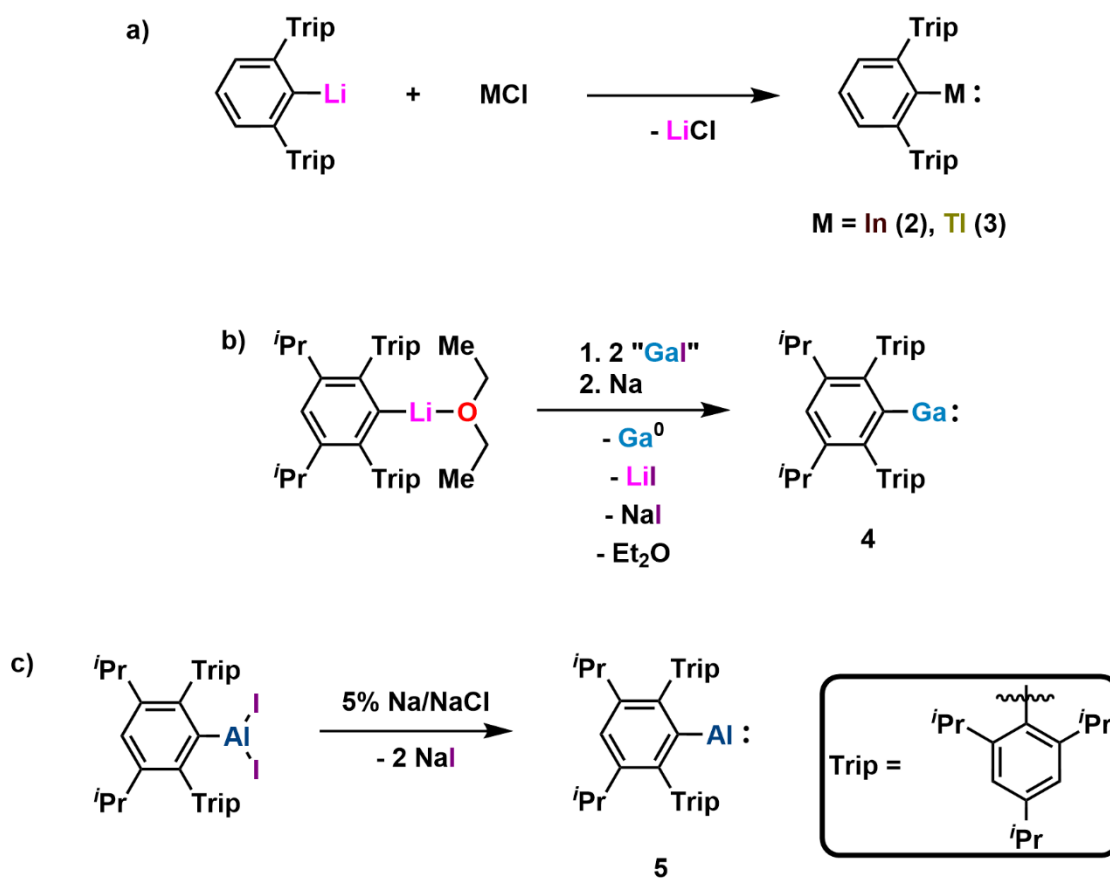


Scheme 1.1. a) Reduction of Cl_2SiMe_2 with sodium metal giving polymethylsilane; b) Reduction of Cl_2SiPh_2 with sodium metal by Kipping; c) West and coworkers' preparation of a kinetically-stabilized disilene $\text{Mes}_2\text{Si}=\text{SiMes}_2$ (**1**) via photolysis.

1.2.1 Kinetic Stabilization of Low-Valent Group 13 Elements

Early examples of element–element (E–E) bonding involving heavier low-valent Group 13 elements were generally supported by cyclopentadienyl (Cp) derivatives, which in the solid state exist as tetramers (e.g., $[\text{Cp}^*\text{Al}]_4$; $\text{Cp}^* = \eta^5\text{-C}_5\text{Me}_5$)²¹ and hexamers (e.g., $[\text{Cp}^*\text{M}]_6$; $\text{M} = \text{Ga}, \text{In}$).²² Monocoordinate silylated ligands, such as $\text{C}(\text{SiMe}_3)_3$ and $\text{Si}(\text{SiMe}_3)_3$, also afford tetrahedron-shaped $[\text{MR}]_4$ oligomers ($\text{M} = \text{Ga}, \text{In}$), which dissociate in solution or in the gas phase to give monomeric species;²³ it should be noted that CpIn ($\text{Cp} = \eta^5\text{-C}_5\text{H}_5$) exists as a zig-zag polymeric structure in the solid state but dissociates into monomers in the gas phase.^{24,25} Power and coworkers demonstrated that monocoordinate $\text{Ga}(\text{I})$, $\text{In}(\text{I})$ and $\text{Tl}(\text{I})$ species could be isolated when supported by the sterically-demanding terphenyl ligand Ar^{Trip}

(Ar^{Trip} = 2,6-Trip₂C₃H₂; Trip = 2,4,6-ⁱPr₂C₆H₂), and were prepared by combining Ar^{Trip}Li with the appropriate MCl (M = In, Tl) source to give Ar^{Trip}In: (**2**)²⁶ and Ar^{Trip}Tl: (**3**),²⁷ respectively (Scheme 1.2a). In the case of Ga, the terphenyl ligand Ar^{*i*Pr⁸}Li•Et₂O (Ar^{*i*Pr⁸} = 2,6-Trip-3,5-ⁱPr₂C₆H) was used instead, and combined with two equivalents of “GaI”, followed by reduction with sodium metal, to give the desired monomeric Ar^{*i*Pr⁸}Ga: (**4**)²⁸ (Scheme 1.2b). More recently, Power, Tuononen and coworkers isolated a stable one-coordinate Al(I) supported by the terphenyl ligand, Ar^{*i*Pr⁸}, by reduction of the precursor Ar^{*i*Pr⁸}AlI₂ with 5% Na/NaCl to give Ar^{*i*Pr⁸}Al: (**5**) as a deep-red solid (Scheme 1.2c).²⁹



Scheme 1.2. a) Synthesis of Ar^{Trip}In: (**2**) and Ar^{Trip}Tl: (**3**); b) Preparation of Ar^{*i*Pr⁸}Ga: (**4**); c) Synthesis of Ar^{*i*Pr⁸}Al: (**5**).

Neutral dimetallenes, of the form $\text{Ar}^{\text{Dipp}}\text{MMAr}^{\text{Dipp}}$ ($\text{M} = \text{Ga}$ (**6**), In (**7**), Tl (**8**)),³⁰ can be considered to be the heavy Group 13 element analogues to acetylene ($\text{HC}\equiv\text{CH}$) and congeners of diborene ($\text{HB}=\text{BH}$).³¹ A key structural feature of these dimetallenes is their *trans*-bent geometries, for example, in the digallene $\text{Ar}^{\text{Dipp}}\text{GaGaAr}^{\text{Dipp}}$ (**6**) the C–Ga–Ga bond angle is $123.16(7)^\circ$,^{30b} which is significantly distorted from the linear H–C–C arrangement in acetylene. The bending in **6** can be rationalized as arising from second-order Jahn–Teller distortion. In a linear molecule, of the general form REER ($D_{\infty h}$) ($\text{E} = \text{Group 13 element}$), the frontier molecular orbitals consist of a bonding σ -orbital and two degenerate π -bonding orbitals, and their corresponding antibonding combinations. When this linear molecule undergoes a *trans*-bending vibration, changing the symmetry to C_{2h} , the degeneracy of the π and π^* orbitals is broken, resulting in a new HOMO that contains a lone pair (n_-), or slipped π -bonding, and a LUMO that consists of an empty π -orbital (n_+); the HOMO and LUMO in this configuration have the same π -symmetry (Figure 1.1).³¹ For heavy main group element multiple-bonded species second order Jahn–Teller distortion is more common due to the separation of the energy levels being smaller than in the lighter congeners (*i.e.*, boron); for this reason, $\text{HB}=\text{BH}$ is calculated to be unstable with a linear geometry and a triplet ground state wherein each of the degenerate π -orbitals are singly occupied,³¹ while the heavier element analogues (REER; $\text{E} = \text{Ga–Tl}$) are stable with a *trans*-bent geometry and a stabilized HOMO in each case.

The multiple bonding in dimetallenes (RMMR; $\text{M} = \text{Ga–Tl}$) is generally considered to be very weak. This is highlighted by the addition of the Lewis acid $\text{B}(\text{C}_6\text{F}_6)_3$ to the diindene $\text{Ar}^{\text{Dipp}}\text{InInAr}^{\text{Dipp}}$ (**7**), which homolytically cleaves the In–In bond affording the adduct $\text{Ar}^{\text{Dipp}}\text{In}\cdot\text{B}(\text{C}_6\text{F}_5)_3$ (**9**) (Scheme 1.3a).^{30a} Likewise, addition of H_2 or NH_3 to $\text{Ar}^{\text{Dipp}}\text{GaGaAr}^{\text{Dipp}}$

(6) gives the corresponding hydrido- or amido-bridging products $[\text{Ar}^{\text{Dipp}}\text{GaH}(\mu\text{-H})]_2$ (**10**) and $[\text{Ar}^{\text{Dipp}}\text{GaH}(\mu\text{-NH}_2)]_2$ (**11**) (Scheme 1.3b).³²

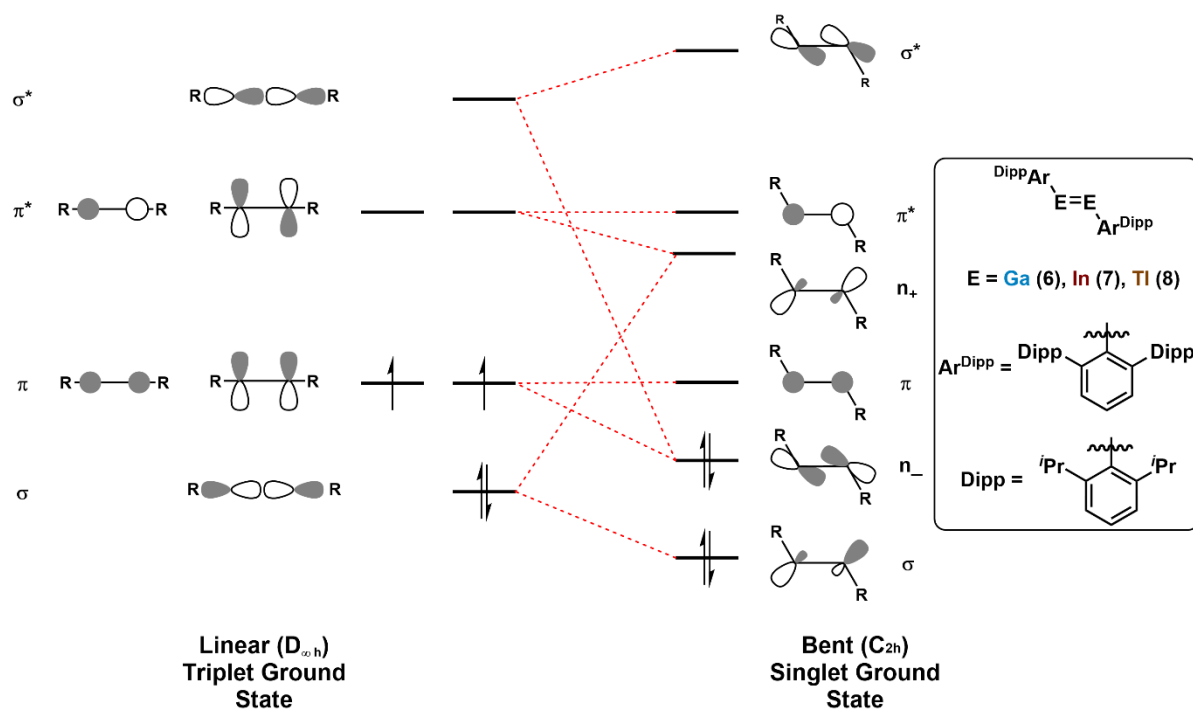
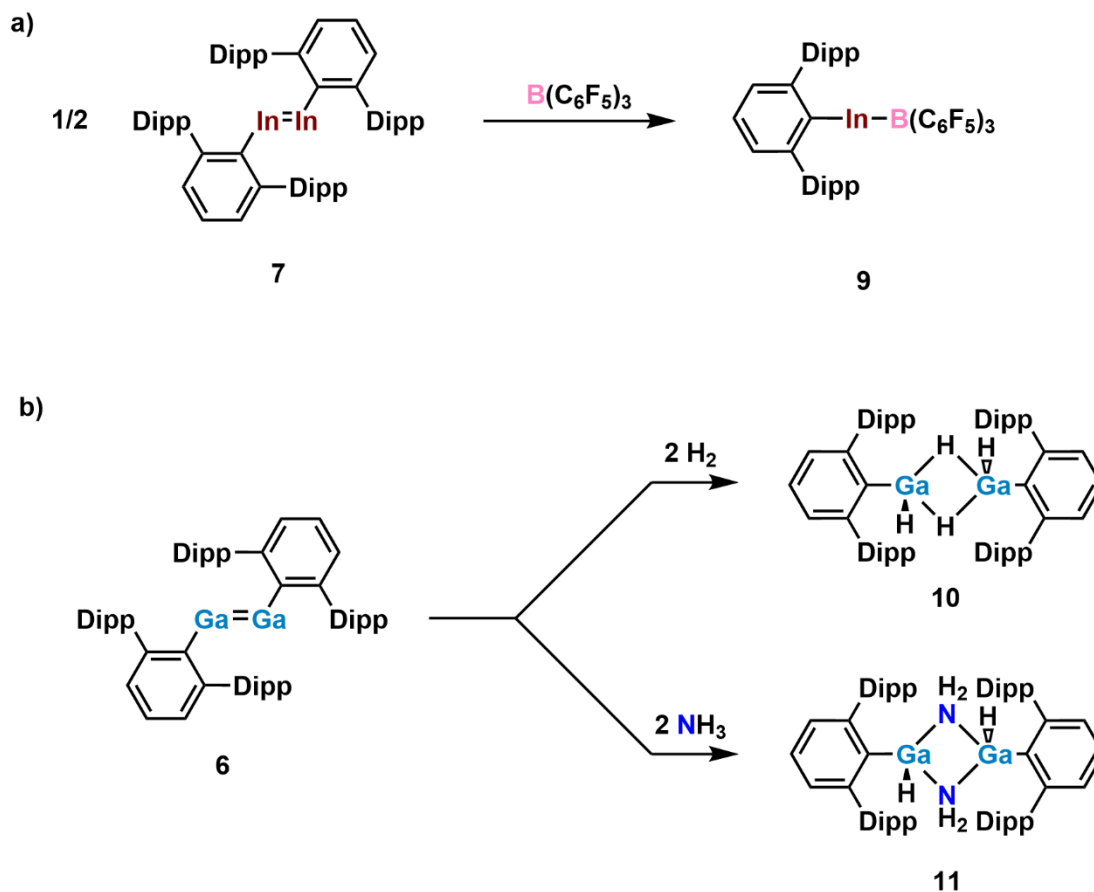


Figure 1.1. Molecular orbital (MO) depiction of linear ($D_{\infty h}$) and *trans*-bent (C_{2h}) heavy Group 13 element dimetallenes with Power and coworkers' *trans*-bent dimetallenes $\text{Ar}^{\text{Dipp}}\text{MMAr}^{\text{Dipp}}$ ($M = \text{Ga}$ (**6**), In (**7**), Tl (**8**)). Adapted from Figure 1 in Ref. 31a.

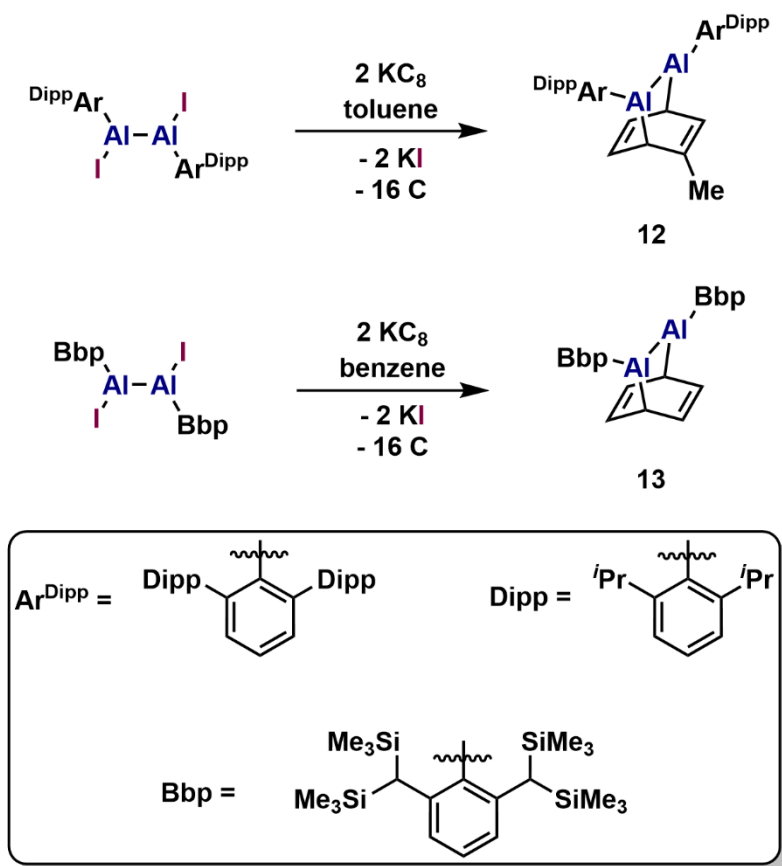
It should be noted that a dialumene (RAlAIR), while postulated to be stable with bulky R groups, has not been isolated to date.³³ Attempts by the Power and Tokitoh groups to prepare and isolate a dialumene resulted in cyclization with aromatic solvents affording $\text{Ar}^{\text{Dipp}}\text{Al}(\text{C}_6\text{H}_5\text{Me})\text{AlAr}^{\text{Dipp}}$ (**12**)^{33a} and $\text{BbpAl}(\text{C}_6\text{H}_6)\text{AlBbp}$ (**13**) ($\text{Bbp} = 2,6\text{-}(\text{CH}(\text{SiMe}_3)_2)_2\text{C}_6\text{H}_3$)^{33b} (Scheme 1.4), respectively.



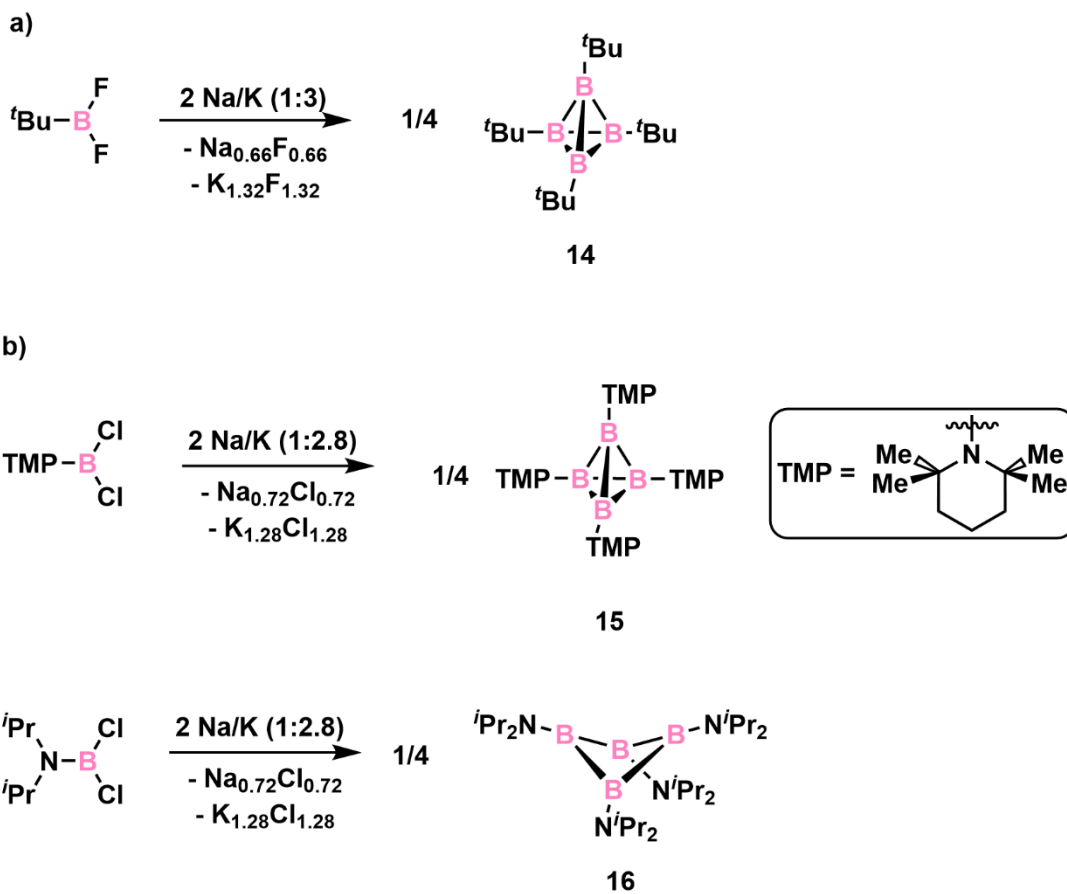
Scheme 1.3. a) Synthesis of $\text{Ar}^{\text{Dipp}}\text{In}\cdot\text{B}(\text{C}_6\text{F}_5)_3$ (**9**); b) Preparation of $[\text{Ar}^{\text{Dipp}}\text{GaH}(\mu\text{-H})_2]$ (**10**) and $[\text{Ar}^{\text{Dipp}}\text{GaH}(\mu\text{-NH}_2)_2]$ (**11**) from H_2 and NH_3 gas, respectively.

Early examples of low-valent boron(I) species include the tetramer $[\text{B}(\text{tBu})_4]$ (**14**), first prepared by reduction of tBuBF_2 with Na/K alloy (1:3) in pentane by Paetzold and Boese in 1991 (Scheme 1.5a).³⁴ In 1999, Siebert and coworkers prepared a similar tetramer supported by 2,2,6,6-tetramethylpiperidide (TMP) groups, $[\text{B}(\text{TMP})_4]$ (**15**), *via* reduction of $(\text{TMP})\text{BCl}_2$ with Na/K (1:2.8). Siebert also described the cyclotetaborane *cyclo*- $[\text{B}(\text{N}^i\text{Pr}_2)]_4$ (**16**) in the same report when the smaller amide N^iPr_2 was used as the supporting ligand (Scheme 1.5b).³⁵ Attempts by Power and Grigsby to prepare a diborene ($\text{RB}=\text{BR}$) supported by the terphenyl ligand Ar^{Mes} ($\text{Ar}^{\text{Mes}} = 2,6\text{-Mes}_2\text{C}_6\text{H}_3$) *via* reduction of $\text{Ar}^{\text{Mes}}\text{BBR}_2$ (e.g., KC_8) gave exclusively

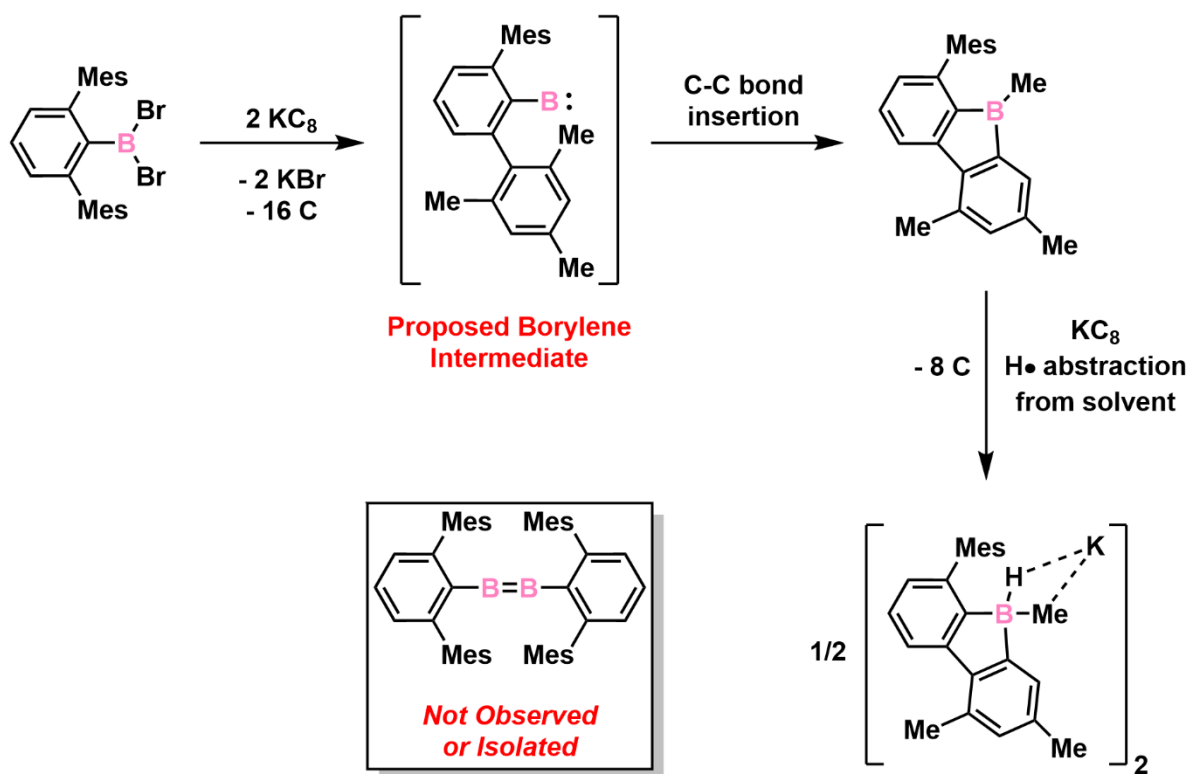
ligand-activated products *via* C–C, C–H bond insertion and proton abstraction by a possible transient borylene ($\text{Ar}^{\text{Mes}}\text{B:}$) (Scheme 1.6).³⁶



Scheme 1.4. Preparation of the dialumene-arene adducts $\text{Ar}^{\text{Dipp}}\text{Al}(\text{C}_6\text{H}_5\text{Me})\text{AlAr}^{\text{Dipp}}$ (**12**) and $\text{BbpAl}(\text{C}_6\text{H}_6)\text{AlBbp}$ (**13**).



Scheme 1.5. a) Synthesis of $[\text{B}(\text{tBu})_4]$ (**14**); b) Preparations of $[\text{B}(\text{TMP})_4]$ (**15**) and *cyclo*- $[\text{B}(\text{N}^i\text{Pr}_2)]_4$ (**16**).



Scheme 1.6. Representative ligand-activation product by a possible transient borylene isolated by Power and Grigsby upon reduction of $\text{Ar}^{\text{Mes}}\text{BBr}_2$.

1.2.2 Kinetic Stabilization of Low-Valent Group 14 Elements

Lappert and coworkers prepared the distannene $\{(\text{Me}_3\text{Si})_2\text{HC}\}_2\text{Sn}=\text{Sn}\{(\text{CH}(\text{SiMe}_3)_2)_2$ (**17**), a tin analogue of an alkene, in the 1970s.¹¹ Unlike West's disilene $\text{Mes}_2\text{Si}=\text{SiMes}_2$ (**1**), which exists as a dimer in both solution and in the solid state, Lappert's distannene **17**, while a dimer in the solid state, dissociates into the monomeric stannylene $\{(\text{Me}_3\text{Si})_2\text{HC}\}_2\text{Sn}$: (**17'**) in solution. Lappert's distannene features a *trans*-bent conformation, with the ligands at each Sn-center being 41° out-of-plane (fold angle) of the Sn–Sn bond axis, indicating the presence of a lone pair character at each Sn center. The sum of the interligand angles at Sn in $\{(\text{Me}_3\text{Si})_2\text{HC}\}_2\text{SnSn}\{(\text{CH}(\text{SiMe}_3)_2)_2$ (**17**) is 340° , supporting the presence of lone pair character at each tin center, while West's disilene (**1**) is nearly planar at each silicon ($\text{Si} =$

356°).¹² These observations indicate that the multiple bonding in $\{(Me_3Si)_2HC\}_2SnSn\{(CH(SiMe_3)_2)_2$ (**17**) is rather weak and could be described by two resonance structures (zwitterionic) with a Sn–Sn single-bond (Figure 1.2). Such *trans*-bent geometries are often observed in heavier Group 14 element alkenes ($R_2E=ER_2$) (E = Ge–Pb). These geometries can be explained by second-order Jahn–Teller distortion (*vide supra*)³¹ but can also be partially explained by the “inert pair effect”, which is also relevant to Group 13 multiplebonded species (*vide infra*).³⁷

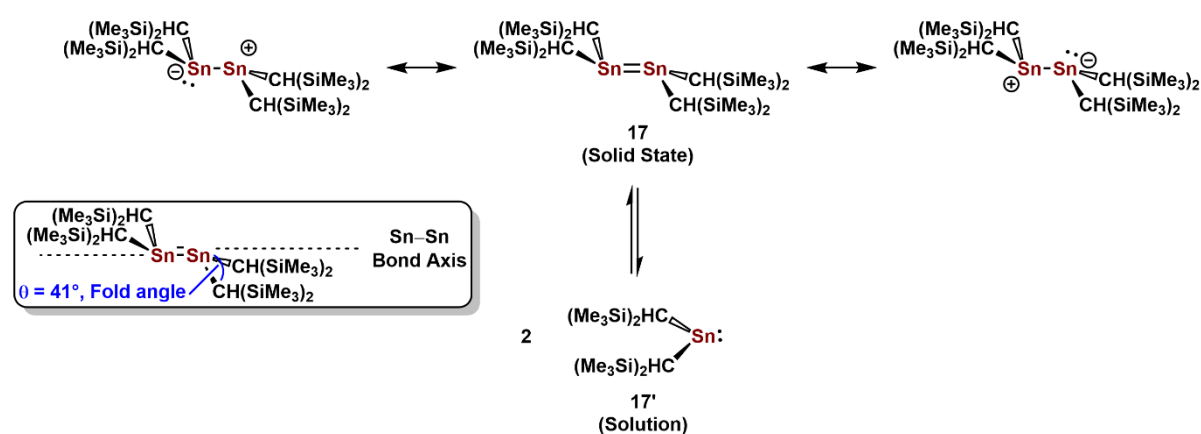


Figure 1.2. Resonance structures of $\{(Me_3Si)_2HC\}_2SnSn\{(CH(SiMe_3)_2)_2$ (**17**), the reversible homolytic cleavage of the Sn–Sn bond of **17** (top) and an illustration of the *trans*-bending in **17** in the solid state (bottom).

The “inert pair effect” describes the tendency of heavier Group 13–16 elements to have stable oxidation states that are two less than the maximum valency as one descends the group. For example, in Group 14, carbon is commonly found in a +4 oxidation state whereas lead is commonly found in a +2 oxidation state preferentially due to a stabilized $6s^2$ lone pair. This stabilization is due to the relatively diffuse *d*- and *f*-orbitals being poorly shielding towards the valence electrons (*e.g.*, $6s^2$), relativistic effects, and decreasing bond enthalpies the lower down a Group an element is.³⁷

The heavy Group 14 alkyne analogues REER (E = Si–Pb) are excellent examples of the effect of second-order Jahn–Teller distortion and the “inert pair effect” associated with heavier main group elements. In 2004, Sekiguchi and coworkers isolated the first disilyne (**18**) (RSi≡SiR; R = Si(ⁱPr){CH(SiMe₃)}₂) utilizing bulky silyl substituents to protect the Si≡Si core.³⁸ Power and coworkers had a few years prior prepared the other heavy element alkynes Ge–Pb by using bulky *meta*-terphenyl ligands, such as Ar^{Dipp}, to afford Ar^{Dipp}GeGeAr^{Dipp} (**19**) and Ar^{Dipp}SnSnAr^{Dipp} (**20**), and Ar^{Tripp} to form Ar^{Dipp}PbPbAr^{Dipp} (**21**).³⁹ Upon descending Group 14 *trans*-bending in the alkyne analogues becomes more pronounced and the multiple-bond character decreases (Figure 1.3). The disilyne (**18**) deviates from linearity with a R–Si–Si bond angle of 137.44(4)° and a Si–Si bond length 2.0622(9) Å,³⁸ which is appreciably shorter than observed bond lengths in dislenes (2.14–2.25 Å).⁴⁰ For the digermynes (**19**) and distannynes (**20**) the *trans*-bending becomes more pronounced and the multiple-bond character decreases with bond lengths closer to measured double-bonds. The diplumbylene Ar^{Tripp}PbPbAr^{Tripp} (**21**) exhibits a C–Pb–Pb angle of 94.26(4)° and a long Pb–Pb bond length of 3.1881(1) Å, consistent with a Pb–Pb single bond and high p-character in the Pb–Pb and Pb–C linkages.^{39a,40}

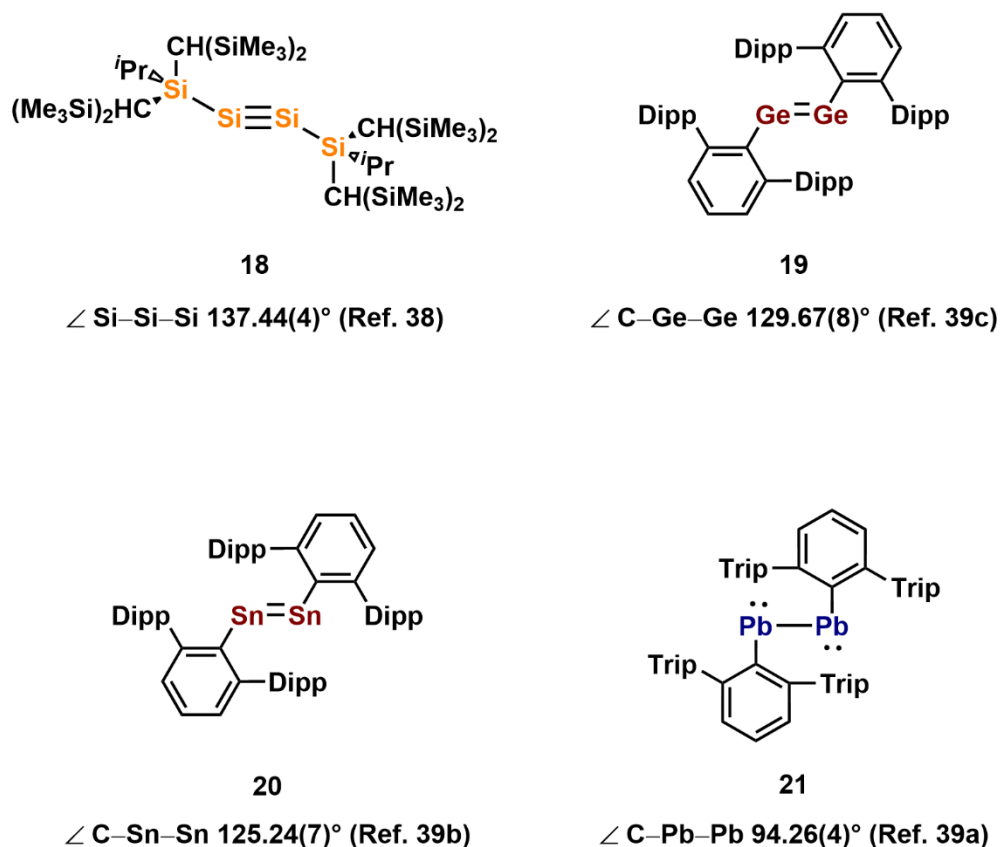


Figure 1.3. The heavy Group 14 alkyne analogues **18–21** with their respective L–E–E bond angles (L = ligand; E = Si–Pb) illustrating a reduction in the multiple bond character descending the Group 14.

While Lappert's tetrelenes $\{(\text{Me}_3\text{Si})_2\text{HC}\}_2\text{E}$: (E = Ge–Pb) dimerize in the solid state, the plumbylene $\{(\text{Me}_3\text{Si})_2\text{HC}\}_2\text{Pb}$ ·, has a $\text{Pb}\cdots\text{Pb}$ contact of 4.13 Å in the solid state,⁴¹ that is significantly longer than a normal Pb–Pb single bond (*ca.*, 2.9 Å).⁴⁰ The dimerization of tetrelenes (R_2E ·) can be prevented by the incorporation of π -donating and/or σ -withdrawing groups (*thermodynamic/electronic* stabilization) in conjunction with sterically-demanding substituents (*kinetic* stabilization).⁴² Thermodynamic/electronic stabilization involves the use of π -donating and σ -withdrawing groups to raise the LUMO (empty *p*-orbital) and HOMO (lone pair) energy gap of the tetrelene. For example, Lappert and coworkers reported a

tetrelene series stabilized by *bis*-amido substituents ($\{(\text{Me}_3\text{Si})_2\text{N}\}_2\text{E}$; E = Ge–Pb) which persist as monomers in solution and the solid state.⁴³ Using the germylene $\{(\text{Me}_3\text{Si})_2\text{N}\}_2\text{Ge}$: as an example, the LUMO (a non-bonding empty *p*-orbital) of the Ge center is raised in energy, by donation of electron density of the π -symmetry lone pairs from the flanking nitrogen atoms. Additionally, the energy of HOMO, a non-bonding lone pair, is lowered due to the σ -withdrawing character of the more electronegative character of the flanking nitrogen centers (Figure 1.4).

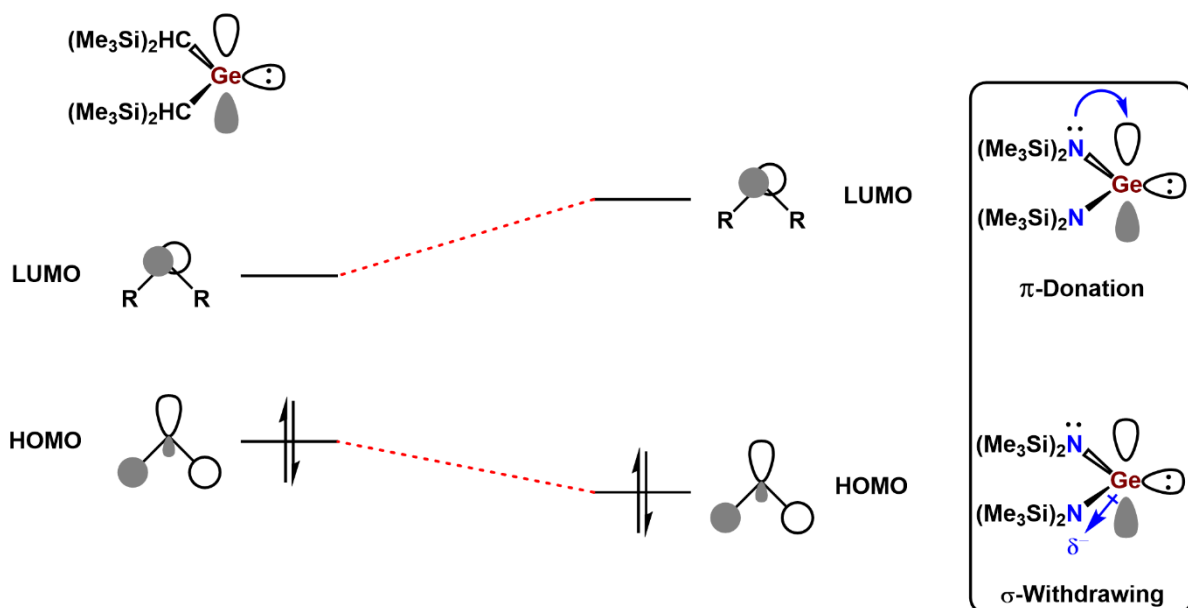
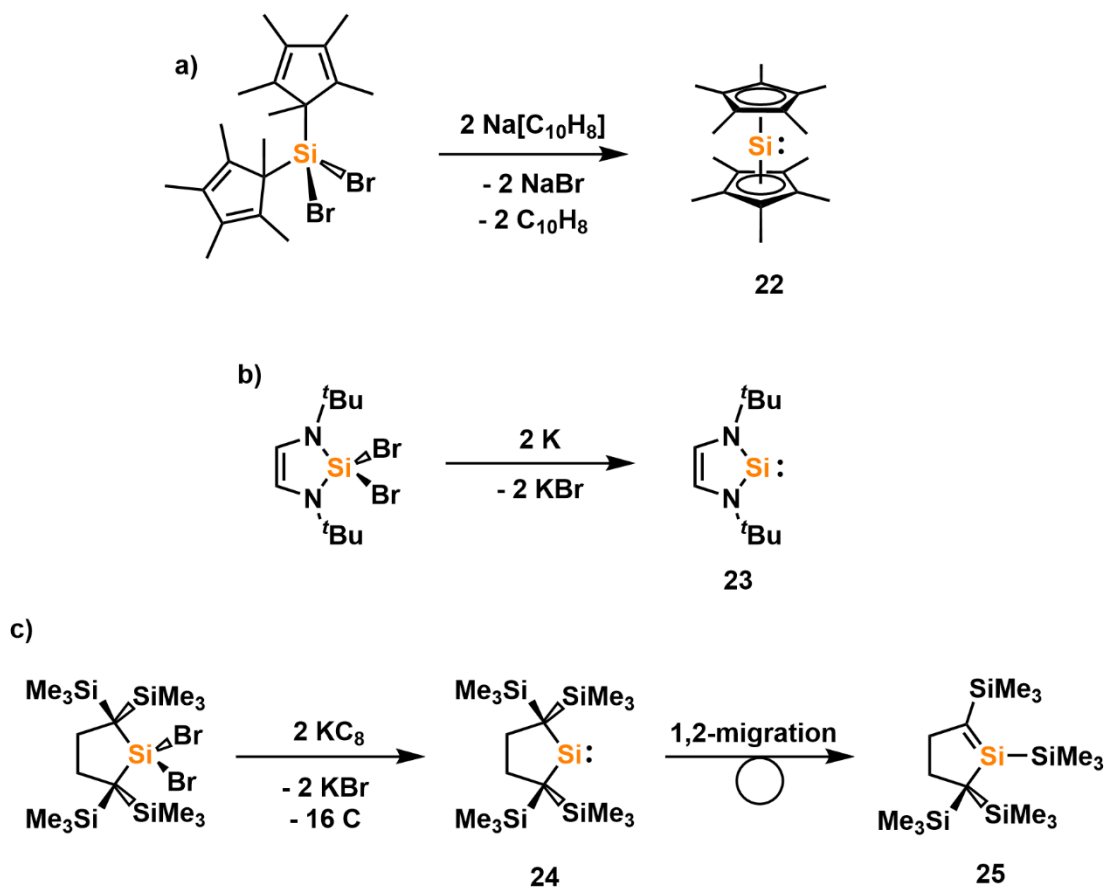


Figure 1.4. Frontier molecular orbitals (FMOs) of $\{(\text{Me}_3\text{Si})_2\text{N}\}_2\text{Ge}$: illustrating σ -withdrawal and π -donation by flanking nitrogen atoms.

Of relevance to this Thesis, select examples of silylenes ($\text{R}_2\text{Si}:$) in which the silylenes are stabilized by both kinetic and/or electron-strategies are shown in Scheme 1.7. Jutzi and coworkers isolated the first stable acyclic diorganosilylene $\text{Cp}^*_2\text{Si}:$ (**22**) by reduction of $\text{Cp}^*_2\text{SiCl}_2$ with $\text{Na}[\text{C}_{10}\text{H}_8]$ (Scheme 1.7a). The Si(II) center in $\text{Cp}^*_2\text{Si}:$ (**22**) is stabilized by the demanding Cp^* moiety ($\text{Cp}^* = \eta^5\text{-C}_5\text{Me}_5$), which coordinatively saturates the silicon center.⁴⁴

Denk, West and coworkers reported the heterocyclic silylene $(\text{HCN}^t\text{Bu})_2\text{Si}$: (**23**) wherein the Si(II) center is electronically-stabilized by the σ -withdrawing and π -donating nitrogen atoms within the ring (Scheme 1.7b).⁴⁵ A cyclic dialkylsilylene $(\text{H}_2\text{CC}(\text{SiMe}_3)_2)_2\text{Si}$: (**24**) was described by Kira and coworkers where the flanking SiMe_3 groups provide effective steric protection preventing dimerization. $(\text{H}_2\text{CC}(\text{SiMe}_3)_2)_2\text{Si}$: (**24**) decomposes in solution at room temperature *via* 1,2-migration of a neighboring trimethylsilyl group (SiMe_3) to give the corresponding silaethene $(\text{H}_2\text{C})_2\text{C}(\text{SiMe}_3)_2(\text{Me}_3\text{Si})\text{C}=\text{SiSiMe}_3$ (**25**) (Scheme 1.7c).⁴⁶

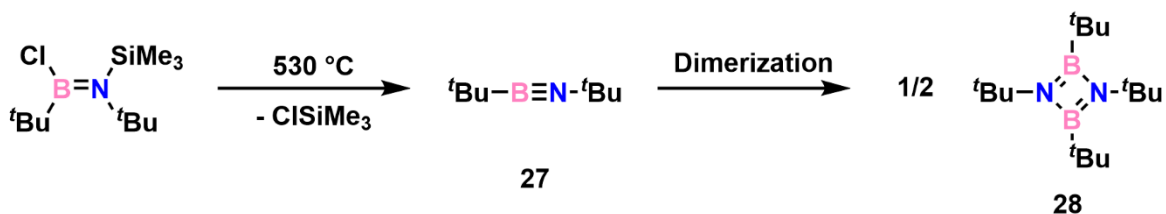


Scheme 1.7. a) Synthesis of Cp^*_2Si : (**22**); b) Preparation of $(\text{HCN}^t\text{Bu})_2\text{Si}$: (**23**); c) Synthesis of $(\text{H}_2\text{CC}(\text{SiMe}_3)_2)_2\text{Si}$: (**24**) and subsequent ligand decomposition *via* 1,2-migration $(\text{H}_2\text{C})_2\text{C}(\text{SiMe}_3)_2(\text{Me}_3\text{Si})\text{C}=\text{SiSiMe}_3$ (**25**).

1.2.3 Kinetic Stabilization of Group 13–Nitrogen Multiply-Bonded Species

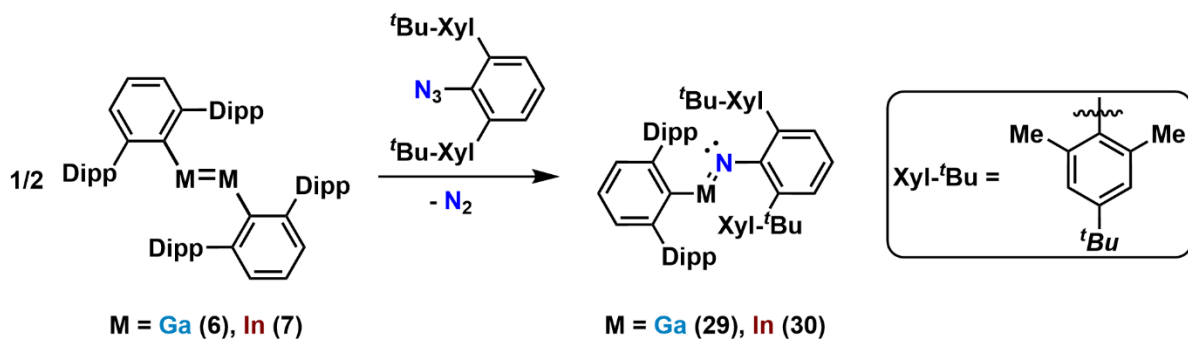
Unsaturated Group 13-nitrogen (Group 13 = B–In) containing species with π -multiple bonding have been of interest for many decades due to such species being isoelectronic to unsaturated organic fragments, such as alkenes and alkynes.⁴⁷ The difference in electronegativity between the Group 13 elements and the nitrogen atom (*e.g.*, B 2.01 *versus* N 3.07)⁴⁸ leads to substantial polarization towards nitrogen. This polarization imparts a high degree of reactivity in Group 13–amides (R_2ENR_2) and Group 13–imides ($RENR$) which both can undergo cyclization and/or oligomerization reactions readily. For example, early work on iminoalanes by Cesari and coworkers found that the iminoalane, $HAlN^rPr$, could form the hexamer $[HAlN^rPr]_6$ or the octamer $[HAlN^rPr]_8$ with alternating nitrogen and aluminum vertices.⁴⁹

Oligomerization of unsaturated Group 13-nitrogen species can be prevented by the incorporation of sterically-demanding substituents on both the nitrogen and Group 13 centers (Group 13 = B–In). Paetzold and coworkers employed such a strategy to isolate the first stable iminoborane. Heating the aminoborane precursor $Cl(tBu)B=N(tBu)SiMe_3$ to 530 °C led to $ClSiMe_3$ elimination to afford the linear iminoborane $tBuB\equiv N^tBu$ (**26**) with a B–N bond length of 1.258(4) Å. It should be noted that $tBuB\equiv N^tBu$ (**27**) dimerizes slowly to give $[tBuBN^tBu]_2$ (**28**) with a substantial increase in the *avg.* B–N bond length to 1.491(6) Å, indicating a decrease in multiple-bond character (Scheme 1.8).⁵⁰



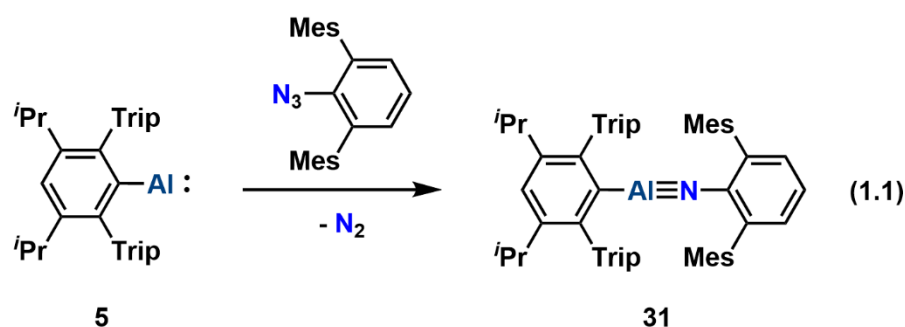
Scheme 1.8. Synthesis of the iminoborane $\text{tBuB}\equiv\text{NtBu}$ (**26**) and its subsequent dimerization to the aminoborane $[\text{tBuBNtBu}]_2$ (**28**).

The heavier Group 13-imide analogues (Group 13 = Ga, In) supported by bulky *meta*-terphenyl ligands were reported by Power and coworkers. Combining the dimetallenes $\text{Ar}^{\text{Dipp}}\text{MMAr}^{\text{Dipp}}$ ($\text{M} = \text{Ga}$ (**6**), In (**7**)) with the bulky terphenyl azide $\text{Ar}^{\text{Xyl-tBu}}\text{N}_3$ ($\text{Ar}^{\text{Xyl-tBu}} = 2,6\text{-}(\text{Xyl-4-}^t\text{Bu})_2\text{C}_6\text{H}_3$; $\text{Xyl} = 2,6\text{-Me}_2\text{C}_6\text{H}_2$) to give the corresponding neutral Group 13-imides $\text{Ar}^{\text{Dipp}}\text{MNAr}^{\text{Xyl-tBu}}$ ($\text{M} = \text{Ga}$ (**29**), In (**30**)) and loss of nitrogen gas (Scheme 1.9).⁵¹ The molecular structures of $\text{Ar}^{\text{Dipp}}\text{MNAr}^{\text{Xyl-tBu}}$ ($\text{M} = \text{Ga}$ (**29**), In (**30**)) display *trans*-bending in the C–M–N–C core with a C–N–M angle of $141.7(3)^\circ$ (**29**) and $134.9(2)^\circ$ (**30**) which deviates from the linear arrangement observed in $\text{tBuB}\equiv\text{NtBu}$ (**28**).⁵⁰



Scheme 1.9. Synthesis of $\text{Ar}^{\text{Dipp}}\text{MNAr}^{\text{Xyl-tBu}}$ ($\text{M} = \text{Ga}$ (**29**), In (**30**)).

As recently as 2021, Power and coworkers were able to isolate a stable monomeric aluminum-imide, also called an iminoalane.⁵² By combining monomeric $\text{Ar}^{i\text{Pr}8}\text{Al}:$ (**5**) with the terphenyl azide $\text{Ar}^{\text{Mes}}\text{N}_3$ ($\text{Ar}^{\text{Mes}} = 2,6\text{-Mes}_2\text{C}_6\text{H}_3$), in a similar fashion to the preparation of their previous Group 13-imides (*vide supra*), liberation of N_2 and formation of $\text{Ar}^{i\text{Pr}8}\text{AlNAr}^{\text{Mes}}$ (**31**) transpired (Equation 1.1).⁵² The molecular structure of $\text{Ar}^{i\text{Pr}8}\text{AlNAr}^{\text{Mes}}$ (**31**) shows a linear C–Al–N–C core and a C–N–Al bond angle of 180° suggesting significant nitrogen lone pair to Al π -donor interaction and the presence of a formal Al–N triple bond with a bond length of 1.625(4) Å.



1.3 *N*-Heterocyclic Carbenes

Carbenes are molecules that contain a dicoordinate carbon (R_2C) with six valence electrons. The non-bonding electrons of the carbene may exist in a triplet state, where the electrons are unpaired, or they can be paired and occupy the formal sp^2 orbital of the carbene carbon atom. While the simplest carbene, H_2C , exists in a triplet ground state, a singlet ground state can be induced by incorporating σ -withdrawing and/or π -donating fragments, typically *N*-aryl/alkyl substituents, which provide steric protection while stabilizing the empty *p*-orbital through π -donation.⁵³ Arduengo and coworkers employed such a strategy in the isolation of the first stable *N*-heterocyclic carbene (NHC) in IAd (IAd = $(\text{HCNAd})_2\text{C}:$; Ad = adamantyl),

prepared by deprotonation of the imidazolium salt [IAdH]Cl.⁵⁴ While IAd is sensitive towards air and moisture, as are most NHCs, it is thermally stable and can be stored indefinitely under an inert atmosphere of N₂ giving NHCs the moniker “botteable carbenes.” Since 1991, NHCs have become the most popular carbon-based ligands in main group element chemistry owing to their stability, structural diversity, and tuneability of the σ -donating/ π -accepting ability of groups bound to the carbene center.⁵⁵

1.3.1 Properties of *N*-Heterocyclic Carbenes and Coordination Chemistry

Highlights

N-Heterocyclic carbenes (NHCs) are strong σ -donating ligands and, for many years, were considered to have little to no π -accepting ability. In 2001, Danopoulos and coworkers found that NHCs can indeed act as weak π -accepting ligands when they prepared an NHC•CuBr complex (NHC = [(H₂C)₂(NDipp)(NPyridyl)]C:; Pyridyl = 2-pyridyl) with a short NHC–Cu bond of 1.880(6) Å, somewhat shorter than previously reported carbon-copper bond lengths [1.90–1.96 Å].⁵⁶ The π -accepting character of carbenes can be increased by the replacement of one of the flanking amino substituents with a quaternary carbon. Bertrand and coworkers demonstrated this concept when they prepared the first cyclic(alkyl)amino carbenes (CAACs) in 2005.⁵⁷ The removal of one of the electronegative atoms not only increases the π -accepting character of the carbene center but also enhances σ -donating ability of the carbene by making it more electron rich (Figure 1.5).

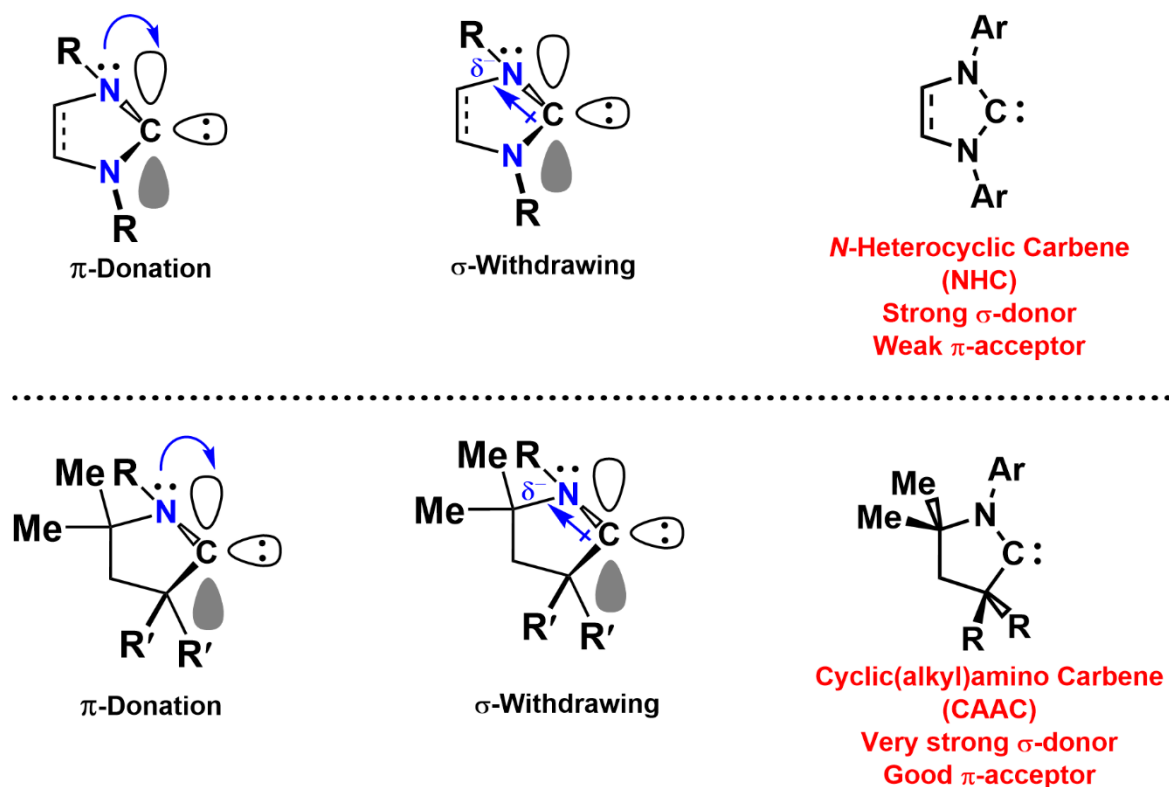


Figure 1.5. Diagram depicting the σ -donating and π -accepting interactions for *N*-heterocyclic carbenes (NHCs) and cyclic(alkyl)amino carbenes (CAAC).

Another important aspect of NHCs is their structural tuneability which has led to a vast catalogue of different carbenes typically, but not always, by altering the group situated on the flanking nitrogen atoms. These alterations can also influence the steric parameters of the carbene.⁵⁸ In recent years, the concept of percent buried volume ($\%V_{\text{Bur}}$) has been developed by Nolan and others as a method of quantifying the steric properties of NHCs.^{58,59} The percent buried volume ($\%V_{\text{Bur}}$) is defined as the percent of the total volume of a sphere that is occupied by a ligand.^{59a} This can be determined by having a sphere of a set radius, typically of 3.5 Å, which represents the potential coordination sphere of a metal, with a metal atom placed at the center of said sphere (*e.g.*, Au(I)). The ligand of choice is then placed coordinating to the metal center at a set distance of 2.0 Å or 2.28 Å (Figure 1.6). From these parameters the spatial

occupation of the ligand (*i.e.*, %V_{Bur}) is determined by the software SambVca (Salerno molecular buried volume calculation).^{59a} As an example of the variability in steric parameters, the most commonly used carbene in main group element chemistry, IPr (IPr = (HCNDipp)₂C:), has a %V_{Bur} of 45.4 % when the NHC-Au distance is set to 2.0 Å, while ImⁱPr₂ (ImⁱPr₂ = (HCNⁱPr₂)₂C:) has a %V_{Bur} of 27.5 % when the same parameters are used.⁵⁸ The concept of %V_{Bur} is of particular interest and relevance for Chapter 6.

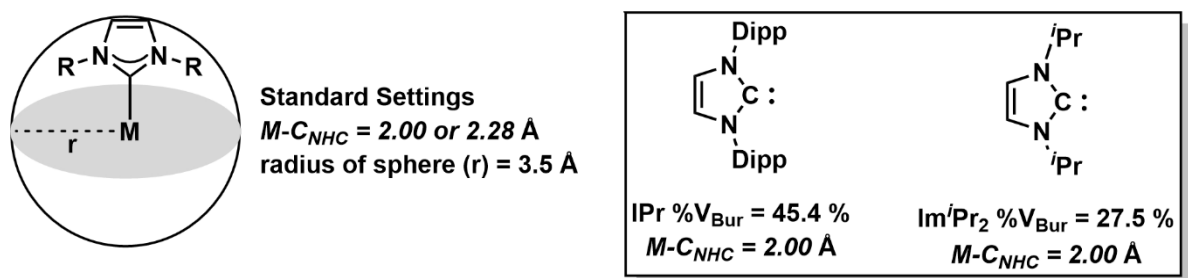
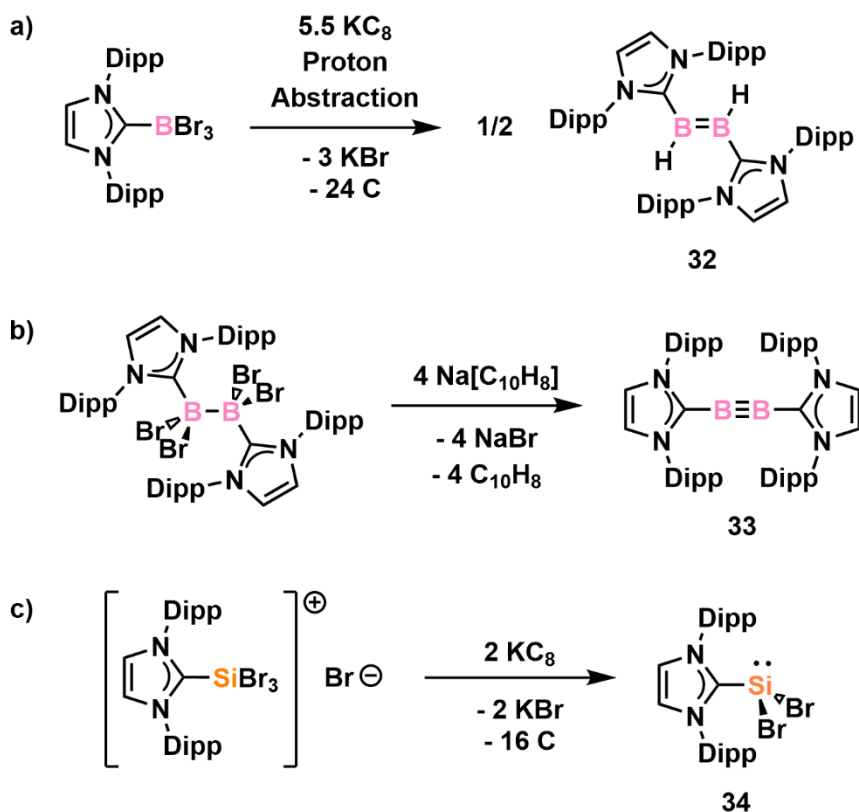


Figure 1.6. Graphical illustration of percent buried volume (%V_{Bur}) and the calculated %V_{Bur} for IPr and ImⁱPr₂ when the NHC-M distance is set to 2.0 Å. Adapted from Figure 2 in Ref. 58.

Select examples of NHC-main group element complexes relevant to this Thesis are shown in Scheme 1.10. Robinson and coworkers, were able to isolate the neutral NHC-stabilized IPr•HB=BH•IPr (**32**), the first example of a stable diborene (Scheme 1.10a) upon reduction of IPr•BBr₃ with 5.5 equivalents of KC₈ and proton abstraction from the solvent.⁶⁰ This was taken a step further in 2012 when Braunschweig and coworkers reported the isolation of a stable boron-boron triple bond, diboryne, by reduction of the NHC-diborane adduct IPr•Br₂B–BBR₂•IPr with four equivalents of Na[C₁₀H₈] to give IPr•B≡B•IPr (**33**) (Scheme 1.10b).⁶¹



Scheme 1.10. a) Synthesis the NHC-stabilized diborene $\text{IPr}\cdot\text{HB}=\text{BH}\cdot\text{IPr}$ (**32**); b) Preparation of an NHC-stabilized boron-boron triple bond $\text{IPr}\cdot\text{B}\equiv\text{B}\cdot\text{IPr}$ (**33**); c) Synthesis of a NHC-stabilized silylene $\text{IPr}\cdot\text{SiBr}_2$ (**34**).

Silylenes ($\text{R}_2\text{Si}:$) can also be stabilized by NHCs as demonstrated by Filippou and coworkers when they were able to reduce $[\text{IPr}\cdot\text{SiBr}_3]\text{Br}$ with two equivalents of KC_8 to give the $\text{IPr}\cdot\text{SiBr}_2$ (**34**) (Scheme 1.10c).⁶² In these examples, the strong electron-donating ability of the NHC IPr occupies the once empty p -orbitals of the boron and silicon centers while also providing sufficient steric protection to prevent oligomerization.

1.4 *N*-Heterocyclic Olefins: An Unassuming Beginning

N-Heterocyclic olefins (NHOs), occasionally referred to as deoxy-Breslow intermediates, are a class of compounds that contain an alkylidene (CR₂) fragment tethered to a heterocyclic carbene framework (Figure 1.7). This structure leads to substantial polarization of the exocyclic C=C π bond causing an increase in the nucleophilicity of the exocyclic ylidic carbon atom,⁶³ reminiscent of methylene phosphoranes, such as Ph₃P=CH₂,⁶⁴ and the Breslow intermediates formed during *N*-heterocyclic carbene (NHC)-catalyzed conjugated addition reactions (Figure 1.8).⁶⁵ While the term NHO was first introduced in 2011,⁶⁶ the first example of an NHO appeared in the literature as early as 1961, 30 years before the isolation of NHCs by Arduengo and coworkers,⁵⁴ when Böhme and Soldan reported the preparation of SImMe₂CH(Ph) (SImMe₂ = (H₂CNMe)₂C) during their studies on derivatives of triaminomethane.⁶⁷ The next example of an NHO appeared in 1979 and was the first example of an NHO-metal complex, [(SImMe₂CH₂)PtCl₂]₂, prepared by Kaska and coworkers.⁶⁸ Reports on NHOs would lay dormant again for almost a decade until Heuschmann reported a general synthetic route to over 20 functionalized NHOs.⁶⁹ Kuhn and coworkers would build upon this work with important trailing blazing investigations leading to a general synthetic route to the sterically unhindered NHO ImMe₄CH₂ (ImMe₄ = (MeCNMe)₂C) and subsequent 1:1 adducts with BX₃ (X = H and F) and M(CO)₅ (M = Mo and W).⁷⁰ Reports on NHOs would once again fade into obscurity until 2010 with a report from Beller and coworkers, wherein they described the *in situ* generation of sterically-demanding NHOs (*e.g.*, IPrCH₂) and their subsequent transformation into cationic phosphine ligands for use in Pd-catalyzed bond forming reactions.⁷¹ This would precipitate a surge in interest in the chemistry of NHOs, initially by the Rivard group^{63,72} and then others,⁷³ as ligands in the stabilization of low-oxidation state main group species and as organocatalysts in a variety of transformations.⁷⁴

The emergence of NHOs from unassuming and scattered reports over the better part of 50 years belies their utility, and their application in the stabilization of reactive fragments remains unabated today.

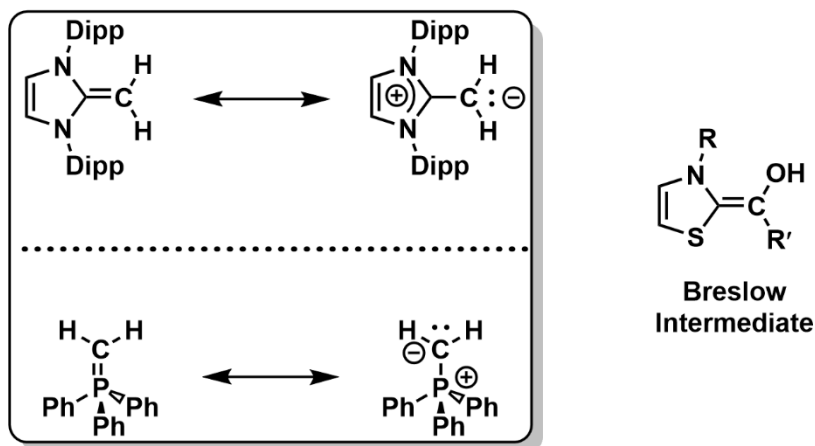


Figure 1.7. Resonance forms of *N*-heterocyclic olefins (NHOs) and the methylene phosphorane Ph_3CH_2 , and the general structure of a Breslow intermediate.

1.4.1 Synthesis of *N*-Heterocyclic Olefins

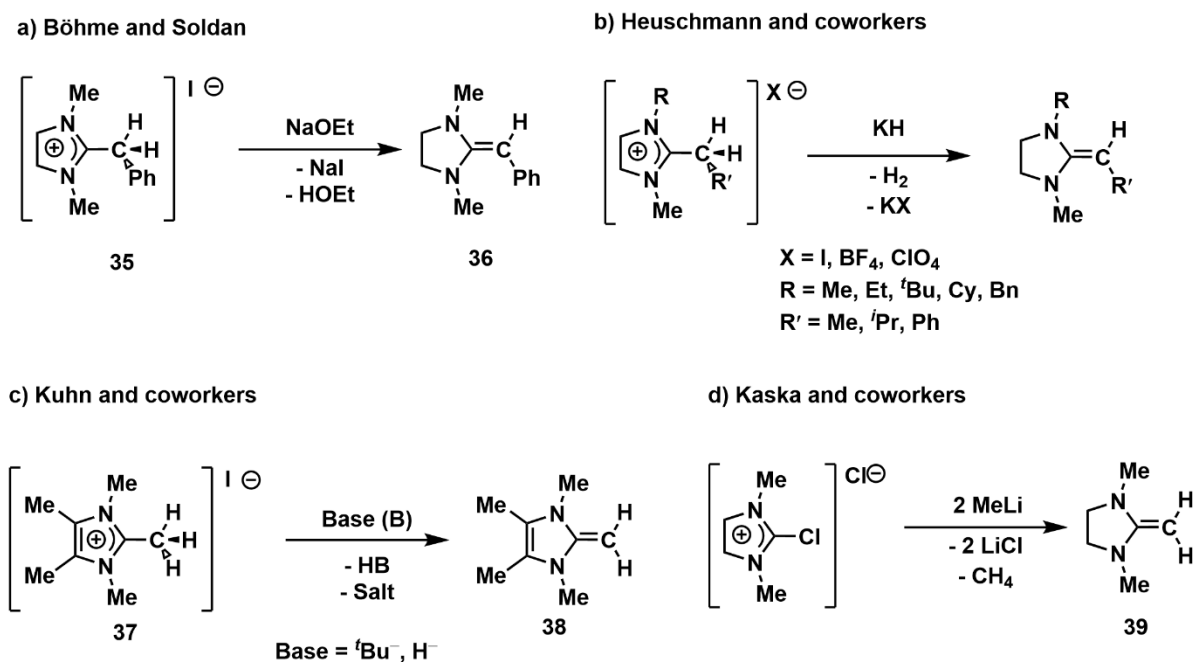
There are multiple established routes to access NHOs with slightly different methods being employed for sterically unhindered NHOs and more sterically demanding aryl-based NHOs, with the key step in all cases being the selective deprotonation of an exocyclic alkyl group. Since sterically unhindered NHOs appeared in the literature the earliest, methods of their preparation will be discussed first.

The first route to an NHO established by Böhme and Soldan, involved deprotonation of the imidazolium salt $[\text{SImMe}_2\text{CH}_2\text{Ph}]\text{I}$ (**35**) with NaOEt (Scheme 1.11a) to give $\text{SImMe}_2\text{CHPh}$ (**36**).⁶⁷ Heuschmann and coworkers reported a similar method of preparing a series of structurally diverse NHOs by simply combining the corresponding imidazolium salts with sodium hydride (NaH) (Scheme 1.11b).⁶⁹ Kuhn and coworkers' method involves the

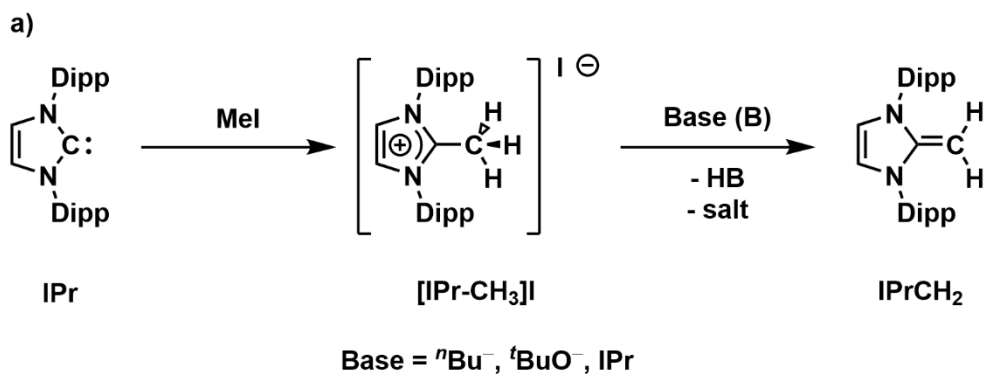
deprotonation of the imidazolium salt [ImMe₄CH₃]I (**37**) with ^tBuLi followed by vacuum thermolysis of the NHO lithium iodide adduct to afford ImMe₄CH₂ (**38**).^{70a} This method was later improved upon by using potassium hydride (KH) as the base, allowing for easy separation of **38** from the by-products H₂ and potassium iodide (KI) (Scheme 1.11c).^{70c} Kaska and coworkers employed an interesting synthetic method for preparing NHOs which involved combining the commercially available 2-chloro-1,3-dimethylimidazolium chloride [SImMe₂Cl]Cl with two equivalents of methyl lithium (MeLi) to afford SImMe₂CH₂ (**39**) (Scheme 1.10d). This method presumably proceeds through the formation of the imidazolium salt, [SImMe₂CH₃]Cl, followed by deprotonation of the exocyclic methyl group with the second equivalent of MeLi resulting in loss of methane (CH₄) and LiCl as by-products.⁶⁸ A key feature in the preparation of these sterically unhindered NHOs, with the exception of the method employed by Kaska and coworkers, is the avoidance of the *in situ* generation of the corresponding NHC, but rather that the methyl group is pre-installed.

For more sterically demanding NHOs, which contain bulky aryl substituents at nitrogen, there are three protocols that can be employed. An important step in each of these protocols is the generation of the parent NHC, which can be isolated or generated *in situ*, and subsequent alkylation of the NHC. The most general method, for example, in the synthesis of IPrCH₂ (IPr = (H₂CNDipp)₂C; Dipp = 2,6-ⁱPr₂C₆H₃), involves the addition of methyl iodide (MeI) to the parent carbene IPr resulting in the formation of the imidazolium salt [IPr-CH₃]I, which is subsequently deprotonated with a strong base (*e.g.*, ⁿBuLi) (Scheme 1.12a).^{63,75} A variation of this synthesis involves the use of a second equivalent of the carbene IPr as the base, with the formation of [IPrH]I as the by-product.⁶⁶ Robinson and coworkers reported a novel synthetic route to IPrCH₂ wherein they form initially the anionic *N*-heterocyclic carbene

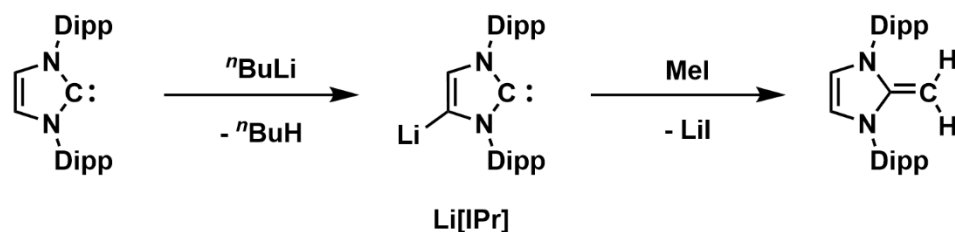
Li[IPr] by lithiation of the alkene backbone. Subsequent addition of MeI to a slurry of Li[IPr] afforded IPrCH₂ (Scheme 1.12b).⁷⁶ However, there are a few limitations with the above methods. In the cases where ⁿBuLi is used in THF, the by-product Li(THF)_xI can be difficult to separate from the desired NHO. Similarly, if IPr is used as the base, separation of the NHO from excess or unreacted IPr can be problematic due to the similar solubilities of the two species. The Rivard group developed an alternative synthetic route toward IPrCH₂ that is both high yielding (*ca.*, 80 %) and applicable on a large scale (*ca.*, 30 g); this method utilizes ClCH₂SiMe₃ as the methylene source and when combined with IPr the volatile by-product ClSiMe₃ is removed easily from IPrCH₂ (Scheme 1.12c).⁷⁵



Scheme 1.11. Early reports on the synthesis of sterically unencumbered NHOs.



b) Robinson and coworkers



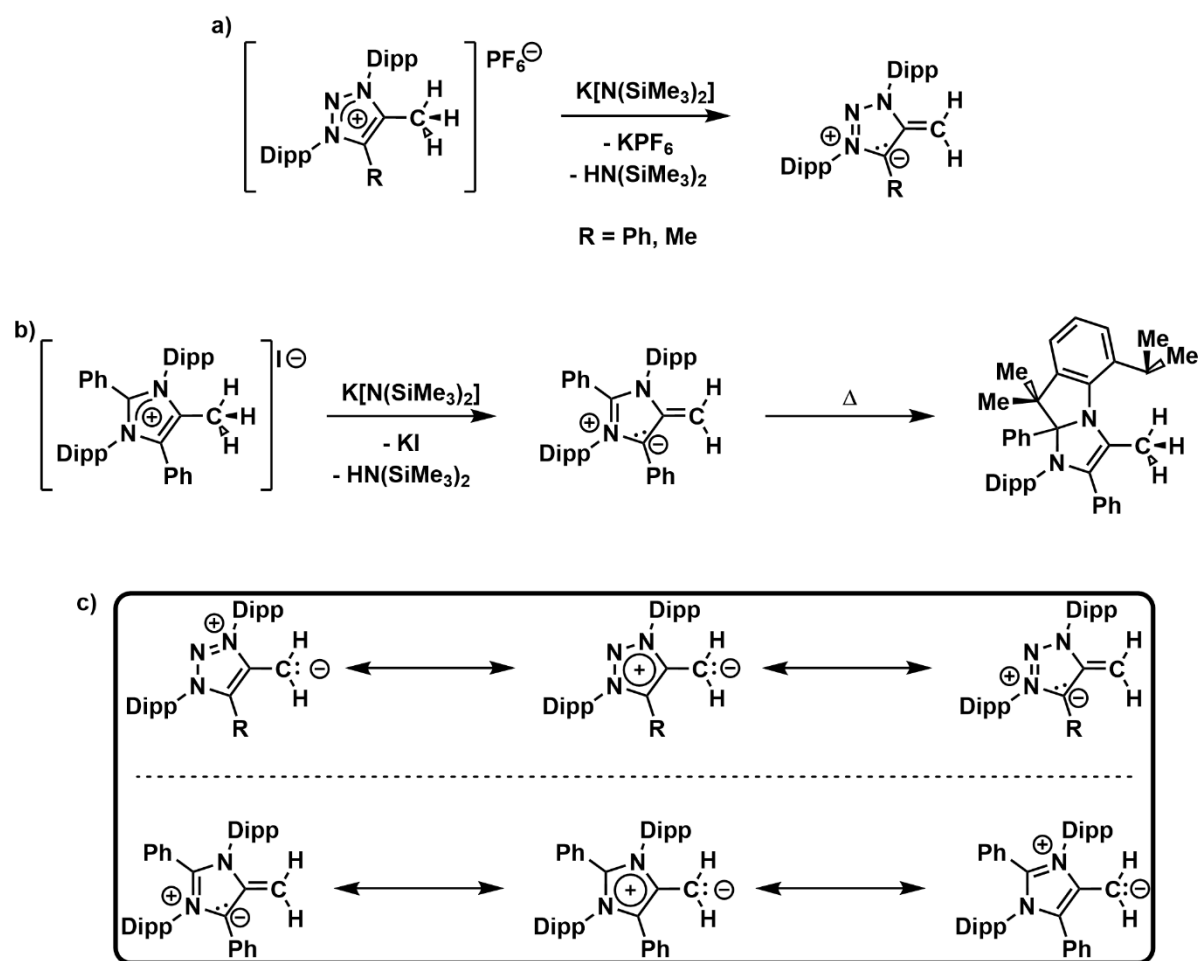
c) Rivard and coworkers



Scheme 1.12. General synthetic routes to NHOs. Adapted from Scheme 1 in Ref. 63.

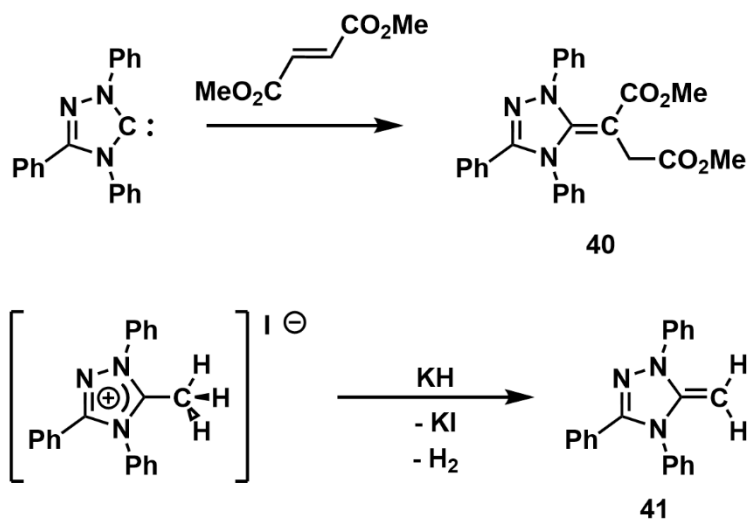
In 2020 Hansmann and coworkers reported the efficient and straightforward synthesis of mesoionic NHOs (mNHOs),⁷⁷ which are formally derived from 1H-1,2,3-triazoles. The synthesis involves a [3+2] cycloaddition of 1,3-diaza-2-azoniaallene salts with the appropriate alkenes, followed by deprotonation of the resulting triazolium salt with K[N(SiMe₃)₂] to give the desired mNHOs (Scheme 1.13a). Hansmann and coworkers in the same report also described the synthesis of a mNHO, Ph(NDipp)₂(Ph)CCH₂, derived from an abnormal NHC

by deprotonation of the imidazolium salt with $\text{K}[\text{N}(\text{SiMe}_3)_2]$. This mNHO, derived from an abnormal NHC, decomposed over the course of a roughly five to six days in solution at room temperature *via* C-H activation of the flanking Dipp group, and subsequent intramolecular attack on to the C2 position of the imidazole ring (Scheme 1.13b). In contrast to classical NHOs, which are typically pale-yellow or colorless, mNHOs are deeply colored, likely due to charge transfer from the exocyclic olefinic moiety to the cationic heterocyclic ring system.⁷⁷



Scheme 1.13. Synthesis of mesoionic NHOs (mNHOs) derived from: a) triazoles, b) abnormal carbenes as described by Hansmann, and c) the salient canonical resonance forms of mNHOs.

It should be noted that examples of triazole NHOs, derived from 1,2,4-triazoles, are known in the literature. Early pioneering work in this area was conducted by Enders and coworkers, wherein they combined the NHC $(\text{PhCN}(\text{NPh})_2)\text{C}:$, commonly referred to as Enders' carbene, with ethylfumarate to give the functionalized triazole NHO $(\text{PhCN}(\text{NPh})_2)\text{CCH}(\text{CHMeCO}_2\text{Me})$ (**40**).^{78,79} More recently, the "free" triazole NHO, $(\text{PhCN}(\text{NPh})_2)\text{CCH}_2$ (**41**), also derived from an Enders' carbene, was reported and prepared by deprotonation of the triazolium salt with KH (Scheme 1.14).⁸⁰



Scheme 1.14. Synthesis of triazole-derived NHOs.

1.4.2 Properties of *N*-Heterocyclic Olefins

The donor properties of NHOs are generally evaluated in relation to their parent NHCs and other related ligands such as phosphines.⁶³ The Tolman electronic parameters (TEPs) of ligands, which is a measure of the electron-donating or -withdrawing ability of said ligand, is generally determined by measuring the average (*avg.*) IR $\nu(\text{CO})$ stretching frequencies in transition metal carbonyl stretches (*e.g.*, $[\text{L}\cdot\text{Rh}(\text{CO})_2\text{Cl}]$, L = ligand). Specifically, a stronger

electron-donating ligand should weaken the C–O π -bonding a result of a corresponding increase in Rh(d)–CO(π^*) backbonding, which results in a lower average $\nu(\text{CO})$ stretching frequency in the IR spectrum and gives a lower TEP.⁸¹

In 2016, the Rivard group determined the *avg.* $\nu(\text{CO})$ stretching frequencies for the NHO-rhodium complexes [IPrCH₂•Rh(CO)₂Cl] (**43**) (2011 cm⁻¹; Nujol) and [IPr•Rh(CO)₂Cl] (**44**) (2045 cm⁻¹; Nujol), which correspond to TEP values of 2029 cm⁻¹ and 2045 cm⁻¹, respectively, indicating that NHOs are stronger electron donors than NHCs.^{75,82} More recently, Hansmann and coworkers determined the *avg.* $\nu(\text{CO})$ stretching frequencies and TEPs of the related mNHO–rhodium complexes [(N(NDipp)₂(CPh)CH₂•Rh(CO)₂Cl] (**45**), [(N(Dipp)₂(CMe)CH₂•Rh(CO)₂Cl] (**46**), and [N(NⁱPr)₂(CPh)CCH₂•Rh(CO)₂Cl] (**47**) (Figure 1.9).^{77,83} When compared to classical NHOs, the TEPs of mNHOs are even lower (*e.g.*, **43** TEP = 2031 cm⁻¹ in CH₂Cl₂ *versus* **45** TEP = 2030 cm⁻¹ in CH₂Cl₂), indicating that mNHOs are even stronger electron donors than NHOs and NHCs. When Rivard and coworkers combined 1:1 mixture of IPr and IPrCH₂ with [Rh(CO)₂(μ -Cl)]₂, as method to probe the relative Lewis basicity of each ligand, it was found that the NHC complex [IPr•Rh(CO)₂Cl] (**44**) formed exclusively.⁷⁵ Similar experiments by Hansmann and coworkers, found that mNHOs displaced IPrCH₂ from the [IPrCH₂•Rh(CO)₂Cl] (**43**) to give the corresponding [mNHO•Rh(CO)₂Cl] complexes in line with mNHOs being stronger Lewis bases than NHOs (Figure 1.9). Notably, Hansmann and coworkers found that addition IPr to the mNHO–rhodium complexes gave exclusively [IPr•Rh(CO)₂Cl] (**44**). It can be rationalized that NHCs act as weak π -acceptors allowing for Rh(d)–NHC(p/π^*) backbonding, whereas NHOs and mNHOs, while strong σ -donors, are poor π -acceptors.^{63,75,77,83} An important aspect of these studies is that while TEP can be used to determine potential electron donor strength, one must

wary when comparing ligand systems with different π -accepting capabilities, especially as a measure of Lewis basicity.

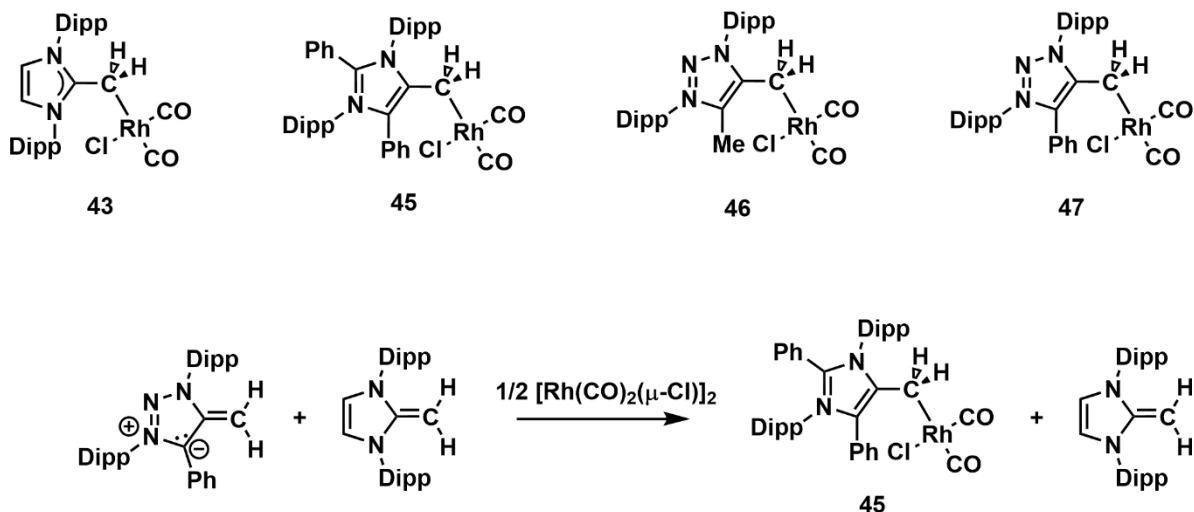


Figure 1.8. NHO and mNHO Rh-complexes (top) and competitive binding experiment between NHOs and mNHOs (bottom).

Another key difference between NHOs and their parent NHCs is a difference in their respective percent buried volumes ($\%V_{\text{Bur}}$). Due to the alkylidene (CR_2) fragment being tethered to a heterocyclic carbene framework, one can intuitively assume that the $\%V_{\text{Bur}}$ of NHOs should be lower than that of the parent NHCs. Gandon and coworkers determined that the $\%V_{\text{Bur}}$ of the NHO ImMe_2CH_2 was 18.7 %, while the parent NHC ImMe_2 had a $\%V_{\text{Bur}}$ of 26.1%.⁸⁴ Gandon and coworkers included the hydrogen atoms in their calculations of the percent buried volumes. It should be noted that normally hydrogen atoms are omitted from the $\%V_{\text{Bur}}$ calculation.⁵⁹ As such, the percent buried volume reported by Gandon and coworkers for ImMe_2 (26.1 %) deviates slightly from the percent buried volume determined by Nolan and coworkers for ImMe_2 (26.3 %).⁵⁸

1.4.3 Neutral *N*-Heterocyclic Olefins as Ligands

Early examples of neutral NHOs acting as ligands involved coordination to transition metals. In 1979 Kaska and coworkers reported the first example of an NHO–transition metal complex wherein $\text{SiImMe}_2\text{CH}_2$ (**36**) was combined with Zeise’s dimer $[(\eta^2\text{-H}_2\text{CCH}_2)\text{PtCl}_2]_2$ to give the dimeric Pt-complex $[(\text{SiImMe}_2\text{CH}_2)\text{PtCl}_2]$ (**48**) (Figure 1.9).⁶ This complex is rather unique, not only in that it is the first example of an NHO being utilized as a ligand, but that this NHO-Pt complex exhibits both η^1 and η^2 -binding modes in the solid state. The majority of NHO-transition metal complexes bind end-on (η^1) *via* the exocyclic methylene carbon. Kuhn and coworkers prepared the metal complex $[\text{ImMe}_4\text{CH}_2 \cdot \text{M}(\text{CO})_5]$ ($\text{M} = \text{W}$ (**49**), Mo (**50**)) from the corresponding hexacarbonyls in the early 1990s (Figure 1.10).^{70a,b}

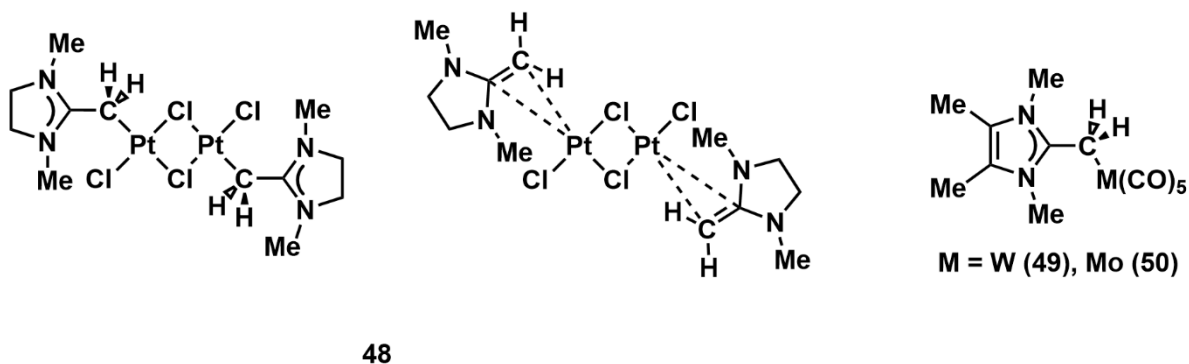


Figure 1.9. Early examples of NHO transition metal complexes.

Many of the first examples of NHOs coordinating to main group Lewis acids were described in the pioneering work of Kuhn and coworkers throughout the 1990s, wherein they reported NHO-borane adducts ($\text{ImMe}_4\text{CH}_2 \cdot \text{BX}_3$; $\text{X} = \text{H}$ (**51**), F (**52**)) and a NHO-tin complex, $\text{ImMe}_4\text{CH}_2 \cdot \text{SnCl}_2\text{Ph}_2$ (**53**).^{70c} An important extension of this work was the preparation of the NHO-stabilized GeH_2 and SnH_2 complexes $\text{IPrCH}_2 \cdot \text{EH}_2 \cdot \text{W}(\text{CO})_5$ ($\text{E} = \text{Ge}$ (**54**), Sn (**55**))⁶⁶ and

the digermene complex $\text{IPrCH}_2 \cdot \text{H}_2\text{Ge}-\text{GeH}_2 \cdot \text{W}(\text{CO})_5$ (**56**), an inorganic ethylene analogue, by the Rivard group (Figure 5.10).⁸⁵

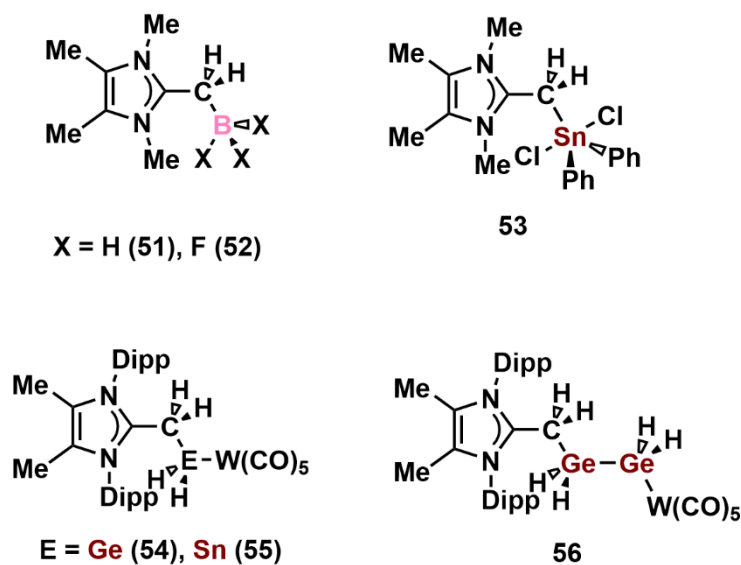
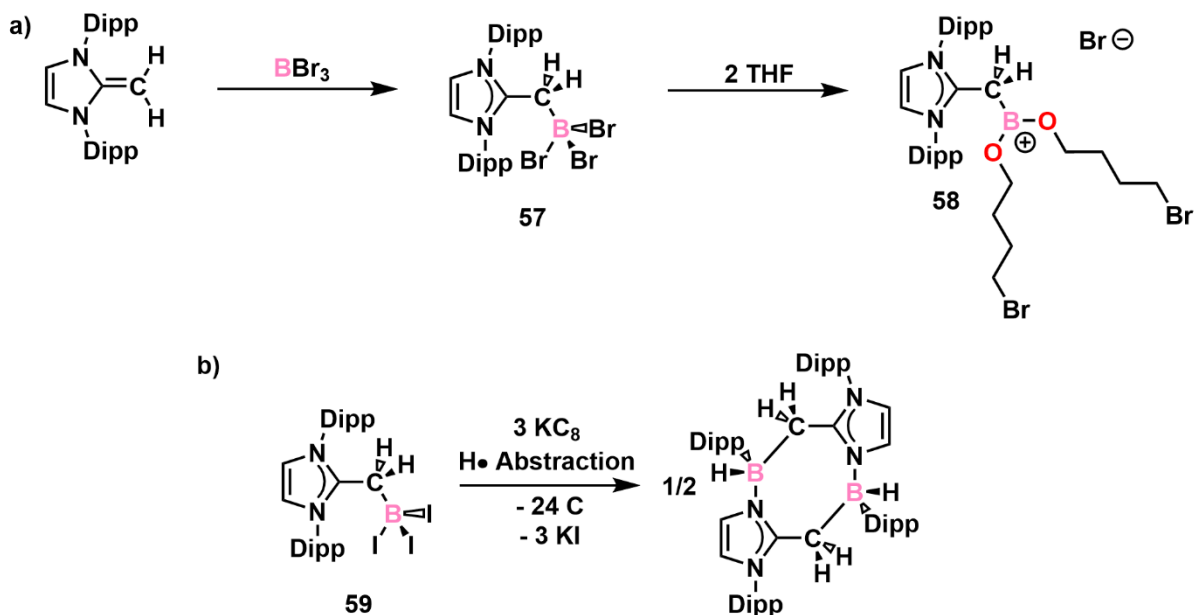


Figure 1.10. Examples of NHOs coordinating to main group halides and hydrides.

An inherent property of *N*-heterocyclic olefins is their lower % V_{Bur} (*vide supra*) owing to the CR_2 spacer between the site of coordination and the imidazolium array. Accordingly, chemistry at the site of coordination between NHCs and NHOs can differ greatly. For example, Robinson and coworkers showed that $\text{IPrCH}_2 \cdot \text{BBr}_3$ (**57**) can be prepared readily in hexanes and is stable in chlorinated solvents such as dichloromethane, but in THF rapid-ring opening is observed to yield the borenium cation $[\text{IPrCH}_2 \cdot \text{B}((\text{OC}_4\text{H}_8)\text{Br})_2]\text{Br}$ (**58**).⁸⁶ Remarkably, the corresponding NHC adduct $\text{IPr} \cdot \text{BBr}_3$ is stable in THF.⁶⁰ This suggests that the $\text{C}_{\text{IPrCH}_2}-\text{B}$ bond in $\text{IPrCH}_2 \cdot \text{BBr}_3$ (**57**) is labile allowing for the dissociation of BBr_3 moiety which ring-opens the THF molecule to give the corresponding bromoalkyloxides (Scheme 1.15a). Ghadwal and coworkers described an unprecedented borylene insertion into a C–N bond of the imidazolium heterocyclic, followed by Dipp-group migration to the boron center and hydrogen abstraction

from the solvent, when they attempted to reduce $\text{IPrCH}_2\cdot\text{BI}_3$ (**59**) with KC_8 .⁸⁷ Notably, the IPr framework is generally stable under most reducing conditions.^{60,88}



Scheme 1.15. Solvent and ligand activation of NHO-borane adducts.

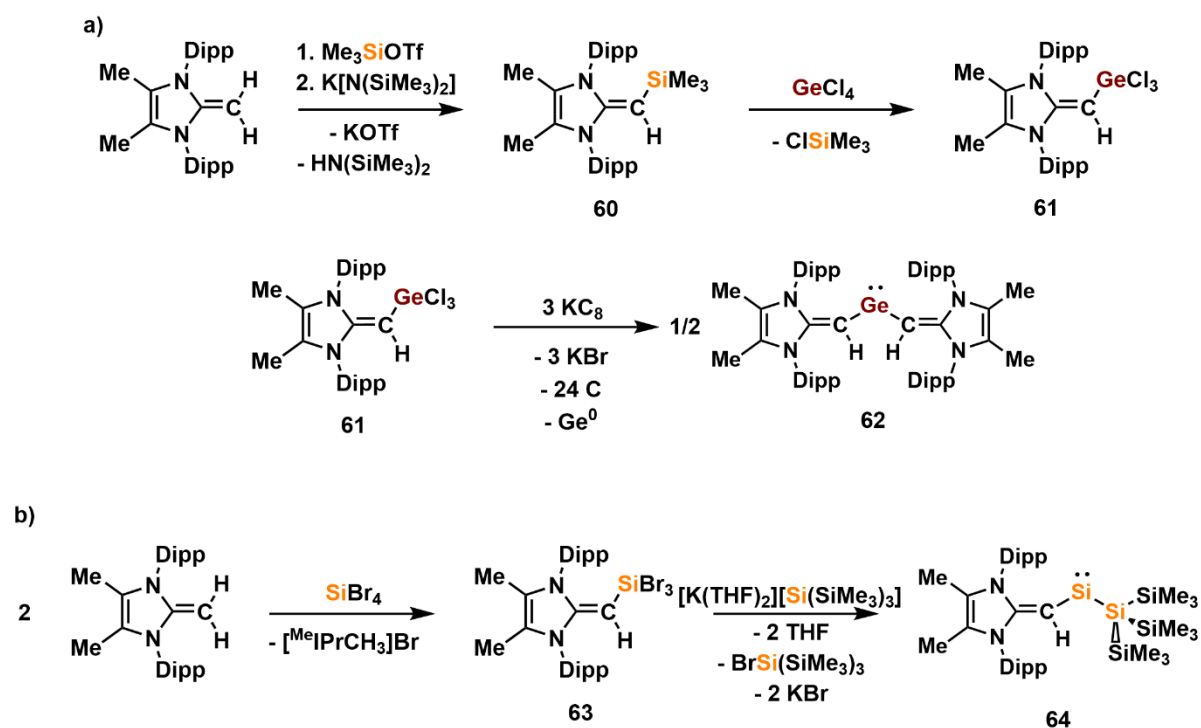
1.4.4 Anionic *N*-Heterocyclic Olefins as Ligands

Anionic *N*-heterocyclic olefins (aNHO) are formally 2σ , 2π -donors, which can be generated by deprotonation of the exocyclic methylene fragment in neutral NHOs (Scheme 1.16). These ligands are potentially strong electron-donating ligands and have become increasingly valuable in the stabilization of low-valent main group elements centers. The earliest example of an aNHO was obtained by Kuhn and coworkers by combining ImMe_4CH_2 (**38**) with ClSiMe_3 , followed by subsequent deprotonation with KH , giving $(\text{ImMe}_4\text{CH})\text{SiMe}_3$ (**60**) (Scheme 1.15).^{8c} The Rivard group would later demonstrate that such silylated-NHOs can act as aNHO transfer agents (*vide infra*).⁸⁹



Scheme 1.16. Synthesis of (ImMe₄CH)SiMe₃ (**60**) and the resonance forms of aNHOs.

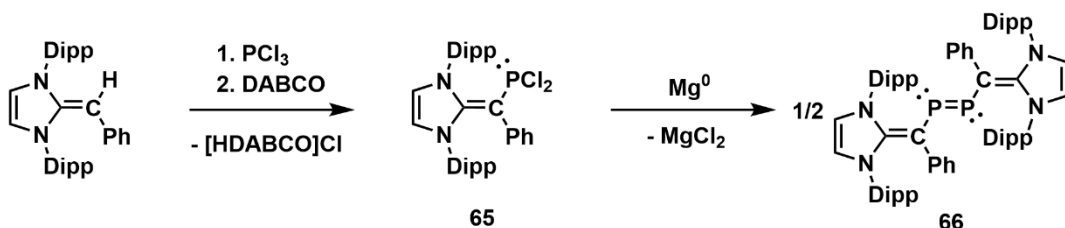
The Rivard group utilized the silylated NHO, (^{Me}IPrCH)SiMe₃ (**60**) (^{Me}IPr = (MeCNDipp)₂C:), which was prepared by combining ^{Me}IPrCH₂ with trimethylsilyl triflate (Me₃SiOTf) followed by deprotonation with the K[N(SiMe₃)₂], as an aNHO transfer agent when they combined **60** with GeCl₄ to give (^{Me}IPrCH)GeCl₃ (**61**).⁸⁹ Reduction of (^{Me}IPrCH)GeCl₃ (**61**) with KC₈ afforded the divinyl germylene (^{Me}IPrCH)₂Ge: (**62**). The use of (^{Me}IPrCH)SiMe₃ (**60**) as an aNHO synthon was a first at the time of its description, however, more common methods to access aNHO complexes include the *in situ* generation of aNHOs with the coordination sphere of an element-halide reagents (E-X; E = Group 14 or 15; X = halide). For example, the Rivard group demonstrated that the addition of two equivalents of ^{Me}IPrCH₂ to SiBr₄ afforded the desired silylated NHO (^{Me}IPrCH)SiBr₃ (**63**) with [^{Me}IPrCH₃]Br as the by-product. Reduction of (^{Me}IPrCH)SiBr₃ (**63**) with two equivalents of [K(THF)₂][Si(SiMe₃)₃] afforded the heteroleptic acyclic silyl vinylsilylene (^{Me}IPrCH)Si{Si(SiMe₃)₃} (**64**) (Scheme 1.18).⁹⁰



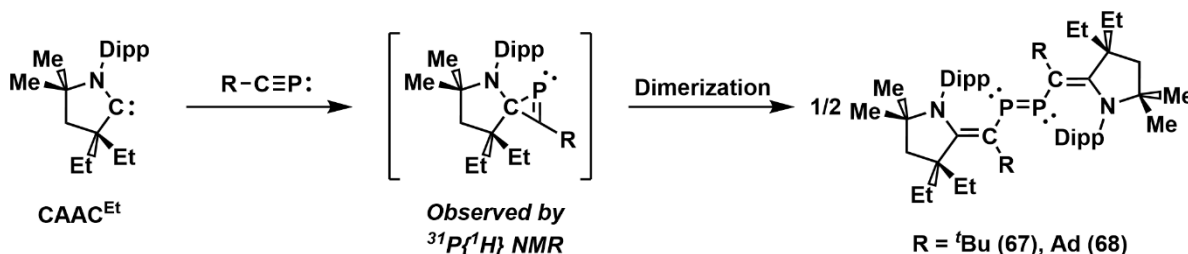
Scheme 1.17. a) Synthesis of the divinyldigermene ($^{\text{Me}}\text{IPrCH}$)₂Ge: (**62**); b) Preparation of the vinyl silylsilylene ($^{\text{Me}}\text{IPrCH}$)Si{Si(SiMe₃)₃} (**64**).

Ghadwal and coworkers have demonstrated that NHOs functionalized at the exocyclic carbon (*e.g.*, with Ph) can be converted to the corresponding aNHO. For example, they described the preparation of a divinyldiphosphene in 2019. By combining the NHO IPrCHPh with PCl_3 and DABCO (1,4-diazabicyclo[2.2.2]octane) they were able to prepare the NHO-functionalized phosphine (IPrCPh) PCl_2 (**65**). Reduction of (IPrCPh) PCl_2 (**65**) with magnesium metal in THF afforded the divinyldiphosphene (IPrCHPh)P=P(CPhIPr) (**66**) (Scheme 1.18a).⁹¹

a) Ghadwal and coworkers



b) Stephan and coworkers



Scheme 1.18. a) Synthesis of divinyldiphosphene (IPrCHPh)P=P(CPhIPr) (**66**); b) Preparation of divinyldiphosphines (CAAC^{Et})C(R)P=PC(R)(CAAC^{Et}) (R = ^tBu (**67**), Ad (**68**)).

Concurrent to Ghadwal and coworkers' report on (IPrCHPh)P=P(CPhIPr) (**66**), Stephan and coworkers described the isolation of a related divinyldiphosphine supported by an aNHO ligand that is formally derived from cyclic(alkyl)amino carbenes (CAAC).⁹² Combining the CAAC^{Et} (CAAC^{Et} = [(Et₂C)H₂C(Me₂C)NDipp]C:) with an equivalent of the phosphalkynes ^tBu-C≡P: or Ad-C≡P: led to the formation of CAAC^{Et}-derived phosphirenes, which rapidly dimerize to the corresponding divinyldiphosphines (CAAC^{Et})C(R)P=PC(R)(CAAC^{Et}) (R = ^tBu (**67**) or Ad (**68**)) (Scheme 1.18b). Notably, this is a rare example of CAAC-derived NHO and could as such be considered a cyclic(alkyl)amino olefin (CAAO).

1.5 Thesis Objectives

As noted in the sections on kinetic stabilization involving low-valent Group 13 and 14 elements, the use of sterically demanding ligands is paramount to prevent unwanted cyclization or oligomerization. However, in some instances, kinetic stabilization is not sufficient alone to prevent unwanted side reactions (*i.e.*, ligand activation or solvent activation). NHOs, and more specifically aNHOs, have been demonstrated to stabilize low-valent Group 14 and 15 species through both steric hindrance and electronic stabilization. A challenge of aNHOs, however, is their use as nucleophiles towards element-halide bonds, specifically those involving Group 13 elements. The main objective of Chapter 2 of this Thesis is the development of a new aNHO synthon and its use in the completion of a homoleptic acyclic tetrelene series $E(\text{aNHO})_2$ ($E = \text{Si-Pb}$). Chapter 3 describes the preparation of In(I) tetramers, which allowed for access to a rare indium-imide supported by an aNHO and a terphenyl ligand. Chapter 4 explores attempts to prepare a stable neutral diborene ($\text{RB}=\text{BR}$) stabilized by aNHOs. In Chapter 5, the preparation of a terphenyl-supported aminoborane, an analogue to styrene, is reported and initial attempts to dehydrogenate said species to afford an iminoborane dimer are described. Finally, the work in Chapter 6 describes the preparation of a new NHC with a modified backbone, increasing the steric demands of NHCs beyond the known (published) upper limit of steric bulk with the eventual aim of using this new NHC to stabilize low-valent transition metal complexes for catalysis.

1.6 References

1. W. C. Zeise, *Annalen der Physik* **1831**, *4*, 497–451.
2. a) M. Black, R. H. B. Mais, P. G. Owston, *Acta. Cryst.* **1969**, *B25*, 1753–1759; b) J. A. J. Jarvis, B. T. Kilbourn, P. G. Owston, *Acta. Cryst.* **1971**, *B27*, 366–372.
3. T. J. Kealy, P. L. Pauson, *Nature* **1951**, *168*, 1039–1040.
4. J. A. Osborn, F. H. Jardine, J. F. Young, G. Wilkinson, *J. Chem. Soc. A.* **1966**, 1711–1732.
5. a) L. Vaska, J. W. DiLuzio, *J. Am. Chem. Soc.* **1961**, *83*, 2784–2785; b) L. Vaska, J. W. DiLuzio, *J. Am. Chem. Soc.* **1962**, *84*, 679–680.
6. a) A. H. Janowicz, R. G. Bergman, *J. Am. Chem. Soc.* **1982**, *104*, 352–354; b) J. K. Hoyano, W. A. G. Graham, *J. Am. Chem. Soc.* **1982**, *104*, 3723–3725.
7. D. Seyferth, *Organometallics* **2001**, *20*, 1488–1498.
8. A. Stock, A. Brandt, H. Fischer, *Ber. Deut. Chemie. Ges. B.* **1925**, *58*, 643–657.
9. a) R. West, *Polyhedron* **2002**, *21*, 467–472; b) T. J. Hadlington, M. Driess, C. Jones, *Chem. Soc. Rev.* **2018**, *47*, 4176–4197.
10. P. P. Power, *Nature* **2010**, *436*, 171–177.
11. a) P. J. Davidson, M. F. Lappert, *J. Chem. Soc., Chem. Commun.* **1973**, 317a; b) D. E. Goldberg, D. E. Harris, M. F. Lappert, K. M. Thomas, *J. Chem. Soc., Chem. Commun.* **1976**, 261–262; c) P. J. Davidson, D. H. Harris, M. F. Lappert, *J. Chem. Soc., Dalton Trans.* **1976**, 2268–2274; d) P. B. Hitchcock, M. F. Lappert, S. J. Miles, A. J. Thorne, *J. Chem. Soc., Chem. Commun.* **1984**, 480–482.

12. R. West, M. J. Fink, J. Michl, *Science* **1981**, *214*, 1343–1344.
13. M. Yoshifuji, I. Shima, N. Inamoto, K. Hirotsu, T. Higuchi, *J. Am. Chem. Soc.* **1981**, *103*, 4587–4589.
14. G. H. Spikes, J. C. Fettinger, P. P. Power, *J. Am. Chem. Soc.* **2005**, *127*, 12232–12233.
15. G. C. Welch, R. R. San Juan, J. D. Masuda, D. W. Stephan, *Science* **2006**, *314*, 1124–1126.
16. D. J. Liptrot, P. P. Power, *Nat. Chem. Rev.* **2017**, *1*, 0004.
17. R. D. Miller, J. Michl, *Chem. Rev.* **1989**, *89*, 1359–1410.
18. F. S. Kipping, J. E. Sands, *J. Chem. Soc., Trans.* **1921**, *119*, 830–847.
19. T. J. Drahnak, J. Michl, R. West, *J. Am. Chem. Soc.* **1979**, *101*, 5427–5428.
20. a) A. G. Moiseev, W. J. Leigh, *Organometallics* **2007**, *26*, 6268–6276; b) A. G. Moiseev, W. J. Leigh, *Organometallics* **2007**, *26*, 6277–6289.
21. C. Dohmeier, C. Robl, M. Tacke, H. Schnöckel, *Angew. Chem. Int. Ed. Engl.* **1991**, *30*, 564–565.
22. D. Loos, E. Baum, A. Ecker, H. Schnöckel, A. J. Downs, *Angew. Chem. Int. Ed.* **1997**, *36*, 860–862.
23. a) R. D. Schluter, A. H. Cowley, D. A. Atwood, R. A. Jones, J. L. Atwood, *J. Coord. Chem.* **1993**, *30*, 25–28; b) W. Uhl, R. Graupner, M. Pohlmann, S. Pohl, W. Saak, *Chem. Ber.* **1996**, *129*, 143–146; c) M. Bühler, G. Linti, *Z. Anorg. Allg. Chem.* **2006**, *632*, 2453–2460; d) A. Seifert, G. Linti, *Eur. J. Inorg. Chem.* **2007**, 5080–5086.

24. a) E. O. Fischer, H. P. Hofmann, *Angew. Chem.* **1957**, *69*, 639–640; b) O. T. Beachley, J. C. Pazik, T. E. Glassman, M. R. Churchill, J. C. Fettinger, R. Blom, *Organometallics* **1988**, *7*, 1051–1059
25. For related work on $[\text{Tl}(\text{C}(\text{SiMe}_3)_3)]_4$, see: W. Uhl, S. U. Keimling, K. W. Klinkhammer, D. Schwarz, *Angew. Chem. Int. Ed.* **1997**, *36*, 64–65.
26. S. T. Haubrich, P. P. Power, *J. Am. Chem. Soc.* **1998**, *120*, 2202–2203.
27. M. Niemeyer, P. P. Power, *Angew. Chem. Int. Ed.* **1998**, *37*, 1277–1279.
28. Z. Zhu, R. C. Fischer, B. D. Ellis, E. Rivard, W. A. Merrill, M. M. Olmstead, P. P. Power, J. D. Guo, S. Nagase, L. Pu, *Chem. Eur. J.* **2009**, *15*, 5263–5272.
29. J. D. Queen, A. Lehmann, J. C. Fettinger, H. M. Tuononen, P. P. Power, *J. Am. Chem. Soc.* **2020**, *142*, 20554–20559.
30. a) R. J. Wright, A. D. Phillips, N. J. Hardman, P. P. Power, *J. Am. Chem. Soc.* **2002**, *124*, 8538–8539; b) N. J. Hardman, A. D. Phillips, P. P. Power, *J. Am. Chem. Soc.* **2003**, *125*, 2667–2679; c) R. J. Wright, A. D. Phillips, S. Hino, P. P. Power, *J. Am. Chem. Soc.* **2005**, *127*, 4794–4799.
31. a) C. A. Caputo, P. P. Power, *Organometallics* **2013**, *32*, 2278–2286; b) H. B. Wedler, P. Wendelboe, P. P. Power, *Organometallics* **2018**, *37*, 2929–2936; c) E. Rivard, *Chem. Soc. Rev.* **2016**, *45*, 989–1003.
32. Z. Zhu, X. Wang, Y. Peng, H. Lei, J. C. Fettinger, E. Rivard, P. P. Power, *Angew. Chem. Int. Ed.* **2009**, *48*, 2031–2034.

33. a) R. J. Wright, A. D. Phillips, P. P. Power, *J. Am. Chem. Soc.* **2003**, *125*, 10784–10785; b) T. Agou, K. Nagata, N. Tokitoh, *Angew. Chem. Int. Ed.* **2013**, *52*, 10818–10821; c) For an example of a dialumene being trapped with an alkyne, see: C. Cui, X. Li, C. Wang, J. Zhang, J. Cheng, X. Zhu, *Angew. Chem. Int. Ed.* **2006**, *45*, 2245–2247.
34. T. Mennekes, P. Paetzold, R. Boese, D. Bläser, *Angew. Chem. Int. Ed. Engl.* **1991**, *30*, 173–175.
35. C.-J. Maier, H. Pritzkow, W. Siebert, *Angew. Chem. Int. Ed.* **1999**, *38*, 1666–1667.
36. W. J. Grigsby, P. P. Power, *J. Am. Chem. Soc.* **1996**, *118*, 7981–7988.
37. P. Schwerdtfeger, G. A. Heath, M. Dolg, M. A. Bennet, *J. Am. Chem. Soc.* **1992**, *114*, 7518–7527.
38. A. Sekiguchi, R. Kinjo, M. Ichinohe, *Science* **2004**, *305*, 1755–1757.
39. a) L. Pu, B. Twamley, P. P. Power, *J. Am. Chem. Soc.* **2000**, *122*, 3524–3525; b) A. D. Phillips, R. J. Wright, M. M. Olmstead, P. P. Power, *J. Am. Chem. Soc.* **2002**, *124*, 5930–5931; c) M. Stender, A. D. Phillips, R. J. Wright, P. P. Power, *Angew. Chem. Int. Ed.* **2002**, *41*, 1785–1787.
40. P. P. Power, *Organometallics* **2007**, *26*, 4362–4372.
41. M. Stürmann, M. Weidenbruch, K. W. Klinkhammer, F. Lissner, H. Marsmann, *Organometallics* **1998**, *17*, 4425–4428.
42. C. Shan, S. Yao, M. Driess, *Chem. Soc. Rev.* **2020**, *49*, 6733–6754.
43. M. J. S. Gynane, D. H. Harris, M. F. Lappert, P. P. Power, P. Rivère, M. Rivière-Baudet, *J. Chem. Soc., Dalton Trans.* **1977**, 2004–2009.

44. P. Jutzi, U. Holtmann, D. Kanna, C. Krüger, R. Blom, R. Gleiter, I. Hyla-Kyrspin, *Chem. Ber.* **1989**, *122*, 1629–1639.
45. M. Denk, R. Lennon, R. Hayashi, R. West, A. V. Belyakov, H. P. Verne, A. Haaland, M. Wagner, N. Metzler, *J. Am. Chem. Soc.* **1994**, *116*, 2691–2692.
46. M. Kira, S. Ishida, T. Iwamoto, C. Kabuto, *J. Am. Chem. Soc.* **1999**, *121*, 9722–9723.
47. a) P. Paetzold, *Pure Appl. Chem.* **1991**, *63*, 345–350; b) Z. X. Giustra, S.-Y. Liu, *J. Am. Chem. Soc.* **2018**, *140*, 1184–1194.
48. E. J. Little, M. M. Jones, *J. Chem. Educ.* **1960**, *37*, 231–233.
49. G. D. Piero, M. Cesari, G. Perego, S. Cucinella, E. Cernia, *J. Organomet. Chem.* **1977**, *129*, 289–298.
50. P. Paetzold, C. von Plotho, G. Schmid, R. Boese, B. Schrader, D. Bougeard, U. Pfeiffer, R. Gleiter, W. Schäfer, *Chem. Ber.* **1984**, *117*, 1089–1102.
51. R. J. Wright, A. D. Phillips, T. L. Allen, W. H. Fink, P. P. Power, *J. Am. Chem. Soc.* **2003**, *125*, 1694–1695.
52. J. D. Queen, S. Irvankoski, J. C. Fettinger, H. M. Tuononen, P. P. Power, *J. Am. Chem. Soc.* **2021**, *143*, 6351–6356.
53. M. N. Hopkinson, C. Richter, M. Schedler, F. Glorius, *Nature* **2014**, *510*, 485–496.
54. A. J. Arduengo III, R. L. Harlow, M. Kline, *J. Am. Chem. Soc.* **1991**, *113*, 361–363.

55. a) V. Nesterov, D. Reiter, P. Bag, P. Frisch, R. Holtzner, A. Porzelt, S. Inoue, *Chem. Rev.* **2018**, *118*, 9678–9842; b) M. Melaimi, R. Jazzar, M. Soleihavoup, G. Bertrand, *Angew. Chem. Int. Ed.* **2017**, *56*, 10046–10068.
56. A. A. D. Tulloch, A. A. Danopoulos, S. Kleinhenz, M. E. Light, M. B. Hursthouse, G. Eastham, *Organometallics* **2001**, *20*, 2027–2031.
57. V. Lavallo, Y. Canac, C. Präsang, B. Donnadiou, G. Bertrand, *Angew. Chem. Int. Ed.* **2005**, *44*, 5705–5709.
58. A. Gómez-Suárez, D. J. Nelson, S. P. Nolan, *Chem. Commun.* **2017**, *53*, 2650–2660.
59. a) H. Clavier, S. P. Nolan, *Chem. Commun.* **2010**, *46*, 841–861; b) L. Falivene, Z. Cao, A. Petta, L. Serra, A. Poater, R. Oliva, V. Scarano, L. Cavallo, *Nat. Chem.* **2019**, *11*, 872–879; c) A. Poater, B. Cosenza, A. Correa, S. Giudice, F. Ragone, V. Scarano, L. Cavallo, *Eur. J. Inorg. Chem.* **2009**, 1759–1766.
60. Y. Wang, B. Quillian, P. Wei, C. S. Wannere, Y. Xie, R. B. King, H. F. Schaefer III, P. v R. Schleyer, G. H. Robinson, *J. Am. Chem. Soc.* **2007**, *129*, 12412–12413.
61. H. Braunschweig, R. D. Dewhurst, K. Hammond, J. Mies, K. Radacki, A. Vargas, *Science* **2012**, *336*, 1420–1422.
62. A. C. Filippou, O. Chernov, G. Schnakenburg, *Angew. Chem. Int. Ed.* **2009**, *48*, 5687–5690.
63. M. M. D. Roy, E. Rivard, *Acc. Chem. Res.* **2017**, *50*, 2017–2025.
64. S. Ling-Chung, K. D. Sales, J. H. P. Utley, *J. Chem. Soc., Chem. Commun.* **1990**, 622–664.
65. M. Pareek, Y. Reddi, R. B. Sunoj, *Chem. Sci.* **2021**, *12*, 7973–7992.

66. S. M. I. Al-Rafia, A. C. Malcolm, S. K. Liew, M. J. Ferguson, R. McDonald, E. Rivard, *Chem. Commun.* **2011**, 47, 6987–6989.
67. H. Böhme, F. Soldan, *Chem. Ber.* **1961**, 94, 3109–3119.
68. P. P. Ponti, J. C. Baldwin, W. C. Kaska, *Inorg. Chem.* **1979**, 18, 873–875.
69. U. Gruseck, M. Heuschmann, *Chem. Ber.* **1987**, 120, 2053–2064.
70. a) N. Kuhn, H. Bohnen, J. Kreuzberg, D. Bläser, R. Boese, *J. Chem. Soc., Chem. Commun.* **1993**, 1136–1137; b) N. Kuhn, H. Bohnen, D. Bläser, R. Boese, *Chem. Ber.* **1994**, 127, 1405–1407; c) N. Kuhn, H. Bohnen, G. Henkel, J. Kreuzberg, *Z. Naturforsch.* **1996**, 51b, 1267–1278.
71. A. Dumrath, X-F. Wu, H. Neumann, A. Spannenberg, R. Jackstell, M. Beller, *Angew. Chem. Int. Ed.* **2010**, 49, 8988–8992.
72. For select articles from the Rivard group on this topic, see: a) I. C. Watson, Y. Zhou, M. J. Ferguson, E. Rivard, *Z. Anorg. Allg. Chem.* **2022**, 68, e202200082; b) I. C. Watson, M. J. Ferguson, E. Rivard, *Inorg. Chem.* **2021**, 60, 18347–18359; c) N. Paisley, M. Lui, R. McDonald, M. J. Ferguson, E. Rivard, *Dalton Trans.* **2016**, 45, 9860–9870; d) M. W. Lui, O. Shynkaruk, M. S. Oakley, R. Sinelnikov, R. McDonald, M. J. Ferguson, A. Meldrum, M. Klobukowski, E. Rivard, *Dalton Trans.* **2017**, 46, 5946–5954.
73. For select reviews and articles, see: a) R. S. Ghadwal, *Acc. Chem. Res.* **2022**, 55, 457–470; b) P. Varava, Z. Dong, R. Scopelliti, F. Fadaei-Tirani, K. Severin, *Nat. Chem.* **2021**, 13, 1055–1060; c) L. Y. M. Eymann, P. Varava, A. M. Shved, B. F. E. Curchod, Y. Liu, O. M. Planes, A. Sienkiewicz, R. Scopelliti, F. F. Tirani, K. Severin, *J. Am. Chem. Soc.* **2019**, 141, 17112–

17116; d) M. K. Sharma, S. Blomeyer, B. Neumann, H.-G. Stammler, M. van Gastel, A. Hinz, R. S. Ghadwal, *Angew. Chem. Int. Ed.* **2019**, *58*, 17599–17603.

74. For select reviews and articles, see: a) M. G. S. Deepika, R. Dandela, V. Dhayalan, *Chem. Eur. J.* **2023**, *29*, e202302106; b) C. Hering-Junghans, I. C. Watson, M. J. Ferguson, R. McDonald, E. Rivard, *Dalton Trans.* **2017**, *46*, 7150–7153; c) I. C. Watson, Y. Zhou, M. J. Ferguson, M. Kranzlein, B. Rieger, E. Rivard, *Z. Anorg. Allen. Chem.* **2020**, *646*, 547–551; d) C. Czysch, T. Dinh, Y. Fröder, L. Bixenmann, P. Komforth, A. Balint, H.-J. Räder, S. Naumann, L. Nuhn, *ACS Polym. Au* **2022**, *2*, 371–379.

75. K. Powers, C. Hering-Junghans, R. McDonald, M. J. Ferguson, E. Rivard, *Polyhedron* **2016**, *108*, 8–14.

76. Y. Wang, M. Y. Abraham, R. J. Gillard, D. R. Sexton, P. Wei, G. H. Robinson, *Organometallics* **2013**, *32*, 6639–6642.

77. M. M. Hansmann, P. W. Antoni, H. Pescht, *Angew. Chem. Int. Ed.* **2020**, *59*, 5782–5787.

78. D. Enders, K. Breuer, G. Raabe, J. Runsink, J. H. Teles, J.-P. Melder, K. Ebel, S. Brode, *Angew. Chem. Int. Ed. Engl.* **1995**, *34*, 1021–1023.

79. For related work by Matusoka and coworkers wherein they combined Enders' carbene with methyl methacrylate (MMA) to give a functionalized triazole NHO, see: S. Matsuoka, Y. Tochigi, K. Takagi, M. Suzuki, *Tetrahedron* **2012**, *68*, 9836–9841.

80. Z. Li, P. Ji, J.-P. Cheng, *J. Org. Chem.* **2021**, *86*, 2974–2985.

81. a) C. A. Tolman, *Chem. Rev.* **1977**, *77*, 313–348; b) T. Dröge, F. Glorius, *Angew. Chem. Int. Ed.* **2010**, *49*, 6940–6952.

82. For earlier reports on NHO–rhodium complexes; see: a) A. Fürstner, M. Alcarazo, R. Goddard, C. W. Lehmann, *Angew. Chem. Int. Ed.* **2008**, *47*, 3210–3214; b) S. Kronig, P. G. Jones, M. Tamm, *Eur. J. Inorg. Chem.* **2013**, 2301–2314.
83. A. Eitzinger, J. Reitz, P. W. Antoni, H. Mayr, A. R. Ofial, M. M. Hansmann, *Angew. Chem. Int. Ed.* **2023**, *62*, e202309790.
84. A. El-Hellani, J. Monot, R. Guillot, C. Bour, V. Gandon, *Inorg. Chem.* **2013**, *52*, 506–514.
85. S. M. I. Al-Rafia, M. R. Momeni, M. J. Ferguson, R. McDonald, A. Brown, E. Rivard, *Organometallics* **2013**, *32*, 6658–6665.
86. Y. W. Wang, M. Y. Abraham, R. J. Gilliard, D. R. Sexton, P. Wei, G. H. Robinson, *Organometallics* **2013**, *32*, 6639–6642.
87. R. J. Ghadwal, C. J. Schürmann, F. Engelhardt, C. Steinmetzger, *Eur. J. Inorg. Chem.* **2014**, 4921–4926.
88. M. W. Lui, C. Merten, M. J. Ferguson, R. McDonald, Y. Xu, E. Rivard, *Inorg. Chem.* **2015**, *54*, 2040–2049.
89. C. Hering-Junghans, P. Andreiuk, M. J. Ferguson, R. McDonald, E. Rivard, *Angew. Chem. Int. Ed.* **2017**, *56*, 6272–6275.
90. M. M. D. Roy, M. J. Ferguson, R. McDonald, Y. Zhou, E. Rivard, *Chem. Sci.* **2019**, *10*, 6476–9481.
91. D. Rottschäfer, M. K. Sharma, B. Neumann, H.-G. Stammer, D. M. Andrada, R. S. Ghadwal, *Chem. Eur. J.* **2019**, *25*, 8127–8134.
92. L. L. Liu, L. L. Cao, J. Zhang, D. W. Stephan, *Angew. Chem. Int. Ed.* **2019**, *58*, 273–277.

Chapter 2 – A Stable Homoleptic Tetrelene Series

2.1 Introduction

In the 1970s Lappert and coworkers reported the isolation of two-coordinate acyclic dialkyl tetrelenes (R_2E ;, $E = Ge, Sn, Pb$; $R = (Me_3Si)_2CH$) (**I**), which while monomeric in solution, dimerize in the solid state.¹ These findings helped spur interest in low-coordinate main group species due to these being examples of heavier Group 14 elements breaking the “Double Bond Rule”, which stated that elements with a principal quantum number greater than 2 could not form element-element double bonds.² The use of sterically-demanding aryl ligands inhibits dimerization in the solid state to afford monomeric germylenes (**II**), stannylenes (**III**) and plumbylenes (**IV**) (Figure 2.1).³ In recent years there has been a renewed interest in tetrelenes due to their transition-metal like reactivity (e.g., H_2 activation) and their important role in main group catalysis.⁴ Absent from the tetrelene family is a stable acyclic diorganosilylene.⁵ It should be noted that organosilylenes are postulated intermediates in the industrial “Direct Synthesis” of Me_2SiCl_2 and in the preparation of polysilanes $[R_2Si]_n$ *via* Wurtz coupling;^{6a,b} moreover, organosilylenes (e.g., $SiMe_2$) have been studied *via* matrix isolation.^{6c}

Known diorganosilylenes are limited to Jutzi’s coordinatively saturated silicocene Cp^*_2Si (**V**; $Cp^* = \eta^5-C_5Me_5$)⁷ and Kira’s cyclic silylene (**VI**; $[H_2CC(SiMe_3)_2]_2Si$:).^{5c} The first stable acyclic silylenes were reported in 2012,^{5a,b} with other examples having since been reported.⁸ In all these cases, the presence of heteroatoms as stabilizing π -donors was used. In recent years, our group^{8f,9} and others^{10,11} have employed a class of ligand termed by the Rivard group as anionic *N*-heterocyclic olefins (aNHOs) to stabilize low-coordinate main group

element species due to the highly electron-donating nature of the ligating sp^2 -hybridized carbon atom in aNHOs.^{9a} I assisted in the preparation of a complete divinyltetrelene series (Si–Pb) supported by the sterically demanding vinylic (aNHO) donor $[\text{Me}^e\text{IPrCH}^-]$ ($\text{Me}^e\text{IPr} = (\text{MeCNDipp})_2\text{C}; \text{Dipp} = 2,6\text{-}i\text{Pr}_2\text{C}_6\text{H}_3$), which involved the development of the new reagent $[(\text{Me}^e\text{IPrCH})\text{Li}]_2$. This project also required the development of a high-yielding route to a Si(II) source that is less prone to degradation, leading to the isolation of the electron-rich divinylsilylene $(\text{Me}^e\text{IPrCH})\text{Si}:$.

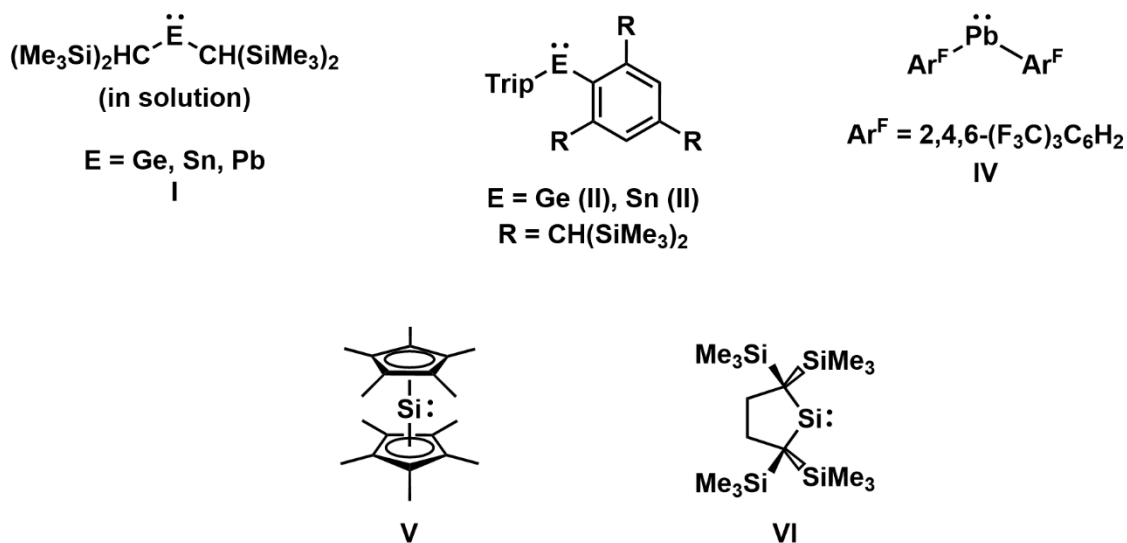


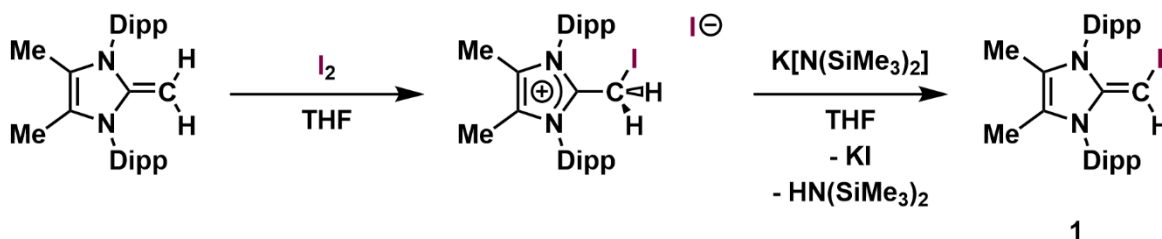
Figure 2.1. Alkyl- and aryl-substituted tetrelenes (Trip = 2,4,6- $i\text{Pr}_3\text{C}_6\text{H}_2$).

2.2 Results and Discussion

This project began with the development of a synthetic strategy to prepare a precursor that could take full advantage of the potential 2σ , 2π -electron properties of anionic N -heterocyclic olefins (*i.e.*, $\text{Me}^e\text{IPrCH}^-$). While anionic N -heterocyclic olefins (aNHOs) can be prepared *via* the *in situ* deprotonation of the neutral ligand NHO within the coordination sphere of an element

halide,¹² this method is not applicable to all elements. Initial attempts to induce deprotonation the exocyclic carbon atom of IPrCH₂ [IPr = (HCNDipp)₂C:], led to deprotonation of the unsaturated backbone in the IPr unit.¹³ Attempts were made to deprotonate the methylated NHO ^{Me}IPrCH₂ with ⁿBuLi, ^tBuLi and TMEDA/ⁿBuLi (TMEDA = tetramethylethylenediamine) mixtures, but no reaction was observed in each attempt. As such, the iodination of ^{Me}IPrCH₂ to afford ^{Me}IPrCH(I) (**1**) was targeted, as this species would likely undergo lithium halogen exchange to give an anionic [^{Me}IPrCH]⁻ unit.

Combining ^{Me}IPrCH₂ with I₂ in tetrahydrofuran led to the immediate formation of a bright-yellow precipitate, tentatively assigned as the iodide salt [^{Me}IPrCH₂(I)]I.¹⁴ Upon subsequent addition of the strong amide base, K[N(SiMe₃)₂], the precipitate was consumed and the target compound ^{Me}IPrCH(I) (**1**) (Scheme 2.1) was obtained in a 57 % yield after extraction of the product with hexanes and recrystallization at -35 °C. X-ray crystallographic analysis of **1** (Figure 2.2) revealed that the exocyclic C=C bond [1.360(5) Å] retained significant double character as it is the same length within error as the corresponding exocyclic C=C distance in ^{Me}IPrCH₂ [1.3489(18) Å].^{12b}



Scheme 2.1. One-pot synthesis of ^{Me}IPrCH(I) (**1**).

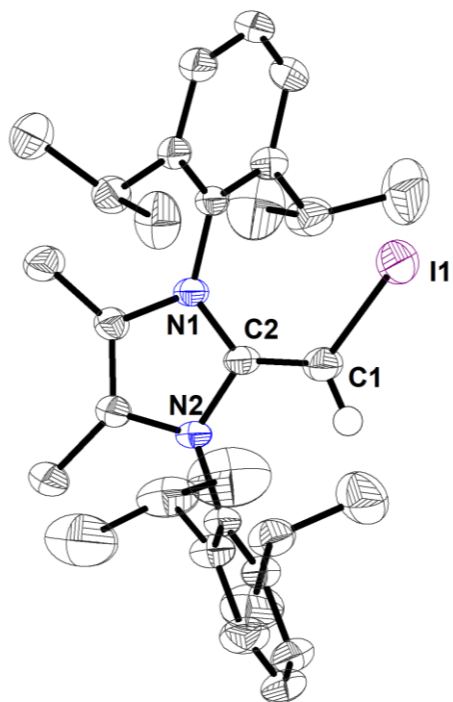
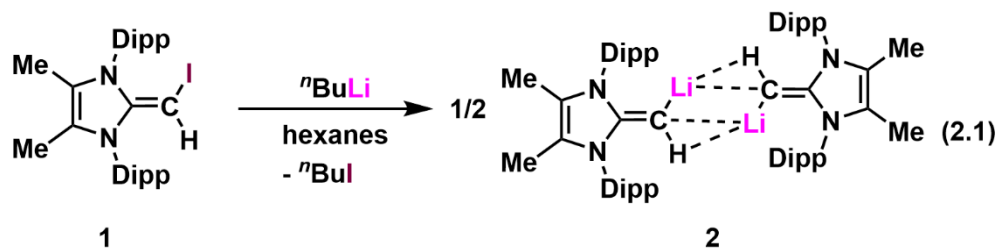


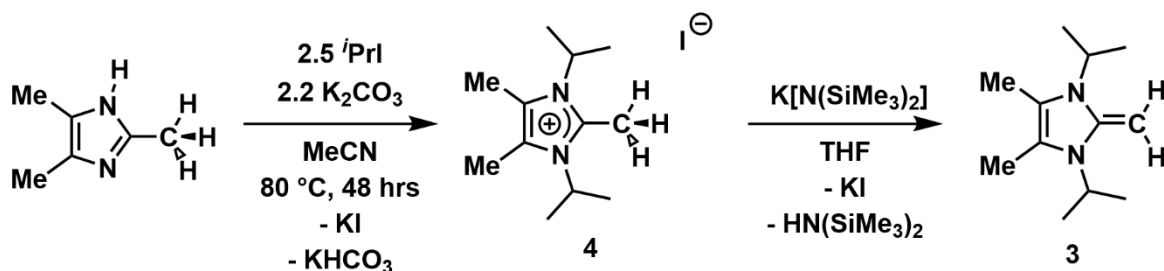
Figure 2.2. Molecular structure of MeIPrCH(I) (**1**) with thermal ellipsoids plotted at 50 % probability. All hydrogen atoms (except for the vinylic hydrogen atom at C1) are omitted for clarity. Selected bond lengths [Å] and angles [°]: C1–I1 2.063(3), C1–C2 1.360(5), N1–C2 1.375(5), N2–C2 1.391(4); C2–C1–I1 128.1(3), N1–C2–C1 133.1(3), N2–C2–C1 122.7(3), N1–C2–N2 104.2(3).

$n\text{-BuLi}$ was added to a solution of MeIPrCH(I) (**1**) in hexanes, which afforded $[(\text{MeIPrCH})\text{Li}]_2$ (**2**) as a bright-orange solid in a yield of 82 % (Equation 2.1). This species exists as a dimer in the solid state (according to X-ray crystallography) and in solution as determined by diffusion-ordered NMR spectroscopy (DOSY). The core of this centrosymmetric dimer is supported by agostic (CH)-Li interactions, with substantial retention of double bond character within the exocyclic olefin units. The $\text{Li}\{^1\text{H}\}$ NMR spectrum of **2** in C_6D_6 shows a resonance at 1.0 ppm. Interestingly, the vinyl proton on the exocyclic olefin unit is located considerably upfield with a shift of 0.89 ppm, indicating a significant amount of electron density located on the exocyclic carbon. Solid samples of **2** decompose over the

course of a few days at room temperature, as such, samples of **2** are used within a few days of preparation and are stored at -35 °C.

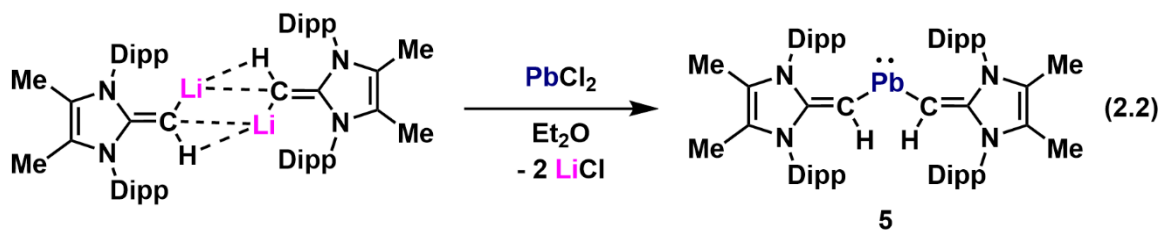


I was interested in the possibility of preparing other aNHO synthons of varying bulk, namely the previously unreported $\text{ImMe}_2^i\text{Pr}_2\text{CH}_2$ (**3**) [$\text{ImMe}_2^i\text{Pr}_2 = (\text{MeCN}^i\text{Pr}_2)_2\text{C}$]. Initial attempts to prepare **3** by methylation of the carbene $\text{ImMe}_2^i\text{Pr}_2$ with methyl iodide and subsequent deprotonation with a strong base (*i.e.*, KO^tBu), in a similar fashion to the preparation of $\text{Me}^e\text{IPrCH}_2$,^{12b} afforded only the free carbene $\text{ImMe}_2^i\text{Pr}_2$ as the detectable species in solution. It was determined that in order to prepare the target NHO, $\text{ImMe}_2^i\text{Pr}_2\text{CH}_2$ (**3**), that pre-installation of the methyl group to the imidazole ring was necessary. As such, 2,4,6-trimethylimidazole¹⁵ was combined with a slight excess of isopropyl iodide (^iPrI) in acetonitrile and the mixture heated to reflux for 48 hours, which afforded [$\text{ImMe}_2^i\text{Pr}_2\text{-CH}_3$]I (**4**) in an isolated yield of 33 % (Scheme 2.2). With an analytically pure sample **4** in hand, its subsequent deprotonation with $\text{K}[\text{N}(\text{SiMe}_3)_2]$ in THF yielded the previously unreported NHO $\text{ImMe}_2^i\text{Pr}_2\text{CH}_2$ (**3**) in an isolated yield of 77 % as a brown oil. Attempts to prepare $\text{ImMe}_2^i\text{Pr}_2\text{CH(I)}$ by employing the same strategy as used in the synthesis of **1** were unsuccessful, yielding an inseparable mixture of two species, tentatively assigned as a mixture of [$\text{ImMe}_2^i\text{Pr}_2\text{CH}_2\text{I}$]I and [$\text{ImMe}_2^i\text{Pr}_2\text{CH}_2\text{I}$]I₃.¹⁴



Scheme 2.2. Synthesis of [ImMe₂^{*i*Pr}Pr₂CH₃]⁺I⁻ (**4**) and ImMe₂^{*i*Pr}Pr₂CH₂ (**3**).

While aNHOs can be prepared *via* the *in situ* deprotonation of a neutral NHO ligand within the coordination sphere of an element halide,¹² it was found that this is not applicable to all elements. For example, the combination of two equivalents of ^{Me}iPrCH₂ and PbBr₂ did not afford the vinylplumbylene (^{Me}iPrCH)PbBr, which highlighted the need for a new aNHO synthon. The divinylplumbylene (^{Me}iPrCH)₂Pb: (**5**) was prepared by combining [(^{Me}iPrCH)Li]₂ (**2**) and PbBr₂ in Et₂O and was isolated as a deep-blue crystalline solid in a yield of 49 % (Equation 2.2). The ¹H NMR spectrum of **5** in C₆D₆ indicated a dramatic peak shift for the exocyclic vinyl protons from 0.89 ppm in **2** to 7.24 ppm. Additionally, the ²⁰⁷Pb{¹H} NMR spectrum of **5** in [d₈]-toluene showed a resonance at 5449 ppm (Figure 2.3), which is positioned considerably downfield when compared to that of (Ar^F)₂Pb: (**IV**; Ar^F = 2,4,6-(F₃C)₃C₆H₂) (δ = 4878 ppm).^{3c}



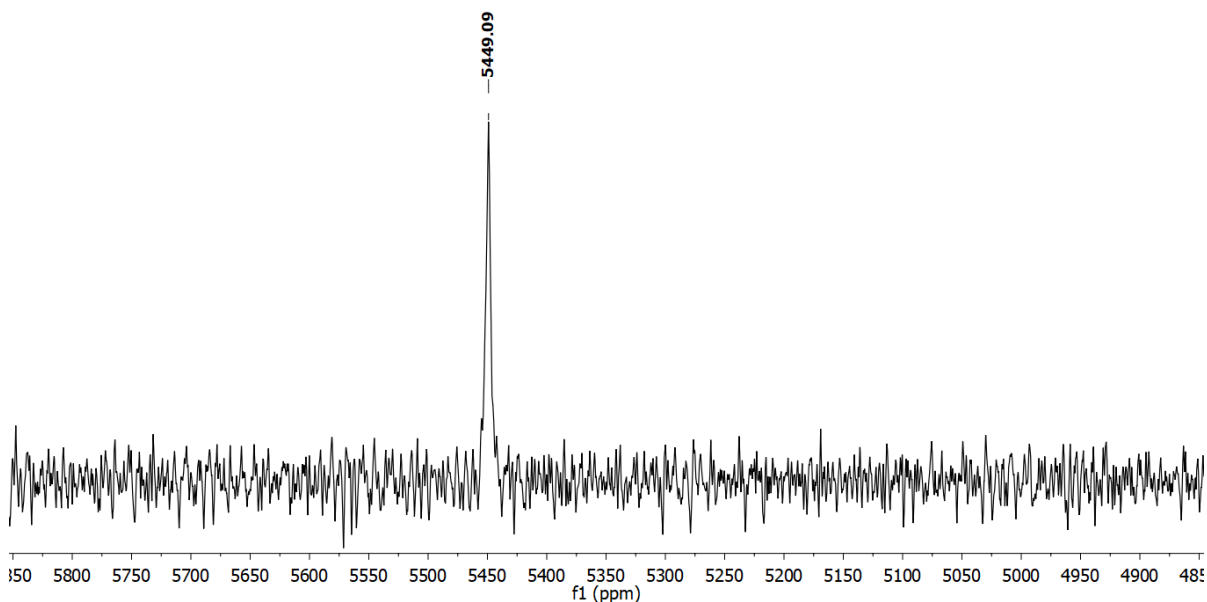
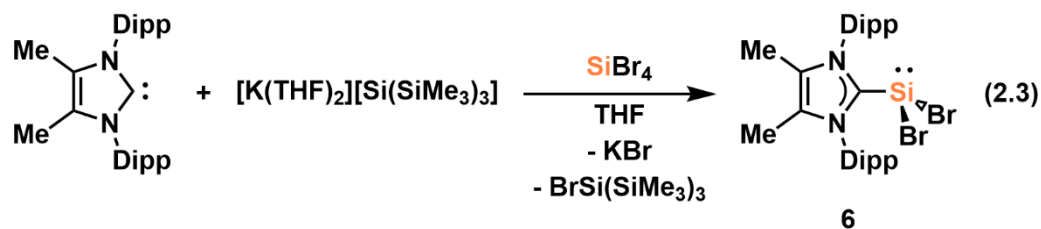
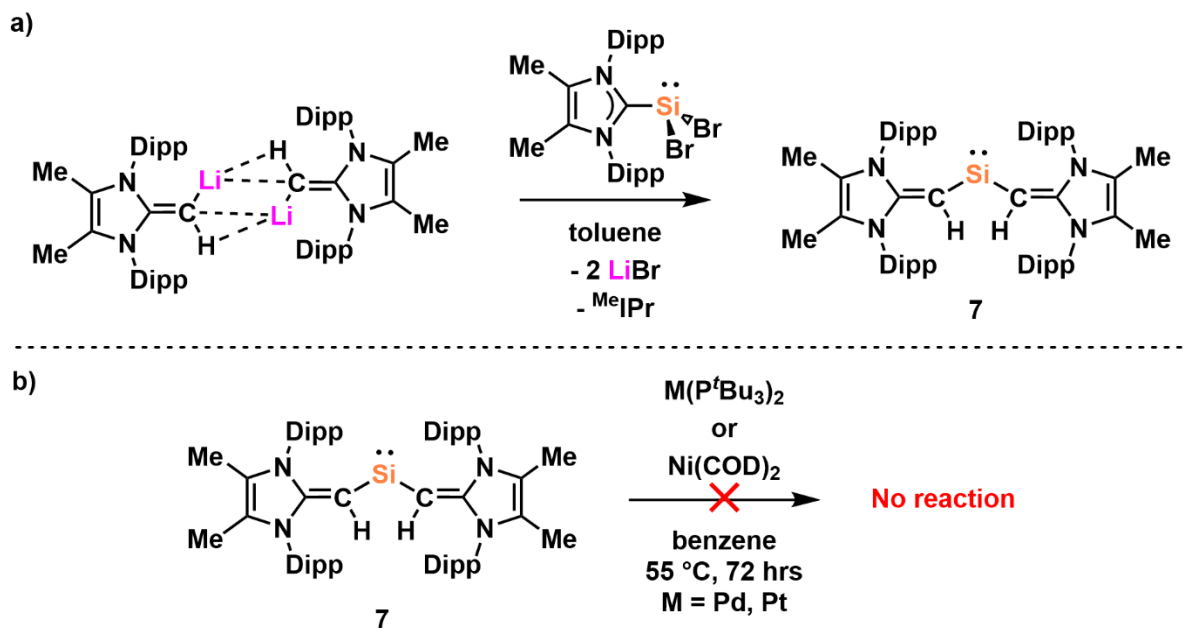


Figure 2.3. $^{207}\text{Pb}\{^1\text{H}\}$ NMR spectrum of $(^{\text{Me}}\text{IPrCH})_2\text{Pb}$ (**7**) in $[\text{d}_8]$ -toluene.

The preparation of the divynylsilylene $(^{\text{Me}}\text{IPrCH})_2\text{Si}$ (**7**) required the development of a suitable Si(II) precursor. When $[(^{\text{Me}}\text{IPrCH})\text{Li}]_2$ (**2**) was combined with either Roesky's $(\text{IPr}\cdot\text{SiCl}_2)^{16}$ or Filippou's $(\text{IPr}\cdot\text{SiBr}_2)^{17}$ as potential Si(II) precursors, undesirable C-H activation/deprotonation of the carbene ligand backbone by **2** and regeneration of $^{\text{Me}}\text{IPrCH}_2$ was observed. As such, attention was turned towards the methylated Si(II) precursor $^{\text{Me}}\text{IPr}\cdot\text{SiBr}_2$ (**6**).¹⁸ While $^{\text{Me}}\text{IPr}\cdot\text{SiBr}_2$ (**6**) had been prepared previously from the carbene-induced disproportionation of Si_2Br_6 , its separation from the coproduct $^{\text{Me}}\text{IPr}\cdot\text{SiBr}_4$ on a significant scale was not reported. The ability of the hypersilyl salt $[\text{K}(\text{THF})_2][\text{Si}(\text{SiMe}_3)_3]^{19}$ to reduce Si(IV) to Si(II) centers^{8a,c,f} inspired us to combine this $[\text{Si}(\text{SiMe}_3)_3]^-$ reagent and $^{\text{Me}}\text{IPr}$ followed by the rapid addition of SiBr_4 affording the Si(II) dibromide adduct **6** as a pure product in a yield of 64 % after washing the final product mixture with cold hexanes cooled to $-30\text{ }^\circ\text{C}$ to remove the hypersilyl bromide $\text{BrSi}(\text{SiMe}_3)_3$ by-product (Equation 2.3).

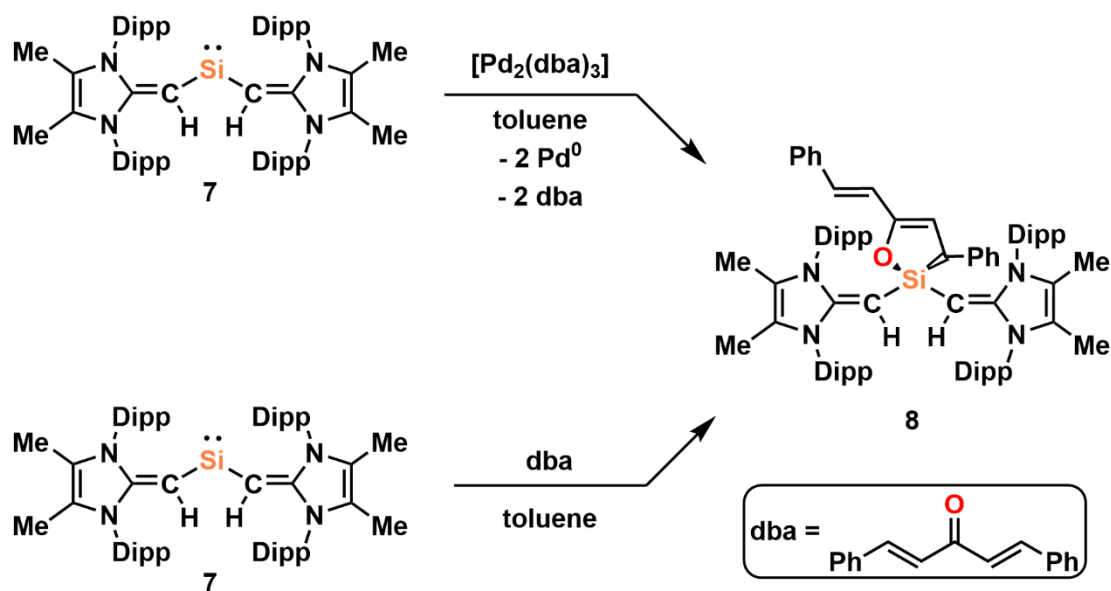


Combining analytically pure $^{\text{Me}}\text{IPr}\cdot\text{SiBr}_2$ (**6**) with $[(^{\text{Me}}\text{IPrCH})\text{Li}]_2$ (**2**) in toluene afforded the target acyclic divinylsilylene $(^{\text{Me}}\text{IPrCH})_2\text{Si}$: (**7**) as a deep-yellow solid in a yield of 27 %. I then turned my attention towards the preparation of silylene d^{10} metal complexes by combining **7** with $\text{Ni}(\text{COD})_2$ (COD = 1,5-cyclooctadiene), $\text{Pd}(\text{P}^t\text{Bu}_3)_2$ and $\text{Pt}(\text{P}^t\text{Bu}_3)_2$. Unfortunately, these attempts did not afford any discernable metal-silylene complexation, even upon heating the reaction mixtures to 55 °C for three days (Scheme 2.3). This may be due to the sterically demanding nature of the supporting Dipp groups of the aNHO preventing the metal centers from interacting with the Si(II) center.



Scheme 2.3. a) Synthesis of the divinylsilylene $(^{\text{Me}}\text{IPrCH})_2\text{Si}$: (**7**); b) Attempted synthesis of silylene d^{10} complexes.

Interestingly, when $(^{\text{Me}}\text{IPrCH})_2\text{Si}$: (**7**) was combined with one equivalent of $[\text{Pd}_2(\text{dba})_3]$ (dba = dibenzylideneacetone) in toluene, a black precipitate formed and the deep-yellow color of the silylene was slowly consumed to afford a pale-yellow solution. Upon removal of the precipitate by filtration and crystallization from a concentrated pentane solution stored at $-35\text{ }^\circ\text{C}$, it was determined by X-ray crystallographic analysis that **7** had undergone a [4+1] cycloaddition with one of the dibenzylideneacetone ligands to afford the silane $(^{\text{Me}}\text{IPrCH})_2\text{Si}(\text{dba})$ (**8**) (Figure 2.4). $(^{\text{Me}}\text{IPrCH})_2\text{Si}(\text{dba})$ (**8**) was then prepared by an independent reaction between **7** and dba in toluene, which upon work-up afforded **8** in a yield of 27% as pale-yellow crystalline solid after recrystallization from pentane (Scheme 2.4). This reaction highlights the dual electrophilic/nucleophilic character of the Si(II) center in **7**.



Scheme 2.4. The synthesis of $(^{\text{Me}}\text{IPrCH})_2\text{Si}(\text{dba})$ (**8**).

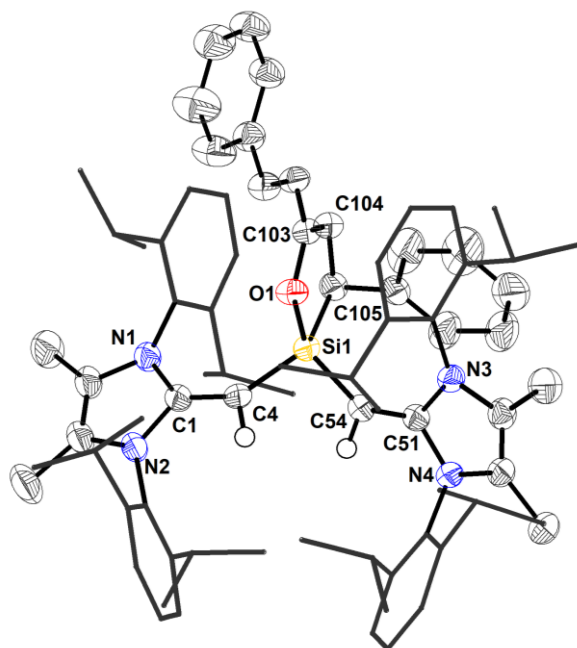


Figure 2.4. Molecular structure of $(^{\text{Me}}\text{IPrCH})_2\text{Si}(\text{dba})$ (**8**) with thermal ellipsoids plotted at 50 % probability. All hydrogen atoms (except for the vinylic hydrogen atoms at C4 and C51) are omitted for clarity; Dipp groups are shown as wireframes. Selected bond lengths [\AA] and bond angles [$^\circ$]: C1–C4 1.394(5), C4–Si1 1.805(4), C51–C54 1.380(5), C54–Si1 1.805(4), Si1–O1 1.700(3), Si1–C105 1.926(4), O1–C103 1.379(4), C103–C104 1.335(5), C104–C105 1.515(5); C1–C4–Si1 145.5(3), C4–Si1–C54 100.57(16), C51–C54–Si1 143.5(3), C4–Si1–O1 113.14(15), C54–Si1–O1 111.97(16), C4–Si1–C105 118.27(17), C54–Si1–C105 120.10(17), O1–Si1–C105 93.35(15), Si1–O1–C103 112.3(2), Si1–C105–C104 100.7(2), O1–C103–C104 117.3(3), C103–C104–C105 116.3(3).

2.3 Conclusions

This Chapter describes the completion of a complete acyclic divinyl tetrelene series stabilized by sterically-demanding anionic NHO ligands, and the development of a new anionic NHO synthon, $[(^{\text{Me}}\text{IPrCH})\text{Li}]$ (**2**) which could be accessed by lithium-halogen exchange from the new iodinated *N*-heterocyclic olefin $^{\text{Me}}\text{IPrCH}(\text{I})$ (**1**). The completion of the tetrelene series required the development of a convenient synthetic route to $^{\text{Me}}\text{IPr}\cdot\text{SiBr}_2$ (**6**), which was shown to be a viable Si(II) precursor *via* halogen substitution to afford the first

acyclic two-coordinate diorganosilylene ($^{\text{Me}}\text{IPrCH})_2\text{Si}$: (**7**). It was found that this species exhibits both nucleophilic and electrophilic character, as demonstrated by its [4+1] cycloaddition reactivity with dibenzylideneacetone (dba) to afford ($^{\text{Me}}\text{IPrCH})_2\text{Si}(\text{dba})$ (**8**).

2.4 Experimental Details

2.4.1 General Considerations

All reactions were performed using Schlenk and glovebox (Innovative Technology, Inc.) techniques under a nitrogen atmosphere. All solvents were purified using a Grubbs-type solvent purification system²⁰ manufactured by Innovative Technology, Inc., degassed (freeze–pump–thaw method), and stored under an atmosphere of nitrogen prior to use. $\text{K}[\text{N}(\text{SiMe}_3)_2]$, PbBr_2 , $n\text{BuLi}$ (2.5 M solution in hexanes), $i\text{PrI}$ and I_2 were purchased from Sigma-Aldrich and used as received. SiBr_4 was purchased from Alfa Aesar and used as received. $^{\text{Me}}\text{IPr}$,²¹ $^{\text{Me}}\text{IPrCH}_2$,^{12b} $[\text{K}(\text{THF})_2][\text{Si}(\text{SiMe}_3)_3]$,¹⁹ 2,4,6-trimethylimidazole,¹⁵ and dibenzylideneacetone (dba)²² were prepared according to literature procedures [$^{\text{Me}}\text{IPr} = (\text{MeCNDipp})_2\text{C}$; Dipp = 2,6- $i\text{Pr}_2\text{C}_6\text{H}_3$]. ^1H , $^{13}\text{C}\{^1\text{H}\}$, $^7\text{Li}\{^1\text{H}\}$, and $^{207}\text{Pb}\{^1\text{H}\}$ NMR spectra were recorded on 400, 500, 600 or 700 MHz Varian Inova instruments and were referenced externally to SiMe_4 (^1H , $^{13}\text{C}\{^1\text{H}\}$), 9.7 M solution of LiCl in D_2O (^7Li) and PbMe_4 (^{207}Pb). Elemental analyses were performed by the Analytical and Instrumentation Laboratory at the University of Alberta using a Thermo Flash 2000 Elemental Analyzer. Melting points were measured in sealed glass capillaries under nitrogen with a MelTemp apparatus and are uncorrected.

2.4.2 Synthetic Procedures

Synthesis of ^{Me}IPrCH(I) (1): A solution of I₂ (1.153 g, 4.543 mmol) in 60 mL of THF was added *via* cannula to a solution of ^{Me}IPrCH₂ (1.997 g, 4.637 mmol) in 150 mL of THF, resulting in the immediate formation of a yellow solid. The mixture was then stirred for a further 40 minutes. *After this point, all manipulations were performed in the absence of ambient light.* A solution of K[N(SiMe₃)₂] (0.920 g, 4.61 mmol) in 40 mL of THF was added *via* cannula to the mixture, the resulting mixture was stirred for 1 hour, followed by removal of the volatiles *in vacuo*. The solid residue was extracted with 100 mL of hexanes and filtered through a frit packed with a 1 cm plug of diatomaceous earth. The resulting dark-yellow filtrate was concentrated to a volume of 15 mL and placed in a -35 °C freezer for 16 hours, which afforded bright-yellow crystals of ^{Me}IPrCH(I) (1) (1.127 g). The mother liquor was then concentrated to half of its original volume and placed in a -35 °C freezer for 16 hours, yielding a second crop of crystals of 1 (0.326 g; combined yield = 57 %). X-ray quality crystals of 1 were obtained from a concentrated hexanes solution stored in a -35 °C freezer for one week. ¹H NMR (400 MHz, C₆D₆): δ 7.32 (t, 1H, ³J_{HH} = 7.6 Hz, *p*-ArH), 7.17–7.22 (m, 3H, *p*- and *m*-ArH), 7.10 (d, 2H, ³J_{HH} = 7.6 Hz, *m*-ArH), 3.24 (sept, 2H, ³J_{HH} = 6.8 Hz, CH(CH₃)₂), 3.13 (sept, 2H, ³J_{HH} = 6.8 Hz, CH(CH₃)₂), 2.25 (s, 1H, =CH(I)), 1.59 (d, 6H, ³J_{HH} = 6.8 Hz, CH(CH₃)₂), 1.52 (s, 3H, NCCH₃), 1.46 (s, 3H, NCCH₃), 1.34 (d, 6H, ³J_{HH} = 6.8 Hz, CH(CH₃)₂), 1.19 (d, 6H, ³J_{HH} = 6.8 Hz, CH(CH₃)₂), 1.16 (d, 6H, ³J_{HH} = 6.8 Hz, CH(CH₃)₂). ¹³C {¹H} NMR (176 MHz, C₆D₆): δ 149.3 (ArC), 149.2 (ArC), 145.6 (NCN), 133.0 (ArC), 132.5 (ArC), 129.8 (ArC), 129.7 (ArC), 124.7 (ArC), 123.8 (ArC), 117.0 (NC-CH₃), 116.6 (NC-CH₃), 29.1 (CH(CH₃)₂), 28.9 (CH(CH₃)₂), 24.8 (CH(CH₃)₂), 24.3 (CH(CH₃)₂), 23.9

(CH(CH₃)₂), 9.4 (NC-CH₃), 9.3 (NC-CH₃), -7.1 (CHI). Anal. Calcd. for C₃₀H₄₁IN₂ (%): C 64.74, H 7.43, N 5.03; Found: C 64.89, H 7.45, N 4.86. M.p. 150 °C (decomp.).

Synthesis of [(^{Me}IPrCH)Li] (2): A 2.5 M solution of ⁿBuLi in hexanes (208 μL, 0.52 mmol) was added to a solution of ^{Me}IPrCH(I) (1) (0.289 g, 0.519 mmol) dissolved in 4 mL of hexanes. After two minutes of stirring, the solution began to turn a bright orange-red. After a further 20 minutes an orange-red solid began to precipitate from the solution. The mixture was placed in a -35 °C freezer for 16 hours after which the mother liquor was decanted from the resulting precipitate and the remaining solid dried *in vacuo* affording [(^{Me}IPrCH)Li]₂ (2) as a bright orange-red solid (0.185 g, 82 %). X-ray quality crystals of 2 were obtained from a concentrated hexanes solution stored in a -35 °C for 10 days. *Compound 2 slowly decomposes at room temperature, even when stored in an inert atmosphere in the solid state. As such, batches of 2 were always stored as a solid at -35 °C in a glovebox.* ¹H NMR (400 MHz, C₆D₆): δ 7.39 (t, 2H, ³J_{HH} = 8.0 Hz, *p*-ArH), 7.32 (d, 4H, ³J_{HH} = 8.0 Hz, *m*-ArH), 7.04 (d, 4H, ³J_{HH} = 8.0 Hz, *m*-ArH), 6.87 (t, 2H, ³J_{HH} = 8.0 Hz, *p*-ArH), 3.13–3.40 (overlapping multiplets, CH(CH₃)₂), 1.66 (s, 6H, NC-CH₃), 1.64 (s, 6H, NC-CH₃), 1.39 (d, 12H, ³J_{HH} = 7.0 Hz, CH(CH₃)₂), 1.31 (d, 12H, ³J_{HH} = 7.0 Hz, CH(CH₃)₂), 1.30 (d, 12H, ³J_{HH} = 7.0 Hz, CH(CH₃)₂), 1.10 (d, 12H, ³J_{HH} = 7.0 Hz, CH(CH₃)₂), 0.87 (broad s, 2H, CHLi). ¹³C{¹H} NMR (176 MHz, C₆D₆): δ 159.0 (NCN), 150.5 (ArC), 150.4 (ArC), 136.6 (ArC), 136.0 (ArC), 129.4 (ArC), 128.3 (ArC), 126.0 (ArC), 123.7 (ArC), 115.6 (NCCH₃), 113.6 (NCCH₃), 69.7 (broad, C=CH), 28.7 (CH(CH₃)₂), 28.5 (CH(CH₃)₂), 25.4 (CH(CH₃)₂), 24.5 (CH(CH₃)₂), 24.3 (CH(CH₃)₂), 23.9 (CH(CH₃)₂), 10.3 (NCCH₃), 10.1 (NCCH₃). ⁷Li{¹H} NMR (194 MHz, C₆D₆): δ 1.0 (s). Anal. Calcd. for C₆₀H₈₂N₄Li₂ (%): C 82.53, H 9.47, N 6.42; Found: C 80.26, H 9.25, N 6.11. M.p. 188–190 °C.

Synthesis of ImMe₂ⁱPr₂CH₂ (3): To a solution of [ImMe₂ⁱPr₂-CH₃]I (4) (0.164 g, 0.510 mmol) in 4 mL of THF was added a solution of K[N(SiMe₃)₂] (0.102 g, 0.509 mmol) in 4 mL of THF. Upon addition of K[N(SiMe₃)₂] a white precipitate was observed. After stirring the reaction mixture for an additional 2 hours the volatiles were removed *in vacuo* to afford a brown residue. The product was combined with 10 mL of toluene and the extract filtered through diatomaceous earth to yield an orange filtrate. The solvent was removed from the filtrate *in vacuo* to give ImMe₂ⁱPr₂CH₂ (3) as a spectroscopically pure dark-brown oil (0.076 g, 77 %). ¹H NMR (700 MHz, C₆D₆): δ 3.89 (sept, 2H, ³J_{HH} = 7.0 Hz, CH(CH₃)₂), 2.98 (s, 2H, C=CH₂), 1.66 (s, 6H, NC(CH₃)), 1.23 (d, 12H, ³J_{HH} = 7.0 Hz, CH(CH₃)₂). ¹³C{¹H} NMR (176 MHz, C₆D₆): δ 128.1 (NCN), 114.8 (NC(CH₃)), 45.8 (CH(CH₃)₂), 43.2 (C=CH₂), 19.5 (CH(CH₃)₂), 10.1 (NC(CH₃)). Anal. Calcd. for C₁₂H₂₂N₂ (%): C 74.17, H 11.41, N 14.42; Found: C 73.40, H 11.38, N 14.15.

Synthesis of [ImMe₂ⁱPr₂-CH₃]I (4): 2,4,5-Trimethylimidazole (2.595 g, 23.56 mmol) and K₂CO₃ (7.243 g, 52.41 mmol) were dissolved in 30 mL of acetonitrile and the mixture was heated to reflux for 2 hours. The reaction mixture was allowed to cool to room temperature, and then ⁱPrI (6.0 mL, 60 mmol) was added. The reaction mixture was then heated to reflux again for another 48 hours, cooled to room temperature, and the volatiles removed under vacuum. The resulting product was then combined with 200 mL of CH₂Cl₂ and the extract filtered; the remaining solid from the filtration was washed with another 50 mL of CH₂Cl₂ and the organic layers combined. The solvent was then removed from the combined CH₂Cl₂ extracts under vacuum to give a black oil. This oil was triturated with 500 mL of Et₂O to yield [ImMe₂ⁱPr₂-CH₃]I (4) as a light-brown solid, which was isolated by filtration and dried (2.520

g, 33 %). ^1H NMR (700 MHz, CD_3CN): δ 4.70 (sept, 2H, $^3J_{\text{HH}} = 7.0$ Hz, $\text{CH}(\text{CH}_3)_2$), 2.65 (s, 3H, $\text{ImMe}_2^i\text{Pr}_2\text{-CH}_3$), 2.26 (s, 6H, $-\text{NC}(\text{CH}_3)$), 1.51 (d, 12H, $^3J_{\text{HH}} = 7.0$ Hz, $\text{CH}(\text{CH}_3)_2$). $^{13}\text{C}\{^1\text{H}\}$ NMR (176 MHz, CD_3CN): δ 142.4 (NCN), 126.6 (NC(CH₃)), 51.3 ($\text{ImMe}_2^i\text{Pr}_2\text{-CH}_3$), 21.3 ($\text{CH}(\text{CH}_3)_2$), 13.0 ($\text{CH}(\text{CH}_3)_2$), 10.3 (NC(CH₃)). Anal. Calcd. for $\text{C}_{12}\text{H}_{23}\text{IN}_2$ (%): C 44.73, H 7.19, N 8.69; Found: C 44.49, H 7.04, N 8.46. M.p. 135–137 °C.

Synthesis of $(^{\text{Me}}\text{IPrCH})_2\text{Pb}$: (5): A solution of $[(^{\text{Me}}\text{IPrCH})\text{Li}]_2$ (0.067 g, 0.076 mmol) in 4 mL of Et_2O was added to a slurry of PbBr_2 (0.033 g, 0.090 mmol) in 1 mL of Et_2O . After stirring for 1 minute, the resulting mixture had turned a deep blue. After stirring for an additional 20 minutes, the volatiles were removed *in vacuo*, the residue extracted with 4 mL of hexanes and filtered. The filtrate was concentrated to 2 mL and placed in a -30 °C freezer for one week. The mother liquor was decanted from the crystals and the product was dried *in vacuo* affording $(^{\text{Me}}\text{IPrCH})_2\text{Pb}$: (5) as a deep-blue crystalline solid (0.047 g, 49 %). ^1H NMR (700 MHz, C_6D_6): δ 7.35 (t, 2H, $^3J_{\text{HH}} = 8.0$ Hz, *p*-ArH), 7.24 (s, 2H, *CHPb*), 7.20 (t, 2H, $^3J_{\text{HH}} = 8.0$ Hz, *p*-ArH), 7.17 (d, 4H, $^3J_{\text{HH}} = 8.0$ Hz, *m*-ArH), 7.14 (d, 4H, $^3J_{\text{HH}} = 8.0$ Hz), 3.24 (sept, 4H, $^3J_{\text{HH}} = 7.0$ Hz, $\text{CH}(\text{CH}_3)_2$), 3.08 (sept, 4H, $^3J_{\text{HH}} = 7.0$ Hz, $\text{CH}(\text{CH}_3)_2$), 1.61 (s, 12H, NC-CH₃), 1.27 (d, 12H, $^3J_{\text{HH}} = 7.0$ Hz, $\text{CH}(\text{CH}_3)_2$), 1.22 (d, 12H, $^3J_{\text{HH}} = 7.0$ Hz, $\text{CH}(\text{CH}_3)_2$), 1.16 (d, 12H, $^3J_{\text{HH}} = 7.0$ Hz, $\text{CH}(\text{CH}_3)_2$), 1.15 (d, 12H, $^3J_{\text{HH}} = 7.0$ Hz, $\text{CH}(\text{CH}_3)_2$). $^{13}\text{C}\{^1\text{H}\}$ NMR (176 MHz, C_6D_6): δ 160.3 (NCN), 149.2 (ArC), 148.4 (ArC), 135.0 (ArC), 133.6 (ArC), 129.3 (ArC), 128.7 (ArC), 125.5 (ArC), 124.1 (ArC), 116.9 (NCCH₃), 116.7 (NCCH₃), 28.8 ($\text{CH}(\text{CH}_3)_2$), 28.7 ($\text{CH}(\text{CH}_3)_2$), 24.9 ($\text{CH}(\text{CH}_3)_2$), 24.9 ($\text{CH}(\text{CH}_3)_2$), 24.1 ($\text{CH}(\text{CH}_3)_2$), 24.0 ($\text{CH}(\text{CH}_3)_2$), 9.9 (NCCH₃), 9.6 (NCCH₃). *The vinylic carbon resonance was not located.* $^{207}\text{Pb}\{^1\text{H}\}$ NMR (84 MHz, [*d*₈]-toluene, 0 °C): δ 5449 (s). Anal. Calcd. for $\text{C}_{60}\text{H}_{82}\text{N}_4\text{Pb}$ (%): C 67.57, H 7.75, N

5.25; Found: C 67.31, H 7.87, N 5.14. M.p. 85 °C (decomp.). *Compound 5 is thermally unstable in both solution and in the solid state at room temperature.*

Synthesis of ^{Me}IPr•SiBr₂ (6): To a vial containing solution of ^{Me}IPr (0.147 g, 0.353 mmol) in 5 mL of THF was added a solution of [K(THF)₂][Si(SiMe₃)₃] (0.152 g, 0.353 mmol) in 3 mL of THF followed by the rapid addition of SiBr₄ (44.0 μL, 0.353 mmol). Upon the addition of SiBr₄, the formation of a white precipitate was observed. The reaction mixture was stirred for 1 hour and filtered through diatomaceous earth affording an orange filtrate. The volatiles were removed from the filtrate *in vacuo* and the resultant residue was washed with 2 × 2 mL of cold (−35 °C) hexanes affording **6** as an orange powder (0.131 g, 61 %). ¹H and ¹³C{¹H} NMR spectra match those reported in the literature.¹⁷

Synthesis of (^{Me}IPrCH)₂Si: (7): A solution of [(^{Me}IPrCH)Li]₂ (0.204 g, 0.234 mmol) in 4 mL of toluene was added to a vial containing a slurry of ^{Me}IPr•SiBr₂ (0.142 g, 0.235 mmol) in 1 mL of toluene. Upon addition of **2**, the reaction mixture turned a dark yellow-brown. After stirring for 15 minutes, the volatiles of the mixture were removed *in vacuo*, the residue was extracted with 5 mL of hexanes and filtered. The dark yellow-brown filtrate was concentrated to a volume of 2 mL and placed in a -35 °C freezer overnight. The resulting bulk crystals were separated from the mother liquor and dried *in vacuo* affording (^{Me}IPrCH)₂Si: (**7**) as a dark-yellow crystalline solid (0.057 g, 27 %). ¹H NMR (700 MHz, C₆D₆): δ 7.30 (t, 2H, ³J_{HH} = 8.0 Hz, *p*-ArH), 7.25 (t, 2H, ³J_{HH} = 8.0 Hz, *p*-ArH), 7.09–7.13 (m, 8H, *m*-ArH), 4.25 (s, 2H, CHSi), 3.11 (sept, 4H, ³J_{HH} = 7.0 Hz, CH(CH₃)₂), 2.96 (sept, 4H, ³J_{HH} = 7.0 Hz, CH(CH₃)₂), 1.62 (s, 6H, NC-CH₃), 1.54 (s, 6H, NC-CH₃), 1.32 (d, 12H, ³J_{HH} = 7.0 Hz, CH(CH₃)₂), 1.23 (d, 12H,

$^3J_{\text{HH}} = 7.0$ Hz, $\text{CH}(\text{CH}_3)_2$), 1.17 (d, 12H, $^3J_{\text{HH}} = 7.0$ Hz, $\text{CH}(\text{CH}_3)_2$), 1.14 (d, 12H, $^3J_{\text{HH}} = 7.0$ Hz, $\text{CH}(\text{CH}_3)_2$). $^{13}\text{C}\{^1\text{H}\}$ NMR (176 MHz, C_6D_6): δ 158.1 (NCN), 148.8 (ArC), 147.7 (ArC), 134.9 (ArC), 132.9 (ArC), 129.2 (ArC), 128.9 (ArC), 124.8 (ArC), 123.9 (ArC), 118.3 (NCCH₃), 116.9 (NCCH₃), 100.0 (C=CH), 28.9 ($\text{CH}(\text{CH}_3)_2$), 28.8 ($\text{CH}(\text{CH}_3)_2$), 24.5 ($\text{CH}(\text{CH}_3)_2$), 23.8 ($\text{CH}(\text{CH}_3)_2$), 9.8 (NCCH₃), 9.3 (NCCH₃). $^{29}\text{Si}\{^1\text{H}\}$ NMR (79 MHz, C_6D_6): δ 271.9 (s). Anal. Calcd. for $\text{C}_{60}\text{H}_{82}\text{N}_4\text{Si}$ (%): C 81.21, H 9.31, N 6.31; Found: C 80.20, H 9.77, N 5.69. M.p. 155–157 °C (decomp.).

Synthesis of (^{Me}IPrCH)₂Si(dba) (8): To a solution of (^{Me}IPrCH)₂Si: (0.035 g, 0.039 mmol) in 1 mL of toluene was added a solution of dibenzylideneacetone (dba) (0.009 g, 0.04 mmol) in 1 mL of toluene. After five minutes of stirring the reaction mixture turned light-yellow. After an additional 25 minutes of stirring the volatiles were removed *in vacuo* to afford a yellow residue. The product was extracted with 2 mL of pentane and filtered. The light-yellow filtrate was concentrated to a volume of *ca.* 1 mL and placed in a -35 °C freezer for 16 hours to afford (^{Me}IPrCH)₂Si(dba) (8) as a yellow crystalline solid (0.012 g, 27 %). X-ray quality crystals were obtained by dissolving 8 in 1 mL of pentane and storing in a -35 °C freezer for one week. ^1H NMR (700 MHz, C_6D_6): δ 7.56 (d, 2H, $^3J_{\text{HH}} = 7.4$ Hz, *o*-Ph), 7.42 (d, 2H, $^3J_{\text{HH}} = 7.7$ Hz, *o*-Ph*H*), 7.33–7.36 (m, 3H, *m*-Ph*H* and *p*-Ph*H*), 7.27–7.31 (m, 3H, *m*-Ph*H* and *p*-Ph*H*), 7.21 (dd, 1H, $^3J_{\text{HH}} = 7.7$, 1.2 Hz, *p*-Dipp*H*), 7.14–7.19 (m, 2H, *m*-Dipp*H*), 7.08–7.13 (m, 2H, *m*-Dipp*H*), 7.10–7.12 (m, 4H, *m*-Dipp*H*), 7.01 (dd, 1H, $^3J_{\text{HH}} = 7.7$, 1.2 Hz, *p*-Dipp*H*), 6.97 (dd, 1H, $^3J_{\text{HH}} = 7.7$, 1.2 Hz, *p*-Dipp*H*), 6.93 (dd, 1H, $^3J_{\text{HH}} = 7.6$, 1.1 Hz, *p*-Dipp*H*), 6.12 (d, 1H, $^3J_{\text{HH}} = 15.8$ Hz, Ph(H)C=C(H)CO), 5.85 (d, 1H, $^3J_{\text{HH}} = 15.8$ Hz, Ph(H)C=C(H)CO), 4.63 (d, 1H, $^3J_{\text{HH}} = 3.1$ Hz, OC=C(H)), 3.17–3.23 (m, 3H, $\text{CH}(\text{CH}_3)_2$), 3.10–3.13 (m, 2H,

$CH(CH_3)_2$ 3.02 (sept, 1H, $^3J_{HH} = 7.0$ Hz, $CH(CH_3)_2$), 2.93 (sept, 1H, $^3J_{HH} = 7.0$ Hz, $CH(CH_3)_2$), 2.84 (sept, 1H, $^3J_{HH} = 7.0$ Hz, $CH(CH_3)_2$), 2.56 (br, 1H, SiCH(Ph)), 2.27 (s, 1H, SiCH(NHC)), 1.67 (s, 1H, SiCH(NHC)), 1.61 (d, 3H, $^3J_{HH} = 7.0$ Hz, $CH(CH_3)_2$), 1.45 (d, 3H, $^3J_{HH} = 7.0$ Hz, $CH(CH_3)_2$), 1.43 (d, 3H, $^3J_{HH} = 7.0$ Hz, $CH(CH_3)_2$), 1.41 (s, 3H, CH_3), 1.36 (s, 3H, CH_3), 1.35 (s, 3H, CH_3), 1.25 (d, 3H, $^3J_{HH} = 7.0$ Hz, $CH(CH_3)_2$), 1.22 (d, 3H, $^3J_{HH} = 7.0$ Hz, $CH(CH_3)_2$), 1.21 (d, 3H, $^3J_{HH} = 7.0$ Hz, $CH(CH_3)_2$), 1.20 (s, 3H, CH_3), 1.19 (d, 3H, $^3J_{HH} = 7.0$ Hz, $CH(CH_3)_2$), 1.18 (d, 3H, $^3J_{HH} = 7.0$ Hz, $CH(CH_3)_2$), 1.09 (d, 3H, $^3J_{HH} = 7.0$ Hz, $CH(CH_3)_2$), 1.06 (d, 3H, $^3J_{HH} = 7.0$ Hz, $CH(CH_3)_2$), 1.02 (d, 6H, $^3J_{HH} = 7.0$ Hz, $CH(CH_3)_2$), 1.01 (d, 3H, $^3J_{HH} = 7.0$ Hz, $CH(CH_3)_2$), 0.97 (d, 3H, $^3J_{HH} = 7.0$ Hz, $CH(CH_3)_2$), 0.88 (d, 3H, $^3J_{HH} = 7.0$ Hz, $CH(CH_3)_2$), 0.80 (d, 3H, $^3J_{HH} = 7.0$ Hz, $CH(CH_3)_2$). $^{13}C\{^1H\}$ NMR (176 MHz, C_6D_6): δ 154.4 (NC(CHSi)N), 154.4 (NC(CHSi)N), 154.2 (CO), 149.1 (CCH(CH_3) $_2$), 149.0 (CCH(CH_3) $_2$), 148.8 (CCH(CH_3) $_2$), 148.6 (CCH(CH_3) $_2$), 148.4 (CCH(CH_3) $_2$), 147.8 (CCH(CH_3) $_2$), 147.7 (CCH(CH_3) $_2$), 147.3 (CCH(CH_3) $_2$), 145.7 (*ipso*-C_{Ph}), 139.2 (*ipso*-C_{Ph}), 135.4 (*ipso*-C_{Dipp}), 135.1 (*ipso*-C_{Dipp}), 133.6 (*ipso*-C_{Dipp}), 133.4 (*ipso*-C_{Dipp}), 130.2 (C_{Ph}), 129.3 (C_{Ph}), 129.2 (C_{Ph}), 129.1 (C_{Ph}), 129.0 (C_{Ph}), 128.9 (C_{Ph}), 128.5 (C_{Ph}), 128.2 (C_{Ph}), 127.6 (PhC(H)=C(H)CO), 127.5 (C_{Dipp}), 126.6 (C_{Dipp}), 126.5 (C_{Ph}), 126.1 (C_{Ph}), 125.8 (C_{Dipp}), 124.8 (C_{Dipp}), 124.7 (C_{Dipp}), 124.6 (C_{Dipp}), 124.5 (C_{Dipp}), 124.4 (C_{Dipp}), 124.3 (C_{Dipp}), 124.2 (C_{Dipp}), 124.1 (PhC(H)=C(H)CO), 123.9 (C_{Dipp}), 123.7 (C_{Dipp}), 118.2 (H₃CC=CCH₃), 118.0 (H₃CC=CCH₃), 117.2 (H₃CC=CCH₃), 117.1 (H₃CC=CCH₃), 111.2 (OC=C(H)), 53.9 (SiCH(NHC)), 49.2 (SiCH(NHC)), 38.9 (SiCH(Ph)), 29.1 ($CH(CH_3)_2$), 28.79 ($CH(CH_3)_2$), 28.77 ($CH(CH_3)_2$), 28.74 ($CH(CH_3)_2$), 28.70 ($CH(CH_3)_2$), 28.6 ($CH(CH_3)_2$), 28.5 ($CH(CH_3)_2$), 28.4 ($CH(CH_3)_2$), 25.9 ($CH(CH_3)_2$), 25.7 ($CH(CH_3)_2$), 25.5 ($CH(CH_3)_2$), 24.8 ($CH(CH_3)_2$), 24.7 ($CH(CH_3)_2$), 24.5 ($CH(CH_3)_2$), 24.5 ($CH(CH_3)_2$), 24.4 ($CH(CH_3)_2$), 24.2 ($CH(CH_3)_2$),

24.03 (CH(CH₃)₂), 24.99 (CH(CH₃)₂), 23.95 (CH(CH₃)₂), 23.8 (CH(CH₃)₂), 23.5 (CH(CH₃)₂), 23.3 (CH(CH₃)₂), 22.7 (CH(CH₃)₂), 10.4 (NCCH₃), 10.2 (NCCH₃), 10.06 (NCCH₃), 10.05 (NCCH₃). Anal. Calcd. for C₇₇H₉₆N₄OSi (%): C 82.45, H 8.63, N 4.99; Found: C 81.33, H 8.19, N 4.05. M.p. 229–232 °C.

2.4.3 X-Ray Crystallography

Appropriate X-ray quality crystals were coated with a small amount of hydrocarbon oil (Paratone-N) and removed from the glovebox in a vial. Crystals were mounted quickly onto a glass fiber and placed in a low temperature stream of nitrogen on the X-ray diffractometer. All data were collected using a Bruker APEX II CCD detector/D8 or PLATFORM diffractometer using Mo K α (0.71073 Å) or Cu K α (1.54178 Å) radiation, with the crystals cooled to -80 °C or -100 °C. The data were corrected for absorption through Gaussian integration from the indexing of crystal faces.²³ Crystal structures were solved using intrinsic phasing (SHELXT)²⁴ and refined using SHELXL-2014.²⁵ The assignment of hydrogen atom positions is based on the sp²- or sp³- hybridization geometries of their attached carbon atoms and were given thermal parameters 20 % greater than those of their parent atoms.

Table 2.1. X-ray crystallographic data details for ^{Me}IPrCH(I) (**1**).*A. Crystal Data*

formula	C ₃₀ H ₄₁ IN ₂
formula weight	556.55
crystal color and habit ^a	colorless fragment
crystal dimensions (mm)	0.32 × 0.23 × 0.17
crystal system	triclinic
space group	<i>P</i> $\bar{1}$ (No. 2)]
unit cell parameters ^a	
<i>a</i> (Å)	9.0297(18)
<i>b</i> (Å)	9.5889(19)
<i>c</i> (Å)	18.373(4)
α (deg)	84.60(3)
β (deg)	86.53(3)
γ (deg)	64.76(3)
<i>V</i> (Å ³)	1432.2(6)
<i>Z</i>	2
ρ _{calcd} (g cm ⁻³)	1.291
μ (mm ⁻¹)	8.905

B. Data Collection and Refinement Conditions

diffractometer	Bruker D8/APEX II CCD ^b
radiation (λ [Å])	Cu Kα (1.54178) (microfocus source)
temperature (°C)	-100
scan type	ω and φ scans (1.0°) (5-5-10 s exposures) ^c
data collection 2θ limit (deg)	149.66
total data collected	5579 (-11 ≤ <i>h</i> ≤ 11, -11 ≤ <i>k</i> ≤ 11, 0 ≤ <i>l</i> ≤ 22)
independent reflections	5579 (<i>R</i> _{int} = 0.0537)
number of observed reflections (<i>NO</i>)	5406 [<i>F</i> _o ² ≥ 2σ(<i>F</i> _o ²)]
structure solution method	intrinsic phasing (<i>SHELXT-2014</i> ^d)
refinement method	full-matrix least-squares on <i>F</i> ² (<i>SHELXL-2017</i> ^e)
absorption correction method	Gaussian integration (face-indexed)
range of transmission factors	0.1340–0.0329
data/restraints/parameters	5579 / 0 / 309
goodness-of-fit (<i>S</i>) ^f [all data]	1.039
final <i>R</i> indices ^g	
<i>R</i> ₁ [<i>F</i> _o ² ≥ 2σ(<i>F</i> _o ²)]	0.0420
<i>wR</i> ₂ [all data]	0.1168
largest difference peak and hole	2.764 and -0.705 e Å ⁻³

^aObtained from least-squares refinement of 9883 reflections with $4.82^\circ < 2\theta < 148.68^\circ$.

^bPrograms for diffractometer operation, data collection, data reduction and absorption correction were those supplied by Bruker. The crystal used for data collection was found to display non-merohedral twinning. Both components of the twin were indexed with the program *CELL_NOW* (Bruker AXS Inc., Madison, WI, 2004). The second twin component can be related to the first component by 179.9° rotation about the [0.499 1.000 0.000] axis in real space and about the [0.144 1 -0.053] axis in reciprocal space. Integrated intensities for the reflections from the two components were written into a *SHELXL-2014* HKLF 5 reflection file with the data integration program *SAINTE* (version 8.38A), using all reflection data (exactly overlapped, partially overlapped and non-overlapped). The refined value of the twin fraction (*SHELXL-2014* BASF parameter) was 0.18486.

^cData were collected with the detector set at three different positions. Low-angle (detector $2\theta = -33^\circ$) data frames were collected using a scan time of 5 s, medium-angle (detector $2\theta = 75^\circ$) frames using a scan time of 5 s, and high-angle (detector $2\theta = 117^\circ$) frames using a scan time of 10 s.

^dG. M. Sheldrick, *Acta Crystallogr.* **2015**, *A71*, 3–8. (*SHELXT-2014*)

^eG. M. Sheldrick, *Acta Crystallogr.* **2015**, *C71*, 3–8. (*SHELXL-2017*)

$fS = [\sum w(F_o^2 - F_c^2)^2 / (n - p)]^{1/2}$ (n = number of data; p = number of parameters varied; $w = [\sigma^2(F_o^2) + (0.0672P)^2 + 1.6197P]^{-1}$ where $P = [\text{Max}(F_o^2, 0) + 2F_c^2]/3$).

$gR_1 = \sum ||F_o| - |F_c|| / \sum |F_o|$; $wR_2 = [\sum w(F_o^2 - F_c^2)^2 / \sum w(F_o^4)]^{1/2}$.

Table 2.2. X-ray crystallographic data details for (^{Me}IPrCH)₂Si(dba) (**8**).*A. Crystal Data*

formula	C ₇₇ H ₉₆ N ₄ OSi
formula weight	1121.66
crystal color and habit ^a	yellow fragment
crystal dimensions (mm)	0.17 × 0.08 × 0.04
crystal system	orthorhombic
space group	<i>P</i> 2 ₁ 2 ₁ 2 ₁ (No. 19)
unit cell parameters ^a	
<i>a</i> (Å)	12.6733(4)
<i>b</i> (Å)	22.4008(7)
<i>c</i> (Å)	23.4422(7)
<i>V</i> (Å ³)	6655.1(4)
<i>Z</i>	4
ρ_{calcd} (g cm ⁻³)	1.119
μ (mm ⁻¹)	0.658

B. Data Collection and Refinement Conditions

diffractometer	Bruker D8/APEX II CCD ^b
radiation (λ [Å])	Cu K α (1.54178) (microfocus source)
temperature (°C)	-100
scan type	ω and ϕ scans (1.0°) (5-10-15 s exposures) ^c
data collection 2θ limit (deg)	142.02
total data collected	113027 ($-15 \leq h \leq 15$, $-27 \leq k \leq 26$, $-27 \leq l \leq 24$)
independent reflections	12607 ($R_{\text{int}} = 0.0877$)
number of observed reflections (<i>NO</i>)	9854 [$F_o^2 \geq 2\sigma(F_o^2)$]
structure solution method	intrinsic phasing (<i>SHELXT-2014</i> ^d)
refinement method	full-matrix least-squares on F^2 (<i>SHELXL-2018</i> ^e)
absorption correction method	Gaussian integration (face-indexed)
range of transmission factors	0.9795--0.8758
data/restraints/parameters	12607 / 36 ^f / 781
extinction coefficient (<i>x</i>) ^g	0.00052(6)
Flack absolute structure parameter ^h	-0.016(14)
goodness-of-fit (<i>S</i>) ⁱ [all data]	1.119
final <i>R</i> indices ^j	
<i>R</i> ₁ [$F_o^2 \geq 2\sigma(F_o^2)$]	0.0533
<i>wR</i> ₂ [all data]	0.1311
largest difference peak and hole	0.206 and -0.236 e Å ⁻³

- ^aObtained from least-squares refinement of 9933 reflections with $5.46^\circ < 2\theta < 137.72^\circ$.
- ^bPrograms for diffractometer operation, data collection, data reduction and absorption correction were those supplied by Bruker
- ^cData were collected with the detector set at three different positions. Low-angle (detector $2\theta = -33^\circ$) data frames were collected using a scan time of 5 s, medium-angle (detector $2\theta = 75^\circ$) frames using a scan time of 10 s, and high-angle (detector $2\theta = 117^\circ$) frames using a scan time of 15 s.
- ^dG. M. Sheldrick, *Acta Crystallogr.* **2015**, *A71*, 3–8. (*SHELXT-2014*)
- ^eG. M. Sheldrick, *Acta Crystallogr.* **2015**, *C71*, 3–8. (*SHELXL-2018/3*)
- ^fThe disordered isopropyl group had the following same distance restraints (**SADI**): C36–C40A & C36–C40B; C40A–C41A & C40B–C41B; C40A–C42A & C40B–C42B; C36···C41A & C36···C41A; C36···C42A & C36···C42B; C41A···C42A & C41A···C42A. Additionally, the rigid bond restraint (**RIGU**) was applied to the anisotropic displacement parameters of the carbon atoms of the disordered isopropyl group.
- ^g $F_c^* = kF_c[1 + x\{0.001F_c^2\lambda^3/\sin(2\theta)\}]^{-1/4}$ where k is the overall scale factor.
- ^hH. D. Flack, *Acta Crystallogr.* **1983**, *A39*, 876–881; H. D. Flack, G. Bernardinelli, *Acta Crystallogr.* **1999**, *A55*, 908–915; H. D. Flack, G. Bernardinelli, *J. Appl. Cryst.* **2000**, *33*, 1143–1148. The Flack parameter will refine to a value near zero if the structure is in the correct configuration and will refine to a value near one for the inverted configuration.
- ⁱ $S = [\sum w(F_o^2 - F_c^2)^2/(n - p)]^{1/2}$ (n = number of data; p = number of parameters varied; $w = [\sigma^2(F_o^2) + (0.0411P)^2 + 2.5833P]^{-1}$ where $P = [\text{Max}(F_o^2, 0) + 2F_c^2]/3$).
- ^j $R_1 = \sum ||F_o| - |F_c||/\sum |F_o|$; $wR_2 = [\sum w(F_o^2 - F_c^2)^2/\sum w(F_o^4)]^{1/2}$.

2.5 References

1. a) P. J. Davidson, M. F. Lappert, *J. Chem. Soc., Chem. Commun.* **1973**, 317a; b) D. E. Goldberg, D. E. Harris, M. F. Lappert, K. M. Thomas, *J. Chem. Soc., Chem. Commun.* **1976**, 261–262; c) P. J. Davidson, D. H. Harris, M. F. Lappert, *J. Chem. Soc., Dalton Trans.* **1976**, 2268–2274; d) P. B. Hitchcock, M. F. Lappert, S. J. Miles, A. J. Thorne, *J. Chem. Soc., Chem. Commun.* **1984**, 480–482.
2. For select reviews and articles, see: a) R. C. Fischer, P. P. Power, *Chem. Rev.* **2010**, *110*, 3877–3923; b) Y. Wang, G. H. Robinson, *Inorg. Chem.* **2011**, *50*, 12326–12337; c) R. S. Ghadwal, R. Azhakar, H. W. Roesky, *Acc. Chem. Res.* **2013**, *46*, 444–456; d) J. Brand, H. Braunschweig, S. S. Sen, *Acc. Chem. Res.* **2014**, *47*, 180–191; e) G. He, O. Shynkaruk, M. W. Lui, E. Rivard, *Chem. Rev.* **2014**, *114*, 7815–7880; f) A. V. Protchenko, M. P. Blake, A. D. Schwarz, C. Jones, P. Mountford, S. Aldridge, *Organometallics* **2015**, *34*, 2126–2129; g) C. Präsang, D. Scheschkewitz, *Chem. Soc. Rev.* **2016**, *45*, 900–921; h) E. Rivard, *Chem. Soc. Rev.* **2016**, *45*, 989–1003; i) T. Ochiai, D. Franz, S. Inoue, *Chem. Soc. Rev.* **2016**, *45*, 6327–6344; j) M. Melaimi, R. Jazzar, M. Soleilhavoup, G. Bertrand, *Angew. Chem. Int. Ed.* **2017**, *56*, 10046–10068; k) J. Schneider, C. P. Sindlinger, K. Eichele, H. Schubert, L. Wesemann, *J. Am. Chem. Soc.* **2017**, *139*, 6542–6545; l) S. Yao, Y. Xiong, M. Driess, *Acc. Chem. Res.* **2017**, *50*, 2026–2037; m) V. Nesterov, D. Reiter, P. Bag, P. Frisch, R. Holzner, A. Porzelt, S. Inoue, *Chem. Rev.* **2018**, *118*, 9678–9842; n) M.-A. Légaré, M. Rang, G. Bélanger-Chabot, J. I. Schweizer, I. Krummenacher, R. Bertermann, M. Arrowsmith, M. C. Holthausen, H. Braunschweig, *Science* **2019**, *363*, 1329–1332; o) Y. Wang, A. Kostenko, T. J. Hadlington, M.-P. Luecke, S. Yao, M. Driess, *J. Am. Chem. Soc.* **2019**, *141*, 626–634.

3. a) N. Tokitoh, K. Manmaru, R. Okazaki, *Organometallics* **1994**, *13*, 167–171; b) N. Tokitoh, M. Saito, R. Okazaki, *J. Am. Chem. Soc.* **1993**, *115*, 2065–2066; c) S. Brooker, J.-K. Buijink, F. T. Edelman, *Organometallics* **1991**, *10*, 25–26.

4. For example: a) K. A. Miller, T. W. Watson, J. E. Bender, M. M. Banaszak Holl, J. W. Kampf, *J. Am. Chem. Soc.* **2001**, *123*, 982–983; b) Y. Peng, B. D. Ellis, X. Wang, P. P. Power, *J. Am. Chem. Soc.* **2008**, *130*, 12268–12269; c) S. K. Mandal, H. W. Roesky, *Acc. Chem. Rev.* **2011**, *45*, 298–307; d) K. Inomata, T. Watanabe, Y. Miyazaki, H. Tobita, *J. Am. Chem. Soc.* **2015**, *137*, 11935–11937; e) A. V. Protchenko, J. I. Bates, L. M. A. Saleh, M. P. Blake, A. D. Schwarz, E. L. Kolychev, A. L. Thompson, C. Jones, P. Mountford, S. Aldridge, *J. Am. Chem. Soc.* **2016**, *138*, 4555–4564; f) M. M. D. Roy, S. Fujimori, M. J. Ferguson, R. McDonald, N. Tokitoh, E. Rivard, *Chem. Eur. J.* **2018**, *24*, 14392–14399; g) T. J. Hadlington, M. Driess, C. Jones, *Chem. Soc. Rev.* **2018**, *47*, 4176–4197; h) B.-X. Leong, J. Lee, Y. Li, M.-C. Yang, C.-K. Siu, M.-D. Su, C.-W. So, *J. Am. Chem. Soc.* **2019**, *141*, 17629–17636.

5. For related acyclic silylenes, see: a) A. V. Protchenko, K. H. Birj Kumar, D. Dange, A. D. Schwarz, D. Vidovic, C. Jones, N. Kaltsoyannis, P. Mountford, S. Aldridge, *J. Am. Chem. Soc.* **2012**, *134*, 6500–6503; b) B. D. Reken, T. M. Brown, J. C. Fettinger, H. M. Tuononen, P. P. Power, *J. Am. Chem. Soc.* **2012**, *134*, 6504–6507; c) Cyclic diorganosilylenes are also known: M. Kira, S. Ishida, T. Iwamoto, C. Kabuto, *J. Am. Chem. Soc.* **1999**, *121*, 9722–9723; d) M. Asay, S. Inoue, M. Driess, *Angew. Chem. Int. Ed.* **2011**, *50*, 9589–9592.

6. a) D. Seyferth, *Organometallics* **2001**, *40*, 4978–4992; b) For a recent example of generating $[\text{Me}_2\text{Si}]_n$ from an isolable complex of SiMe_2 , see: A. A. Omaña, R. K. Green, R. Kobayashi, Y. He, E. R. Antoniuk, M. J. Ferguson, Y. Zhou, J. G. C. Veinot, T. Iwamoto, A. Brown, E.

Rivard, *Angew. Chem. Int. Ed.* **2021**, *60*, 228–231; c) T. J. Drahnak, J. Michl, R. West, *J. Am. Chem. Soc.* **1979**, *101*, 5427–5428.

7. P. Jutzi, U. Holtmann, D. Kanne, C. Krüger, R. Blom, R. Gleiter, I. Hyla-Kryspin, *Chem. Ber.* **1989**, *122*, 1629–1939.

8. a) A. V. Protchenko, A. D. Schwarz, M. P. Blake, C. Jones, N. Kaltsoyannis, P. Mountford, S. Aldridge, *Angew. Chem. Int. Ed.* **2012**, *52*, 568–571; b) T. J. Hadlington, J. A. B. Adballa, R. Tirfoin, S. Aldridge, C. Jones, *Chem. Commun.* **2016**, *52*, 1717–1720; c) D. Wendel, A. Porzelt, F. A. D. Herz, D. Sarkar, C. Jandl, S. Inoue, B. Rieger, *J. Am. Chem. Soc.* **2017**, *139*, 8134–8137; d) D. Wendel, D. Reiter, A. Porzelt, P. J. Altmann, S. Inoue, B. Rieger, *J. Am. Chem. Soc.* **2017**, *139*, 17193–17198; e) Y. K. Loh, L. Ying, M. Á. Fuentes, D. C. H. Do, S. Aldridge, *Angew. Chem. Int. Ed.* **2019**, *58*, 4847–4851; f) M. M. D. Roy, M. J. Ferguson, R. McDonald, Y. Zhou, E. Rivard, *Chem. Sci.* **2019**, *10*, 6476–6481; g) S. Fujimori, S. Inoue, *Eur. J. Inorg. Chem.* **2020**, 3131–3142; h) C. Shan, S. Yao, M. Driess, *Chem. Soc. Rev.* **2020**, *49*, 6733–6754; h) C. Ganesamoorthy, J. Schoening, C. Wölper, L. Song, P. R. Schreiner, S. Schulz, *Nat. Chem.* **2020**, *12*, 608–614; j) D. Reiter, R. Holzner, A. Porzelt, P. Frisch, S. Inoue, *Nat. Chem.* **2020**, *12*, 1131–1135.

9. a) M. M. D. Roy, E. Rivard, *Acc. Chem. Rev.* **2017**, *50*, 2017–2025; b) S. M. I. Al-Rafia, M. J. Ferguson, E. Rivard, *Inorg. Chem.* **2011**, *50*, 10543–10545; c) C. Hering-Junghans, P. Andreiuk, M. J. Ferguson, R. McDonald, E. Rivard, *Angew. Chem. Int. Ed.* **2017**, *56*, 6272–6275.

10. a) N. Kuhn, M. Göhner, M. Siemann, *Z. Anorg. Allg. Chem.* **2002**, *628*, 1108–1115; b) R. S. Ghadwal, *Acc. Chem. Res.* **2022**, *55*, 457–470; c) L. Y. M. Eymann, P. Varava, A. M. Shved,

B. F. E. Curchod, Y. Liu, O. M. Planes, A. Sienkiewicz, R. Scopelliti, F. F. Tirani, K. Severin, *J. Am. Chem. Soc.* **2019**, *141*, 17112–17116; d) A. Causero, H. Elsen, J. Pahl, S. Harder, *Angew. Chem. Int. Ed.* **2017**, *56*, 6906–6910.

11. For related work on *N*-heterocyclic imines, see: a) T. Ochiai, D. Franz, S. Inoue, *Chem. Soc. Rev.* **2016**, *45*, 6327–6344; b) M. W. Lui, C. Merten, M. J. Ferguson, R. McDonald, Y. Xu, E. Rivard, *Inorg. Chem.* **2015**, *54*, 2040–2049.

12. a) R. S. Ghawdal, S. O. Reichmann, F. Engelhardt, D. M. Andrada, G. Frenking, *Chem. Commun.* **2013**, *49*, 9440–9442; b) K. Powers, C. Hering-Junghans, R. McDonald, M. J. Ferguson, E. Rivard, *Polyhedron* **2016**, *108*, 8–18; c) R. S. Ghawdal, *Dalton Trans.* **2016**, *45*, 16081–16095; d) R. D. Crocker, T. B. Nguyen, *Chem. Eur. J.* **2016**, *22*, 2208–2213; e) M. A. Wünsche, T. Witteler, F. Dielmann, *Angew. Chem. Int. Ed.* **2018**, *57*, 7234–7239; f) M. K. Sharma, S. Blomeyer, B. Neumann, N.-G. Stammer, M. von Gastel, A. Hinz, R. S. Ghadwal, *Angew. Chem. Int. Ed.* **2019**, *58*, 17599–17603; g) S. Naumann, *Chem. Commun.* **2019**, *55*, 11658–11670; h) P. Gupta, J.-E. Siewart, T. Wellnitz, M. Fischer, W. Baumann, T. Beweries, C. Hering-Junghans, *Dalton Trans.* **2021**, *50*, 1838–1844.

13. T. X. Gentner, G. Ballmann, J. Pahl, H. Elsen, S. Harder, *Organometallics* **2018**, *37*, 4473–4480.

14. NHOs are known to react with I₂ to form [(NHO)I]₃ salts: N. Kuhn, H. Bohnen, G. Henkel, J. Kreutzberg, *Z. Naturforsch.* **1996**, *51b*, 1267–1278.

15. S. Evjen, A. Fiksdahl, *Synth. Commun.* **2017**, *47*, 1392–1399.

16. R. S. Ghadwal, H. W. Roesky, S. Merkel, J. Henn, D. Stalke, *Angew. Chem. Int. Ed.* **2009**, *48*, 5683–5686.

17. A. C. Filippou, O. Chernov, G. Schnakenburg, *Angew. Chem. Int. Ed.* **2009**, *48*, 5687–5690.
18. J. I. Schweizer, A. G. Sturm, T. Porsch, M. Berger, M. Bolte, N. Auner, M. C. Holtausen, *Z. Anorg. Allg. Chem.* **2018**, *114*, 982–988.
19. C. Marschner, *Eur. J. Inorg. Chem.* **1998**, 221–226.
20. A. B. Pangborn, M. A. Giardello, R. H. Grubbs, R. K. Rosen, F. J. Timmers, *Organometallics* **1996**, *15*, 1518–1520.
21. S. J. Ryan, S. D. Schimler, D. C. Bland, M. S. Sanford, *Org. Lett.* **2017**, *17*, 1866–1869.
22. G. Blankson, A. K. Parhi, M. Kaul, D. S. Pilch, E. J. LaVoie, *Eur. J. Med. Chem.* **2019**, *178*, 30–38.
23. H. Hope, *Prog. Inorg. Chem.* **1994**, *41*, 1–19.
24. G. M. Sheldrick, *Acta Crystallogr.* **2015**, *A71*, 3–8.
25. G. M. Sheldrick, *Acta Crystallogr.* **2015**, *C71*, 3–8.

Chapter 3 – An Indium(I) Tetramer Bound by Anionic *N*-Heterocyclic Olefins: Ambiphilic Reactivity, Transmetallation and a Rare Indium-Imide

3.1 Introduction

Indium(I) compounds of the general form (RIn)_x appeared early in the development of organometallic chemistry with the report of CpIn in 1957 (Cp = η⁵-C₅H₅).^{1,2} Subsequent examples serve to highlight the structural variety in this class of molecules, as evidenced by the octahedral-shaped In₈ oligomer [Cp*In]₈ (Cp* = η⁵-C₅Me₅),³ Hill and coworkers' linear In₆ catenate [(Nacnac)InI]-[(Nacnac)In]₄-[(Nacnac)InI] (Nacnac = β-diketiminiate),⁴ and Power's dimetallene Ar^{Dipp}InInAr^{Dipp} (Ar^{Dipp} = 2,6-Dipp₂C₆H₃; Dipp = 2,6-ⁱPr₂C₆H₃).⁵ The lability of the In-In bonds in such systems leads to an isolable In(I) monomer Ar^{Trip}In: when a bulky terphenyl ligand (Ar^{Trip} = 2,6-Trip₂C₆H₃; Trip = 2,4,6-ⁱPr₃C₆H₂) is bound to In.⁶ Another interesting bonding motif exists within tetrahedron-shaped oligomers [RIn]₄ bearing silylated ligands: R = C(SiMe₃)₃, C(SiMe₂Et)₃ and Si(SiMe₃)₃.⁷

Over the past few years, the Rivard group⁸ and others⁹⁻¹¹ have explored a class of ligands, termed by us as anionic *N*-heterocyclic olefins (aNHOs). Hallmarks of these ligands include the highly electron-donating nature of the ligating sp²-hybridized carbon and the possibility of added ligand-to-element π-donation, as found in the monomeric acyclic silylene (^{Me}eIPrCH)₂Si: (^{Me}eIPrCH = [(MeCNDipp)₂C=CH]⁻), as shown in Figure 3.1.¹² Given the recent exploration of low-oxidation state main group complexes in catalysis (*e.g.*, with bismuth),¹³ I wondered if aNHOs could be used to form reactive In(I) complexes and if E-H bond (E =

element)¹⁴ and redox chemistry at In would be supported by these low-oxidation state p-block complexes.

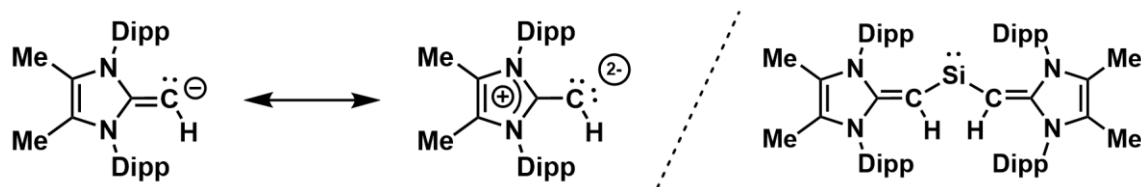


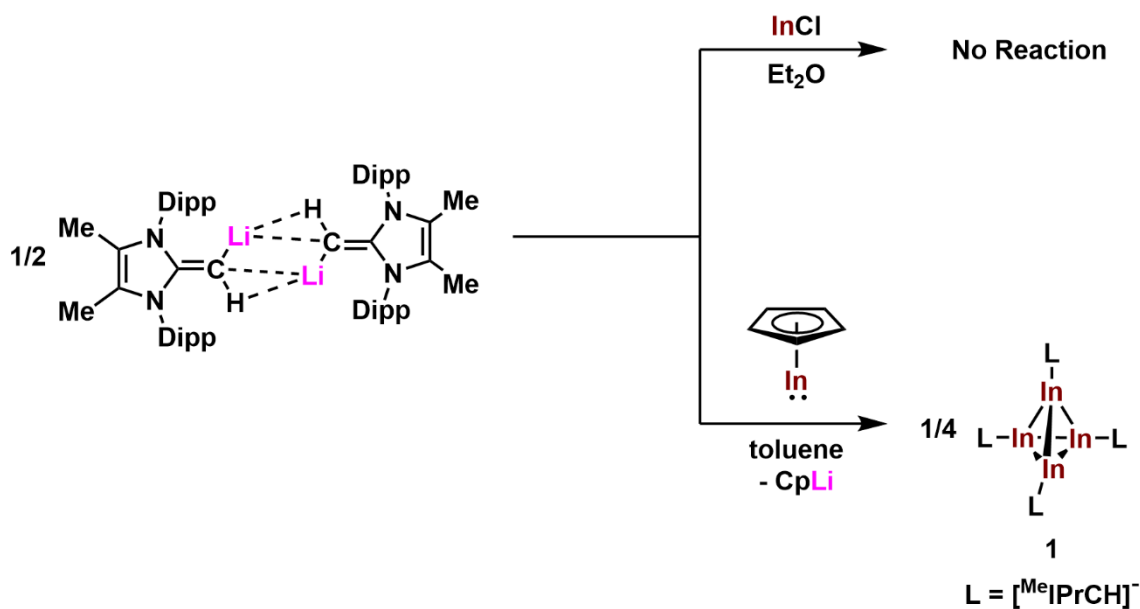
Figure 3.1. Major resonance forms of the anionic *N*-heterocyclic olefin (aNHO) ^{Me}IPrCH⁻ (left) and structure of (^{Me}IPrCH)₂Si: (right).

3.2 Results and Discussion

The initial starting point of this project involved combining half an equivalent of the previously reported aNHO reagent, [(^{Me}IPrCH)Li]₂ (Chapter 2),¹² with InCl in diethyl ether (Et₂O) or toluene, as it had been previously established that [(^{Me}IPrCH)Li]₂ could react with a variety of element halides EX_n (E = Ti, Zr, Hf, Zn, Si, Ge, Sn, Pb; X = Cl or Br).^{12,15} Interestingly, no reaction was observed between [(^{Me}IPrCH)Li]₂ and InCl, thus CpIn became the targeted indium(I) source as cyclopentadienyl-type ligands have been found to be good leaving groups when bound to main group elements.¹⁶

Upon addition of half an equivalent of [(^{Me}IPrCH)Li]₂ to CpIn in toluene, a deep-red solution formed along with the expected insoluble co-product, LiCp, from Cp⁻/aNHO ligand exchange (Scheme 3.1).¹⁷ The indium(I) tetramer [(^{Me}IPrCH)In]₄ (**1**) could be isolated from the reaction mixture in a yield of 30 % as a deep-red solid by recrystallization from hexanes, and crystals suitable for X-ray crystallography were obtained from a concentrated toluene solution of **1** at -35 °C. Examination of the ¹H NMR spectrum of **1** in C₆D₆ showed the

expected chemical shifts for a $[\text{Me}^e\text{IPrCH}]^-$ ligand, with the vinylic protons appearing collectively as a singlet at 3.72 ppm, which is significantly shifted when compared to the vinylic protons in $[(\text{Me}^e\text{IPrCH})\text{Li}]_2$ (0.89 ppm in C_6D_6).¹² Solid samples of **1** decompose within 16 hours at room temperature and even decompose slowly at $-35\text{ }^\circ\text{C}$; as such, compound **1** was used within a few days of preparation.



Scheme 3.1. Synthetic route to $[(\text{Me}^e\text{IPrCH})\text{In}]_4$ (**1**).

The solid-state structure of **1** (Figure 3.2) consists of a tetrahedron-shaped In_4 core with an average In-In bond length of $2.9818(5)\text{ \AA}$, which falls in the range $[2.887(2)\text{--}3.165(2)\text{ \AA}]$ of those found within $[\text{RIn}]_4$ tetramers reported previously ($\text{R} = \text{C}(\text{SiMe}_3)_3$, $\text{C}(\text{SiMe}_2\text{Et})_3$ and $\text{Si}(\text{SiMe}_3)_3$).⁷ The average In-C bond length in **1** of $2.150(4)\text{ \AA}$ is appreciably shorter than the corresponding bonds within Power's In(I) complexes $\text{Ar}^{\text{Dipp}}\text{InInAr}^{\text{Dipp}}$ and $\text{Ar}^{\text{Trip}}\text{In}$: $[2.256(6)\text{ \AA}$ (*avg.*) and $2.260(7)\text{ \AA}$, respectively].^{5,6} The exocyclic C=C bonds with the $[\text{Me}^e\text{IPrCH}]^-$ ligands in **1** [$1.345(5)\text{ \AA}$ (*avg.*)] are the same length within error as found in free $\text{Me}^e\text{IPrCH}_2$ [$1.3489(18)\text{ \AA}$],¹⁷ indicating the retention of substantial C=C double bond character.

The interior In-In-In angles that make up the In₄ core in **1** [59.112(13) to 61.104(13)°] approach the ideal angle of 60° expected for a tetrahedron. Density functional theory (DFT) computations on a truncated model of **1**, [(^{Me}I^{Ph}CH)In]₄ (**1**^M; ^{Me}I^{Ph}CH = [(MeCNPh)₂C=CH]⁻), gave Wiberg bond indices (WBI) of 0.58 for the In–In bonds, while WBI values of 0.57 were obtained for the capping In–C_{aNHO} bonds, indicating long single bonds.

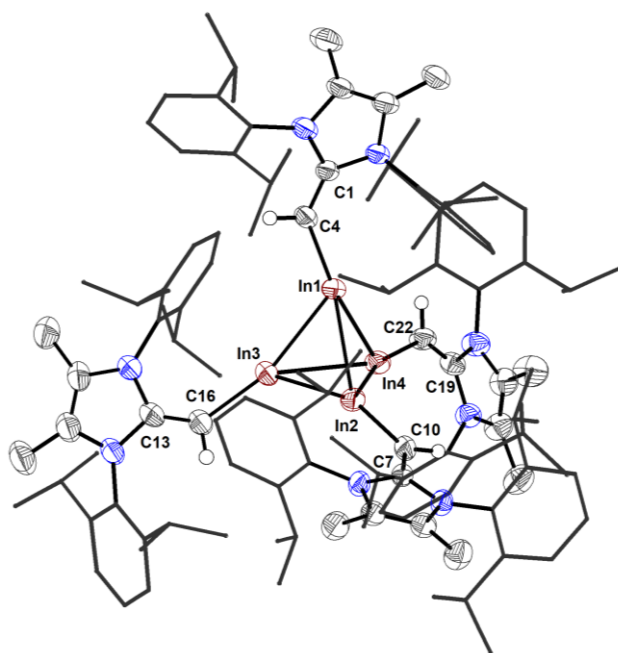


Figure 3.2. Molecular structure of [(^{Me}I^{Pr}CH)In]₄ (**1**) with thermal ellipsoids plotted at 50 % probability. All hydrogen atoms (except for the vinylic hydrogens at C4, C10, C16 and C22) are omitted for clarity; Dipp groups are shown as wireframes. The toluene solvent molecules are not shown. Selected bond lengths [Å] and angles [°]: In1–In2 2.30082(6), In1–In3 2.9854(5), In1–In4 2.911(5), In1–C4 2.154(4), C1–C4 1.356(5); In2–In1–In3 59.112(13), In2–In1–In4 59.380(12), In3–In1–In4 61.104(13), In1–C4–C1 134.7(3), C4–In1–In2 124.90(11).

Diffusion-ordered NMR spectroscopy (DOSY) revealed that the tetrameric nature of **1** is maintained in benzene. Interestingly, DOSY of **1** in a THF/C₆D₆ mixture (4:1) revealed that the tetramer dissociates and forms what is most likely a dimer in solution, suggesting that the indium-indium bonds can be broken in **1**, at least partially, by a polar coordinating solvent.

The deep color of **1** prompted further computational and spectroscopic investigations. The UV-vis spectrum of **1** in hexanes shows intense absorptions at 439 and 515 nm respectively ($\epsilon = 4970$ and $4390 \text{ L mol}^{-1} \text{ cm}^{-1}$). The λ_{max} at 515 nm in **1** is slightly red-shifted when compared to known $[\text{RIn}]_4$ tetramers [$\lambda_{\text{max}} = 490 \text{ nm}$, $\text{R} = \text{C}(\text{SiMe}_3)_3$, $\text{C}(\text{SiMe}_2\text{Et})_3$].⁷ Time-dependent DFT (TD-DFT) studies on a truncated model for **1** (**1^M**), provided a computed UV-vis spectrum [$\lambda_{\text{max}} = 457$ and 549 nm] that matched well with the experiment (Figure 3.3). The lowest energy band arises from a combination of HOMO/HOMO–1/HOMO–2 to LUMO+1 transitions with overall charge transfer from aNHO ligand-based orbitals to the LUMO+1, which is localized mainly on the In_4 core; the HOMO–LUMO transition is transition dipole forbidden.¹⁸

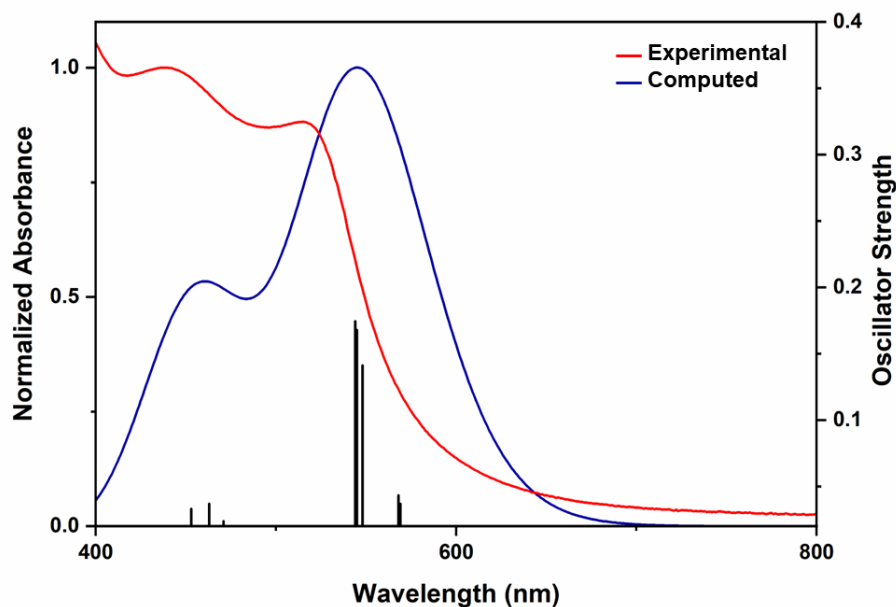
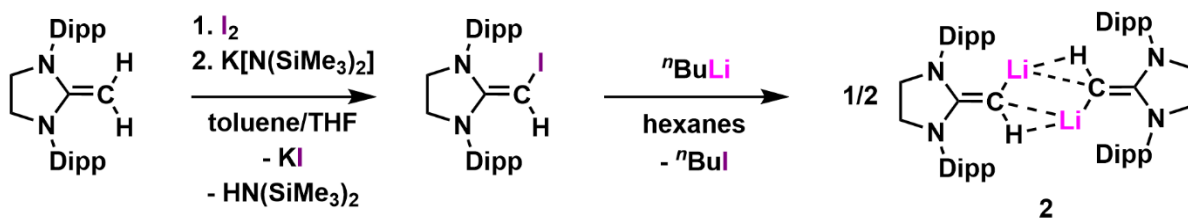


Figure 3.3. Experimentally determined UV-vis spectrum of $[(^{\text{Me}}\text{IPrCH})\text{In}]_4$ (**1**) in hexanes with computed UV-vis spectra overlay with corresponding oscillator strengths for $[(^{\text{Me}}\text{PhCH})\text{In}]_4$ (**1^M**). Computed at B3LYP/cc-pVDZ(-PP) level of theory.

A new aNHO reagent, $[(\text{SIPrCH})\text{Li}]_2$ (**2**) ($\text{SIPrCH} = [(\text{H}_2\text{CNDipp})_2\text{C}=\text{CH}^-]$) was also prepared, in an attempt to isolate another indium(I) tetramer. Compound **2** was synthesized in a one-pot procedure, without the isolation of the probable intermediate $\text{SIPrCH}(\text{I})$, as shown in Scheme 3.2. $[(\text{SIPrCH})\text{Li}]_2$ (**2**) could be isolated as an off-white solid in a yield of 54 %. Crystals suitable for X-ray crystallographic analysis were grown from a concentrated toluene solution of **2** at $-35\text{ }^\circ\text{C}$. Similar to $[(^{\text{Me}}\text{IPrCH})\text{Li}]_2$, **2** adopts a centrosymmetric dimeric arrangement in the solid state (Figure 3.4).



Scheme 3.2. One-pot synthesis of $[(\text{SIPrCH})\text{Li}]_2$ (**2**).

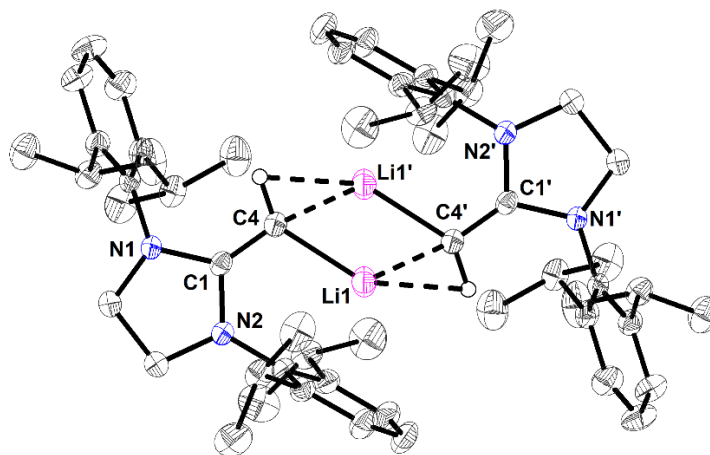


Figure 3.4. Molecular structure of $[(\text{SIPrCH})\text{Li}]_2$ (**2**) with thermal ellipsoids plotted at 50 % probability. All hydrogen atoms (except for the vinylic hydrogens at C4 and C4') are omitted for clarity. The toluene solvent molecule is not shown. Selected bond lengths [\AA] and angles [$^\circ$]: C1–C4 1.3440(13), C4–Li1 2.072(2), C4–Li1' 2.122(2); C1–C4–Li1 147.92(10), C1–C4–Li1' 112.37(9).

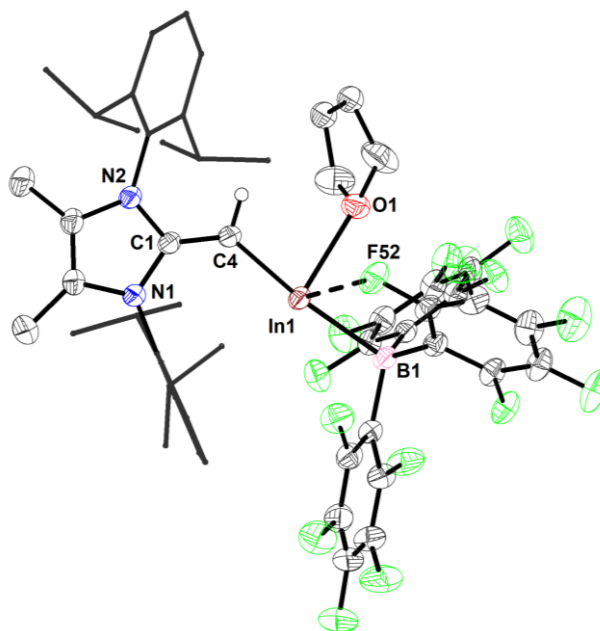
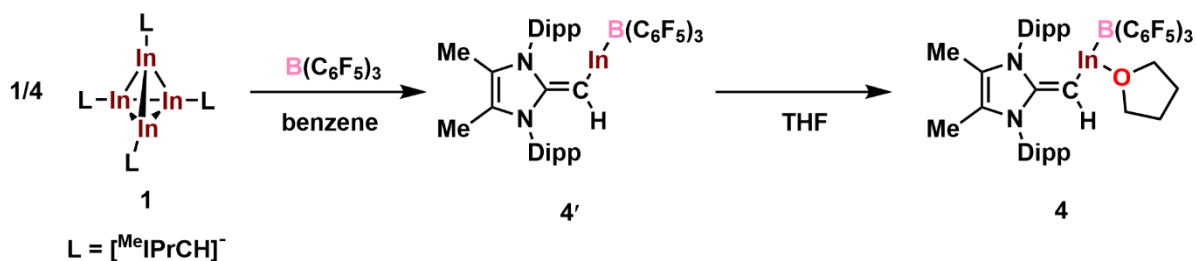


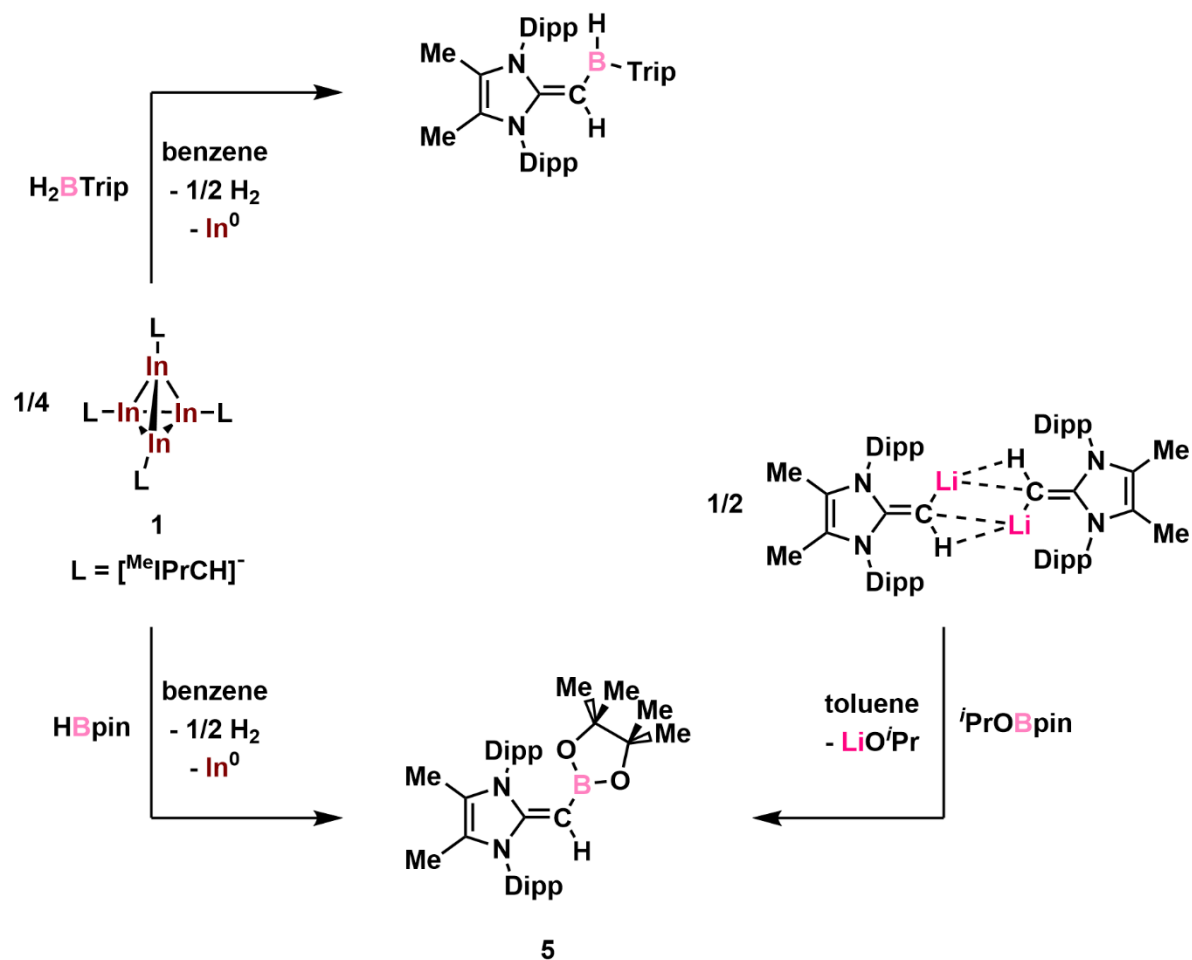
Figure 3.5. Molecular structure of $(^{\text{Me}}\text{IPrCH})\text{In}(\text{THF})\cdot\text{B}(\text{C}_6\text{F}_5)_3$ (**4**) with thermal ellipsoids plotted at 50 % probability. All hydrogen atoms (except for the vinylic hydrogen at C4) are omitted for clarity, while all Dipp groups are shown in wireframe. The pentane solvent molecule is not shown. Only one part of the disordered tetrahydrofuran group is shown. Selected bond lengths [Å] and angles [°]: C1–C4 1.371(2), C4–In1 2.0699(16), In1–B1 2.3103(18), In1–O1 2.4734(12), In1–F52 2.7177(14); C1–C4–In1 133.12(12), C4–In1–B1 173.72(6), C4–In1–O1 83.85(6).

An In(I)-borane complex free of coordinating THF, $(^{\text{Me}}\text{IPrCH})\text{In}\cdot\text{B}(\text{C}_6\text{F}_5)_3$ (**4'**), could be prepared by careful exclusion of THF when **1** is combined with $\text{B}(\text{C}_6\text{F}_5)_3$, as shown in Scheme 3.3; however, attempts to grow crystals of this species were unsuccessful as **4'** readily absorbs THF from the glovebox atmosphere to give **4**. The $^{11}\text{B}\{^1\text{H}\}$ NMR spectrum of the crude reaction mixture of **4'** in C_6D_6 , showed a chemical shift of -14.4 ppm, similar to that of **4**, while the ^1H NMR spectrum of **4'** in C_6D_6 showed that the vinylic proton as a singlet at 3.57 ppm, which is shifted considerably when compared to the vinylic proton of **4** ($\delta = 4.07$ ppm). Attempts to remove THF from **4** by prolonged exposure to dynamic vacuum to obtain **4'** were unsuccessful.



Scheme 3.3. Synthesis of $(^{\text{Me}^i\text{PrCH}}\text{In})\cdot\text{B}(\text{C}_6\text{F}_5)_3$ (**4'**) and $(^{\text{Me}^i\text{PrCH}}\text{In}(\text{THF}))\cdot\text{B}(\text{C}_6\text{F}_5)_3$ (**4**).

Attention was then turned to B-H bond activation at indium. To start, compound **1** was combined with $\text{H}_2\text{B}^i\text{Trip}$, resulting in an immediate color change from a deep-red homogenous mixture to a pale-yellow solution over a black precipitate (presumably indium metal). ^1H NMR spectroscopic analysis showed formation of the known bulky borane $(^{\text{Me}^i\text{PrCH}}\text{B}(\text{H})^i\text{Trip})$,^{15a} derived from a formal aNHO/hydride exchange at boron. In a similar fashion, rapid ligand exchange transpired between **1** and HB^ipin (*pin* = pinacolato) occurred to give $(^{\text{Me}^i\text{PrCH}}\text{B}^i\text{pin})$ (**5**) along with a metallic by-product. Alternatively, compound **5** can be prepared from $[(^{\text{Me}^i\text{PrCH}}\text{Li})_2]$ and $^i\text{PrOB}^i\text{pin}$ in an isolated yield of 20 % (Scheme 3.4). Notably, both $(^{\text{Me}^i\text{PrCH}})_2\text{Zn}^{15a}$ and $[(^{\text{Me}^i\text{PrCH}}\text{Li})_2]$ are unreactive towards HB^ipin , indicating a higher propensity for B-H bond activation/ligand transfer with $[(^{\text{Me}^i\text{PrCH}}\text{In})_4]$ (**1**).



Scheme 3.4. Synthesis of $(\text{Me}^i\text{PrCH})\text{B}^i\text{Trip}$ and $(\text{Me}^i\text{PrCH})\text{B}^i\text{pin}$ (**5**).

$(\text{Me}^i\text{PrCH})\text{B}^i\text{pin}$ (**5**) was structurally characterized by single-crystal X-ray crystallography (Figure 3.6) from which an exocyclic C=C bond length of 1.3757(19) Å is present, indicating that there is minimal π -donation from the exocyclic aNHO ligand to the boron (Figure 3.6). This is most likely due to the quenched Lewis acidity of the boron center resulting from electron donation from the pinacolato group.

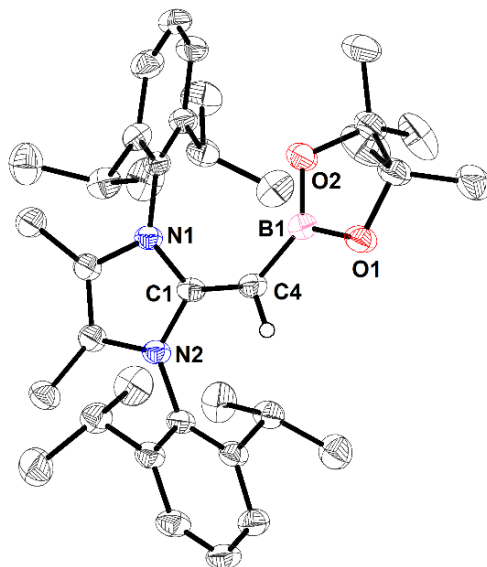


Figure 3.6. Molecular structure of $(^{\text{Me}}\text{IPrCH})\text{Bpin}$ (**5**) with thermal ellipsoids plotted at 50 % probability. All hydrogen atoms (except for the vinylic hydrogen at C4) are omitted for clarity. Selected bond lengths [Å] and angles [°]: C1–C4 1.3757(19), C4–B1 1.513(2), B1–O1 1.3948(19), B1–O2 1.3770(19); C1–C4–B1 134.02(12).

The aNHO/hydride exchange at boron described above could go *via* initial oxidative addition^{14b} with In(I) to In(III) conversion, direct σ -bond metathesis at In,^{15a} or *via* radical processes.¹⁹ As such, possible mechanisms for the reaction of **1** with HBpin were investigated computationally. Notably, the dissociation of **1^M** into four monomers, $(^{\text{Me}}\text{IPrCH})\text{In}$, was endothermic ($\Delta H = 17.5 \text{ kcal mol}^{-1}$ of **1^M**), while this process becomes favorable in the gas phase when entropy is considered ($\Delta G = -13.6 \text{ kcal mol}^{-1}$ of **1^M**); hence, it is possible that there is some monomeric/reactive $(^{\text{Me}}\text{IPrCH})\text{In}$ is present when **1** is dissolved. The direct oxidative addition of a B–H bond at the In center in $(^{\text{Me}}\text{IPrCH})\text{In}$ to give $(^{\text{Me}}\text{IPrCH})\text{In}(\text{H})\text{Bpin}$ is disfavored energetically with a large computed Gibbs free energy of $\Delta G = 26.8 \text{ kcal mol}^{-1}$; thus, it is not likely to happen at room temperature. Instead, a more favorable method for aNHO/hydride exchange at In is pre-coordination of HBpin to the terminal olefinic aNHO

carbon to give the energetically low-lying transition state species $\text{pinB(H)\cdot(aNHO)In}$ ($\Delta\Delta G^\ddagger = -30.4 \text{ kcal mol}^{-1}$) prior to B to In hydride transfer, as shown in Figure 3.7. The overall reaction: $(^{\text{Me}}\text{IPrCH})\text{In} + \text{HBpin} \rightarrow (^{\text{Me}}\text{IPrCH})\text{Bpin} + \text{InH}$ is predicted to be quite exoergic with $\Delta_r G = -30.4 \text{ kcal mol}^{-1}$. It should be noted that InH is not expected to be stable and should decompose immediately into In and H_2 under ambient conditions,^{14a} which would be supported by the observation of a black precipitate and bubbling during the reaction. It cannot be ruled out at this stage that the reaction can proceed through the interaction of HBpin with In(I) oligomers.

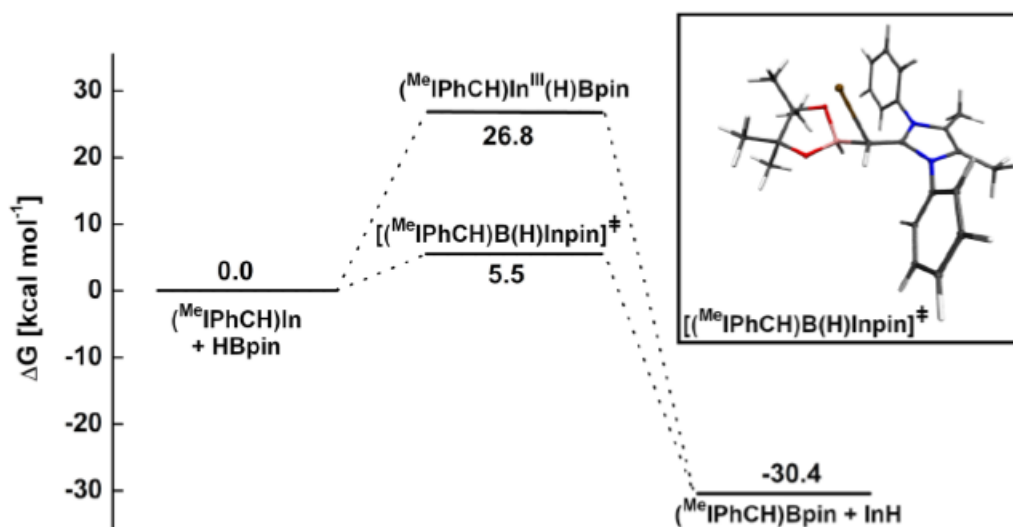
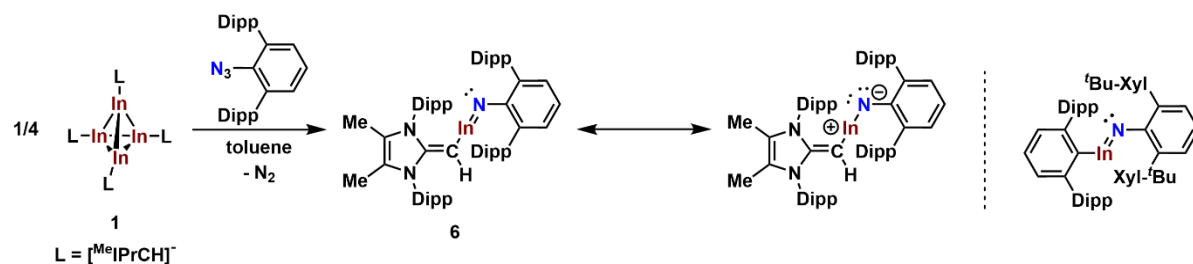


Figure 3.7. Possible reaction mechanism of the reaction of monomeric 1^{M} with HBpin. $(^{\text{Me}}\text{IPrCH})\text{BH(In)pin}$ represents a transition state, all other geometries are minima on the potential energy surface.

Given that only one example of a neutral indium-imide, $\text{Ar}^{\text{Dipp}}\text{InNAr}^{\text{Xyl-}t\text{Bu}} \text{Ar}^{\text{Xyl-}t\text{Bu}} = 2,6\text{-(Xyl-4-}t\text{Bu)}_2\text{C}_6\text{H}_3$; $\text{Xyl} = 2,6\text{-Me}_2\text{C}_6\text{H}_3$), is known,²⁰ $[(^{\text{Me}}\text{IPrCH})\text{In}]_4$ (**1**) was combined with the sterically hindered terphenylazide $\text{Ar}^{\text{Dipp}}\text{N}_3$ ($\text{Ar}^{\text{Dipp}} = 2,6\text{-Dipp}_2\text{C}_6\text{H}_3$)²¹ which formed the monomeric indium-imide $(^{\text{Me}}\text{IPrCH})\text{InNAr}^{\text{Dipp}}$ (**6**) (Scheme 3.5), compound **6** was isolated

as an orange crystalline solid in a yield of 31 % after cooling a toluene solution to $-35\text{ }^{\circ}\text{C}$. Single-crystal X-ray analysis gave (Figure 3.8) an In-N length of $1.949(3)\text{ \AA}$ in **6** with this unit located within the steric pocket created by four flanking Dipp groups from the aNHO and terphenyl ligands; of note, the resulting In-N distance in **6** is only slightly longer than in Power's imide $\text{Ar}^{\text{Dipp}}\text{InNAr}^{\text{Xyl-}t\text{Bu}}$ [$1.928(3)\text{ \AA}$];^{20a} further, the In-N bond length in **6** is similar to that found in Coles' anionic imide $[\{\text{O}(\text{SiMe}_2\text{NDipp})_2\}\text{InNMes}]^-$ [$1.984(2)\text{ \AA}$].²²



Scheme 3.5. Synthetic route to $(\text{MeIPrCH})\text{InNAr}^{\text{Dipp}}$ (**6**) and its major resonance forms (left) and the structure of Power's imide $\text{Ar}^{\text{Dipp}}\text{InNAr}^{\text{Xyl-}t\text{Bu}}$ (right).

The computed HOMO-1 of $(\text{MeIPrCH})\text{InNAr}^{\text{Dipp}}$ (**6**) (Figure 3.9) does show C–In π -character, however, the structural impact of this interaction on the exocyclic C=C bond length [$\text{C1}–\text{C4} = 1.360(4)\text{ \AA}$] seems minimal, as this distance is the same within experimental error as in $(\text{MeIPrCH})_2\text{Sn}$: [$1.352(5)\text{ \AA}$],¹² a species that lacks $\text{C}_{\text{aNHO}}–\text{E}$ π -bonding. As in Power's indium-imide, the geometry at N in **6** is bent [$\text{In1}–\text{N3}–\text{C51} = 122.5(2)^\circ$], while the geometry at In in **6** is close to linear, with an $\text{C4}–\text{In1}–\text{N3}$ angle of $170.39(12)^\circ$; the related angle in $\text{Ar}^{\text{Dipp}}\text{InNAr}^{\text{Xyl-}t\text{Bu}}$ is narrower [$142.2(1)^\circ$].^{20a} One possible reason for the quasi linear geometry at the indium center in **6** is the presence of added close aryl \cdots In contacts (as short as $3.0821(15)\text{ \AA}$) at either side of the C–In–N array. These interactions were also present when inspecting the computed non-covalent interaction (NCI) indices in **6** and are seen *via*

additional In-C/H bond critical points (bcp) in a topological Atoms-In-Molecules (AIM) analysis.

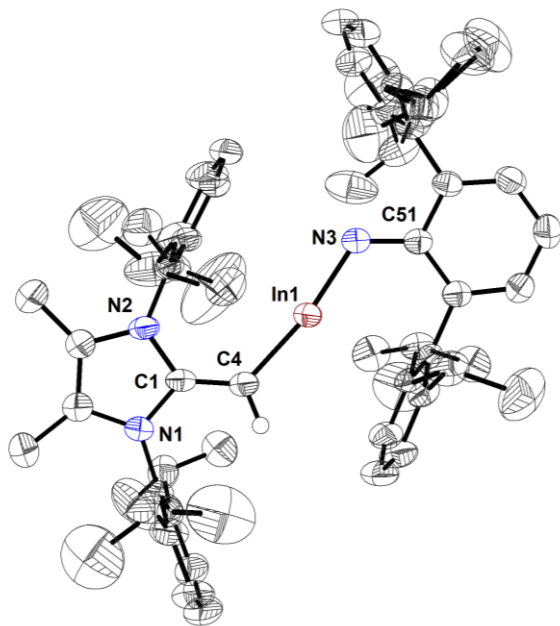


Figure 3.8. Molecular structure of $(^{\text{Me}}\text{IPrCH})\text{InNAr}^{\text{Dipp}}$ (**6**) with thermal ellipsoids plotted at 50 % probability. All hydrogen atoms (except for the vinylic hydrogen at C4) are omitted for clarity. The toluene solvent molecule is not shown. Selected bond lengths [\AA] and [$^{\circ}$]: In1–N3 1.949(3), C4–In1 2.035(3), C1–C4 1.630(4), N3–C51 1.361(4); C1–C4–In1 170.39(12), In1–N3–C51 122.5(2).

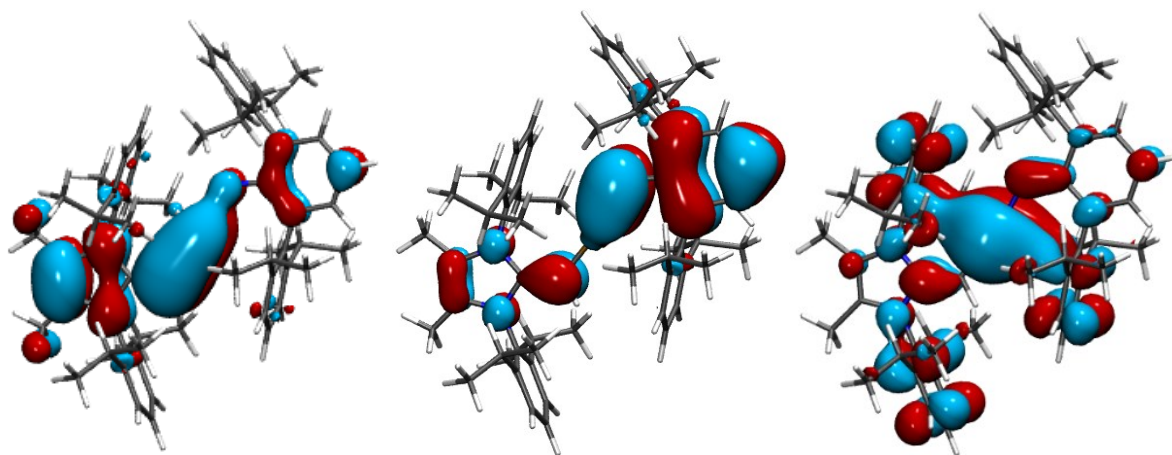


Figure 3.9. HOMO-1 (left), HOMO (middle), and LUMO (right) of $(^{\text{Me}}\text{IPrCH})\text{InNAr}^{\text{Dipp}}$ (**6**) computed at the B3LYP/cc-pVDZ(-PP) level of theory with the orbitals plotted with an *iso*-value of ± 0.02 .

AIM analysis of the InN array in **6** gave bond critical points (bcps) with key parameters that are characteristic of predominantly ionic bonding contributions. The delocalization index, $\delta(\text{In}, \text{N})$, for the InN unit in **6** of (1.13) is rather low for In–N π -bonding. For comparison, the delocalization indices $\delta(\text{In}, \text{N})$ were determined for HInNH (1.73), HInNPh (1.51), PhInNPh (1.44), $(\text{H}_2\text{C}=\text{CH})\text{InNPh}$ (1.45) and $(\text{HCNH})_2\text{C}=\text{CH})\text{InNPh}$ (1.39), and gave significantly larger values than in **6**. Natural bonding orbital (NBO) analysis for HInNH revealed both σ and π In–N bonding, but only a σ -bonding NBO was found in **6**. Second-order perturbation theory uncovered strong $\sigma(\text{In}-\text{N})$ to $\sigma^*(\text{In}-\text{C})$, $\sigma(\text{In}-\text{C})$ to $\sigma^*(\text{In}-\text{N})$ and $\pi(\text{N}-\text{C})$ to $\text{In}(\text{p})$ interactions of $E_2 = 65.8, 48.1$ and $14.3 \text{ kcal mol}^{-1}$ respectively. Lastly, the computed frontier orbitals of **6** show a discernible In–N π interaction in the HOMO, contradicting the results derived from the AIM and NBO analyse. Interestingly, increasing the *iso*-surface from ± 0.02 to ± 0.04 decreased dramatically the $\text{In}(\text{p})$ contribution to the HOMO, as shown in Figure 3.10. All told, one can describe the In–N linkage in **6** as containing a very polarized/weak π -bond.

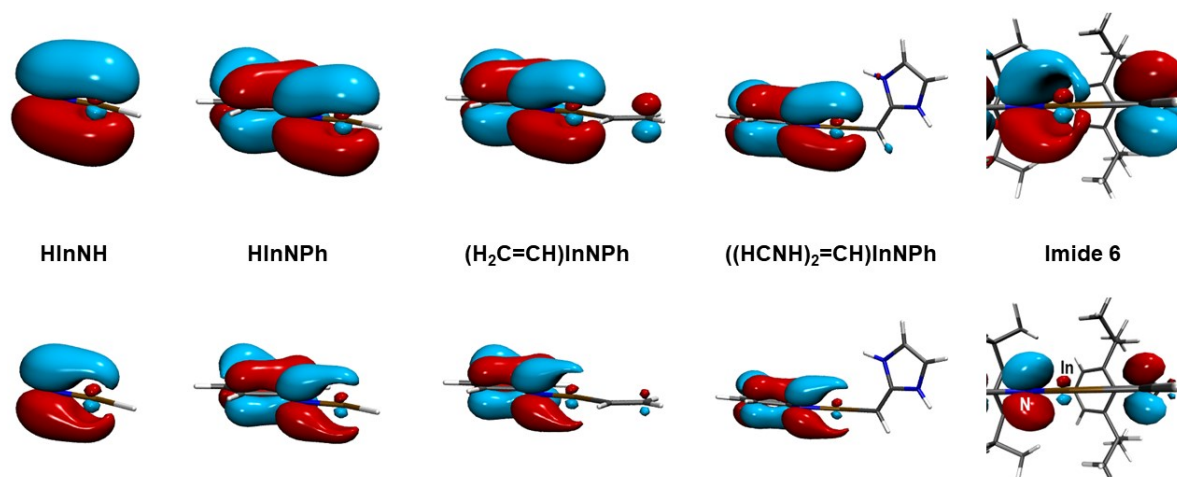


Figure 3.10. Highest occupied molecular orbitals of modeled imides and $(^{\text{Me}}\text{IPrCH})\text{InNAr}^{\text{Dipp}}$ (**6**) at *iso*-values of ± 0.02 (top) and ± 0.04 (bottom).

The deep-orange color of $(^{\text{Me}}\text{IPrCH})\text{InNAr}^{\text{Dipp}}$ (**6**) prompted further computational and spectroscopic analysis. The UV-vis spectrum of **6** in hexanes showed two intense absorptions at 459 and 341 nm ($\epsilon = 3690$ and $8040 \text{ L mol}^{-1} \text{ cm}^{-1}$). TD-DFT studies of **6** provided a computed spectrum [$\lambda_{\text{max}} = 457$ and 378] that matched well with the experimental data (Figure 3.11). Furthermore, this identified the band at 459 nm as being a HOMO–LUMO transition [$\text{In–N } \pi$ to $\text{In–N } \pi^*$]. The second transition at 341 nm consists of a HOMO–LUMO+7 transition [$\text{In–N } \pi$ to $\text{C–In } \pi^*$].

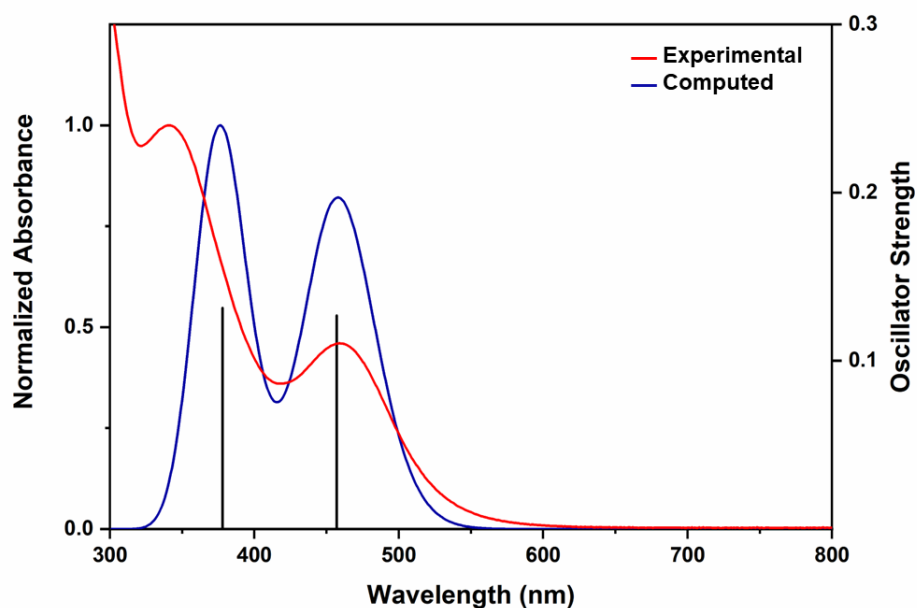
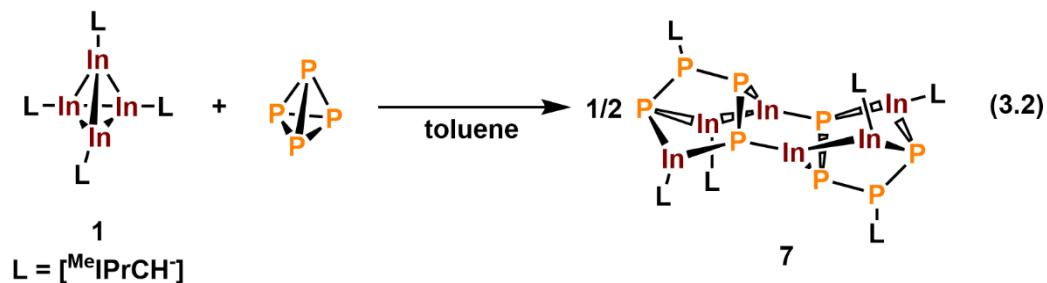


Figure 3.11. Experimentally determined UV-vis spectrum of $(^{\text{Me}}\text{IPrCH})\text{InNAr}^{\text{Dipp}}$ (**6**) in hexanes with computed UV-vis spectra overlay with corresponding oscillator strengths. Computed at B3LYP/cc-pVDZ(-PP) level of theory.

On one occasion, $[(^{\text{Me}}\text{IPrCH})\text{In}]_4$ (**1**) was quickly combined with white phosphorus (P_4) and purple crystals of the novel In_6P_8 cluster $[(^{\text{Me}}\text{IPrCH})\text{In}_6\text{P}_8]$ (**7**) were obtained (Equation 3.2 and Figure 3.12). Unfortunately, repeated attempts to reproduce this result on a preparative scale gave $^{\text{Me}}\text{IPrCH}_2$ as the major soluble species.



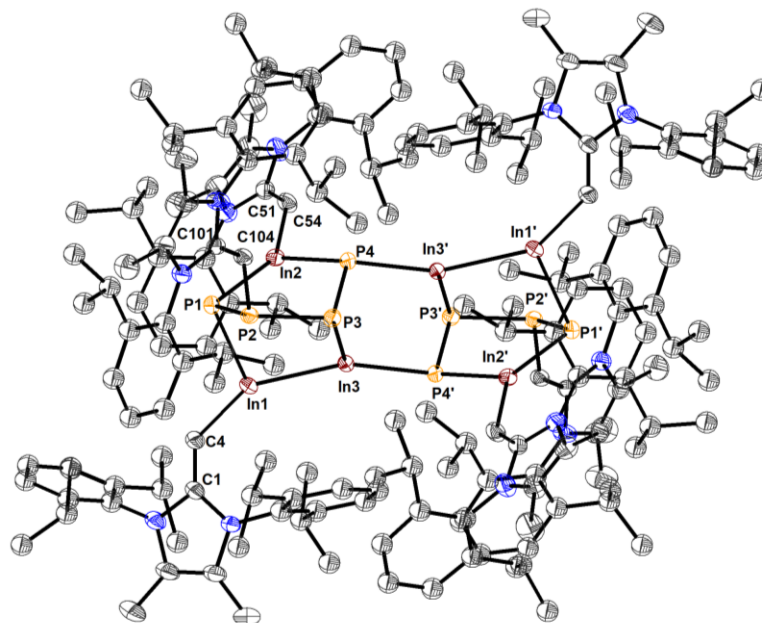


Figure 3.12. Molecular structure of $[(^{\text{Me}}\text{IPrCH})_6\text{In}_6\text{P}_8]$ (**7**) with thermal ellipsoids plotted at 50 % probability. All hydrogen atoms are omitted for clarity. Selected bond lengths [\AA] and angles [$^\circ$]: C4–In1 2.1065(19), In1–P1 2.5623(3), In1–In3 2.73726(16), C54–In2 2.1008(18), In2–P1 2.4936(6), In2–P4 2.5274(5), C104–P2 1.7863(18), P1–P2 2.2346(6), P2–P3 2.2374(6), P3–P4 2.2045(6), P4–In3' 2.5702(2); C1–C4–In1 135.06(15), C4–In1–In3 147.91(5), In1–In3–P4' 80.913(13), In3–P3–P4 73.145(18), In3–P4'–P3' 107.68(2), P4–P3–P2 102.21(2), P3–P2–P1 113.87(2), P1–P2–C104 98.69(6), P2–P1–In2 101.88(2), In1–P2–In2 89.271(14), P1–In2–C54 145.42(5), P4–In2–C54 110.21(5).

3.3 Conclusions

This Chapter explores the isolation of the tetrameric In(I) complex, $[(^{\text{Me}}\text{IPrCH})\text{In}]_4$ (**1**), stabilized by the steric bulk afforded by an anionic NHO ligand. Scission of this tetramer into monomeric units was possible by addition of the Lewis acid $\text{B}(\text{C}_6\text{F}_5)_3$, leading to $(^{\text{Me}}\text{IPrCH})\text{In}(\text{THF}) \cdot \text{B}(\text{C}_6\text{F}_5)_3$ (**2**), which highlights the ambiphilic character of the In(I) center. Activation of strong H–B bonds in boranes by the In(I) centers in **1** was possible, affording rapid H/aNHO ligand exchange at boron to yield $(^{\text{Me}}\text{IPrCH})\text{Bpin}$ (**5**). Lastly a rare example of an indium-imide was isolated, $(^{\text{Me}}\text{IPrCH})\text{InNAr}^{\text{Dipp}}$ (**6**), featuring a highly polar/weak In–N π

bond. This last result places anionic *N*-heterocyclic olefins (aNHOs) amongst the rank of versatile ligands of tunable bulk for the advancement of low-coordination inorganic chemistry, with future catalysis *via* low-oxidation state elements envisioned.

3.4 Experimental Details

3.4.1 General Considerations

All reactions were performed using Schlenk and glovebox (Innovative Technology, Inc.) techniques under a nitrogen atmosphere. All solvents were purified using a Grubbs-type solvent purification system²³ manufactured by Innovative Technology, Inc., degassed (freeze–pump–thaw method), and stored under an atmosphere of nitrogen prior to use. 2-Isopropoxy-4,4,5,5-tetramethyl-1,3,2-dioxaborolane (*i*PrOBpin) and pinacolborane (HBpin) were purchased from Oakwood Chemical and used as received. Tris(pentafluorophenyl)borane (B(C₆F₅)₃) was purchased from TCI and used as received. I₂, K[N(SiMe₃)₂] and ⁿBuLi (2.5 M solution in hexanes) were purchased from Sigma-Aldrich and used as received. [MeⁱIPrCH)Li]₂,¹² TripBH₂,^{15a} Ar^{Dipp}N₃,²¹ SIPrCH₂²⁴ and CpIn²⁵ were prepared according to literature procedures [SIPr = (H₂CNDipp)₂C; MeⁱIPr = (MeCNDipp)₂C; Ar^{Dipp} = 2,6-Dipp₂C₆H₃; Dipp = 2,6-*i*Pr₂C₆H₃; Trip = 2,4,6-*i*Pr₃C₆H₂]. ¹H, ¹³C{¹H}, ¹¹B{¹H}, ¹⁹F, and ⁷Li NMR spectra were recorded on 400, 500, 600 or 700 MHz Varian Inova instruments and were referenced externally to SiMe₄ (¹H, ¹³C{¹H}), 15 % F₃B•OEt₂ (¹¹B}, Cl₃CF (¹⁹F) and 9.7 M solution of LiCl in D₂O (⁷Li). UV-vis spectroscopic measurements were carried out with a Varian Carry 300 Scan spectrophotometer. Elemental analyses were performed by the Analytical and Instrumentation Laboratory at the University of Alberta using a Thermo Flash

2000 Elemental Analyzer. Melting points were measured in sealed glass capillaries under nitrogen with a MelTemp apparatus and are uncorrected.

3.4.2 Synthetic Procedures

Synthesis of [(^{Me}IPrCH)In]₄ (1): A solution of [(^{Me}IPrCH)Li]₂ (0.151 g, 0.173 mmol) in 10 mL of toluene was added to a solution of CpIn (0.061 g, 0.34 mmol) in 3 mL of toluene. After one minute the solution had turned deep red. After a further 40 minutes of stirring the volatiles were removed *in vacuo*, and the remaining solid residue was extracted with 18 mL of hexanes and the mixture was filtered through a plug of diatomaceous earth. The resulting deep-red filtrate was concentrated to a volume of 1 mL and stored in a -35 °C freezer for 16 hours to afford deep-red microcrystals of [(^{Me}IPrCH)In]₄ (1) (0.056 g, 30 %). X-ray quality crystals were obtained by dissolving 1 in 1 mL of toluene and storing in a -35 °C freezer for one month.

¹H NMR (700 MHz, C₆D₆): δ 7.37-7.40 (m, 4H, ArH), 7.34-7.35 (m, 8H, ArH), 7.24 (t, 4H, ³J_{HH} = 7.0 Hz, *p*-ArH), 7.16-7.17 (m, 8H, *m*-ArH), 3.72 (s, 4H, CHIn), 3.39 (sept, 8H, ³J_{HH} = 7.0 Hz, CH(CH₃)₂), 3.29 (sept, 8H, ³J_{HH} = 7.0 Hz, CH(CH₃)₂), 1.68 (s, 12H, CN-CH₃), 1.66 (s, 12H, CN(CH₃)), 1.64 (d, 24H, ³J_{HH} = 7.0 Hz, CH(CH₃)₂), 1.40 (d, 24H, ³J_{HH} = 7.0 Hz, CH(CH₃)₂), 1.30 (d, 24H, ³J_{HH} = 7.0 Hz, CH(CH₃)₂), 1.28 (d, 24H, ³J_{HH} = 7.0 Hz, CH(CH₃)₂).

¹³C{¹H} NMR (176 MHz, C₆D₆): δ 154.9 (NCN), 149.4 (ArC), 147.6 (ArC), 134.7 (ArC), 134.5 (ArC), 130.3 (ArC), 128.8 (ArC), 128.1 (CHIn), 126.6 (ArC), 124.2 (ArC), 116.6 (NC-CH₃), 115.8 (NC-CH₃), 28.8 (CH(CH₃)₂), 28.7 (CH(CH₃)₂), 26.3 (CH(CH₃)₂), 25.5 (CH(CH₃)₂), 24.2 (CH(CH₃)₂), 24.1 (CH(CH₃)₂), 10.3 (CN-CH₃), 9.9 (CN-CH₃). Anal. Calcd. for C₁₂₀H₁₆₄In₄N₈ (%): C 66.18, H 7.59, N 5.14; Found: C 66.11, H 8.11, N 4.55. M.p. 126 °C

(decomp). The exocyclic vinyl carbon resonance was located indirectly by HSQC and overlaps with a residual benzene resonance by coincidence. UV-vis (in hexanes): $\lambda_{\text{max}} = 515 \text{ nm}$, $\epsilon = 4390 \text{ L mol}^{-1} \text{ cm}^{-1}$; $\lambda_{\text{max}} = 439 \text{ nm}$, $\epsilon = 4970 \text{ L mol}^{-1} \text{ cm}^{-1}$.

Synthesis of [(SIPrCH)Li]₂ (2): Iodine (0.4598 g, 1.811 mmol) dissolved in 10 mL of toluene was added *via* cannula to a solution of SIPrCH₂ (0.7325 g, 1.811 mmol) in 50 mL of toluene, resulting in the immediate formation of a yellow solid. The mixture was then stirred for 1 hour. *After this point, all manipulations were performed in the absence of ambient light.* A solution of K[N(SiMe₃)₂] (0.5060 g, 2.536 mmol) in 10 mL of THF was added *via* cannula and the resulting mixture was stirred for 1 hour, followed by removal of the volatiles *in vacuo*. The residue was extracted with 100 mL of hexanes and filtered through a plug of diatomaceous earth. The volatiles were removed from the filtrate *in vacuo* and the residue was dissolved in 15 mL of hexanes, followed by the addition of ⁿBuLi (0.797 mL, 2.5 M solution in hexanes, 2.0 mmol). The mixture was stirred for 15 minutes, after which a white precipitate had formed. The supernatant was decanted away and the volatiles were removed from the remaining white solid *in vacuo* to yield [(SIPrCH)Li]₂ (2) (0.3790 g, 54 %). X-ray quality crystals of 2 were obtained by dissolving the product in 1 mL of toluene and storing in a -35 °C freezer for 72 hours. ¹H NMR (700 MHz, C₆D₆): δ 7.36 (t, 2H, ³J_{HH} = 7.0 Hz, *p*-ArH), 7.27 (d, 4H, ³J_{HH} = 7.0 Hz, *m*-ArH), 6.93 (d, 4H, ³J_{HH} = 7.0 Hz, *m*-ArH), 6.79 (t, 2H, ³J_{HH} = 7.0 Hz, *p*-ArH), 3.57 (t, 4H, ³J_{HH} = 7.0 Hz, NCH₂), 3.46 (t, 4H, ³J_{HH} = 7.0 Hz, NCH₂), 3.31-3.40 (overlapping multiplets, 8H, CH(CH₃)₂), 1.36 (d, 12H, ³J_{HH} = 7.0 Hz, CH(CH₃)₂), 1.32 (d, 12H, ³J_{HH} = 7.0 Hz, CH(CH₃)₂), 1.23 (d, 12H, ³J_{HH} = 7.0 Hz, CH(CH₃)₂), 1.11 (d, 12H, ³J_{HH} = 7.0 Hz, CH(CH₃)₂), 1.03 (s, 2H, CHLi). ¹³C{¹H} NMR (176 MHz, C₆D₆): δ 161.8 (NCN), 150.4

(ArC), 150.1 (ArC), 140.6 (ArC), 140.3 (ArC), 128.9 (ArC), 127.5 (ArC), 125.8 (ArC), 124.6 (ArC), 123.9 (ArC), 77.4 (CHLi), 50.3 (NCH₂), 48.7 (NCH₂), 28.6 (CH(CH₃)₂), 28.5 (CH(CH₃)₂), 25.3 (CH(CH₃)₂), 24.7 (CH(CH₃)₂), 24.5 (CH(CH₃)₂), 23.9 (CH(CH₃)₂). ⁷Li{¹H} NMR (194 MHz, C₆D₆): δ 0.7(s) Anal. Calcd. for C₅₆H₇₈Li₂N₄ (%): C 81.91, H 9.57, N 6.82; Found: C 81.43, H 9.60, N 6.61. M.p. 182–183 °C.

Synthesis of [(SIPrCH)In]₄ (3): A solution of [(SIPrCH)Li]₂ (**2**) (0.199 g, 0.195 mmol) in 8 mL of toluene was added to a slurry of CpIn (0.69 g, 0.38 mmol) in 8 mL of toluene. After one minute the solution had turned deep red. After a further 45 minutes of stirring the volatiles were removed *in vacuo*, and the remaining solid was extracted with 18 mL of hexanes and the mixture filtered through a plug of diatomaceous earth. The resulting deep-red filtrate was concentrated to a volume of 5 mL and stored in a -35 °C freezer for 16 hours, which afforded [(SIPrCH)In]₄ (**3**) as an analytically pure deep-orange solid (0.048 g, 24 %). ¹H NMR (700 MHz, C₆D₆): δ 7.38 (t, 4H, ³J_{HH} = 7.0 Hz, *p*-ArH), 7.30 (d, 8H, ³J_{HH} = 7.0 Hz, *m*-ArH), 7.16–7.18 (m, 4H, ³J_{HH} = 7.0 Hz, *p*-ArH), 6.95 (d, 8H, ³J_{HH} = 7.0 Hz, *m*-ArH), 3.56 (t, 8H, ³J_{HH} = 7.0 Hz, NCH₂), 3.55 (s, 4H, CHIn), 3.44–3.47 (m, 16H, NCH₂ and CH(CH₃)₂), 3.30 (sept, 8H, ³J_{HH} = 7.0 Hz, CH(CH₃)₂), 1.55 (d, 24H, ³J_{HH} = 7.0 Hz, CH(CH₃)₂), 1.32 (d, 48H, ³J_{HH} = 7.0 Hz, CH(CH₃)₂), 1.28 (d, 24H, ³J_{HH} = 7.0 Hz, CH(CH₃)₂). ¹³C{¹H} NMR (176 MHz, C₆D₆): δ 157.9 (NCN), 149.8 (ArC), 148.3 (ArC), 138.5 (ArC), 138.2 (ArC), 130.7 (=CHIn), 129.9 (ArC), 129.3 (ArC), 126.8 (ArC), 124.4 (ArC), 50.7 (NCH₂), 50.0 (NCH₂), 28.9 (CH(CH₃)₂), 28.7 (CH(CH₃)₂), 25.9 (CH(CH₃)₂), 25.6 (CH(CH₃)₂), 25.2 (CH(CH₃)₂), 24.7 (CH(CH₃)₂). Anal. Calcd. for C₁₂₈H₁₅₆N₈In₄ (%): C 64.87, H 7.58, N 5.40; Found: C 64.56, H 7.18, N 5.01. M.p. 129 °C (decomp).

Synthesis of (^{Me}IPrCH)In(THF)•B(C₆F₅)₃ (4): A solution of B(C₆F₅)₃ (0.052 g, 0.10 mmol) in 3 mL of benzene was added to a solution of **1** (0.055 g, 0.025 mmol) in 4 mL of benzene. After one minute of stirring the color of the reaction mixture had turned dark yellow-brown. After a further three minutes of stirring the volatiles were removed *in vacuo*, and the remaining solid was extracted in 18 mL of pentane and the mixture was filtered through a plug of diatomaceous earth. The resulting orange filtrate was concentrated to volume of 1 mL and 1 mL of THF was added. Storing the solution in a -35 °C freezer for 24 hours afforded (^{Me}IPrCH)In(THF)•B(C₆F₅)₃ (**4**) as a bright-yellow powder (0.024 g, 21 %). X-ray quality crystals of **4** were grown from a solution in pentane/THF over the course of one month. ¹H NMR (700 MHz, C₆D₆): δ 7.18 (t, 1H, ³J_{HH} = 7.0 Hz, *p*-ArH), 7.07 (d, 2H, ³J_{HH} = 7.0 Hz, *m*-ArH), 7.06 (d, 2H, ³J_{HH} = 7.0 Hz, *m*-ArH), 6.79 (t, 1H, ³J_{HH} = 7.0 Hz, *p*-ArH), 3.45 (t, 4H, ³J_{HH} = 7.0 Hz, OCH₂CH₂), 4.07 (s, 1H, CHIn), 2.85 (sept, 4H, ³J_{HH} = 7.0 Hz, CH(CH₃)₂), 1.42 (s, 3H, CN-CH₃), 1.36 (s, 3H, CN-CH₃), 1.31-1.32 (m, 10H, ³J_{HH} = 7.0 Hz, CH(CH₃)₂ overlapping with OCH₂CH₂), 1.27 (d, 6H, ³J_{HH} = 7.0 Hz, CH(CH₃)₂), 1.08 (d, 6H, ³J_{HH} = 7.0 Hz, CH(CH₃)₂), 0.95 (d, 6H, ³J_{HH} = 7.0 Hz, CH(CH₃)₂). ¹³C{¹H} NMR (176 MHz, C₆D₆): δ 159.6 (NCN), 148.0-148.2 (m, ArF), 147.8 (ArC), 147.0 (ArC), 146.7-146.9 (m, ArF), 144.7 (ArC), 139.7-139.9 (m, ArF), 138.3-138.5 (m, ArF), 137.7-137.9 (m, ArF), 136.3-136.5 (m, ArF), 131.9 (ArC), 131.0 (ArC), 130.4 (ArC), 129.9 (ArC), 127.9 (ArC), 127.8 (ArC), 127.1 (ArC), 124.4 (ArC), 118.8 (NC-CH₃), 117.4 (NC-CH₃), 81.7 (C=CHIn), 67.8 (OCH₂), 28.6 (CH(CH₃)₂), 28.5 (CH(CH₃)₂), 25.2 (OCH₂CH₂), 24.2 (CH(CH₃)₂), 23.8 (CH(CH₃)₂), 23.4 (CH(CH₃)₂), 23.1 (CH(CH₃)₂), 8.9 (NCCH₃), 8.8 (NCCH₃). ¹¹B{¹H} NMR (128 MHz, C₆D₆): δ -14.3 (s). ¹⁹F NMR (376 MHz, C₆D₆): δ -129.8 (d, 6F, ³J_{FF} = 37.6 Hz, *o*-ArF), -159.0 (t, 3F,

$^3J_{FF} = 37.6$ Hz, *p*-ArF), -163.7 to -163.8 (m, 6F, *m*-ArF). Anal. Calcd. for C₅₂H₄₉BF₁₅IN₂O (%): C 55.34, H, 4.38, N 2.48; Found: C 55.12, H 4.41, N 2.50. M.p. 147–149 °C.

Synthesis of (MeIPrCH)In•B(C₆F₅)₃ (4'): A solution of B(C₆F₅)₃ (0.026 g, 0.051 mmol) in 1 mL of C₆D₆ was added to a solution of **1** (0.028 g, 0.013 mmol) in 1 mL of C₆D₆. After one minute of stirring the color of the reaction mixture had turned a dark yellow-brown. After a further five minutes of stirring the reaction mixture was filtered through glass filter paper and the volatiles were removed from the filtrate *in vacuo* to afford (MeIPrCH)In•B(C₆F₅)₃ (**4'**) as an orange solid (0.040 g, 74 %). ¹H NMR (700 MHz, C₆D₆): δ 7.19 (t, 1H, ³J_{HH} = 7.0 Hz, *p*-Ar), 7.06 (overlapping d, 4H, ³J_{HH} = 7.0 Hz, *m*-Ar), 6.80 (t, 1H, ³J_{HH} = 7.0 Hz, *p*-Ar), 3.57 (s, 1H, CHIn), 2.84 (sept, 4H, ³J_{HH} = 7.0 Hz, CH(CH₃)₂), 1.41 (s, 3H, CN-CH₃), 1.35 (s, 3H, CN-CH₃), 1.31 (d, 6H, ³J_{HH} = 7.0 Hz, CH(CH₃)₂), 1.28 (d, 6H, ³J_{HH} = 7.0 Hz, CH(CH₃)₂), 1.09 (d, 6H, ³J_{HH} = 7.0 Hz, CH(CH₃)₂), 0.94 (d, 6H, ³J_{HH} = 7.0 Hz, CH(CH₃)₂). ¹³C {¹H} NMR (176 MHz, C₆D₆): δ 160.2 (NCN), 148.4–148.5 (m, ArF), 148.1 (ArC), 147.6 (ArC), 147.1–147.2 (m, ArF), 140.2–140.3 (m, ArF), 138.8–138.9 (m, ArF), 138.1–138.3 (m, ArF), 136.7–136.9 (m, ArF), 132.3 (ArC), 131.2 (ArC), 130.9 (ArC), 130.4 (ArC), 128.3 (ArC), 127.7 (ArC), 124.8 (ArC), 119.4 (NC-CH₃), 117.8 (NC-CH₃), 83.0 (CHIn), 31.9 (CH(CH₃)₂), 28.9 (CH(CH₃)₂), 28.8 (CH(CH₃)₂), 24.6 (CH(CH₃)₂), 24.2 (CH(CH₃)₂), 23.7 (CH(CH₃)₂), 23.6 (CH(CH₃)₂), 23.0 (CH(CH₃)₂), 9.2 (NCCH₃), 9.1 (NCCH₃). ¹¹B {¹H} NMR (128 MHz, C₆D₆): δ -14.4 (s). ¹⁹F NMR (376 MHz, C₆D₆): δ -129.9 (d, 6F, ³J_{FF} = 37.6 Hz, *o*-ArF), -158.7 (t, 3F, ³J_{FF} = 37.6 Hz, *p*-ArF), -163.5 to -163.6 (m, 6F, *m*-ArF). Anal. Calcd. for C₄₈H₄₁BF₁₅IN₂ (%): C 54.57, H 3.91, N 2.65; Found: C 56.66, H 4.34, N 2.76; *the discrepancy in calculated and*

experimental elemental analysis values may be due to absorbance of residue THF from the glovebox atmosphere. M.p. 92 °C (decomp).

Synthesis of (^{Me}IPrCH)B(H)Trip: To a solution of TripBH₂ (0.008 g, 0.04 mmol) in 2 mL of toluene was added **1** (0.020 g, 0.0092 mmol) in 2 mL of toluene. After one minute, the deep-red color of **1** had faded with bubbling H₂ gas observed and the formation of a black precipitate, presumably indium metal. After a further seven minutes of stirring, the reaction mixture was filtered through a plug of diatomaceous earth resulting in a colorless solution. The volatiles were removed from the filtrate *in vacuo* to afford (^{Me}IPrCH)B(H)Trip as a white solid (0.021 g, 86 %). ¹H and ¹¹B{¹H} NMR spectral data matched previously reported literature values.^{15a}

Synthesis of (^{Me}IPrCH)Bpin (5): Route A. A solution of [(^{Me}IPrCH)Li]₂ (0.170 g, 0.195 mmol) in 5 mL of toluene was added dropwise to a solution of ⁱPrOBpin (79 μL, 0.39 mmol) in 3 mL of toluene. After stirring for 3 hours a pale-orange supernatant was formed along with a white precipitate. The volatiles were removed *in vacuo*, the residue was extracted with 15 mL of hexanes and filtered. The filtrate was concentrated to a volume of 1 mL and stored in a -35 °C freezer for 16 hours, leading to the formation of colorless microcrystals of (^{Me}IPrCH)Bpin (**5**) (0.044 g, 20 %). X-ray quality crystals of **5** were grown from hexanes at -35 °C over the course of one month. ¹H NMR (700 MHz, C₆D₆): δ 7.31 (t, 1H, ³J_{HH} = 7.0 Hz, *p*-ArH), 7.22 (t, 1H, ³J_{HH} = 7.0 Hz, *p*-ArH), 7.15 (d, 2H, ³J_{HH} = 7.0 Hz, *m*-ArH), 7.10 (d, 2H, ³J_{HH} = 7.0 Hz, *m*-ArH), 3.17 (sept, 2H, ³J_{HH} = 7.0 Hz, CH(CH₃)₂), 3.07 (sept, 2H, ³J_{HH} = 7.0

Hz, CH(CH₃)₂), 2.65 (s, 1H, CH(Bpin)), 1.54 (s, 3H, CN-CH₃), 1.51 (s, 3H, CN-CH₃), 1.50 (d, 6H, ³J_{HH} = 7.0 Hz, CH(CH₃)₂), 1.36 (d, 6H, ³J_{HH} = 7.0 Hz, CH(CH₃)₂), 1.24 (d, 6H, ³J_{HH} = 7.0 Hz, CH(CH₃)₂), 1.15 (d, 6H, ³J_{HH} = 7.0 Hz, CH(CH₃)₂), 0.89 (s, 12H, OC(CH₃)₂). ¹³C{¹H} NMR (176 MHz, C₆D₆): δ 155.9 (NCN), 148.6 (ArC), 148.4 (ArC), 134.3 (ArC), 132.6 (ArC), 129.6 (ArC), 129.0 (ArC), 124.5 (ArC), 123.8 (ArC), 117.7 (NC-CH₃), 117.0 (NC-CH₃), 79.9 (OC(CH₃)₂), 48.0 (CHBpin), 29.1 (CH(CH₃)₂), 28.9 (CH(CH₃)₂), 24.7 (OC(CH₃)₂), 24.6 (CH(CH₃)₂), 24.0 (CH(CH₃)₂), 23.8 (CH(CH₃)₂), 9.7 (NCCH₃), 9.5 (NCCH₃). ¹¹B{¹H} NMR (128 MHz, C₆D₆): δ 28.4 (s). Anal. Calcd. for C₃₆H₅₃BN₂O₂ (%): C 77.68, H 9.60, N 5.75; Found: C 76.55, H, 9.53, N 4.98. M.p. 145–147 °C. *The exocyclic vinyl carbon resonance was not found in the ¹³C{¹H} NMR but located indirectly by HSQC.*

Route B. To a solution of **1** (0.045 g, 0.021 mmol) in 2 mL of C₆D₆ was added HBpin (12 μL, 0.083 mmol). After one minute, the deep-red color of **1** had faded and a black precipitate had formed, presumably indium metal. After a further four minutes of stirring, the reaction mixture was filtered through a plug of diatomaceous earth resulting in a colorless solution. ¹H and ¹¹B{¹H} NMR analysis of the reaction mixture showed the formation of (^{Me}IPrCH)Bpin (**5**), which was not isolated.

Synthesis of (^{Me}IPrCH)InNAr^{Dipp} (6**):** A solution of [(^{Me}IPrCH)Li]₂ (0.029 g, 0.033 mmol) in 2 mL of toluene was added to a solution of CpIn (0.011 g, 0.061 mmol) in 2 mL of toluene. After one minute the color of the reaction mixture had turned deep red. After a further 50 minutes the reaction mixture was filtered through a plug of diatomaceous earth. To the resulting deep-red solution containing **1** was added rapidly Ar^{Dipp}N₃ (0.029 g, 0.066 mmol) in 2 mL of toluene. After one minute the reaction mixture became red-orange. After a further 40

minutes the reaction mixture was concentrated to a volume of 1 mL and placed in a -35 °C freezer for 16 hours, which afforded bright-orange microcrystals of (^{Me}IPrCH)InNAr^{Dipp} (**6**) (0.018 g, 31 %). Crystals of **6** that were suitable for X-ray diffraction analysis were obtained by dissolving **6** in 1 mL of toluene and storing the solution at -35 °C for 16 hours. ¹H NMR (700 MHz, C₆D₆): δ 7.35 (t, 1H, ³J_{HH} = 7.0 Hz, *p*-ArH), 7.28 (d, 2H, ³J_{HH} = 7.0 Hz, *m*-ArH), 7.22 (d, 2H, ³J_{HH} = 7.0 Hz, *m*-ArH), 7.21 (d, 2H, ³J_{HH} = 7.0 Hz, *m*-ArH), 7.13 (t, 1H, ³J_{HH} = 7.0 Hz, *p*-ArH), 7.11 (d, 2H, ³J_{HH} = 7.0 Hz, *m*-ArH), 7.05 (t, 1H, ³J_{HH} = 7.0 Hz, *p*-ArH), 7.02 (d, 1H, ³J_{HH} = 7.0 Hz, *p*-ArH), 6.82 (t, 1H, ³J_{HH} = 7.0 Hz, *p*-ArH), 6.75 (t, 1H, ³J_{HH} = 7.0 Hz, *p*-ArH), 3.17-3.21 (overlapping septets, 4H, ³J_{HH} = 7.0 Hz, CH(CH₃)₂), 2.83 (sept, 2H, ³J_{HH} = 7.0 Hz, CH(CH₃)₂), 2.73 (sept, 2H, ³J_{HH} = 7.0 Hz, CH(CH₃)₂), 1.66 (s, 1H, CHI_n), 1.45 (s, 3H, CN-CH₃), 1.43 (s, 3H, CN-CH₃), 1.37 (d, 12H, ³J_{HH} = 7.0 Hz, CH(CH₃)₂), 1.28 (d, 6H, ³J_{HH} = 7.0 Hz, CH(CH₃)₂), 1.26 (d, 6H, ³J_{HH} = 7.0 Hz, CH(CH₃)₂), 1.22 (d, 12H, ³J_{HH} = 7.0 Hz, CH(CH₃)₂), 1.16 (d, 6H, ³J_{HH} = 7.0 Hz, CH(CH₃)₂), 1.01 (d, 6H, ³J_{HH} = 7.0 Hz, CH(CH₃)₂). ¹³C{¹H} NMR (176 MHz, C₆D₆): δ 162.8 (NCN), 158.3 (ArC), 148.8 (ArC), 148.7 (ArC), 146.2 (ArC), 143.4 (ArC), 134.0 (ArC), 131.9 (ArC), 129.9 (ArC), 129.8 (ArC), 129.3 (ArC), 129.2 (ArC), 128.5 (ArC), 128.3 (ArC), 128.2 (ArC), 127.7 (ArC), 125.6 (ArC), 124.5 (ArC), 124.3 (ArC), 57.6 (=CHI_n), 30.6 (CH(CH₃)₂), 28.8 (CH(CH₃)₂), 28.6 (CH(CH₃)₂), 25.0 (CH(CH₃)₂), 24.9 (CH(CH₃)₂), 24.8 (CH(CH₃)₂), 24.7 (CH(CH₃)₂), 24.0 (CH(CH₃)₂), 23.7 (CH(CH₃)₂), 9.4 (CH(CH₃)₂), 9.2 (CH(CH₃)₂). Anal. Calcd. for C₈₀H₇₈N₃In (%): C 75.37, H 8.22, N 4.39; Found: C 68.51, H 7.60, N 3.75; *repeated attempts to obtain satisfactory elemental analysis led to low values for carbon*. M.p. 203–205 °C. UV-vis (in hexanes): λ_{max} = 459 nm, ε = 3690 L mol⁻¹ cm⁻¹; λ_{max} = 341 nm, ε = 8040 L mol⁻¹ cm⁻¹.

Synthesis of [(^{Me}IPrCH)₆In₆P₈] (7): To a solution of P₄ (0.002 g, 0.02 mmol) in 4 mL of toluene was added **1** (0.032 g, 0.015 mmol) in 5 mL of toluene. After one minute of stirring the initially deep-red mixture became red-purple along with the formation of a black precipitate. After one hour the volatiles were removed *in vacuo*. 15 mL of hexanes was then added and the mixture filtered through a plug of diatomaceous earth. The filtrate was then concentrated to a volume of 1 mL and stored in a -35 °C freezer for one week affording a single X-ray quality crystal of [(^{Me}IPrCH)₆In₆P₈] (**7**). *Attempts to repeat the preparation of 7 on a larger scale for further characterization were unsuccessful with the major isolated product being ^{Me}IPrCH₂.*

3.4.3 X-Ray Crystallography

Appropriate X-ray quality crystals were coated with a small amount of hydrocarbon oil (Paratone-N) and removed from the glovebox in a vial. Crystals were mounted quickly onto a glass fiber and placed in a low temperature stream of nitrogen on the X-ray diffractometer. All data were collected using a Bruker APEX II CCD detector/D8 or PLATFORM diffractometer using Mo K α (0.71073 Å) or Cu K α (1.54178 Å) radiation, with the crystals cooled to -80 °C or -100 °C. The data were corrected for absorption through Gaussian integration from the indexing of crystal faces.²⁶ Crystal structures were solved using intrinsic phasing (SHELXT)²⁷ and refined using SHELXL-2014.²⁸ The assignment of hydrogen atom positions is based on the sp²- or sp³ hybridization geometries of their attached carbon atoms and were given thermal parameters 20 % greater than those of their parent atoms.

Table 3.1. X-ray crystallographic data details for [(^{Me}IPrCH)In]₄ (**1**)•2 toluene.*A. Crystal Data*

formula	C ₁₃₄ H ₁₈₀ In ₄ N ₈
formula weight	2362.13
crystal color and habit ^a	red block
crystal dimensions (mm)	0.68 × 0.20 × 0.13
crystal system	triclinic
space group	<i>P</i> $\bar{1}$ (No. 2)
unit cell parameters ^b	
<i>a</i> (Å)	16.114(3)
<i>b</i> (Å)	22.258(4)
<i>c</i> (Å)	22.529(4)
α (deg)	86.035(2)
β (deg)	78.839(2)
γ (deg)	70.732(2)
<i>V</i> (Å ³)	7484(2)
<i>Z</i>	2

 ρ_{calcd} (g cm⁻³)

1.048

 μ (mm⁻¹)

0.650

B. Data Collection and Refinement Conditions

diffractometer	Bruker PLATFORM/APEX II CCD ^c
radiation (λ [Å])	graphite-monochromated Mo K α (0.71073)
temperature (°C)	-80
scan type	ω scans (0.3°) (20 s exposures)
data collection 2θ limit (deg)	52.86
total data collected	119804 ($-20 \leq h \leq 20$, $-27 \leq k \leq 27$, $-28 \leq l \leq 28$)
independent reflections	30703 ($R_{\text{int}} = 0.0707$)
number of observed reflections (<i>NO</i>)	20334 [$F_o^2 \geq 2\sigma(F_o^2)$]
structure solution method	intrinsic phasing (<i>SHELXT-2014^d</i>)
refinement method	full-matrix least-squares on F^2 (<i>SHELXL-2018^{e,f}</i>)
absorption correction method	Gaussian integration (face-indexed)
range of transmission factors	1.0000–0.6234
data/restraints/parameters	30703 / 45 g / 1357
goodness-of-fit (<i>S</i>) ^h [all data]	1.017
final <i>R</i> indices ⁱ	
<i>R</i> ₁ [$F_o^2 \geq 2\sigma(F_o^2)$]	0.0501
<i>wR</i> ₂ [all data]	0.1484
largest difference peak and hole	1.647 and -0.726 e Å ⁻³

^aObtained by recrystallization from a toluene solution.

^bObtained from least-squares refinement of 9829 reflections with $4.58^\circ < 2\theta < 46.06^\circ$.

^cPrograms for diffractometer operation, data collection, data reduction and absorption correction were those supplied by Bruker.

^dG. M. Sheldrick, *Acta Crystallogr.* **2015**, *A71*, 3–8. (*SHELXT-2014*)

^eG. M. Sheldrick, *Acta Crystallogr.* **2015**, *C71*, 3–8. (*SHELXL-2018/3*)

^fAttempts to refine peaks of residual electron density as disordered or partial-occupancy solventtoluene carbon atoms were unsuccessful. The data were corrected for disordered electron density through use of the SQUEEZE procedure as implemented in *PLATON* (A. L. Spek, *Acta Crystallogr.* **2015**, *C71*, 9–18. *PLATON* – a multipurpose crystallographic tool. Utrecht University, Utrecht, The Netherlands). A total solvent-accessible void volume of 1734 Å³ with a total electron count of 399 (consistent with and additional 8 molecules of solvent toluene, or 4 molecules per formula unit of the indium cluster compound) was found in the unit cell.

^{42he} rigid-bond restraint (**RIGU**) was applied to solvent toluene carbon atoms C11S to C17S to improve the quality of their anisotropic displacement parameters.

^h $S = [\sum w(F_o^2 - F_c^2)^2 / (n - p)]^{1/2}$ (n = number of data; p = number of parameters varied; $w = [\sigma^2(F_o^2) + (0.0770P)^2 + 0.8458P]^{-1}$ where $P = [\text{Max}(F_o^2, 0) + 2F_c^2]/3$).

ⁱ $R_1 = \sum ||F_o| - |F_c|| / \sum |F_o|$; $wR_2 = [\sum w(F_o^2 - F_c^2)^2 / \sum w(F_o^4)]^{1/2}$.

Table 3.2. X-ray crystallographic data details for [(SIPrCH)Li]₂ (**2**)•toluene.*A. Crystal Data*

formula	C ₆₃ H ₈₆ Li ₂ N ₄
formula weight	913.23
crystal color and habit ^a	colorless block
crystal dimensions (mm)	0.33 × 0.30 × 0.21
crystal system	monoclinic
space group	C2/c (No. 15)
unit cell parameters ^b	
<i>a</i> (Å)	19.5691(4)
<i>b</i> (Å)	15.1755(3)
<i>c</i> (Å)	21.1457(4)
β (deg)	114.3497(8)
<i>V</i> (Å ³)	5721.1(2)
<i>Z</i>	4
ρ _{calcd} (g cm ⁻³)	1.060
μ (mm ⁻¹)	0.449

B. Data Collection and Refinement Conditions

diffractometer	Bruker D8/APEX II CCD ^c
radiation (λ [Å])	Cu Kα (1.54178) (microfocus source)
temperature (°C)	-100
scan type	ω and φ scans (1.0°) (5 s exposures)
data collection 2θ limit (deg)	147.73
total data collected	119852 (-24 ≤ <i>h</i> ≤ 24, -18 ≤ <i>k</i> ≤ 18, -26 ≤ <i>l</i> ≤ 26)
independent reflections	5789 (<i>R</i> _{int} = 0.0343)
number of observed reflections (<i>NO</i>)	5491 [<i>F</i> _o ² ≥ 2σ(<i>F</i> _o ²)]
structure solution method	intrinsic phasing (<i>SHELXT-2014</i> ^d)
refinement method	full-matrix least-squares on <i>F</i> ² (<i>SHELXL-2018</i> ^e)
absorption correction method	Gaussian integration (face-indexed)
range of transmission factors	0.9790–0.8648
data/restraints/parameters	5789 / 0 / 349
extinction coefficient (<i>x</i>) ^f	0.00042(6)
goodness-of-fit (<i>S</i>) ^g [all data]	1.059
final <i>R</i> indices ^h	
<i>R</i> ₁ [<i>F</i> _o ² ≥ 2σ(<i>F</i> _o ²)]	0.0388
<i>wR</i> ₂ [all data]	0.1068
largest difference peak and hole	0.246 and -0.229 e Å ⁻³

^aObtained by recrystallization from a toluene solution.

^bObtained from least-squares refinement of 9507 reflections with $7.66^\circ < 2\theta < 147.00^\circ$.

^cPrograms for diffractometer operation, data collection, data reduction and absorption correction were those supplied by Bruker.

^dG. M. Sheldrick, *Acta Crystallogr.* **2015**, *A71*, 3–8. (*SHELXT-2014*)

^eG. M. Sheldrick, *Acta Crystallogr.* **2015**, *C71*, 3–8. (*SHELXL-2018/3*)

^f $F_c^* = kF_c[1 + x\{0.001F_c^2\lambda^3/\sin(2\theta)\}]^{-1/4}$ where k is the overall scale factor.

^g $S = [\sum w(F_o^2 - F_c^2)^2/(n - p)]^{1/2}$ (n = number of data; p = number of parameters varied; $w = [\sigma^2(F_o^2) + (0.0520P)^2 + 2.8094P]^{-1}$ where $P = [\text{Max}(F_o^2, 0) + 2F_c^2]/3$).

^h $R_1 = \sum ||F_o| - |F_c||/\sum |F_o|$; $wR_2 = [\sum w(F_o^2 - F_c^2)^2/\sum w(F_o^4)]^{1/2}$.

Table 3.3. X-ray crystallographic data details for (^{Me}IPrCH)In(THF)•B(C₆F₅)₃ (**4**)•pentane.*A. Crystal Data*

formula	C ₅₇ H ₆₁ BF ₁₅ InN ₂ O
formula weight	1200.70
crystal color and habit ^a	yellow block
crystal dimensions (mm)	0.34 × 0.27 × 0.24
crystal system	triclinic
space group	$P\bar{1}$ (No. 2)
unit cell parameters ^b	
<i>a</i> (Å)	10.7833(8)
<i>b</i> (Å)	13.3363(10)
<i>c</i> (Å)	21.1279(16)
<i>α</i> (deg)	107.7613(11)
<i>β</i> (deg)	102.8104(12)
<i>γ</i> (deg)	91.5239(12)
<i>V</i> (Å ³)	2807.0(4)
<i>Z</i>	2
ρ_{calcd} (g cm ⁻³)	1.421
μ (mm ⁻¹)	0.511

B. Data Collection and Refinement Conditions

diffractometer	Bruker PLATFORM/APEX II CCD ^c
radiation (λ [Å])	graphite-monochromated Mo K α (0.71073)
temperature (°C)	-80
scan type	ω scans (0.3°) (20 s exposures)
data collection 2θ limit (deg)	57.51
total data collected	52526 ($-14 \leq h \leq 14$, $-18 \leq k \leq 18$, $-28 \leq l \leq 28$)
independent reflections	14557 ($R_{\text{int}} = 0.0283$)
number of observed reflections (<i>NO</i>)	12804 [$F_o^2 \geq 2\sigma(F_o^2)$]
structure solution method	intrinsic phasing (<i>SHELXT-2014^d</i>)
refinement method	full-matrix least-squares on F^2 (<i>SHELXL-2018^e</i>)
absorption correction method	Gaussian integration (face-indexed)
range of transmission factors	0.9359–0.8825
data/restraints/parameters	14557 / 21 ^f / 715
goodness-of-fit (<i>S</i>) ^g [all data]	1.039
final <i>R</i> indices ^h	
<i>R</i> ₁ [$F_o^2 \geq 2\sigma(F_o^2)$]	0.0321
<i>wR</i> ₂ [all data]	0.0854
largest difference peak and hole	0.584 and -0.480 e Å ⁻³

^aObtained by recrystallization from a pentane solution.

^bObtained from least-squares refinement of 9764 reflections with $4.84^\circ < 2\theta < 56.24^\circ$.

^cPrograms for diffractometer operation, data collection, data reduction and absorption correction were those supplied by Bruker.

^dG. M. Sheldrick, *Acta Crystallogr.* **2015**, *A71*, 3–8. (*SHELXT-2014*)

^eG. M. Sheldrick, *Acta Crystallogr.* **2015**, *C71*, 3–8. (*SHELXL-2018/3*)

^{45he} C–C distances within the disordered tetrahydrofuran group were restrained to be approximately the same by use of the *SHELXL SAME* instruction. Likewise, the C–C distances within the solvent pentane molecule were similarly treated.

^g $S = [\sum w(F_o^2 - F_c^2)^2 / (n - p)]^{1/2}$ (n = number of data; p = number of parameters varied; $w = [\sigma^2(F_o^2) + (0.0411P)^2 + 1.0816P]^{-1}$ where $P = [\text{Max}(F_o^2, 0) + 2F_c^2]/3$).

^h $R_1 = \sum ||F_o| - |F_c|| / \sum |F_o|$; $wR_2 = [\sum w(F_o^2 - F_c^2)^2 / \sum w(F_o^4)]^{1/2}$.

Table 3.4. X-ray crystallographic details for (^{Me}IPrCH)Bpin (**5**).*A. Crystal Data*

formula	C ₃₆ H ₅₃ BN ₂ O ₂
formula weight	556.61
crystal color and habit	colorless block
crystal dimensions (mm)	0.13 × 0.10 × 0.08
crystal system	monoclinic
space group	<i>P</i> 2 ₁ / <i>c</i> (No. 14)
unit cell parameters ^a	
<i>a</i> (Å)	13.2848(3)
<i>b</i> (Å)	15.2957(3)
<i>c</i> (Å)	16.2903(4)
β (deg)	91.8769(13)
<i>V</i> (Å ³)	3308.42(13)
<i>Z</i>	4
ρ _{calcd} (g cm ⁻³)	1.117
μ (mm ⁻¹)	0.516

B. Data Collection and Refinement Conditions

diffractometer	Bruker D8/APEX II CCD ^b
radiation (λ [Å])	Cu Kα (1.54178) (microfocus source)
temperature (°C)	-100
scan type	ω and φ scans (1.0°) (5-10-15 s exposures) ^c
data collection 2θ limit (deg)	144.55
total data collected	70416 (-16 ≤ <i>h</i> ≤ 15, -18 ≤ <i>k</i> ≤ 18, -20 ≤ <i>l</i> ≤ 20)
independent reflections	6473 (<i>R</i> _{int} = 0.0622)
number of observed reflections (<i>NO</i>)	5245 [<i>F</i> _o ² ≥ 2σ(<i>F</i> _o ²)]
structure solution method	intrinsic phasing (<i>SHELXT-2014</i> ^d)
refinement method	full-matrix least-squares on <i>F</i> ² (<i>SHELXL-2018</i> ^e)
absorption correction method	Gaussian integration (face-indexed)
range of transmission factors	0.9784–0.9161
data/restraints/parameters	6473 / 0 / 373
extinction coefficient (<i>x</i>) ^f	0.00105(14)
goodness-of-fit (<i>S</i>) ^g [all data]	1.050
final <i>R</i> indices ^h	
<i>R</i> ₁ [<i>F</i> _o ² ≥ 2σ(<i>F</i> _o ²)]	0.0433
<i>wR</i> ₂ [all data]	0.1232
largest difference peak and hole	0.329 and -0.194 e Å ⁻³

^aObtained from least-squares refinement of 9875 reflections with 6.66° < 2θ < 144.28°.

^bPrograms for diffractometer operation, data collection, data reduction and absorption correction were those supplied by Bruker.

^cData were collected with the detector set at three different positions. Low-angle (detector $2\theta = -33^\circ$) data frames were collected using a scan time of 5 s, medium-angle (detector $2\theta = 75^\circ$) frames using a scan time of 10 s, and high-angle (detector $2\theta = 117^\circ$) frames using a scan time of 15 s.

^dG. M. Sheldrick, *Acta Crystallogr.* **2015**, *A71*, 3–8. (*SHELXT-2014*)

^eG. M. Sheldrick, *Acta Crystallogr.* **2015**, *C71*, 3–8. (*SHELXL-2018/3*)

^f $F_c^* = kF_c[1 + x\{0.001F_c^2\lambda^3/\sin(2\theta)\}]^{-1/4}$ where k is the overall scale factor.

^g $S = [\sum w(F_o^2 - F_c^2)^2/(n - p)]^{1/2}$ (n = number of data; p = number of parameters varied; $w = [\sigma^2(F_o^2) + (0.0595P)^2 + 0.8852P]^{-1}$ where $P = [\text{Max}(F_o^2, 0) + 2F_c^2]/3$).

^h $R_1 = \sum ||F_o| - |F_c||/\sum |F_o|$; $wR_2 = [\sum w(F_o^2 - F_c^2)^2/\sum w(F_o^4)]^{1/2}$.

Table 3.5. X-ray crystallographic details for (MeIPrCH)InNAr^{Dipp} (**6**)•toluene.*A. Crystal Data*

formula	C ₇₄ H ₉₄ InN ₃
formula weight	1140.34
crystal color and habit ^a	orange plate
crystal dimensions (mm)	0.37 × 0.17 × 0.05
crystal system	monoclinic
space group	<i>P</i> 2 ₁ / <i>n</i> (an alternate setting of <i>P</i> 2 ₁ / <i>c</i> [No. 14])
unit cell parameters ^b	
<i>a</i> (Å)	10.9546(16)
<i>b</i> (Å)	25.751(4)
<i>c</i> (Å)	23.267(3)
β (deg)	91.891(3)
<i>V</i> (Å ³)	6560.0(16)
<i>Z</i>	4
ρ _{calcd} (g cm ⁻³)	1.155
μ (mm ⁻¹)	0.402

B. Data Collection and Refinement Conditions

diffractometer	Bruker PLATFORM/APEX II CCD ^c
radiation (λ [Å])	graphite-monochromated Mo Kα (0.71073)
temperature (°C)	-80
scan type	ω scans (0.3°) (20 s exposures)
data collection 2θ limit (deg)	51.56
total data collected	80035 (-13 ≤ <i>h</i> ≤ 13, -31 ≤ <i>k</i> ≤ 31, -28 ≤ <i>l</i> ≤ 28)
independent reflections	12545 (<i>R</i> _{int} = 0.0901)
number of observed reflections (<i>NO</i>)	8925 [<i>F</i> _o ² ≥ 2σ(<i>F</i> _o ²)]
structure solution method	intrinsic phasing (<i>SHELXT-2014</i> ^d)
refinement method	full-matrix least-squares on <i>F</i> ² (<i>SHELXL-2018</i> ^{e,f})
absorption correction method	Gaussian integration (face-indexed)
range of transmission factors	1.0000–0.7633
data/restraints/parameters	12545 / 118 <i>g</i> / 720
goodness-of-fit (<i>S</i>) ^h [all data]	1.015
final <i>R</i> indices ⁱ	
<i>R</i> ₁ [<i>F</i> _o ² ≥ 2σ(<i>F</i> _o ²)]	0.0479
<i>wR</i> ₂ [all data]	0.1401
largest difference peak and hole	1.006 and -0.785 e Å ⁻³

^aObtained by recrystallization from a toluene solution.^bObtained from least-squares refinement of 9104 reflections with 4.36° < 2θ < 41.76°.

^cPrograms for diffractometer operation, data collection, data reduction and absorption correction were those supplied by Bruker.

^dG. M. Sheldrick, *Acta Crystallogr.* **2015**, *A71*, 3–8. (*SHELXT-2014*)

^eG. M. Sheldrick, *Acta Crystallogr.* **2015**, *C71*, 3–8. (*SHELXL-2018/3*)

^fAttempts to refine peaks of residual electron density as disordered or partial-occupancy solvent toluene carbon atoms were unsuccessful. The data were corrected for disordered electron density through use of the SQUEEZE procedure as implemented in *PLATON* (A. L. Spek, *Acta Crystallogr.* **2015**, *C71*, 9–18. *PLATON* – a multipurpose crystallographic tool. Utrecht University, Utrecht, The Netherlands). A total solvent-accessible void volume of 872 Å³ with a total electron count of 197 (consistent with 4 molecules of solvent toluene, or 1 molecule per formula unit of the indium complex) was found in the unit cell.

¹¹⁴*he* C–C distances within the disordered isopropyl group were restrained to be approximately the same by use of the *SHELXL SADI* instruction. Additionally, the C66–C70A and C66–C70B distances were similarly restrained. The rigid-bond restraint (**RIGU**) was applied to the carbon atoms of the disordered isopropyl group to improve the quality of their anisotropic displacement parameters. The phenyl ring of the disordered solvent toluene molecule was constrained to be an idealized hexagon; the C_{me}–C_{ipso} distances were restrained to be approximately the same, as were the C_{me}···C_{ortho} distances; the rigid-bond restraint was applied to all of the carbon atoms of the solvent toluene molecule. [total restraints: 10 **SADI**, 108 **RIGU**]

^h $S = [\sum w(F_o^2 - F_c^2)^2 / (n - p)]^{1/2}$ (n = number of data; p = number of parameters varied; $w = [\sigma^2(F_o^2) + (0.0770P)^2 + 0.5782P]^{-1}$ where $P = [\text{Max}(F_o^2, 0) + 2F_c^2]/3$).

ⁱ $R_1 = \sum ||F_o| - |F_c|| / \sum |F_o|$; $wR_2 = [\sum w(F_o^2 - F_c^2)^2 / \sum w(F_o^4)]^{1/2}$.

Table 3.6. X-ray crystallographic details for [(^{Me}IPrCH)₆In₆P₈] (7).*A. Crystal Data*

formula	C ₂₀₄ H ₃₀₂ In ₆ N ₁₂ P ₈
formula weight	3859.24
crystal color and habit ^a	purple block
crystal dimensions (mm)	0.35 × 0.09 × 0.05
crystal system	triclinic
space group	$P\bar{1}$ (No. 2)
unit cell parameters ^b	
<i>a</i> (Å)	17.9240(3)
<i>b</i> (Å)	18.1563(3)
<i>c</i> (Å)	19.0661(3)
α (deg)	66.0552(7)
β (deg)	69.6779(7)
γ (deg)	71.9143(8)
<i>V</i> (Å ³)	5212.76(15)
<i>Z</i>	1
ρ _{calcd} (g cm ⁻³)	1.229
μ (mm ⁻¹)	6.171

B. Data Collection and Refinement Conditions

diffractometer	Bruker D8/APEX II CCD ^c
radiation (λ [Å])	Cu Kα (1.54178) (microfocus source)
temperature (°C)	-100
scan type	ω and φ scans (1.0°) (5 s exposures)
data collection 2θ limit (deg)	145.17
total data collected	237205 (-22 ≤ <i>h</i> ≤ 22, -21 ≤ <i>k</i> ≤ 19, -23 ≤ <i>l</i> ≤ 23)
independent reflections	19848 (<i>R</i> _{int} = 0.0447)
number of observed reflections (<i>NO</i>)	18289 [<i>F</i> _o ² ≥ 2σ(<i>F</i> _o ²)]
structure solution method	intrinsic phasing (<i>SHELXT-2014</i> ^d)
refinement method	full-matrix least-squares on <i>F</i> ² (<i>SHELXL-2018</i> ^{e,f})
absorption correction method	Gaussian integration (face-indexed)
range of transmission factors	0.8060–0.3321
data/restraints/parameters	19848 / 0 / 934
goodness-of-fit (<i>S</i>) ^g [all data]	1.038
final <i>R</i> indices ^h	
<i>R</i> ₁ [<i>F</i> _o ² ≥ 2σ(<i>F</i> _o ²)]	0.0237
<i>wR</i> ₂ [all data]	0.0645
largest difference peak and hole	0.834 and -0.554 e Å ⁻³

^aObtained by recrystallization from a hexanes solution.

^bObtained from least-squares refinement of 9206 reflections with $5.44^\circ < 2\theta < 144.70^\circ$.

^cPrograms for diffractometer operation, data collection, data reduction and absorption correction were those supplied by Bruker.

^dG. M. Sheldrick, *Acta Crystallogr.* **2015**, *A71*, 3–8. (*SHELXT-2014*)

^eG. M. Sheldrick, *Acta Crystallogr.* **2015**, *C71*, 3–8. (*SHELXL-2018/3*)

^fAttempts to refine peaks of residual electron density as disordered or partial-occupancy solvent hexane carbon atoms were unsuccessful. The data were corrected for disordered electron density through use of the SQUEEZE procedure as implemented in *PLATON* (A. L. Spek, *Acta Crystallogr.* **2015**, *C71*, 9–18. *PLATON* – a multipurpose crystallographic tool. Utrecht University, Utrecht, The Netherlands). A total solvent-accessible void volume of 1177 Å³ with a total electron count of 195 (consistent with 4 molecules of solvent hexane) was found in the unit cell.

^g $S = [\sum w(F_o^2 - F_c^2)^2 / (n - p)]^{1/2}$ (n = number of data; p = number of parameters varied; $w = [\sigma^2(F_o^2) + (0.0337P)^2 + 2.7250P]^{-1}$ where $P = [\text{Max}(F_o^2, 0) + 2F_c^2]/3$).

^h $R_1 = \sum ||F_o| - |F_c|| / \sum |F_o|$; $wR_2 = [\sum w(F_o^2 - F_c^2)^2 / \sum w(F_o^4)]^{1/2}$.

3.4.4 Density Functional Theory (DFT) Computations and UV-vis Data

All computations were performed with Gaussian16.²⁹ Gas-phase geometries were optimized using density functional theory (DFT) with the B3LYP functional³⁰ and the cc-pVDZ basis set.³¹ For indium, the cc-pVDZ-PP basis set³² was used in conjunction with effective core potentials, as obtained from the Basis Set Exchange Library.³³ Frequency analysis confirmed all obtained structures to be local minima on the potential energy surfaces. Optimized geometries, orbitals and Atoms-In-Molecules (AIM) molecules graphs were visualized with Visual Molecular Dynamics (VMD).³⁴ Natural Bond Orbital (NBO) analyses were performed with NBO 6.0³⁵ and the wavefunction files were used for a topological analysis of the electron density according to the Atoms-In-Molecules partitioning scheme³⁶ using AIMAll.³⁷ The NCI

grids were computed with NCIplot.³⁸ The vertical excitation energy of the first fifty singlet states have been predicted by TD-DFT computations using the same level as stated above using the respective optimized gas-phase S_0 geometries of **1** and **6**. Computations regarding $[(^{\text{Me}}\text{IPrCH})\text{In}]_4$ (**1**), were conducted on the truncated model $[(^{\text{Me}}\text{IPhCH})\text{In}]_4$ (**1^M**) ($^{\text{Me}}\text{IPhCH} = [(\text{MeCNPh})_2\text{C}=\text{CH}]^-$ wherein the isopropyl groups were removed from the aryl rings. For comparison the first ten singlet states have been computed for $[\text{InC}(\text{SiMe}_3)_3]_4$, notably for $[\text{InC}(\text{SiMe}_3)_3]_4$ two geometries have been obtained, which both represent minima on the potential energy surface by a subsequent frequency analysis.

3.5 References

1. E. O. Fischer, H. P. Hofmann, *Angew. Chem.* **1957**, *69*, 639–640.
2. a) O. T. Beachley, J. C. Pazik, T. E. Glassman, M. R. Churchill, J. C. Fettinger, R. Blom, *Organometallics* **1988**, *7*, 1051–1059; b) O. T. Beachley, R. Blom, M. R. Churchill, K. Kaegri, J. C. Fettinger, J. C. Pazik, L. Victoriano, *Organometallics* **1989**, *8*, 346–356.
3. O. T. Beachley, M. R. Churchill, J. C. Fettinger, J. C. Pazik, L. Victoriano, *J. Am. Chem. Soc.* **1986**, *108*, 4666–4668.
4. M. S. Hill, P. B. Hitchcock, R. Pongtavornpinyo, *Science* **2006**, *311*, 1904–1907.
5. R. J. Wright, A. D. Phillips, N. J. Hardman, P. P. Power, *J. Am. Chem. Soc.* **2002**, *124*, 8538–8539.
6. S. T. Haubrich, P. P. Power, *J. Am. Chem. Soc.* **1998**, *120*, 2202–2203.

7. a) R. D. Schluter, A. H. Cowley, D. A. Atwood, R. A. Jones, J. L. Atwood, *J. Coord. Chem.* **1993**, *30*, 25–28; b) W. Uhl, R. Graupner, M. Pohlmann, S. Pohl, W. Saak, *Chem. Ber.* **1996**, *129*, 143–146; c) M. Bühler, G. Linti, *Z. Anorg. Allg. Chem.* **2006**, *632*, 2453–2460; d) For a novel cyclic $[\text{RIn}]_4^{2-}$ species, see: A. Protchenko, J. Urbano, J. A. B. Abdalla, J. Campos, D. Vidovic, A. D. Schwarz, M. P. Blake, P. Mountford, C. Jones, S. Aldridge, *Angew. Chem. Int. Ed.* **2017**, *56*, 15098–15102; e) See also: O. Kysliak, S. H. F. Schreiner, N. Grabicki, P. Liebing, F. Weigend, O. Dumele, R. Kretschmer, *Angew. Chem. Int. Ed.* **2022**, *61*, e202206963.

8. a) M. M. D. Roy, E. Rivard, *Acc. Chem. Rev.* **2017**, *50*, 2017–2025; b) S. M. I. Al-Rafia, M. J. Ferguson, E. Rivard, *Inorg. Chem.* **2011**, *50*, 10543–10545; c) C. Hering-Junghans, P. Andreiuk, M. J. Ferguson, R. McDonald, E. Rivard, *Angew. Chem. Int. Ed.* **2017**, *56*, 6272–6275.

9. a) N. Kuhn, M. Göhner, M. Siemann, *Z. Anorg. Allg. Chem.* **2002**, *628*, 1108–1115; b) R. S. Ghadwal, *Acc. Chem. Res.* **2022**, *55*, 457–470; c) L. Y. M. Eymann, P. Varava, A. M. Shved, B. F. E. Curchod, Y. Liu, O. M. Planes, A. Sienkiewicz, R. Scopelliti, F. F. Tirani, K. Severin, *J. Am. Chem. Soc.* **2019**, *141*, 17112–17116; d) A. Causero, H. Elsen, J. Pahl, S. Harder, *Angew. Chem. Int. Ed.* **2017**, *56*, 6906–6910.

10. For related work on formally dianionic NHOs, see: a) Z. Li, X. Chen, D. M. Andrada, G. Frenking, Z. Benkö, Y. Li, J. R. Harmer, C.-Y. Su, H. Grützmacher, *Angew. Chem. Int. Ed.* **2017**, *56*, 5744–5749; b) H. Steffenausewach, Y. V. Vishnevskiy, B. Neumann, H.-G. Stammler, D. M. Andrada, R. S. Ghadwal, *Angew. Chem. Int. Ed.* **2022**, *61*, e202207415.

11. For related work on *N*-heterocyclic imines, see: a) T. Ochiai, D. Franz, S. Inoue, *Chem. Soc. Rev.* **2016**, *45*, 6327–6344; b) M. W. Lui, C. Merten, M. J. Ferguson, R. McDonald, Y. Xu, E. Rivard, *Inorg. Chem.* **2015**, *54*, 2040–2049.
12. M. M. D. Roy, S. R. Baird, E. Dornsiepen, L. A. Paul, L. Miao, M. J. Ferguson, Y. Zhou, I. Siewart, E. Rivard, *Chem. Eur. J.* **2021**, *27*, 8572–8579.
13. H. W. Moon, J. Cornella, *ACS Catal.* **2022**, *12*, 1382–1393.
14. a) M. M. D. Roy, A. A. Omaña, A. S. S. Wilson, M. S. Hill, S. Aldridge, E. Rivard, *Chem. Rev.* **2021**, *121*, 12784–12965; b) T. Chu, G. I. Nikonov, *Chem. Rev.* **2018**, *118*, 3608–3680.
15. For examples of aNHOs bound to transition metals, see: a) I. C. Watson, M. J. Ferguson, E. Rivard, *Inorg. Chem.* **2021**, *60*, 18347–18359; b) I. C. Watson, Y. Zhou, M. J. Ferguson, E. Rivard, *Z. Anorg. Allg. Chem.* **2022**, *648*, e202200082.
16. For similar reactions involving the substitution of Cp (and derivatives), see: a) C. Dohmeier, E. Baum, A. Ecker, R. Köppe, H. Schnöckel, *Organometallics* **1996**, *15*, 4702–4706; b) L. Denker, B. Trzaskowski, R. Frank, *Chem. Commun.* **2021**, *57*, 2816–2819; c) P. Dabringhaus, J. Willrett, I. Krossing, *Nat. Chem.* **2022**, *14*, 1151–1157.
17. K. Powers, C. Hering-Junghans, R. McDonald, M. J. Ferguson, E. Rivard, *Polyhedron* **2016**, *108*, 8–14.
18. For related work on [RGa]₄ tetramers, see: A. Seifert, G. Linti, *Eur. J. Inorg. Chem.* **2007**, 5080–5086.

19. A. V. Protchneko, D. Dange, J. R. Harmer, C. Y. Tang, A. D. Schwarz, M. J. Kelly, N. Phillips, R. Tirfoin, K. Hassomal Birjkumar, C. Jones, N. Kaltsoyannis, P. Mountford, S. Aldridge, *Nat. Chem.* **2014**, *6*, 315–319.
20. a) R. J. Wright, A. D. Phillips, T. L. Allen, W. H. Fink, P. P. Power, *J. Am. Chem. Soc.* **2003**, *125*, 1694–1695; b) R. C. Fischer, P. P. Power, *Chem. Rev.* **2010**, *110*, 3877–3923.
21. T. B. Ditri, B. J. Fox, C. E. Moore, A. L. Rheingold, J. S. Figueroa, *Inorg. Chem.* **2009**, *48*, 8362–8375.
22. M. D. Anker, M. Lein, M. P. Coles, *Chem. Sci.* **2019**, *10* 1212–1218.
23. A. B. Pangborn, M. A. Giardello, R. H. Grubbs, R. K. Rosen, F. J. Timmers, *Organometallics* **1996**, *15*, 1518–1520.
24. I. C. Watson, A. Schumann, H. Yu, E. C. Davy, R. McDonald, M. J. Ferguson, C. Hering-Junghans, E. Rivard, *Chem. Eur. J.* **2019**, *25*, 9678–9690.
25. O. T. Beachley, J. C. Pazik, T. E. Glassman, M. R. Churchill, J. C. Fettinger, R. Blom, *Organometallics* **1988**, *7*, 1051–1059.
26. H. Hope, *Prog. Inorg. Chem.* **1994**, *41*, 1–19.
27. G. M. Sheldrick, *Acta Crystallogr.* **2015**, *A71*, 3–8.
28. G. M. Sheldrick, *Acta Crystallogr.* **2015**, *C71*, 3–8.
29. M. J. Frisch, G. W. Trucks, H. B. Schlegel, G. E. Scuseria, M. A. Robb, J. R. Cheeseman, G. Scalmani, V. Barone, G. A. Petersson, H. Nakatsuji, X. Li, M. Caricato, A. V. Marenich, J. Bloino, B. G. Janesko, R. Gomperts, B. Mennucci, H. P. Hratchian, J. V. Ortiz, A. F. Izmaylov, J. L. Sonnenberg, D. Williams-Young, F. Ding, F. Lipparini, F. Egidi, J. Goings, B. Peng, A.

Petrone, T. Henderson, D. Ranasinghe, V. G. Zakrzewski, J. Gao, N. Rega, G. Zheng, W. Liang, M. Hada, M. Ehara, K. Toyota, R. Fukuda, J. Hasegawa, M. Ishida, T. Nakajima, Y. Honda, O. Kitao, H. Nakai, T. Vreven, K. Throssell, J. A. Montgomery, Jr., J. E. Peralta, F. Ogliaro, M. J. Bearpark, J. J. Heyd, E. N. Brothers, K. N. Kudin, V. N. Staroverov, T. A. Keith, R. Kobayashi, J. Normand, K. Raghavachari, A. P. Rendell, J. C. Burant, S. S. Iyengar, J. Tomasi, M. Cossi, J. M. Millam, M. Klene, C. Adamo, R. Cammi, J. W. Ochterski, R. L. Martin, K. Morokuma, O. Farkas, J. B. Foresman, D. J. Fox, Gaussian 16, Revision A. 03, Gaussian Inc., Wallingford CT, 2016.

30. a) C. Lee, W. Yang, R. G. Parr, *Phys. Rev. B* **1988**, *37*, 785–789.; b) A. D. Becke, *Phys. Rev. A* **1988**, *38*, 3098–3100; c) P. J. Stephens, F. J. Devlin, C. F. Chabalowski, M. J. Frisch, *J. Phys. Chem.* **1994**, *98*, 11623–11627.

31. T. H. Dunning, *J. Chem. Phys.* **1989**, *90*, 1007–1023.

32. K. A. Peterson, *J. Chem. Phys.* **2003**, *119*, 11099–11123.

33. a) B. P. Pritchard, D. Altarawy, B. Didier, T. D. Gibson, T. L. Windus, *J. Chem. Inf. Model.* **2019**, *59*, 4814–4820; b) D. J. Feller *J. Comput. Chem.* **1996**, *17*, 1571–1586; c) K. L. Schuchardt, B. T. Didier, T. Elsethagen, L. Sun, V. Gurumoorthi, J. Chase, J. Li, T. L. Windus, *J. Chem. Inf. Model.* **2007**, *47*, 1045–1052.

34. W. Humphrey, A. Dalke, and K. Schulten, *J. Molec. Graphics* **1996**, *14*, 33–38.

35. E. D. Glendening, J. K. Badenhoop, A. E. Reed, J. E. Carpenter, J. A. Bohmann, C. M. Morales, C. R. Landis, F. Weinhold, NBO 6.0, Theoretical Chemistry Institute, University of Wisconsin, Madison WI, 2013.

36. R. W. F. Bader, *Atoms in Molecules. A Quantum Theory*, Cambridge University Press: Oxford U. K., 1991.
37. T. A. Keith, AIMAll (Version 15.09.27), TK Gristmill Software, Overland Park KS, USA, 2015 (aim.tkgristmill.com).
38. J. Contreras-García, E. Johnson, S. Keinan, R. Chaudret, J.-P. Piquemal, D. Beratan, W. Yang, *J. Chem. Theory Comput.* **2011**, 7, 625–632.

Chapter 4 – C-N Activation by a Possible Transient Diborene Supported by an Anionic *N*-Heterocyclic Olefin

4.1 Introduction

Molecular species containing boron-boron bonds have been of synthetic interest for a long time. The first identified molecular species to contain a boron-boron single bond was $\text{Cl}_2\text{B}-\text{BCl}_2$, reported in 1925 by Stock.¹ While $\text{Cl}_2\text{B}-\text{BCl}_2$ was at first a structural curiosity, it would open the door to a broad class of compounds known as diborane(4)s, each with the general formula $\text{R}_2\text{B}-\text{BR}_2$. Diborane(4)s are now employed in the development of pharmaceuticals, catalysis (*e.g.*, for Suzuki-Miyaura cross-coupling) and within borylative cyclizations.² The first stable tetraorgano-substituted diborane(4) was reported in the 1980's with kinetic stabilization provided by bulky *tert*-butyl groups, ${}^t\text{Bu}_2\text{B}-\text{B}{}^t\text{Bu}_2$.³ While tetralkyl diborane(4)s are highly reactive, the corresponding tetraaryl diborane(4)s are more stable and can undergo two-electron reduction to yield isoelectronic boron analogues to ethylene, $[\text{R}_2\text{B}=\text{BR}_2]^{2-}$, with formal boron-boron double bonds.⁴

The neutral diborane(2), diborene $\text{HB}=\text{BH}$, is the simplest boron species containing boron-boron multiple bonding and can be considered as the boron analogue to acetylene. This species exists in a triplet ground state and as such has been isolated only within a frozen argon matrix.⁵ The electron-deficient nature of the boron atoms in $\text{HB}=\text{BH}$ allows for the coordination of stabilizing Lewis base (LB) ligands, as demonstrated by Robinson in 2007 with the landmark report of a neutral diborene coordinated by *N*-heterocyclic carbenes (NHCs), $[\text{IPr}\cdot(\text{H})\text{B}=\text{B}(\text{H})\cdot\text{IPr}]$; $\text{IPr} = (\text{HCNDipp})_2\text{C}$; $\text{Dipp} = 2,6\text{-}^i\text{Pr}_2\text{C}_6\text{H}_3$] (Figure 4.1).⁶ Since then, a variety of neutral diborene adducts of NHCs, cyclic (alkyl)(amino)carbenes (CAACs),

and phosphines have been reported each featuring a B=B double bond, $\text{LB}\cdot(\text{R})\text{B}=\text{B}(\text{R})\cdot\text{LB}$.⁷ To date, a stable neutral singlet diborene $\text{RB}=\text{BR}$ without the need of supporting Lewis base donors has not been reported.

Recently the Rivard group⁸ and others⁹ have explored a class of ligands termed as anionic *N*-heterocyclic olefins (aNHOs). These ligands are notable for the highly electron-donating nature of the ligating/anionic sp^2 -hybridized carbon center, and the possibility of added ligand-to-element π -donation *via* a polarized exocyclic olefin.¹⁰ Given recent reports on the stabilization of an acyclic divinylsilylene ($^{\text{Me}}\text{IPrCH})_2\text{Si}:$ ($^{\text{Me}}\text{IPrCH} = [(\text{MeCNDipp})_2\text{C}=\text{CH}]^-$) a potentially strong $2e^-$ reducing agent (see Chapter 2)^{8d} and an indium(I) tetramer supported by aNHOs (see Chapter 3),^{8a} I speculated that aNHOs may be able to stabilize a neutral singlet diborene ($\text{RB}=\text{BR}$) without the need for exogenous Lewis bases.

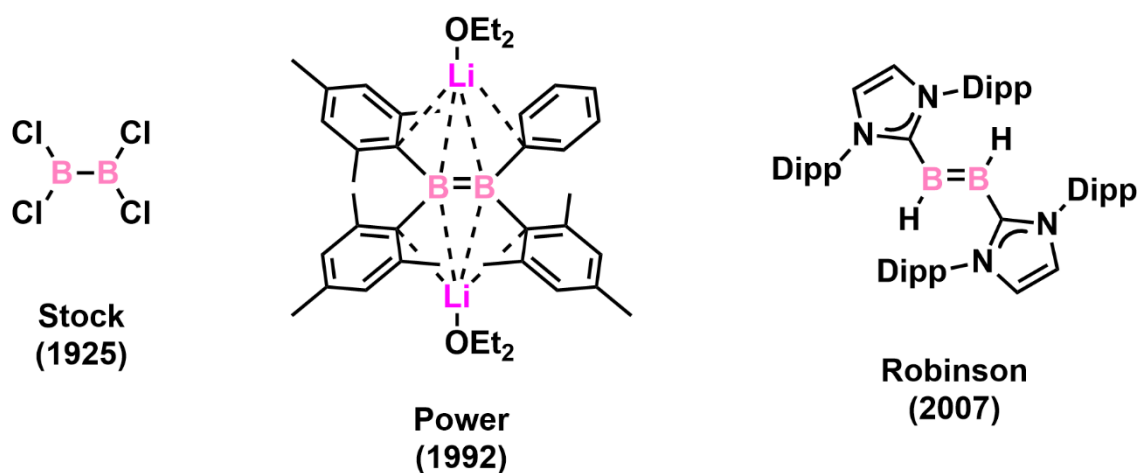
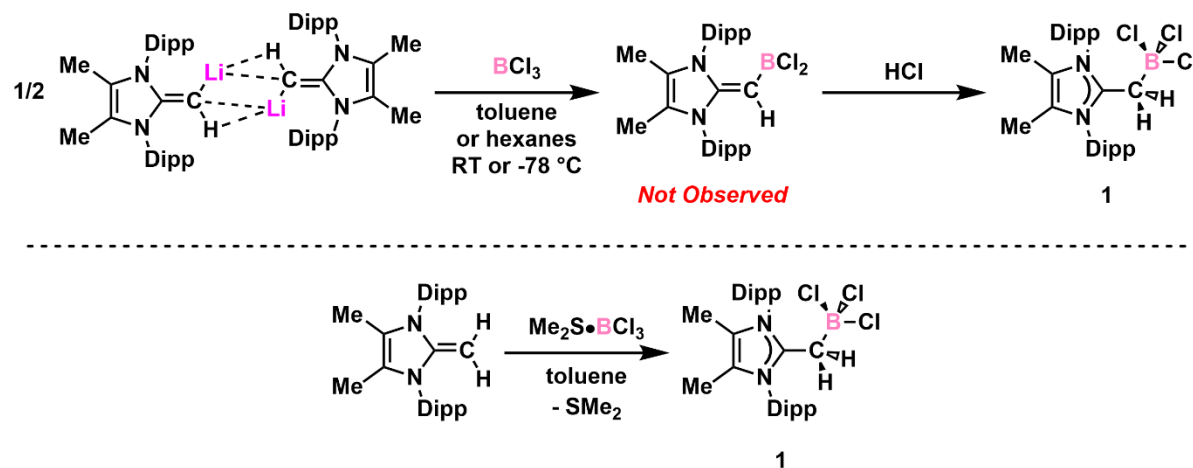


Figure 4.1. $\text{Cl}_2\text{B}-\text{BCl}_2$ the first diborane(4) isolated, $[\text{Mes}_2\text{B}=\text{BMes}(\text{Ph})]^{2-}$, and a parent diborene stabilized by *N*-heterocyclic carbene ligands.

4.2 Results and Discussion

The starting point of this project involved the preparation of an aNHO-supported haloborane, which might be reduced to afford the target compound (aNHO)B=B(aNHO). As an entry to a suitable boron-aNHO precursor, half of an equivalent of the previously reported lithiated aNHO reagent, $[(^{\text{Me}}\text{IPrCH})\text{Li}]_2$ (Chapter 2),^{8d} was combined with BCl_3 in hexanes (at room temperature and $-78\text{ }^\circ\text{C}$) in an attempt to prepare $(^{\text{Me}}\text{IPrCH})\text{BCl}_2$. Unfortunately, the only isolable species was the hydrolysis product $^{\text{Me}}\text{IPrCH}_2\cdot\text{BCl}_3$ (**1**), which is likely formed due to hydrolysis and the *in situ* generation of HCl in solution. Compound **1** could be prepared independently by combining $\text{Me}_2\text{S}\cdot\text{BCl}_3$ and $^{\text{Me}}\text{IPrCH}_2$ in toluene and was isolated in a yield of 82 % as a white solid (Scheme 4.1).



Scheme 4.1. Synthesis of $^{\text{Me}}\text{IPrCH}_2\cdot\text{BCl}_3$ (**1**).

The molecular structure of **1** (Figure 4.2) features elongation of the C=C double bond from a distance of $1.3489(18)\text{ \AA}$ in free $^{\text{Me}}\text{IPrCH}_2$ ¹¹ to a length of $1.476(3)\text{ \AA}$, indicative of a carbon-carbon single bond; this C-C bond in **1** is comparable to the C-C bond length in

Robinson's adduct $\text{IPrCH}_2 \cdot \text{BBr}_3$ ($\text{IPrCH}_2 = [(\text{HCNDipp})_2\text{CCH}_2]$) [1.497(14) Å].¹² The B–C bond in **1** is 1.642(3) Å, which is the same within experimental error as in the related carbene adducts $\text{IPr} \cdot \text{BCl}_3$ [1.636(4) Å]¹³ and $\text{IPrCH}_2 \cdot \text{BBr}_3$ [1.576(18) Å].¹² The $^{11}\text{B}\{^1\text{H}\}$ NMR spectrum of **1** displays a sharp singlet at 6.9 ppm in CD_2Cl_2 , while the methylene protons bound to C4 (Figure 4.2) appear as a singlet at 2.63 ppm in the ^1H NMR spectrum.

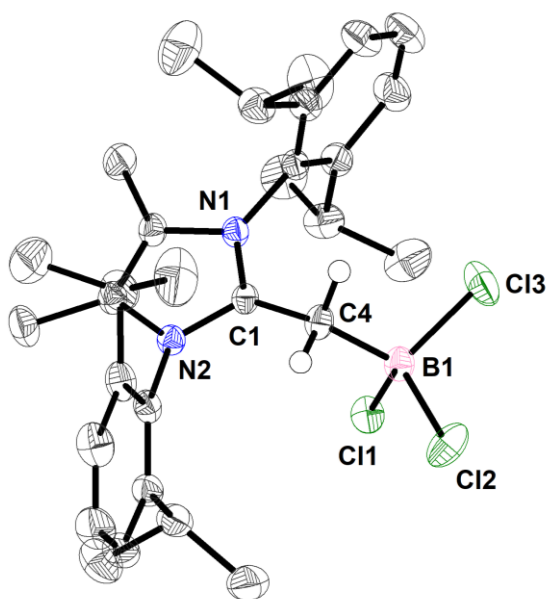
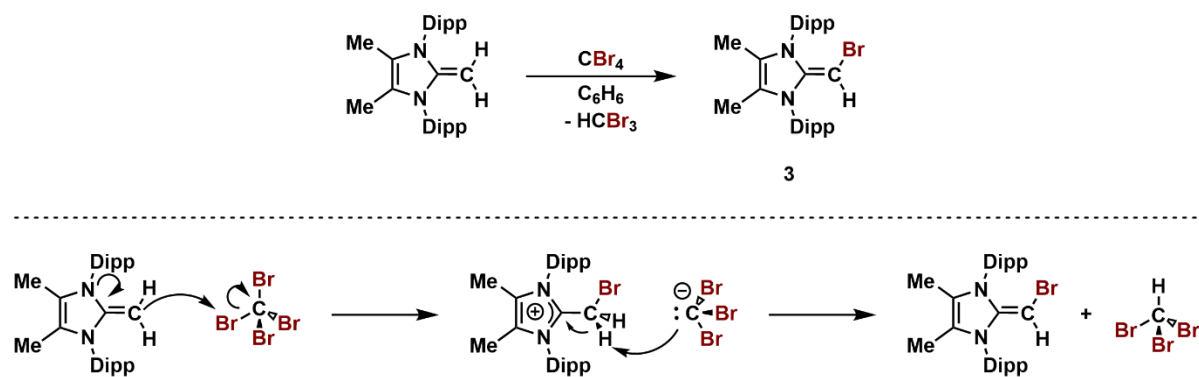


Figure 4.2. Molecular structure of $^{\text{Me}}\text{IPrCH}_2 \cdot \text{BCl}_3$ (**1**) plotted with thermal ellipsoids at 50 % probability. All hydrogen atoms (except for the methylene protons at C4) are omitted for clarity. The hexane solvent molecule not shown. Selected bond lengths [Å] and angle [°]: C1–C4 1.476(3), C4–B1 1.642(3); C1–C4–B1 118.51(16).

$[(^{\text{Me}}\text{IPrCH})\text{Li}]_2$ was combined with the tetrahaloborane complex $\text{Me}_2\text{S} \cdot \text{Br}_2\text{B}-\text{BBR}_2 \cdot \text{SMe}_2$ ¹⁴ in toluene with the goal to prepare $(^{\text{Me}}\text{IPrCH})(\text{Br})\text{B}-\text{B}(\text{Br})(\text{CH}^{\text{Me}}\text{IPr})$ as a precursor for the target diborene, $(^{\text{Me}}\text{IPrCH})\text{B}=\text{B}(\text{CH}^{\text{Me}}\text{IPr})$. However, this reaction afforded the neutral NHO adduct $^{\text{Me}}\text{IPrCH}_2 \cdot \text{Br}_2\text{B}-\text{BBR}_2 \cdot \text{CH}_2^{\text{Me}}\text{IPr}$ (**2**) and free $^{\text{Me}}\text{IPrCH}_2$ as soluble products. This result contrasts sharply with previous work where it had been established that

$[(^{\text{Me}}\text{IPrCH})\text{Li}]_2$ could react cleanly with a variety of element halides EX_n ($\text{E} = \text{Ti, Zr, Hf, Zn, Si, Ge, Sn, Pb; X} = \text{Cl, Br}$).^{8c,d} The most immediate concern was that hydrolysis was occurring; however, other possible side reactions such as ligand activation¹⁵ or the formation of the brominated NHO $^{\text{Me}}\text{IPrCH}(\text{Br})$ (**3**) *via* Li/Br exchange were considered; in relation to the latter, formation of copious amounts of $\text{Ar}^{\text{Dipp}}\text{PCl}$ during the synthesis of $\text{Ar}^{\text{Dipp}}\text{PCl}_2$ from $\text{LiAr}^{\text{Dipp}}$ and PCl_3 has been reported ($\text{Ar}^{\text{Dipp}} = 2,6\text{-Dipp}_2\text{C}_6\text{H}_3$).¹⁶

The first step in the investigation of possible side reactions was the preparation of $^{\text{Me}}\text{IPrCH}(\text{Br})$ (**3**), which was achieved by combining $^{\text{Me}}\text{IPrCH}_2$ with CBr_4 , and afforded **3** in a yield of 63 % as a light-brown solid. Compound **3** is sensitive to light but is stable at room temperature indefinitely when stored in the dark as a solid. When the reaction progress was monitored by ^1H NMR spectroscopy in C_6D_6 , the formation of HCBBr_3 was observed with quantitative conversion to **3** within ten minutes. The formation of **3** is envisioned to occur through the initial coordination and subsequent bromide abstraction to give the ion pair $[(^{\text{Me}}\text{IPrCH}_2\text{Br})][\text{CBr}_3]$ in which the CBr_3 anion rapidly deprotonates the exocyclic methylene fragment to afford $^{\text{Me}}\text{IPrCH}(\text{Br})$ (**3**) and HCBBr_3 (Scheme 4.2), reminiscent of an Appel-like reaction.¹⁷ Analysis of **3** by ^1H NMR spectroscopy in C_6D_6 identified that the $=\text{CH}(\text{Br})$ resonance as a sharp singlet at 3.16 ppm, which is shifted downfield when compared to $^{\text{Me}}\text{IPrCH}(\text{I})$ [2.25 ppm in C_6D_6] (Chapter 2).^{8d} The molecular structure of $^{\text{Me}}\text{IPrCH}(\text{Br})$ (**3**) (Figure 4.3) features a $\text{C}=\text{C}$ bond length of 1.361(5) Å and sp^2 -character at the exocyclic carbon as evidenced by a $\text{C}-\text{C}-\text{Br}$ bond angle of 123.7(4)°.



Scheme 4.2. Synthesis of $^{\text{Me}}\text{IPrCH}(\text{Br})$ (**3**) (top) and proposed mechanism of formation of $^{\text{Me}}\text{IPrCH}(\text{Br})$ (**3**) (bottom).

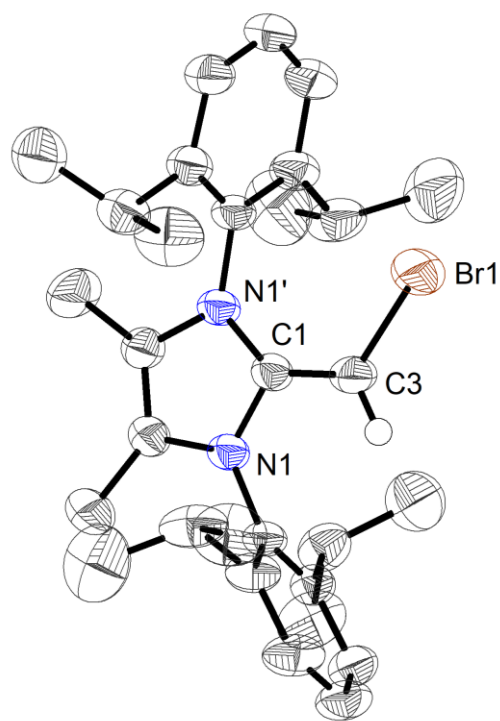
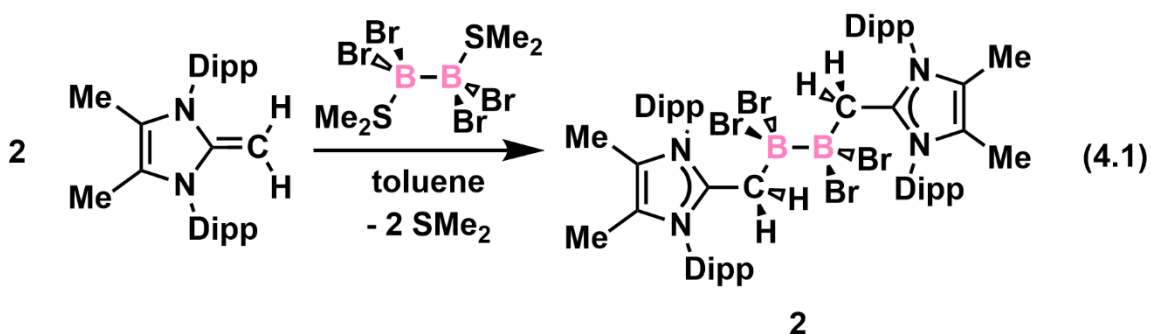


Figure 4.3. Molecular structure $^{\text{Me}}\text{IPrCH}(\text{Br})$ (**3**) with thermal ellipsoids plotted at 50 % probability. All hydrogen atoms (except for the vinylic proton at C3) are omitted for clarity. Selected bond lengths [Å] and angle [°]: C1–C3 1.361(5), C3–Br1 1.878(6); C1–C3–Br1 123.7(4).

Now that the ^1H NMR spectrum of $^{\text{Me}}\text{IPrCH}(\text{Br})$ (**3**) is known, monitoring the reaction between $[(^{\text{Me}}\text{IPrCH})\text{Li}]_2$ and $\text{Me}_2\text{S}\cdot\text{Br}_2\text{B}\cdot\text{BBR}_2\cdot\text{SMe}_2$ in C_6D_6 indicated the formation of

$^{\text{Me}}\text{IPrCH}_2\cdot\text{Br}_2\text{B-BBr}_2\cdot\text{CH}_2^{\text{Me}}\text{IPr}$ (**2**), as well as other unidentified species; the possible by-product **3** was not detected. $^{11}\text{B}\{^1\text{H}\}$ NMR spectroscopy indicated the presence of unreacted $\text{Me}_2\text{S}\cdot\text{Br}_2\text{B-BBr}_2\cdot\text{SMe}_2$ and **2** as the only observable soluble boron-containing species. Attempts to prepare $(^{\text{Me}}\text{IPrCH})(\text{Br})\text{B-B}(\text{Br})(\text{CH}^{\text{Me}}\text{IPr})$ by generating “ $(^{\text{Me}}\text{IPrCH})\text{Cu}$ ” *in situ*,¹⁸ by combining $[(^{\text{Me}}\text{IPrCH})\text{Li}]_2$ with $\text{Me}_2\text{S}\cdot\text{CuBr}$ also afforded **2** as the only isolable product. These results indicate that hydrolysis is most likely occurring in all cases, although ligand activation can not be entirely ruled out due to the presence of added unidentified NHO-based products in the ^1H NMR spectrum of the reaction mixture.

$^{\text{Me}}\text{IPrCH}_2\cdot\text{Br}_2\text{B-BBr}_2\cdot\text{CH}_2^{\text{Me}}\text{IPr}$ (**2**) can be prepared independently as an off-white solid in an isolated yield of 83 % by combining $^{\text{Me}}\text{IPrCH}_2$ with $\text{Me}_2\text{S}\cdot\text{Br}_2\text{B-BBr}_2\cdot\text{SMe}_2$ in toluene (Equation 4.1). Attempts to prepare $(^{\text{Me}}\text{IPrCH})(\text{Br})\text{B-B}(\text{Br})(\text{CH}^{\text{Me}}\text{IPr})$ from **2** *via* base-induced dehydrohalogenation with bases such as $n\text{BuLi}$, $\text{K}[\text{N}(\text{SiMe}_3)_2]$, KO^tBu , $^{\text{Me}}\text{IPr}$, $^{\text{Me}}\text{IPrCH}_2$ and $[(^{\text{Me}}\text{IPrCH})\text{Li}]_2$ were unsuccessful with either no reaction in the cases $^{\text{Me}}\text{IPrCH}_2$ and $[(^{\text{Me}}\text{IPrCH})\text{Li}]_2$, and with $n\text{BuLi}$, $\text{K}[\text{N}(\text{SiMe}_3)_2]$, KO^tBu , $^{\text{Me}}\text{IPr}$ only the formation of the free *N*-heterocyclic ligand $^{\text{Me}}\text{IPrCH}_2$ were observed. Attempts to prepare $(^{\text{Me}}\text{IPrCH})(\text{Br})\text{B-B}(\text{Br})(\text{CH}^{\text{Me}}\text{IPr})$ by combining $(^{\text{Me}}\text{IPrCH})\text{SiMe}_3$ ¹⁹ (a mild source of an anionic NHO fragment) with $\text{Me}_2\text{S}\cdot\text{Br}_2\text{B-BBr}_2\cdot\text{SMe}_2$ at room temperature led to no reaction; heating this reaction mixture to 80 °C for 16 hours led exclusively to the formation of $^{\text{Me}}\text{IPrCH}_2\cdot\text{Br}_2\text{B-BBr}_2\cdot\text{CH}_2^{\text{Me}}\text{IPr}$ (**2**) as determined by NMR spectroscopic analysis.



Crystals of $^{\text{Me}}\text{IPrCH}_2\cdot\text{Br}_2\text{B-BBr}_2\cdot\text{CH}_2^{\text{Me}}\text{IPr}$ (**2**) suitable for X-ray crystallographic analysis were grown from a toluene solution heated to 80 °C in a Teflon valve-capped NMR tube over the course of 16 hours with the crystals forming just above the solvent level in the NMR tube (Figure 4.4). The molecular structure of **2** features an exocyclic C–C bond length of 1.476(2) Å within the $^{\text{Me}}\text{IPrCH}_2$ donor, which is the same value as in $^{\text{Me}}\text{IPrCH}_2\cdot\text{BCl}_3$ (**1**) [1.476(3) Å]; the adjacent C–B bond distance in **2** [1.630(2) Å] is also similar to the C–B distance in **1** [1.642(3) Å]. The core B–B bond length in **2** [1.716(3) Å] matches the B–B single bond distance in $\text{Me}_2\text{S}\cdot\text{Br}_2\text{B-BBr}_2\cdot\text{SMe}_2$ [1.715(4) Å].¹⁴ Unlike $^{\text{Me}}\text{IPrCH}_2\cdot\text{BCl}_3$ (**1**) and $\text{IPrCH}_2\cdot\text{BBR}_3$,¹² compound **2** decomposes rapidly in dichloromethane into a complicated mixture of products. As such, the ^1H NMR data of **2** was collected in C_6D_6 , despite the low solubility of **2** in this solvent, which revealed the expected methylene resonance at 3.55 ppm for a neutral NHO adduct. The $^{11}\text{B}\{^1\text{H}\}$ NMR spectrum of **2** consisted of a singlet resonance centered at -3.5 ppm indicative of a four-coordinate boron environment.

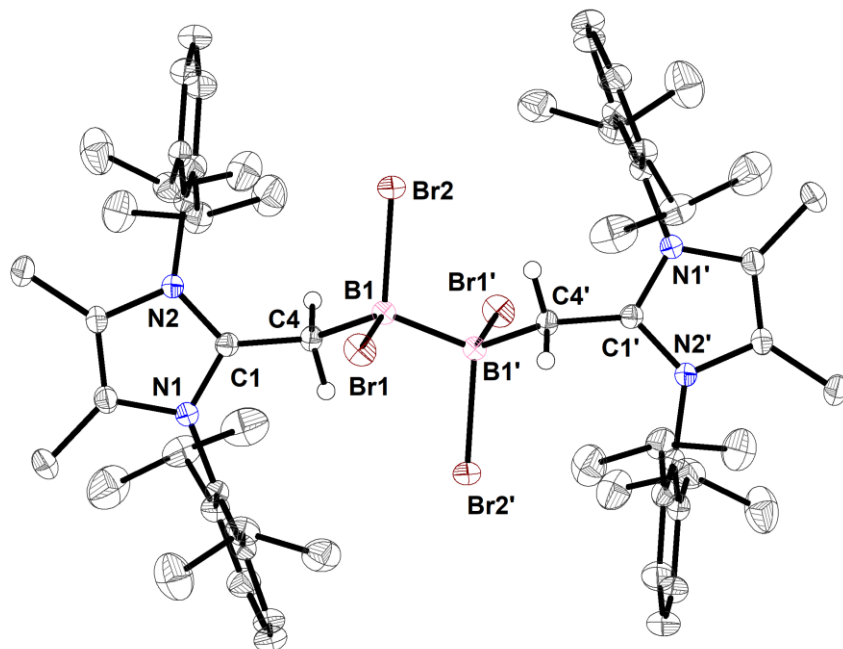
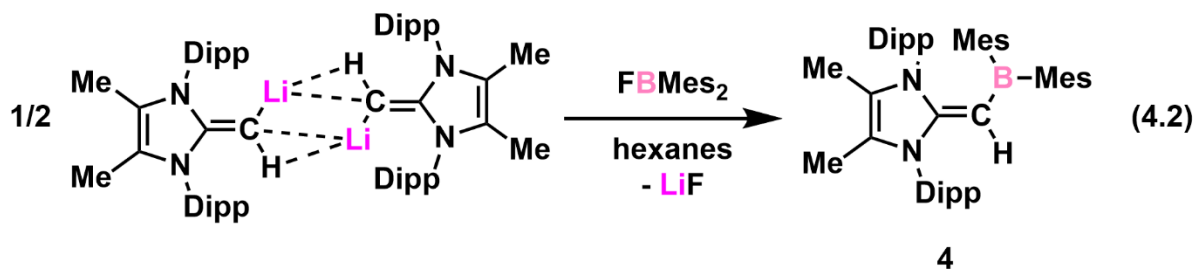


Figure 4.4. Molecular structure of $^{\text{Me}}\text{IPrCH}_2\cdot\text{Br}_2\text{B-BBr}_2\cdot\text{CH}_2^{\text{Me}}\text{IPr}$ (**2**) with thermal ellipsoids plotted at 50 % probability. All hydrogen atoms (except for the methylene protons at C4 and C4') are omitted for clarity. Selected bond lengths [\AA] and angles [$^\circ$]: C1–C4 1.476(2), C4–B1 1.630(2), B1–B1' 1.716(3), B1–Br1 2.0841(17), B1–Br2 2.1026(17); C1–C4–B1 124.55(13), C4–B1–B1' 124.55(13).

While I had previously demonstrated that $[(^{\text{Me}}\text{IPrCH})\text{Li}]_2$ could be a viable aNHO synthon for the preparation of $(^{\text{Me}}\text{IPrCH})\text{Bpin}$,^{8a} from $^t\text{PrOBpin}$ (Chapter 3; $\text{Bpin} = [\text{B}(\text{OCMe}_2\text{CMe}_2\text{O})]$), there was concern that boron-bound halides may not be ideal leaving groups for the preparation of a diborene precursor. As a probe of general reactivity, half of an equivalent of $[(^{\text{Me}}\text{IPrCH})\text{Li}]_2$ was combined with FBMes_2 ²⁰ ($\text{Mes} = 2,4,6\text{-Me}_3\text{C}_6\text{H}_2$) in hexanes, which led to the formation of a bright-yellow solution and the formation of an insoluble precipitate, presumably LiF (Equation 4.2). The desired borylated NHO $(^{\text{Me}}\text{IPrCH})\text{BMes}_2$ (**4**) was then isolated in a yield of 40 % as a bright-yellow solid. After work up, analysis of **4** by ^1H NMR spectroscopy in C_6D_6 indicated a shift of the vinylic proton to 4.44 ppm from a value of 0.87 ppm in $[(^{\text{Me}}\text{IPrCH})\text{Li}]_2$ (Chapter 2);^{8d} the accompanying

$^{11}\text{B}\{^1\text{H}\}$ NMR spectrum of **4** gave a broad resonance at 50.9 ppm, in line with a three-coordinate boron environment.



The molecular structure of $(^{\text{Me}}\text{IPrCH})\text{BMes}_2$ (**4**) features significant elongation of the exocyclic C–C moiety within the $^{\text{Me}}\text{IPrCH}$ unit [1.4038(18) Å] (Figure 4.5) when compared to the corresponding distance in $[(^{\text{Me}}\text{IPrCH})\text{Li}]_2$ [1.341(6) Å]^{8d} and to the values found in the related borylated aNHOs, such as $(^{\text{Me}}\text{IPrCH})\text{Bpin}$ [1.3757(19) Å] (Chapter 3)^{8a} and $(^{\text{Me}}\text{IPrCH})\text{Bcat}$ [1.3867(17) Å; Bcat = B(OC₆H₄O)],^{8b} indicating possible donation of electron density from carbon (C1). This bonding situation is similar to other aNHO-supported aryl boranes such as $(^{\text{Me}}\text{IPrCH})\text{B(H)Mes}$ [1.4022(15) Å] and $(^{\text{Me}}\text{IPrCH})\text{B(H)Trip}$ [1.4033(14) Å] (Trip = 2,4,6-*t*-Pr₃C₆H₂).^{8b} As expected (*vide supra*), the B–C bond length in **4** [1.4833(19) Å] is similar in length as the B–C(aNHO) distances in $(^{\text{Me}}\text{IPrCH})\text{B(H)Mes}$ [1.4783(16) Å] and $(^{\text{Me}}\text{IPrCH})\text{B(H)Trip}$ [1.4741(15) Å].^{8b}

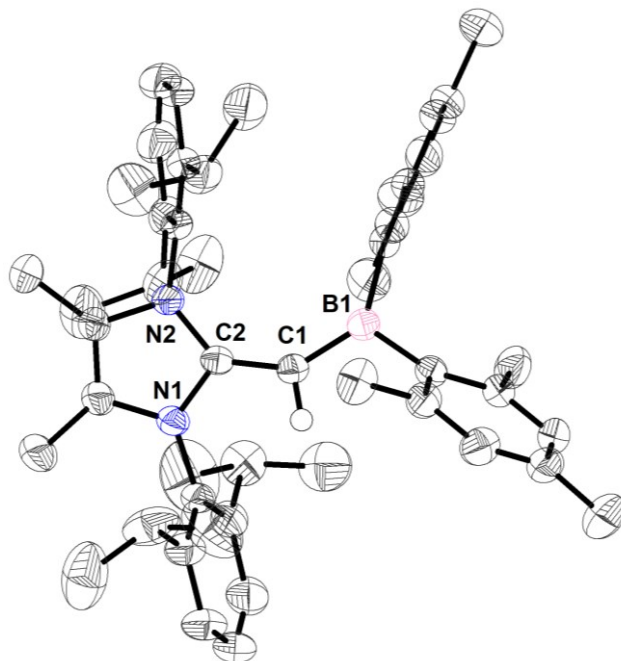
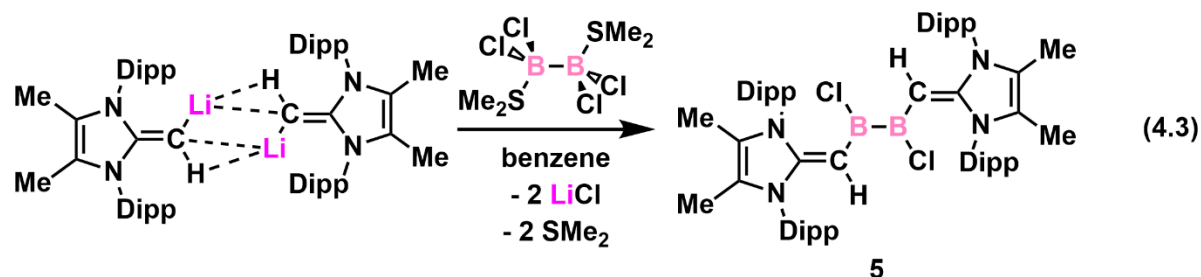


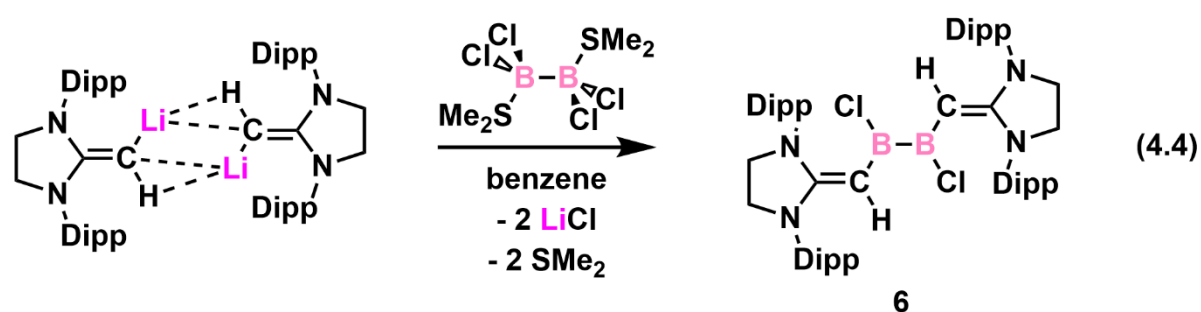
Figure 4.5. Molecular structure of (^{Me}IPrCH)BMes₂ (**4**) with thermal ellipsoids plotted at 50 % probability. All hydrogen atoms (except for the vinylic protons at C1) are omitted for clarity. Selected bond lengths [Å] and angle [°]: C2–C1 1.4038(18); C1–B1 1.4883(19); C2–C1–B1 140.94(13).

With the successful synthesis of (^{Me}IPrCH)BMes₂ (**4**) it was established that [(^{Me}IPrCH)Li]₂ could indeed participate in halide metathesis chemistry at boron. I turned my attention towards Me₂S•Cl₂B–BCl₂•SMe₂¹⁴ a potentially easier-to-handle precursor with a preformed B–B bond. Combining [(^{Me}IPrCH)Li]₂ with Me₂S•Cl₂B–BCl₂•SMe₂ in benzene led to the formation of a deep-yellow solution along with a fine white precipitate (Equation 4.3). After work-up, the diborane(**4**) (^{Me}IPrCH)ClB–BCl(CH^{Me}IPr) (**5**) was isolated as a bright-yellow solid in a yield of 90 %. ¹H NMR spectroscopic analysis of **5** in C₆D₆ showed that the vinylic protons appeared as a singlet at 4.76 ppm, which is expected for a coordinated [^{Me}IPrCH][–] ligand.^{8d} The ¹¹B{¹H} NMR spectrum of **5** gave a broad singlet at 49.1 ppm, indicative of a three-coordinate boron environment. Despite numerous attempts, X-ray quality

crystals of $(^{\text{Me}}\text{IPrCH})\text{ClB-BCl}(\text{CH}_2^{\text{Me}}\text{IPr})$ (**5**) could not be obtained and as such atom connectivity could not be determined with this method.



In an effort to determine atom connectivity in a close structural analogue to $(^{\text{Me}}\text{IPrCH})\text{ClB-BCl}(\text{CH}^{\text{Me}}\text{IPr})$ (**5**), I turned my attention to our recently reported lithiated aNHO, $[(\text{SIPrCH})\text{Li}]_2^{\text{8a}}$ ($\text{SIPrCH} = [(\text{H}_2\text{CNDipp})_2\text{C}=\text{CH}]$) (Chapter 3). Combining $[(\text{SIPrCH})\text{Li}]_2$ with $\text{Me}_2\text{S}\cdot\text{Cl}_2\text{B-BCl}_2\cdot\text{SMe}_2$ led to a pale-yellow solution along with a white precipitate (presumably LiCl). Work-up of the reaction mixture gave the diborane(**4**) $(\text{SIPrCH})\text{ClB-BCl}(\text{CHSIPr})$ (**6**) as a yellow solid in a yield of 95 % (Equation 4.4). Compound **6** gave an ^1H NMR spectrum in C_6D_6 that had the expected signals for the anticipated product, including a singlet resonance at 4.11 ppm for the vinylic protons, similar to the vinylic protons in $(^{\text{Me}}\text{IPrCH})\text{ClB-BCl}(\text{CH}^{\text{Me}}\text{IPr})$ (**5**) [$\delta = 4.76$ ppm]. The $^{11}\text{B}\{^1\text{H}\}$ NMR spectrum of **6** consists of a broad singlet at 55.6 ppm.



X-ray quality crystals of (SIPrCH)CIB-BCl(CHSIPr) (**6**) were grown from a saturated Et₂O solution (*ca.* 0.5 mL) that was stored at -35 °C for 16 hours. The molecular structure of **6** features a B–B single bond length of 1.694(4) Å (Figure 4.6), which is marginally shorter than the B–B separation within the bis(dimethylsulfide) adduct Me₂S•Cl₂B-BCl₂•SMe₂ [1.719(2) Å], and similar to the B–B distance found within Braunschweig’s corresponding cyclic(alkyl)aminoimine dibromodiborane (DippN(Me₂C)CH₂(Me₂C)C=N-(Br)B-B(Br)-N=C(Me₂C)CH₂(Me₂C)NDipp) [1.692(4) Å].²¹

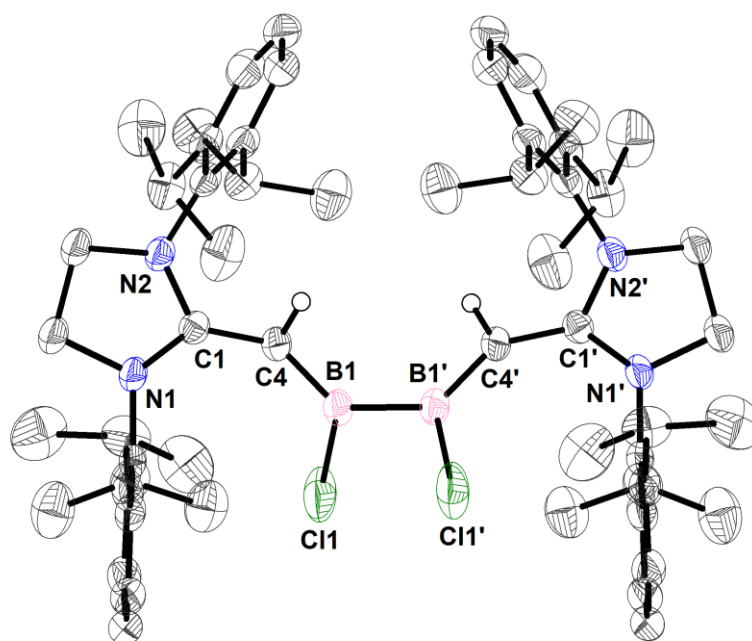
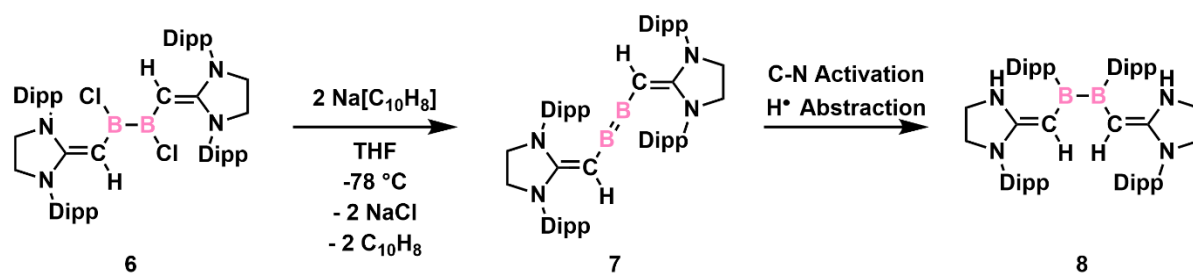


Figure 4.6. Molecular structure of (SIPrCH)CIB-BCl(CHSIPr) (**6**) with thermal ellipsoids plotted at 50 % probability. All hydrogen atoms (except for the vinylic protons at C4 and C4') are omitted for clarity. Selected bond lengths [Å] and angles [°]: C1–C4 1.387(3), C4–B1 1.495(3), B1–B1' 1.694(4), B1–Cl1 1.816(2); C1–C4–B1 139.41(19), C4–B1–B1' 123.34(16), C4–B1–Cl1 125.23(16).

With an spectroscopically pure diborene precursor in hand, I explored potential methods to reduce (SIPrCH)CIB-BCl(CHSIPr) (**6**) to afford the target diborene,

(SIPrCH)B=B(CHSIPr) (**7**). Attempts to reductively cleave the boron chloride bonds with lithium metal, KC_8 ,⁷ Cp_2Co ($\text{Cp} = \eta^5\text{-C}_5\text{H}_5$),²² $[\text{K}(\text{THF})_2][\text{Si}(\text{SiMe}_3)_3]$,^{8d,23} and Mashima's reagent $\text{Me}_3\text{SiN}\{(\text{Me})\text{C}=\text{C}(\text{Me})\}_2\text{NSiMe}_3$ ²⁴ were unsuccessful with either the formation of free SIPrCH₂ being observed in the cases of lithium metal and KC_8 , and in the cases of Cp_2Co , $[\text{K}(\text{THF})_2][\text{Si}(\text{SiMe}_3)_3]$, and Mashima's reagent no reactions were observed. Reduction of **6** with sodium naphthalenide, $\text{Na}[\text{C}_{10}\text{H}_8]$, in THF at $-78\text{ }^\circ\text{C}$ ²⁵ led to the formation of a dark-blue solution (Scheme 4.2). This blue solution persisted (by eye) for up to four hours with no noticeable change at $-78\text{ }^\circ\text{C}$. Upon warming, even slowly, the color faded to pale yellow. After removal of the volatiles from the warmed-up reaction mixture, ¹H NMR spectroscopic analysis of the resulting yellow residue in C_6D_6 determined that the predominant species formed was the free ligand SIPrCH₂ as well as other unidentified products. The residue was redissolved in a minimal amount of pentane (*ca.* 1 mL) and placed in a $-35\text{ }^\circ\text{C}$ freezer for two weeks, which afforded a crop of colorless crystals that were subsequently identified by single crystal X-ray crystallography as the ligand-activated product $[(\{\text{HN}(\text{H}_2\text{C})_2\text{N}(\text{Dipp})\}\text{C}=\text{CH})\text{B}(\text{Dipp})]_2$ (**8**). The proposed route to **8** involves intramolecular C-N activation of the flanking Dipp-groups by the transient diborene (SIPrCH)B=B(CHSIPr) (**7**) and subsequent hydrogen atom abstraction from the solvent (Scheme 4.3);⁶ although, one cannot rule out that this process occurs in a stepwise fashion by reduction at a single boron atom followed by subsequent ligand activation. Such ligand activation is not without precedent as recently the Hicks' group reported C-N activation of a flanking Dipp group within a transient boryl anion.²⁶



Scheme 4.3. Synthesis of $[(\{\text{HN}(\text{H}_2\text{C})_2\text{N}(\text{Dipp})\}\text{C}=\text{CH})\text{B}(\text{Dipp})_2]$ (**8**).

The molecular structure of $[(\{\text{HN}(\text{H}_2\text{C})_2\text{N}(\text{Dipp})\}\text{C}=\text{CH})\text{B}(\text{Dipp})_2]$ (**8**) features an average exocyclic C=C bond length of 1.385(3) Å, which is elongated slightly relative to the corresponding distances in ^{Me}IPrCH₂ [1.3489(18) Å]¹¹ and SIPrCH₂ [1.3346(19) Å],²⁷ suggesting possible π -donation from the vinylic C=C π -bond an adjacent empty boron-based *p*-orbital (Figure 4.7). However, this is contrasted by the C–B bond lengths in **8**, which have an average length of 1.502(3) Å and are the same within error as the B–C bond length of 1.513(2) Å in (^{Me}IPrCH)Bpin, a species that lacks appreciable C_aNHO–E π -bonding (according to DFT calculations).^{8a} The B–B bond in **8** is marginally longer [1.716(3) Å] than the B–B distance in (SIPrCH)ClB–BCl(CH₂SIPr) (**5**) [1.694(4) Å]. ¹H NMR analysis of the remaining crystals of **8** in C₆D₆ revealed that the vinylic protons appear as a singlet at 4.16 ppm; a broad ¹¹B{¹H} NMR resonance is located at 67.4 ppm.

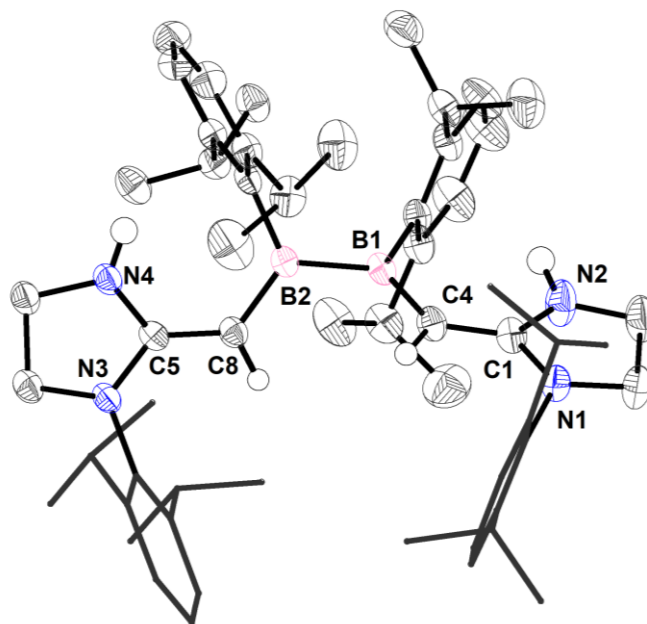


Figure 4.7. Molecular structure of $[(\{\text{HN}(\text{H}_2\text{C})_2\text{N}(\text{Dipp})\}\text{C}=\text{CH})\text{B}(\text{Dipp})]_2$ (**8**) with thermal ellipsoids plotted at 50 % probability. All hydrogen atoms (except for the vinylic and amine hydrogen atoms) are omitted for clarity. The Dipp-groups on the imidazole rings are shown in wireframe for clarity. Selected bond lengths [Å] and angles [°]: C1–C4 1.386(3), C4–B1 1.501(3), B1–B2 1.716(3), B2–C8 1.503(3), C8–C5 1.383(3); C1–C4–B1 127.6(2), C4–B1–B2 119.08(17), B1–B2–C8 119.85(19), B2–C8–C5 127.1(2).

The computed singlet-triplet energy gap of $(^{\text{Me}}\text{IPrCH})\text{B}=\text{B}(\text{CH}^{\text{Me}}\text{IPr})$ (**9**) was determined to be -0.5 kcal/mol at the B3LYP/cc-pVDZ level of theory indicating the ground state of anionic *N*-heterocyclic olefin-supported diborenes will likely be a triplet, as in the parent diborene $\text{HB}=\text{BH}$.⁷ The computed structure of $(^{\text{Me}}\text{IPrCH})\text{B}=\text{B}(\text{CH}^{\text{Me}}\text{IPr})$ (**9**) shows a nearly linear C–B=B–C core and two degenerate, half-filled, π -bonding orbitals (Figure 4.8). Computational investigations involving the related aryl diborene $\text{PhB}=\text{BPh}$ reveals a triplet ground state when the C–B=B–C core is linear. However, by bending the C–B=B–C unit in $\text{PhB}=\text{BPh}$ away from linearity, the degeneracy of the half-filled orbitals is broken leading to a singlet state.^{7a,28} Taking these insights into consideration, the isolation of singlet ground state diborene stabilized by any ligand system, not just aNHOs, will need sufficient steric demands

to enforce a bent geometry. Applying increased steric bulk to the exocyclic carbon moiety of the aNHO by incorporation of Dipp or Trip substituents (*e.g.*, within [^{Me}IPrC(Trip)]⁻) may induce a bent geometry through the C-B=B-C core possibly resulting in a stable singlet diborene supported by aNHOs.

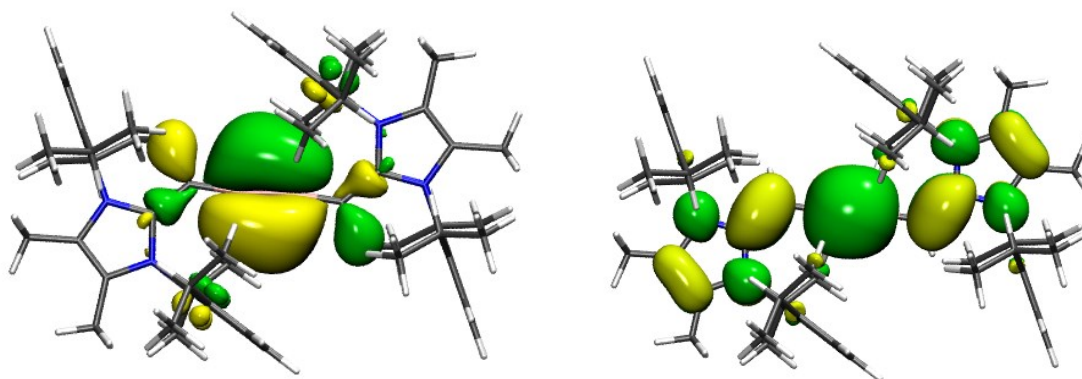


Figure 4.8. Computed SOMOs of (^{Me}IPrCH)B=B(CH^{Me}IPr) (**9**) at the B3LYP/cc-pVDZ level of theory.

4.3 Conclusion

This Chapter explores the attempted isolation of a diborene stabilized by anionic NHO ligands. The search for an appropriate precursor led to the development of the diborane(4) (SIPrCH)ClB-BCl(CH₂SIPr) (**6**), which contains a pre-formed B-B bond. Attempts to reductively cleave the B-Cl bonds in **6** to afford the diborene (SIPrCH)B=B(CH₂SIPr) (**7**) led to the formation of the ligand-activated product [($\{HN(H_2C)_2N(Dipp)\}C=CH)B(Dipp)]_2$ (**8**), which is postulated to arise through intramolecular C-N activation of the flanking Dipp-groups and subsequent hydrogen atom abstraction from the solvent. Computational investigations

found that the dibroene ($^{\text{Me}}\text{IPrCH})\text{B}=\text{B}(\text{CH}^{\text{Me}}\text{IPr})$ (**9**) likely exists in a triplet ground state. Future work will focus on computational studies on aNHOs with sterically-demanding aryl groups on the olefinic fragment to induce bending of the R–B=B–R core and formation of a singlet ground state.

4.4 Experimental Details

4.4.1 General Considerations

All reactions were performed using Schlenk and glovebox (Innovative Technology, Inc.) techniques under a nitrogen atmosphere. All solvents were purified using a Grubbs-type solvent purification system³⁰ manufactured by Innovative Technology, Inc., degassed (freeze–pump–thaw method), and stored under an atmosphere of nitrogen prior to use. BCl_3 (1.0 M solution in hexanes), $\text{Me}_2\text{S}\cdot\text{BCl}_3$, sodium, and naphthalene (C_{10}H_8) were purchased from Sigma-Aldrich and used as received. $^{\text{Me}}\text{IPrCH}_2$,¹¹ $[(^{\text{Me}}\text{IPrCH})\text{Li}]_2$,^{8d} $[(\text{SIPrCH})\text{Li}]_2$,^{8a} FBMes_2 ,²¹ $\text{Me}_2\text{S}\cdot\text{Cl}_2\text{B}\cdot\text{BCl}_2\cdot\text{SMe}_2$ and $\text{Me}_2\text{S}\cdot\text{Br}_2\text{B}\cdot\text{BBr}_2\cdot\text{SMe}_2$ ¹⁴ were prepared according to literature procedures [$^{\text{Me}}\text{IPr} = (\text{MeCNDipp})_2\text{C}$; $\text{SIPr} = (\text{H}_2\text{CNDipp})_2\text{C}$; $\text{Dipp} = 2,6\text{-}i\text{Pr}_2\text{C}_6\text{H}_3$; $\text{Mes} = 2,4,6\text{-Me}_3\text{C}_6\text{H}_2$]. ^1H , $^{13}\text{C}\{^1\text{H}\}$, and $^{11}\text{B}\{^1\text{H}\}$ NMR spectra were recorded on 400, 500, 600 or 700 MHz Varian Inova instruments and were referenced externally to SiMe_4 (^1H , $^{13}\text{C}\{^1\text{H}\}$), and 15 % $\text{F}_3\text{B}\cdot\text{Et}_2\text{O}$ (^{11}B). Elemental analyses were performed by the Analytical and Instrumentation Laboratory at the University of Alberta using a Thermo Flash 2000 Elemental Analyzer. Melting points were measured in sealed glass capillaries under nitrogen with a MelTemp apparatus and are uncorrected.

4.4.2 Synthetic Procedures

Synthesis of $\text{Me}^e\text{IPrCH}_2\cdot\text{BCl}_3$ (1): A solution of $\text{Me}^e\text{IPrCH}_2$ (0.153 g, 0.355 mmol) in 5 mL of toluene was added to a solution of $\text{Me}_2\text{S}\cdot\text{BCl}_3$ (0.064 g, 0.36 mmol) in 5 mL of toluene. After one minute a white precipitate had formed. After a further 16 hours of stirring the precipitate was allowed to settle, the mother liquor was decanted away and the remaining precipitate dried *in vacuo*. The resulting residue was washed with hexanes (3×5 mL) and dried affording $\text{Me}^e\text{IPrCH}_2\cdot\text{BCl}_3$ (1) as a white solid (0.160 g, 82 %). X-ray quality crystals were obtained from a saturated solution of hexanes stored at -35 °C for one week. ^1H NMR (700 MHz, CD_2Cl_2): δ 7.60 (t, 2H, $^3J_{\text{HH}} = 7.0$ Hz, *p*-ArH), 7.41 (d, 4H, $^3J_{\text{HH}} = 7.0$ Hz, *m*-ArH), 2.63 (s, 2H, CH_2), 2.56 (sept, 4H, $^3J_{\text{HH}} = 7.0$ Hz, $\text{CH}(\text{CH}_3)_2$), 2.01 (s, 6H, $\text{CN}(\text{CH}_3)$), 1.38 (d, 12H, $^3J_{\text{HH}} = 7.0$ Hz, $\text{CH}(\text{CH}_3)_2$), 1.18 (d, 12H, $^3J_{\text{HH}} = 7.0$ Hz, $\text{CH}(\text{CH}_3)_2$). $^{13}\text{C}\{^1\text{H}\}$ NMR (176 MHz, CD_2Cl_2): δ 153.4 (NCN), 146.6 (ArC), 131.8 (*p*-ArC), 129.8 (CN- CH_3), 127.7 (ArC), 125.8 (*m*-ArC), 37.8 (C- CH_2), 29.1 ($\text{CH}(\text{CH}_3)_2$), 25.2 ($\text{CH}(\text{CH}_3)_2$), 24.6 ($\text{CH}(\text{CH}_3)_2$), 10.4 (CN- CH_3). $^{11}\text{B}\{^1\text{H}\}$ NMR (128 MHz, CD_2Cl_2): δ 6.1 (s). Anal. Calcd. for $\text{C}_{30}\text{H}_{42}\text{BCl}_3\text{N}_2$ (%): C 65.77, H 7.73, N 5.11; Found: C 65.28, H 7.79, N 4.89. M.p. 294–296 °C.

Synthesis of $\text{Me}^e\text{IPrCH}_2\cdot\text{Br}_2\text{B}\cdot\text{BBr}_2\cdot\text{CH}_2\text{Me}^e\text{IPr}$ (2): A solution of $\text{Me}^e\text{IPrCH}_2$ (0.152 g, 0.352 mmol) in 3 mL of toluene was added to a solution of $\text{Me}_2\text{S}\cdot\text{Br}_2\text{B}\cdot\text{BBr}_2\cdot\text{SMe}_2$ (0.082 g, 0.18 mmol) dissolved in 3 mL of toluene; after 10 minutes a white precipitate had formed. Following a further 16 hours of stirring the precipitate was allowed to settle, the mother liquor was decanted away and the remaining precipitate dried *in vacuo*. The resulting solid was washed with hexanes (3×5 mL) and dried *in vacuo* affording $\text{Me}^e\text{IPrCH}_2\cdot\text{Br}_2\text{B}\cdot\text{BBr}_2\cdot\text{CH}_2\text{Me}^e\text{IPr}$

(2) as an off-white solid (0.175 g, 83 %). X-ray quality crystals were grown from a solution of C₆D₆ heated to 80 °C for 16 hours in a Teflon valve-capped NMR tube with the crystals forming just above the solvent level. ¹H NMR (700 MHz, C₆D₆): δ 7.21 (t, 4H, ³J_{HH} = 7.0 Hz, *p*-ArH), 7.12 (d, 8H, ³J_{HH} = 8.0 Hz, *m*-ArH), 3.55 (s, 4H, CH₂), 2.80 (br s, 8H, CH(CH₃)₂), 1.60 (d, 24H, ³J_{HH} = 8.0 Hz, CH(CH₃)₂), 1.35 (s, 12H, CN-CH₃), 0.91 (d, 24H, ³J_{HH} = 8.0 Hz, CH(CH₃)₂). ¹³C {¹H} NMR (178 MHz, C₆D₆): δ 160.8 (NCN), 146.0 (ArC), 131.2 (*p*-ArC), 129.6 (CN-CH₃), 128.9 (ArC), 124.7 (*m*-ArC), 30.9 (C-CH₂), 28.6 (CH(CH₃)₂), 24.7 (CH(CH₃)₂), 24.5 (CH(CH₃)₂), 9.6 (CN-CH₃). ¹¹B {¹H} NMR (128 MHz, C₆D₆): δ -3.4 (s). Anal. Calcd. for C₆₀H₈₄B₂Br₄N₄ (%): C 59.93, H 7.04, N 4.66; Found: C 59.88, H 7.07, N 4.50. M.p. 280–282 °C.

Synthesis of ^{Me}IPrCH(Br) (3): In the absence of ambient light, a solution of CBr₄ (0.390 g, 1.18 mmol) in 3 mL of benzene was added to a solution of ^{Me}IPrCH₂ (0.507 g, 1.18 mmol) in 2 mL of benzene. After ten minutes of stirring the volatiles were removed *in vacuo* affording a purple residue. The residue was extracted with 20 mL of pentane and filtered through a plug of diatomaceous earth. The volatiles were removed from the filtrate *in vacuo* affording ^{Me}IPrCH(Br) (3) as a light-brown solid (0.375 g, 63 %). Light-brown X-ray quality crystals of 3 were grown from a saturated solution of hexanes stored in a -35 °C freezer for 16 hours. ¹H NMR (700 MHz, C₆D₆): δ 7.29 (t, 1H, ³J_{HH} = 7.0 Hz, *p*-ArH), 7.21 (t, 1H, ³J_{HH} = 7.0 Hz, *p*-ArH), 7.15 (d, 2H, ³J_{HH} = 7.0 Hz, *m*-ArH), 7.11 (d, 2H, ³J_{HH} = 7.0 Hz, *m*-ArH), 3.31 (sept, 2H, ³J_{HH} = 7.0 Hz, CH(CH₃)₂), 3.18 (sept, 2H, ³J_{HH} = 7.0 Hz, CH(CH₃)₂), 3.16 (s, 1H, =CHBr), 1.55 (d, 6H, ³J_{HH} = 7.0 Hz, CH(CH₃)₂), 1.51 (s, 3H, CN-CH₃), 1.47 (s, 3H, CN-CH₃), 1.35 (d, 6H, ³J_{HH} = 7.0 Hz, CH(CH₃)₂), 1.22 (d, 6H, ³J_{HH} = 7.0 Hz, CH(CH₃)₂), 1.17 (d, 6H, ³J_{HH} = 7.0

Hz, CH(CH₃)₂). ¹³C{¹H} NMR (178 MHz, C₆D₆): δ 205.7 (NCN), 148.8 (ArC), 148.5 (ArC), 145.4 (ArC), 133.2 (ArC), 131.9 (ArC), 129.3 (*p*-ArC), 129.2 (*p*-ArC), 127.9 (ArC), 124.4 (*m*-ArC), 123.1 (*m*-ArC), 116.4 (CN-CH₃), 116.3 (CN-CH₃), 38.7 (=CHBr), 28.7 (CH(CH₃)₂), 28.4 (CH(CH₃)₂), 24.4 (CH(CH₃)₂), 23.7 (CH(CH₃)₂), 23.6 (CH(CH₃)₂), 23.5 (CH(CH₃)₂), 9.0 (CN-CH₃), 8.9 (CN-CH₃). Anal. Calcd. for C₃₀H₄₁BrN₂ (%): C 70.71, H 8.11, N 5.50; Found: C 70.08, H 8.08, N 5.49. M.p. 152 °C (decomposed). *Me*^eIPrCH(Br) decomposes in the presence of light, both in solution and in the solid state, but is stable as a solid for up to 3 months when stored at room temperature with the exclusion of light and indefinitely when stored in a -35 °C freezer.

Synthesis of (^{Me}eIPrCH)BMes₂ (4): A solution of [(^{Me}eIPrCH)Li]₂ (0.120 g, 0.138 mmol) in 6 mL of hexanes was added dropwise to a solution of FBMes₂ (0.068 g, 0.25 mmol) in 8 mL of hexanes. The reaction mixture was allowed to stir for two hours after which the reaction mixture was filtered through a plug of diatomaceous earth to yield a bright-yellow filtrate. This solution was concentrated to a final volume of *ca.* 5 mL and placed in a -35 °C freezer for two weeks affording (^{Me}eIPrCH)BMes₂ (4) (0.061 g, 40 %) as bright-yellow crystals. X-ray quality crystals were grown by dissolving 4 in hexanes and storing the solution in a -35 °C freezer for two days. ¹H NMR (700 MHz, C₆D₆): δ 7.04 (t, 2H, ³J_{HH} = 7.0 Hz, *p*-ArH), 6.98 (d, 4H, ³J_{HH} = 7.0 Hz, *m*-ArH), 6.67 (s, 1H, *m*-ArH), 6.60 (s, 1H, *m*-ArH), 4.41 (s, 1H, C=CH), 3.16 (br s, 4H, CH(CH₃)₂), 2.48 (s, 6H, Mes-CH₃), 2.78 (s, 6H, Mes-CH₃), 2.23 (s, 3H, CN-CH₃), 2.08 (s, 3H, CN-CH₃), 1.37 (s, 6H, Mes-CH₃), 1.29 (br, 12H, CH(CH₃)₂), 1.04 (d, 12H, ³J_{HH} = 7.0 Hz, CH(CH₃)₂). ¹³C{¹H} NMR (176 MHz, C₆D₆): δ 157.2 (NCN), 148.9 (ArC), 146.6 (ArC-B), 140.0 (ArC), 139.9 (ArC), 134.1 (ArC), 133.8 (ArC), 129.8 (ArC), 128.3

(ArC), 127.9 (*m*-ArC), 127.7 (*m*-ArC), 124.9 (CN-CH₃), 83.8 (C=CH), 28.7 (CH(CH₃)₂), 24.7 (Mes-CH₃), 24.6 (Mes-CH₃), 24.5 (CH(CH₃)₂), 24.4 (CH(CH₃)₂), 21.2 (CN-CH₃), 20.9 (CN-CH₃). ¹¹B{¹H} NMR (128 MHz, C₆D₆): δ 50.9 (br). Anal. Calcd. for C₅₆H₇₈N₄B₂Cl₂ (%): C 84.93, H 8.74, N 4.13; Found: C 84.08, H 9.33, N 4.15. M.p. 224 °C (decomposed).

Synthesis of (^{Me}IPrCH)CIB-BCl(CH^{Me}IPr) (5): A solution of [(^{Me}IPrCH)Li]₂ (0.100 g, 0.115 mmol) in 8 mL of benzene was added dropwise to a solution of Me₂S•Cl₂B-BCl₂•SMe₂ (0.035 g, 0.12 mmol) in 8 mL of benzene. After one minute the reaction mixture had taken on a dark-yellow color. After a further 16 hours of stirring the reaction mixture was filtered through a plug of diatomaceous earth and the volatiles removed from the filtrate *in vacuo* to give (^{Me}IPrCH)CIB-BCl(CH^{Me}IPr) (5) as a dark-yellow powder (0.098 g, 90 %). ¹H NMR (700 MHz, C₆D₆): δ 7.20 (t, 4H, ³J_{HH} = 7.0 Hz, *p*-ArH), 7.11 (d, 8H, ³J_{HH} = 7.0 Hz, *m*-ArH), 4.75 (s, 2H, C=CH), 2.85 (sept, 8H, ³J_{HH} = 7.0 Hz, CH(CH₃)₂), 1.39 (s, 12H, NC-CH₃), 1.36 (d, 24H, ³J_{HH} = 7.0 Hz, CH(CH₃)₂), 1.12 (d, 24H, ³J_{HH} = 7.0 Hz, CH(CH₃)₂). ¹³C{¹H} NMR (176 MHz, C₆D₆): δ 152.7 (NCN), 147.3 (ArC), 132.9 (ArC), 129.5 (*p*-ArC), 127.9 (ArC), 123.8 (*m*-ArC), 119.2 (NC-CH₃), 80.8 (C=CH), 28.7 (CH(CH₃)₂), 24.1 (CH(CH₃)₂), 23.3 (CH(CH₃)₂), 9.2 (NC-CH₃). ¹¹B{¹H} NMR (128 MHz, C₆D₆): δ 49.1 (br). Anal. Calcd. for C₆₀H₈₂N₄B₂Cl₂ (%): C 75.71, H 8.68, N 5.89; Found: C 67.18, H 8.17, N 4.90. M.p. 170 °C (decomposed). *Repeated attempts at elemental analysis consistently resulted in carbon values lower than the calculated, possibly due to incomplete combustion.*

Synthesis of (SIPrCH)ClB-BCl(CHSIPr) (6): A solution of [(SIPrCH)Li]₂ (0.117 g, 0.143 mmol) in 5 mL of benzene was added dropwise to a solution of Me₂S•Cl₂B-BCl₂•SMe₂ (0.041 g, 0.14 mmol) in 5 mL of benzene. After one minute the reaction mixture had taken on a bright-yellow color. After a further 60 minutes of stirring the reaction mixture was filtered through a plug of diatomaceous earth and the volatiles removed from the filtrate *in vacuo* affording (SIPrCH)ClB-BCl(CHSIPr) (**6**) as a bright-yellow powder (0.121 g, 95 %). X-ray quality crystals were obtained by dissolving **6** in Et₂O and storing the solution in a -35 °C freezer for 16 hours. ¹H NMR (700 MHz, C₆D₆): δ 7.15 (t, 4H, ³J_{HH} = 7.0 Hz, *p*-ArH), 7.04 (d, 8H, ³J_{HH} = 7.0 Hz, *m*-ArH), 4.10 (s, 2H, C=CH), 3.30 (s, 8H, CH₂), 3.14 (sept, 8H, ³J_{HH} = 7.0 Hz, CH(CH₃)₂), 1.27 (d, 12H, ³J_{HH} = 7.0 Hz, CH(CH₃)₂), 1.19 (d, 12H, ³J_{HH} = 7.0 Hz, CH(CH₃)₂). ¹³C{¹H} NMR (176 MHz, C₆D₆): δ 164.6 (NCN), 147.5 (ArC), 128.8 (*p*-ArC), 128.5 (ArC), 128.3 (ArC), 124.6 (*m*-ArC), 81.0 (C=CH), 51.3 (CH₂), 28.9 (CH(CH₃)₂), 25.0 (CH(CH₃)₂), 24.2 (CH(CH₃)₂). ¹¹B{¹H} NMR (128 MHz, C₆D₆): δ 55.1 (br). Anal. Calcd. for C₅₆H₇₈N₄B₂Cl₂ (%): C 74.75, H 8.74, N 6.23; Found: C 65.18, H 8.21, N 5.96. M.p. 122 °C (decomposed). *Repeated attempts at elemental analysis consistently resulted in carbon values lower than the calculated, possibly due to incomplete combustion.*

Synthesis of [(HN(H₂C)₂N(Dipp))C=CH)B(Dipp)]₂ (8): A solution of (SIPrCH)ClB-BCl(CHSIPr) (**6**) (0.100 g, 0.111 mmol) in 5 mL of THF was cooled to -78 °C and added dropwise to a freshly prepared solution of Na[C₁₀H₈] (Na: 0.006 g, 0.3 mmol; C₁₀H₈: 0.028 g, 0.22 mmol) in 5 mL of THF at -78 °C. After one minute the reaction mixture had turned deep blue. The mixture was allowed to warm slowly from -78 °C to room temperature over the course of 16 hours, after which the solution had turned a pale-yellow color. The volatiles were

removed *in vacuo* and vacuum applied for 5 hours at room temperature to remove the naphthalene. The resulting yellow residue was extracted with 10 mL of pentane and filtered through a plug of diatomaceous earth affording a pale-yellow filtrate, which was concentrated to a volume of 1 mL and placed in a -35 °C freezer for two weeks to give a crop of colorless crystals. A few crystals were removed and determined by X-ray crystallography to be $[(\{\text{HN}(\text{H}_2\text{C})_2\text{N}(\text{Dipp})\}\text{C}=\text{CH})\text{B}(\text{Dipp})]_2$ (**8**). The remaining crystals were washed with 2 mL of cold pentane (-35 °C) and dried affording **8** as a white solid (0.021 g, 23 %). ^1H NMR (700 MHz, C_6D_6): δ 7.30 (t, 2H, $^3J_{\text{HH}} = 7.0$ Hz, *p*-ArH), 7.27 (t, 2H, $^3J_{\text{HH}} = 7.0$ Hz, *p*-ArH), 7.21 (d, 4H, $^3J_{\text{HH}} = 7.0$ Hz, *m*-ArH), 7.12 (d, 4H, $^3J_{\text{HH}} = 7.0$ Hz, *m*-ArH), 4.49 (s, 2H, NH), 4.16 (s, 2H, C=CH), 2.88–2.95 (overlapping multiplets, 12H, CH(CH₃)₂ and CH₂), 2.53 (t, 4H, $^3J_{\text{HH}} = 7.0$ Hz, CH₂), 1.45 (d, 12H, $^3J_{\text{HH}} = 7.0$ Hz, CH(CH₃)₂), 1.31 (d, 12H, $^3J_{\text{HH}} = 7.0$ Hz, CH(CH₃)₂), 1.16 (d, 12H, $^3J_{\text{HH}} = 7.0$ Hz, CH(CH₃)₂), 1.05 (d, 12H, $^3J_{\text{HH}} = 7.0$ Hz, CH(CH₃)₂). $^{13}\text{C}\{^1\text{H}\}$ NMR (176 MHz, C_6D_6): δ 166.4 (NCN), 148.5 (ArC), 147.5 (ArC), 135.0 (ArC), 128.3 (*p*-ArC), 126.1 (*p*-ArC), 124.5 (*m*-ArC), 122.3 (*m*-ArC), 84.5 (C=CH), 51.0 (CH₂), 41.9 (CH₂), 34.1 (CH(CH₃)₂), 28.7 (CH(CH₃)₂), 26.0 (CH(CH₃)₂), 25.5 (CH(CH₃)₂), 24.4 (CH(CH₃)₂), 24.2 (CH(CH₃)₂). $^{11}\text{B}\{^1\text{H}\}$ NMR (128 MHz, C_6D_6): δ 67.4 (br). The exocyclic vinyl carbon resonance was not found in the $^{13}\text{C}\{^1\text{H}\}$ NMR but located indirectly by HSQC. The purity of the sample by ^1H NMR spectroscopy is ca. 80 % with the remaining 20 % being SiPrCH₂.

4.4.3 X-Ray Crystallography

Appropriate X-ray quality crystals were coated with a small amount of hydrocarbon oil (Paratone-N) and removed from the glovebox in a vial. Crystals were mounted quickly onto a glass fiber and placed in a low temperature stream of nitrogen on the X-ray diffractometer. All data was collected using a Bruker D8 Venture/PHOTON3, Bruker APEX II CCD detector/D8 or PLATFORM diffractometer using Mo K α (0.71073 Å) and Cu K α (1.54178 Å) radiation, with crystals cooled to -80 °C or -100 °C. The data was corrected for absorption through Gaussian integration from the indexing of crystal faces.³⁰ Molecular structures were solved using intrinsic phasing (SHELXT)³¹ and refined using SHELXL-2014.³² The assignment of hydrogen atom positions is based on the sp²- or sp³-hybridization geometries of their attached carbon atoms and were given thermal parameters 20 % greater than those of their parent atoms.

Table 4.1. X-ray crystallographic details for $\text{MeIPrCH}_2\cdot\text{BCl}_3$ (**1**) \cdot 0.5 hexane.*A. Crystal Data*

formula	$\text{C}_{33}\text{H}_{49}\text{BCl}_3\text{N}_2$
formula weight	590.90
crystal color and habit ^a	colorless fragment
crystal dimensions (mm)	$0.32 \times 0.11 \times 0.05$
crystal system	monoclinic
space group	$P2_1/n$ (an alternate setting of $P2_1/c$ [No. 14])
unit cell parameters ^a	
<i>a</i> (Å)	12.7802(3)
<i>b</i> (Å)	20.2877(5)
<i>c</i> (Å)	12.8223(3)
β (deg)	91.8182(14)
<i>V</i> (Å ³)	3322.90(14)
<i>Z</i>	4
ρ_{calcd} (g cm ⁻³)	1.181
μ (mm ⁻¹)	2.661

B. Data Collection and Refinement Conditions

diffractometer	Bruker D8/APEX II CCD ^b
radiation (λ [Å])	Cu K α (1.54178) (microfocus source)
temperature (°C)	-100
scan type	ω and ϕ scans (1.0°) (5 s exposures)
data collection 2θ limit (deg)	144.83
total data collected	23076 ($-15 \leq h \leq 15$, $-25 \leq k \leq 25$, $-15 \leq l \leq 15$)
independent reflections	6534 ($R_{\text{int}} = 0.0477$)
number of observed reflections (<i>NO</i>)	6234 [$F_o^2 \geq 2\sigma(F_o^2)$]
structure solution method	intrinsic phasing (<i>SHELXT-2014</i> ^c)
refinement method	full-matrix least-squares on F^2 (<i>SHELXL-2017</i> ^{d,e})
absorption correction method	Gaussian integration (face-indexed)
range of transmission factors	0.9539–0.5751
data/restraints/parameters	6534 / 0 / 355
goodness-of-fit (S) ^f [all data]	1.036
final <i>R</i> indices ^g	
R_1 [$F_o^2 \geq 2\sigma(F_o^2)$]	0.0442
wR_2 [all data]	0.1214
largest difference peak and hole	0.973 and -0.479 e Å ⁻³

^aObtained from least-squares refinement of 9941 reflections with $8.72^\circ < 2\theta < 144.34^\circ$.

^bPrograms for diffractometer operation, data collection, data reduction and absorption correction were those supplied by Bruker.

^cG. M. Sheldrick, *Acta Crystallogr.* **2015**, *A71*, 3–8. (*SHELXT-2014*)

^dG. M. Sheldrick, *Acta Crystallogr.* **2015**, *C71*, 3–8. (*SHELXL-2017*)

^eThe data were tested for non-merohedral twinning using the TwinRotMat procedure as implemented in *PLATON* (A. L. Spek, *Acta Crystallogr.* **1990**, *A46*, C34; A. L. Spek, *J. Appl. Cryst.* **2003**, *36*, 7–13. *PLATON* - a multipurpose crystallographic tool. Utrecht University, Utrecht, The Netherlands). The second twin component can be related to the first component by twofold rotation about the [0 1 0] axis (twin law [0 0 1 0 -1 0 1 0 0]). The refined value of the twin fraction (*SHELXL-2014* BASF parameter) was 0.2646(10).

^f $S = [\Sigma w(F_o^2 - F_c^2)^2 / (n - p)]^{1/2}$ (n = number of data; p = number of parameters varied; $w = [\sigma^2(F_o^2) + (0.0742P)^2 + 0.8705P]^{-1}$ where $P = [\text{Max}(F_o^2, 0) + 2F_c^2]/3$).

^g $R_1 = \Sigma ||F_o| - |F_c|| / \Sigma |F_o|$; $wR_2 = [\Sigma w(F_o^2 - F_c^2)^2 / \Sigma w(F_o^4)]^{1/2}$.

Table 4.2. X-ray crystallographic details for (^{Me}IPrCH₂)Br₂B-BBr₂(CH₂^{Me}IPr) (**2**).*A. Crystal Data*

formula	C ₆₀ H ₈₄ B ₂ Br ₄ N ₄
formula weight	1202.57
crystal color and habit ^a	colorless fragment
crystal dimensions (mm)	0.34 × 0.28 × 0.20
crystal system	monoclinic
space group	<i>P</i> 2 ₁ / <i>n</i> (an alternate setting of <i>P</i> 2 ₁ / <i>c</i> [No. 14])
unit cell parameters ^a	
<i>a</i> (Å)	11.4022(6)
<i>b</i> (Å)	17.6498(9)
<i>c</i> (Å)	15.3380(8)
β (deg)	101.6852(8)
<i>V</i> (Å ³)	3022.7(3)
<i>Z</i>	4
ρ _{calcd} (g cm ⁻³)	1.321
μ (mm ⁻¹)	2.702

B. Data Collection and Refinement Conditions

diffractometer	Bruker D8/APEX II CCD ^b
radiation (λ [Å])	graphite-monochromated Mo Kα (0.71073)
temperature (°C)	-100
scan type	ω scans (0.3°) (20 s exposures)
data collection 2θ limit (deg)	53.00
total data collected	24593 (-14 ≤ <i>h</i> ≤ 14, -22 ≤ <i>k</i> ≤ 22, -19 ≤ <i>l</i> ≤ 19)
independent reflections	6272 (<i>R</i> _{int} = 0.0203)
number of observed reflections (<i>NO</i>)	5733 [<i>F</i> _o ² ≥ 2σ(<i>F</i> _o ²)]
structure solution method	intrinsic phasing (<i>SHELXT-2014</i> ^c)
refinement method	full-matrix least-squares on <i>F</i> ² (<i>SHELXL-2017</i> ^d)
absorption correction method	Gaussian integration (face-indexed)
range of transmission factors	0.6025--0.4637
data/restraints/parameters	6272 / 0 / 318
goodness-of-fit (<i>S</i>) ^e [all data]	1.056
final <i>R</i> indices ^f	
<i>R</i> ₁ [<i>F</i> _o ² ≥ 2σ(<i>F</i> _o ²)]	0.0228
<i>wR</i> ₂ [all data]	0.0610
largest difference peak and hole	1.157 and -0.316 e Å ⁻³

^aObtained from least-squares refinement of 9795 reflections with 4.32° < 2θ < 65.86°.

^bPrograms for diffractometer operation, data collection, data reduction and absorption correction were those supplied by Bruker.

^c G. M. Sheldrick, *Acta Crystallogr.* **2015**, *A71*, 3–8. (*SHELXT-2014*)

^d G. M. Sheldrick, *Acta Crystallogr.* **2015**, *C71*, 3–8. (*SHELXL-2018/3*)

^e $S = [\sum w(F_o^2 - F_c^2)^2 / (n - p)]^{1/2}$ (n = number of data; p = number of parameters varied; $w = [\sigma^2(F_o^2) + (0.0325P)^2 + 1.3155P]^{-1}$ where $P = [\text{Max}(F_o^2, 0) + 2F_c^2]/3$).

^f $R_1 = \sum ||F_o| - |F_c|| / \sum |F_o|$; $wR_2 = [\sum w(F_o^2 - F_c^2)^2 / \sum w(F_o^4)]^{1/2}$.

Table 4.3. X-ray crystallographic details for ^{Me}IPrCH(Br) (**3**).*A. Crystal Data*

formula	C ₃₀ H ₄₁ BrN ₂
formula weight	509.56
crystal color and habit ^a	colorless fragment
crystal dimensions (mm)	0.11 × 0.06 × 0.06
crystal system	monoclinic
space group	C2/c (No. 15)
unit cell parameters ^b	
<i>a</i> (Å)	15.9200(6)
<i>b</i> (Å)	9.5233(3)
<i>c</i> (Å)	18.6286(6)
β (deg)	92.650(3)
<i>V</i> (Å ³)	2821.28(17)
<i>Z</i>	4
ρ _{calcd} (g cm ⁻³)	1.200
μ (mm ⁻¹)	2.108

B. Data Collection and Refinement Conditions

diffractometer	Bruker D8/APEX II CCD ^c
radiation (λ [Å])	Cu Kα (1.54178) (microfocus source)
temperature (°C)	-100
scan type	ω and φ scans (1.0°) (5 s exposures)
data collection 2θ limit (deg)	144.54
total data collected	20936 (-19 ≤ <i>h</i> ≤ 19, -11 ≤ <i>k</i> ≤ 11, -22 ≤ <i>l</i> ≤ 22)
independent reflections	2767 (<i>R</i> _{int} = 0.0429)
number of observed reflections (<i>NO</i>)	2149 [<i>F</i> _o ² ≥ 2σ(<i>F</i> _o ²)]
structure solution method	intrinsic phasing (<i>SHELXT-2014</i> ^d)
refinement method	full-matrix least-squares on <i>F</i> ² (<i>SHELXL-2018</i> ^e)
absorption correction method	Gaussian integration (face-indexed)
range of transmission factors	0.9510–0.8545
data/restraints/parameters	2767 / 18 ^f / 194
goodness-of-fit (<i>S</i>) ^g [all data]	1.050
final <i>R</i> indices ^h	
<i>R</i> ₁ [<i>F</i> _o ² ≥ 2σ(<i>F</i> _o ²)]	0.0489
<i>wR</i> ₂ [all data]	0.1522
largest difference peak and hole	0.177 and -0.710 e Å ⁻³

^aObtained by recrystallization from a hexanes solution.

^bObtained from least-squares refinement of 3652 reflections with $9.50^\circ < 2\theta < 143.82^\circ$.

^cPrograms for diffractometer operation, data collection, data reduction and absorption correction were those supplied by Bruker.

^dG. M. Sheldrick, *Acta Crystallogr.* **2015**, *A71*, 3–8. (*SHELXT-2014*)

^eG. M. Sheldrick, *Acta Crystallogr.* **2015**, *C71*, 3–8. (*SHELXL-2018/3*)

^fThe equivalent C–C and C···C distances within the disordered isopropyl group were restrained to be approximately the same by use of the *SHELXL SADI* instruction. The anisotropic displacement parameters of the carbon atoms of the disordered isopropyl group were restrained by use of the *SHELXL RIGU* instruction.

^g $S = [\sum w(F_o^2 - F_c^2)^2 / (n - p)]^{1/2}$ (n = number of data; p = number of parameters varied; $w = [\sigma^2(F_o^2) + (0.0840P)^2 + 1.5583P]^{-1}$ where $P = [\text{Max}(F_o^2, 0) + 2F_c^2]/3$).

^h $R_1 = \sum ||F_o| - |F_c|| / \sum |F_o|$; $wR_2 = [\sum w(F_o^2 - F_c^2)^2 / \sum w(F_o^4)]^{1/2}$.

Table 4.4. X-ray crystallographic details for (^{Me}IPrCH)BMes₂ (**4**).*A. Crystal Data*

formula	C ₄₈ H ₆₃ BN ₂
formula weight	678.81
crystal color and habit ^a	yellow fragment
crystal dimensions (mm)	0.42 × 0.40 × 0.21
crystal system	monoclinic
space group	<i>P</i> 2 ₁ / <i>n</i> (an alternate setting of <i>P</i> 2 ₁ / <i>c</i> [No. 14])
unit cell parameters ^a	
<i>a</i> (Å)	12.8505(13)
<i>b</i> (Å)	15.6844(15)
<i>c</i> (Å)	22.0078(19)
β (deg)	106.975(2)
<i>V</i> (Å ³)	4242.5(7)
<i>Z</i>	4
ρ _{calcd} (g cm ⁻³)	1.063
μ (mm ⁻¹)	0.060

B. Data Collection and Refinement Conditions

diffractometer	Bruker PLATFORM/APEX II CCD ^b
radiation (λ [Å])	graphite-monochromated Mo Kα (0.71073)
temperature (°C)	-80
scan type	ω scans (0.3°) (20 s exposures)
data collection 2θ limit (deg)	55.77
total data collected	78309 (-16 ≤ <i>h</i> ≤ 16, -20 ≤ <i>k</i> ≤ 20, -28 ≤ <i>l</i> ≤ 28)
independent reflections	10114 (<i>R</i> _{int} = 0.0413)
number of observed reflections (<i>NO</i>)	7099 [<i>F</i> _o ² ≥ 2σ(<i>F</i> _o ²)]
structure solution method	intrinsic phasing (<i>SHELXT-2014</i> ^c)
refinement method	full-matrix least-squares on <i>F</i> ² (<i>SHELXL-2017</i> ^d)
absorption correction method	Gaussian integration (face-indexed)
range of transmission factors	1.0000–0.9301
data/restraints/parameters	10114 / 0 / 476
goodness-of-fit (<i>S</i>) ^e [all data]	1.034
final <i>R</i> indices ^f	
<i>R</i> ₁ [<i>F</i> _o ² ≥ 2σ(<i>F</i> _o ²)]	0.0514
<i>wR</i> ₂ [all data]	0.1506
largest difference peak and hole	0.271 and -0.307 e Å ⁻³

^aObtained from least-squares refinement of 9943 reflections with 4.66° < 2θ < 51.22°.

^bPrograms for diffractometer operation, data collection, data reduction and absorption correction were those supplied by Bruker.

^cG. M. Sheldrick, *Acta Crystallogr.* **2015**, *A71*, 3–8. (*SHELXT-2014*)

^dG. M. Sheldrick, *Acta Crystallogr.* **2015**, *C71*, 3–8. (*SHELXL-2017*)

^e $S = [\Sigma w(F_o^2 - F_c^2)^2 / (n - p)]^{1/2}$ (n = number of data; p = number of parameters varied; $w = [\sigma^2(F_o^2) + (0.0660P)^2 + 1.0171P]^{-1}$ where $P = [\text{Max}(F_o^2, 0) + 2F_c^2]/3$).

^f $R_1 = \Sigma ||F_o| - |F_c|| / \Sigma |F_o|$; $wR_2 = [\Sigma w(F_o^2 - F_c^2)^2 / \Sigma w(F_o^4)]^{1/2}$.

Table 4.5. X-ray crystallographic details for (SIPrCH)ClB-BCl(CHSIPr) (6).*A. Crystal Data*

formula	C ₅₆ H ₇₈ B ₂ Cl ₂ N ₄
formula weight	899.74
crystal color and habit ^a	yellow plate
crystal dimensions (mm)	0.18 × 0.11 × 0.05
crystal system	monoclinic
space group	C2/c (No. 15)
unit cell parameters ^b	
<i>a</i> (Å)	26.0566(8)
<i>b</i> (Å)	11.3328(4)
<i>c</i> (Å)	18.6437(7)
β (deg)	103.5742(18)
<i>V</i> (Å ³)	5351.6(3)
<i>Z</i>	4
ρ _{calcd} (g cm ⁻³)	1.117
μ (mm ⁻¹)	1.371

B. Data Collection and Refinement Conditions

diffractometer	Bruker D8 Venture/PHOTON3 ^c
radiation (λ [Å])	Cu Kα (1.54178) (microfocus source)
temperature (°C)	-100
scan type	ω and φ scans (1.0°) (θ-dependent exposures, 5-20 s)
data collection 2θ limit (deg)	160.03
total data collected	102234 (-32 ≤ <i>h</i> ≤ 32, -13 ≤ <i>k</i> ≤ 12, -23 ≤ <i>l</i> ≤ 23)
independent reflections	5744 (<i>R</i> _{int} = 0.0685)
number of observed reflections (<i>NO</i>)	4971 [<i>F</i> _o ² ≥ 2σ(<i>F</i> _o ²)]
structure solution method	intrinsic phasing (<i>SHELXT-2014</i> ^d)
refinement method	full-matrix least-squares on <i>F</i> ² (<i>SHELXL-2018</i> ^e)
absorption correction method	Gaussian integration (face-indexed)
range of transmission factors	1.0000–0.8357
data/restraints/parameters	5744 / 0 / 297
goodness-of-fit (<i>S</i>) ^f [all data]	1.044
final <i>R</i> indices ^g	
<i>R</i> ₁ [<i>F</i> _o ² ≥ 2σ(<i>F</i> _o ²)]	0.0709
<i>wR</i> ₂ [all data]	0.2192
largest difference peak and hole	0.984 and -0.936 e Å ⁻³

^aObtained by recrystallization from a diethylether solution.

^bObtained from least-squares refinement of 9392 reflections with 6.98 ° < 2θ < 158.26°.

^cPrograms for diffractometer operation, data collection, data reduction and absorption correction were those supplied by Bruker.

^dG. M. Sheldrick, *Acta Crystallogr.* **2015**, *A71*, 3–8. (*SHELXT-2014*)

^eG. M. Sheldrick, *Acta Crystallogr.* **2015**, *C71*, 3–8. (*SHELXL-2018/3*)

$fS = [\sum w(F_o^2 - F_c^2)^2 / (n - p)]^{1/2}$ (n = number of data; p = number of parameters varied; $w = [\sigma^2(F_o^2) + (0.1290P)^2 + 7.6997P]^{-1}$ where $P = [\text{Max}(F_o^2, 0) + 2F_c^2]/3$).

$gR_1 = \sum ||F_o| - |F_c|| / \sum |F_o|$; $wR_2 = [\sum w(F_o^2 - F_c^2)^2 / \sum w(F_o^4)]^{1/2}$.

Table 4.6. X-ray crystallographic details for $[(\{\text{HN}(\text{H}_2\text{C})_2\text{N}(\text{Dipp})\}\text{C}=\text{CH})\text{B}(\text{Dipp})]_2$ (**8**).*A. Crystal Data*

formula	$\text{C}_{56}\text{H}_{80}\text{B}_2\text{N}_4$
formula weight	830.86
crystal color and habit ^a	colorless plate
crystal dimensions (mm)	$0.23 \times 0.08 \times 0.02$
crystal system	triclinic
space group	$P\bar{1}$ (No. 2)
unit cell parameters ^b	
<i>a</i> (Å)	11.0887(5)
<i>b</i> (Å)	12.6189(6)
<i>c</i> (Å)	18.6687(8)
α (deg)	89.400(4)
β (deg)	84.718(4)
γ (deg)	89.701(3)
<i>V</i> (Å ³)	2601.0(2)
<i>Z</i>	2
ρ_{calcd} (g cm ⁻³)	1.061
μ (mm ⁻¹)	0.451

B. Data Collection and Refinement Conditions

diffractometer	Bruker D8/APEX II CCD ^c
radiation (λ [Å])	Cu K α (1.54178) (microfocus source)
temperature (°C)	-100
scan type	ω and ϕ scans (1.0°) (5-15-45 s exposures) ^d
data collection 2θ limit (deg)	144.56
total data collected	65435 ($-13 \leq h \leq 13$, $-15 \leq k \leq 15$, $-22 \leq l \leq 23$)
independent reflections	9856 ($R_{\text{int}} = 0.1948$)
number of observed reflections (<i>NO</i>)	6428 [$F_o^2 \geq 2\sigma(F_o^2)$]
structure solution method	intrinsic phasing (<i>SHELXT-2014</i> ^e)
refinement method	full-matrix least-squares on F^2 (<i>SHELXL-2018</i> ^f)
absorption correction method	Gaussian integration (face-indexed)
range of transmission factors	1.0000–0.7228
data/restraints/parameters	9856 / 0 / 584
extinction coefficient (<i>x</i>) ^g	0.0083(10)
goodness-of-fit (<i>S</i>) ^h [all data]	1.032
final <i>R</i> indices ⁱ	
R_1 [$F_o^2 \geq 2\sigma(F_o^2)$]	0.0814
wR_2 [all data]	0.2206
largest difference peak and hole	0.407 and -0.371 e Å ⁻³

^aObtained by recrystallization from a pentane solution.

^bObtained from least-squares refinement of 2992 reflections with $7.00^\circ < 2\theta < 142.32^\circ$.

^cPrograms for diffractometer operation, data collection, data reduction and absorption correction were those supplied by Bruker.

^dData were collected with the detector set at three different positions. Low-angle (detector $2\theta = -33^\circ$) data frames were collected using a scan time of 5 s, medium-angle (detector $2\theta = 75^\circ$) frames using a scan time of 15 s, and high-angle (detector $2\theta = 117^\circ$) frames using a scan time of 45 s.

^eG. M. Sheldrick, *Acta Crystallogr.* **2015**, *A71*, 3–8. (*SHELXT-2014*)

^fG. M. Sheldrick, *Acta Crystallogr.* **2015**, *C71*, 3–8. (*SHELXL-2018/3*)

^g $F_c^* = kF_c[1 + x\{0.001F_c^2\lambda^3/\sin(2\theta)\}]^{-1/4}$ where k is the overall scale factor.

^h $S = [\sum w(F_o^2 - F_c^2)^2/(n - p)]^{1/2}$ (n = number of data; p = number of parameters varied; $w = [\sigma^2(F_o^2) + (0.0832P)^2]^{-1}$ where $P = [\text{Max}(F_o^2, 0) + 2F_c^2]/3$).

ⁱ $R_1 = \sum||F_o| - |F_c||/\sum|F_o|$; $wR_2 = [\sum w(F_o^2 - F_c^2)^2/\sum w(F_o^4)]^{1/2}$.

4.4.4 Density Functional Theory (DFT) Computations

All computations were performed with Gaussian16.³³ Gas-phase geometries were optimized using density functional theory (DFT) with the B3LYP functional³⁴ and the cc-pVDZ basis set.³⁵ Frequency analysis confirmed all obtained structures to be local minima on the potential energy surfaces. Optimized geometries and orbitals were visualized with Visual Molecular Dynamics (VMD).³⁶

4.5 References

1. A. Stock, A. Brandt, H. Fischer, *Ber. Deutsch. Chemie Ges. B* **1925**, *58*, 643–657.
2. E. C. Neeve, S. J. Geier, I. A. I. Mkhaliid, S. A. Westcott, T. B. Marder, *Chem. Rev.* **2016**, *116*, 9091–9161.
3. a) W. Biffar, H. Nöth, H. Pommerening, *Angew. Chem. Int. Ed. Engl.* **1980**, *19*, 56–57; b) K. Schlüter, A. Berndt, *Angew. Chem. Int. Ed. Engl.* **1980**, *19*, 57–58.
4. a) A. Moezzi, M. M. Olmstead, P. P. Power, *J. Am. Chem. Soc.* **1992**, *114*, 2715–2717; b) W. J. Grigsby, P. P. Power, *Chem. Commun.* **1996**, 2235–2236; c) H. Braunschweig, R. D. Dewhurst, J. O. C. Jiménez-Halla, E. Matito, J. H. Muessig, *Angew. Chem, Int. Ed.* **2018**, *57*, 412–416; d) S. Akiyama, S. Ikemoto, S. Muratsugu, M. Tada, M. Yamashita, *Organometallics* **2020**, *39*, 500–504.
5. a) T. J. Tague, L. Andrews, *J. Am. Chem. Soc.* **1994**, *116*, 4970–4976; b) L. B. Knight, K. Kerr, P. K. Miller, C. A. Arrington, *J. Phys. Chem.* **1995**, *99*, 16482–16484.
6. Y. Wang, B. Quillian, P. Wei, C. S. Wannere, Y. Xie, R. B. King, H. F. Schaefer III, P. v R. Schleyer, G. H. Robinson, *J. Am. Chem. Soc.* **2007**, *129*, 12412–12413.
7. For select reviews on boron-boron multiple-bonded species, see: a) H. Braunschweig, R. D. Dewhurst, *Angew. Chem. Int. Ed.* **2013**, *52*, 3574–3583; b) M. Arrowsmith, H. Braunschweig, T. E. Stennett, *Angew. Chem. Int. Ed.* **2017**, *56*, 96–115; c) R. Borthakur, K. Saha, S. Kar, S. Ghosh, *Coord. Chem. Rev.* **2019**, *399*, 213021.
8. a) S. R. Baird, E. Hupf, I. C. Watson, M. J. Ferguson, E. Rivard, *Chem. Commun.* **2023**, *59*, 2903–2906; b) I. C. Watson, Y. Zhou, M. J. Ferguson, E. Rivard, *Z. Anorg. Allg. Chem.* **2022**,

- 68, e202200082; c) I. C. Watson, M. J. Ferguson, E. Rivard, *Inorg. Chem.* **2021**, *60*, 18347–18359; d) M. M. D. Roy, S. R. Baird, E. Dornsiepen, L. A. Paul, L. Miao, M. J. Ferguson, Y. Zhou, I. Siewert, E. Rivard, *Chem. Eur. J.* **2021**, *27*, 8572–8579.
9. a) T. Eisner, A. Kostenko, F. J. Kiefer, S. Inoue, *Chem. Commun.* **2024**, *60*, 558–561; b) H. Steffenfauseweh, Y. V. Vishnevskiy, B. Neumann, H.-G. Stammler, D. M. Andrada, R. S. Ghadwal, *Angew. Chem. Int. Ed.* **2022**, *61*, e202207415; c) M. K. Sharma, S. Blomeyer, T. Glodde, B. Neumann, H.-G. Stammler, A. Hinz, M. van Gastel, R. S. Ghadwal, *Chem. Sci.* **2020**, *11*, 1975–1984; d) M. K. Sharma, S. Blomeyer, B. Neumann, H.-G. Stammler, M. van Gastel, A. Hinz, R. S. Ghadwal, *Angew. Chem. Int. Ed.* **2019**, *58*, 17599–17603; e) R. S. Ghadwal, *Acc. Chem. Res.* **2022**, *55*, 457–470.
10. M. M. D. Roy, E. Rivard, *Acc. Chem. Res.* **2017**, *50*, 2017–2025.
11. K. Powers, C. Hering-Junghans, R. McDonald, M. J. Ferguson, M. J. Ferguson, E. Rivard, *Polyhedron* **2016**, *108*, 8–14.
12. Y. Wang, M. Y. Abraham, R. J. Gilliard, D. R. Sexton, P. Wei, G. H. Robinson, *Organometallics* **2013**, *32*, 6639–6642.
13. S. Muthaiah, D. C. Do, R. Ganguly, D. Vidović, *Organometallics* **2013**, *32*, 6718–6724.
14. M. Arrowsmith, J. Böhnke, H. Braunschweig, A. Deußenberger, R. D. Dewhurst, W. C. Ewing, C. Hörl, J. Mies, J. H. Muessig, *Chem. Commun.* **2017**, *53*, 8265–8267.
15. Ligand activation of lithium amides, and lithium β -diketiminato ligands upon the addition to some element chlorides ECl_n ($E = Si, Ge, P$) is known, see: a) D. Dhara, T. Vijayakanth, M. K. Nayak, P. Kalita, R. Boomishankar, C. B. Yildiz, V. Chandrasekhar, A. Jana, *Dalton. Trans.*

- 2018**, *47*, 14411–14415. b) P. B. Hitchcock, M. F. Lappert, J. E. Nycz, *Chem. Commun.* **2003**, 1142–1143. c) B. Räge, F. Zülch, Y. Ding, J. Prust, H. W. Roesky, M. Notlemeyer, H.-G. Schmidt, *Z. Anorg. Allg. Chem.* **2001**, *627*, 836–840.
16. The formation of $\text{Ar}^{\text{Dipp}}\text{PCl}$ ($\text{Ar}^{\text{Dipp}} = 2,6\text{-Dipp}_2\text{C}_6\text{H}_3$) has been observed during the synthesis of $\text{Ar}^{\text{Dipp}}\text{PPCl}_2$, see: B. Buster, A. A. Diaz, T. Graham, R. Khan, M. A. Khan, D. R. Powell, R. J. Wehmschulte, *Inorg. Chim. Acta* **2009**, *362*, 3465–3474.
17. a) S. Kumar, T. A. Shah, T. Punniyamurthy, *Org. Chem. Front.* **2021**, *8*, 4288–4314; b) R. Appel, *Angew. Chem. Int. Ed. Engl.* **1975**, *12*, 801–811.
18. S. C. Rasmussen, *ChemTexts* **2021**, *7*, 1–8.
19. C. Hering-Junghans, P. Andreiuk, M. J. Ferguson, R. McDonald, E. Rivard, *Angew. Chem. Int. Ed.* **2017**, *56*, 6272–6275.
20. C. Li, S. K. Mellerup, X. Wang, S. Wang, *Organometallics* **2018**, *37*, 3360–3367.
21. J. T. Goettel, H. Gao, S. Dotzauer, H. Braunschweig, *Chem. Eur. J.* **2020**, *26*, 1136–1143.
22. H. Braunschweig, S. Demeshko, W. C. Ewing, I. Krummenacher, B. B. Macha, J. D. Mattock, F. Meyer, J. Mies, M. Schäfer, A. Vargas, *Angew. Chem. Int. Ed.* **2016**, *55*, 7708–7711.
23. M. M. D. Roy, M. J. Ferguson, R. McDonald, Y. Zhou, E. Rivard, *Chem. Sci.* **2019**, *10*, 6476–6481.
24. H. Tsurugi, K. Mashima, *Acc. Chem. Res.* **2019**, *52*, 769–779.
25. H. Braunschweig, R. D. Dewhurst, K. Hammond, J. Mies, K. Radacki, A. Vargas, *Science* **2012**, *336*, 1420–1422.

26. E. E. Nahon, G. R. Nelmes, P. J. Brothers, J. Hicks, *Chem. Commun.* **2023**, 59, 14281–14284.
27. I. C. Watson, A. Schumann, H. Yu, E. C. Davy, R. McDonald, M. J. Ferguson, C. Hering-Junghans, E. Rivard, *Chem. Eur. J.* **2019**, 25, 9678–9690.
28. H. Braunschweig, A. Damme, R. D. Dewhurst, A. Vargas, *Nat. Chem.* **2013**, 5, 115–121.
29. A. B. Pangborn, M. A. Giardello, R. H. Grubbs, R. K. Rosen, F. J. Timmers, *Organometallics* **1996**, 15, 1518–1520.
30. H. Hope, *Prog. Inorg. Chem.* **1994**, 41, 1–19.
31. G. M. Sheldrick, *Acta Crystallogr. Sect. A* **2015**, 71, 3–8.
32. G. M. Sheldrick, *Acta Crystallogr. Sect. C* **2015**, 71, 3–8.
33. M. J. Frisch, G. W. Trucks, H. B. Schlegel, G. E. Scuseria, M. A. Robb, J. R. Cheeseman, G. Scalmani, V. Barone, G. A. Petersson, H. Nakatsuji, X. Li, M. Caricato, A. V. Marenich, J. Bloino, B. G. Janesko, R. Gomperts, B. Mennucci, H. P. Hratchian, J. V. Ortiz, A. F. Izmaylov, J. L. Sonnenberg, D. Williams-Young, F. Ding, F. Lipparini, F. Egidi, J. Goings, B. Peng, A. Petrone, T. Henderson, D. Ranasinghe, V. G. Zakrzewski, J. Gao, N. Rega, G. Zheng, W. Liang, M. Hada, M. Ehara, K. Toyota, R. Fukuda, J. Hasegawa, M. Ishida, T. Nakajima, Y. Honda, O. Kitao, H. Nakai, T. Vreven, K. Throssell, J. A. Montgomery, Jr., J. E. Peralta, F. Ogliaro, M. J. Bearpark, J. J. Heyd, E. N. Brothers, K. N. Kudin, V. N. Staroverov, T. A. Keith, R. Kobayashi, J. Normand, K. Raghavachari, A. P. Rendell, J. C. Burant, S. S. Iyengar, J. Tomasi, M. Cossi, J. M. Millam, M. Klene, C. Adamo, R. Cammi, J. W. Ochterski, R. L.

Martin, K. Morokuma, O. Farkas, J. B. Foresman, D. J. Fox, Gaussian 16, Revision A. 03, Gaussian Inc., Wallingford CT, 2016.

34. a) C. Lee, W. Yang, R. G. Parr, *Phys. Rev. B* **1988**, *37*, 785–789; b) A. D. Becke, *Phys. Rev. A* **1988**, *38*, 3098–3100; c) P. J. Stephens, F. J. Devlin, C. F. Chabalowski, M. J. Frisch, *J. Phys. Chem.* **1994**, *98*, 11623–11627.

35. T. H. Dunning, *J. Chem. Phys.* **1989**, *90*, 1007–1023.

36. W. Humphrey, A. Dalke, K. Schulten, *J. Molec. Graphics* **1996**, *14*, 33–38.

Chapter 5 – The Synthesis of a Terphenyl-Supported Aminoborane an Inorganic Analogue to Styrene

5.1 Introduction

Boron-nitrogen (BN) containing species have been of interest for many decades owing to their utility as from abrasive materials (*e.g.*, cubic boron-nitride, *c*-BN) and as a lubricants (*e.g.*, hexagonal boron-nitride *h*-BN),¹ and ammonia borane ($\text{H}_3\text{N}\cdot\text{BH}_3$) is being explored as a potential candidate for hydrogen storage.² Unsaturated species containing B-N π -bonding are of particular interest to chemists due to such species being isoelectronic to unsaturated organic fragments, *e.g.*, alkenes and alkynes.³ Due to the inherent polarization of the B-N π bonds towards the nitrogen atom in aminoboranes (R_2BNR_2) and iminoboranes (RBNR) these species generally display high reactivity and readily undergo cyclization and oligomerization reactions in the absence of steric protection.⁴ The first example of a kinetically-stabilized iminoborane ($\text{tBuB}\equiv\text{NtBu}$) was reported by Paetzold and coworkers in 1984.⁵ The stabilization of iminoboranes has allowed exploration of their reactivity ranging from ring-expansion,⁶ metal complexation,⁷ boration reactions,⁸ and cycloadditions.⁹

The Rivard group has previously reported the stabilization of the parent iminoborane HBNH, by utilizing a donor-acceptor approach affording $\text{IPr}\cdot\text{HBNH}\cdot\text{BAr}^{\text{F}}_3$ (IPr = $(\text{HCNDipp})_2\text{C}$; Dipp = 2,6-*i*-Pr₂C₆H₃; Ar^F = 3,5-(F₃C)₂C₆H₃), the first example of an isolable complex of HBNH.¹⁰ More recently, the Rivard group has reported the stabilization of the parent iminoborane isomer HBNH and NBH₂ utilizing the intramolecular frustrated Lewis pair $\text{}^i\text{Pr}_2\text{P}(\text{C}_6\text{H}_4)\text{BCy}_2$ (**PB**) (Cy = cyclohexyl) affording the chelates **PB**{HBNH} and **PB**{NBH₂} (Figure 5.1).¹¹ Liu, Kong and coworkers have shown that boraiminolithium

species ($\text{RB}\equiv\text{NLi}$; R = terphenyl ligand), which are inorganic analogues to lithium acetylides ($\text{RC}\equiv\text{CLi}$), can act as iminoborane transfer agents to afford novel heterocycles.¹² Given that sterically-demanding terphenyl ligands have been used in the stabilization of a variety of E–N multiple bonded species ($\text{E} = \text{Al}, \text{Ga}, \text{and In}$)¹³ I set out to prepare an aminoborane supported by the terphenyl ligand Ar^{Dipp} ($\text{Ar}^{\text{Dipp}} = 2,6\text{-Dipp}_2\text{C}_6\text{H}_3$) and attempt to dehydrogenate said species to afford an iminoborane stabilized by terphenyl ligands with the overall goal of using these species as amino- and iminoborane transfer agents towards main group elements (*e.g.*, $\text{Cl}_2\text{Ge}\cdot\text{diox}$; $\text{diox} = 1,4\text{-dioxane}$). This Chapter describes the preparation and characterization of a terphenyl-supported aminoborane and initial attempts of transition metal-mediated dehydrogenation of said aminoborane.

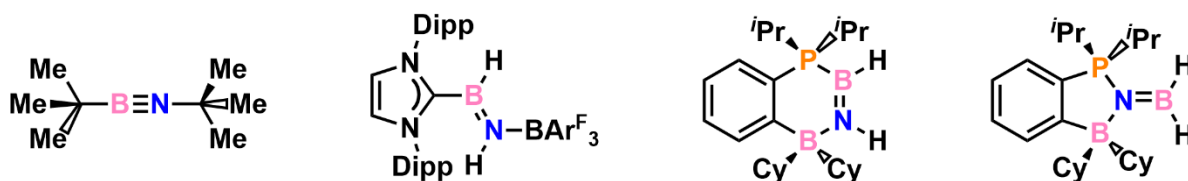
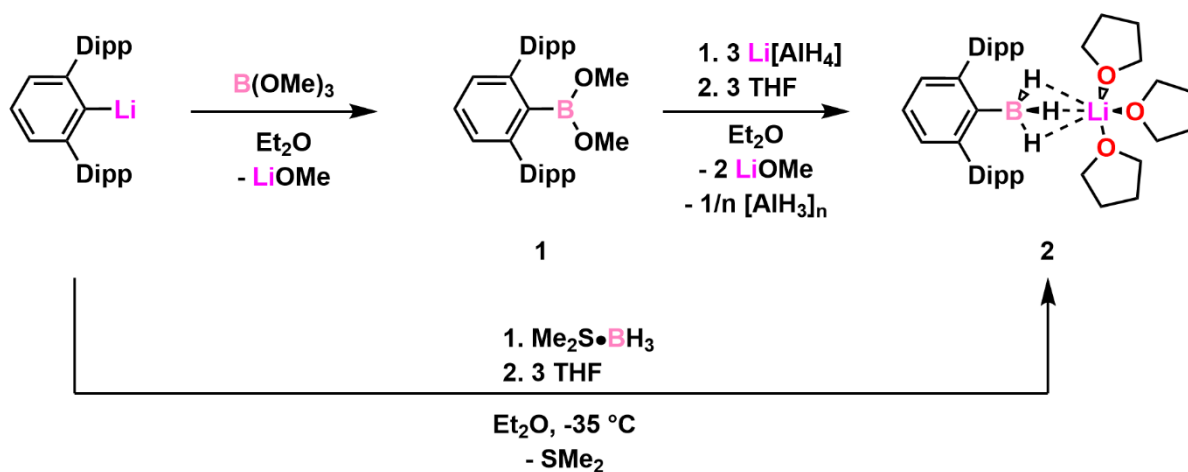


Figure 5.1. Iminoboranes stabilized kinetically and by inter/intramolecular FLPs.

5.2 Results and Discussion

This study to access unsaturated B–N systems began with combining $\text{Ar}^{\text{Dipp}}\text{Li}$ ¹⁴ with one equivalent of $\text{B}(\text{OMe})_3$ leading to the precursor aryl boronate $\text{Ar}^{\text{Dipp}}\text{B}(\text{OMe})_2$ (**1**) as a colorless oil. Compound **1** was then combined with $\text{Li}[\text{AlH}_4]$ to afford the terphenyl borohydride lithium complex $[\text{Ar}^{\text{Dipp}}\text{BH}_3]\text{Li}(\text{THF})_3$ (**2**) in an isolated yield of 84 % as a colorless crystalline solid (Scheme 5.1) after recrystallization from a mixture of THF/hexanes (1:1). Crystals suitable for X-ray crystallographic analysis were obtained from a concentrated

THF/hexanes solution of **2** stored at -35 °C (Figure 5.2). Examination of the $^{11}\text{B}\{^1\text{H}\}$ NMR spectrum of **2** in C_6D_6 showed the expected four-coordinate chemical shift associated with the $-\text{BH}_3$ fragment as a singlet at -30 ppm and a quartet pattern emerged in the $^{11}\text{B}-^1\text{H}$ coupled spectrum. Solid samples of **2** decompose within 16 hours at room temperature and decompose slowly even at -35 °C, affording $\text{Li}[\text{BH}_4]$ and other unidentified products; as such, samples of compound **2** were used within 24 hours of preparation. Alternatively, compound **2** can be prepared in a more direct fashion by combining $\text{Ar}^{\text{Dipp}}\text{Li}$ and $\text{Me}_2\text{S}\cdot\text{BH}_3$ (Scheme 5.1) in Et_2O , followed by recrystallization from THF/hexanes (1:1), with an isolated yield of 89 %. The molecular structure of **2** (Figure 5.2) yields a C1–B1 bond length of 1.608(4) Å, which is identical within experimental error to the C–B bond lengths within $\text{IME}_4\cdot\text{BH}_3$ [1.603(3) Å]¹⁵ ($\text{IME}_4 = (\text{MeCNMe})_2\text{C}$) and $\text{IPr}\cdot\text{BH}_3$ [1.585(4) Å].¹⁶



Scheme 5.1. Synthetic routes to $\text{Ar}^{\text{Dipp}}\text{B}(\text{OMe})_2$ (**1**) and $[\text{Ar}^{\text{Dipp}}\text{BH}_3]\text{Li}(\text{THF})_3$ (**2**).

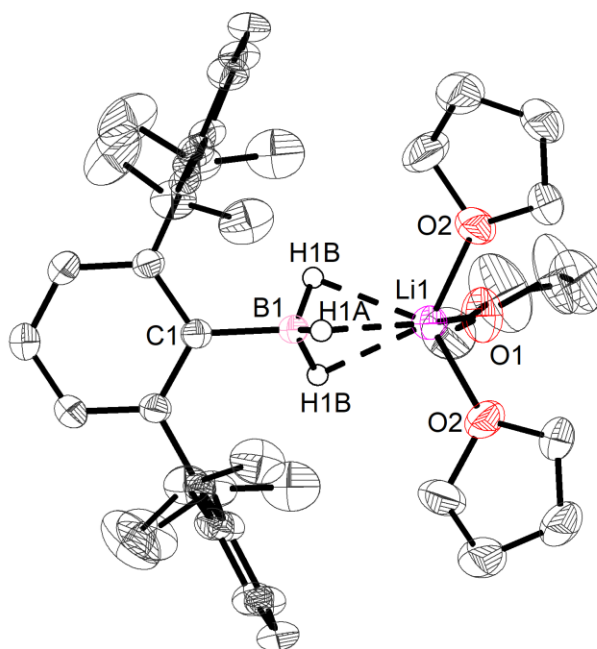
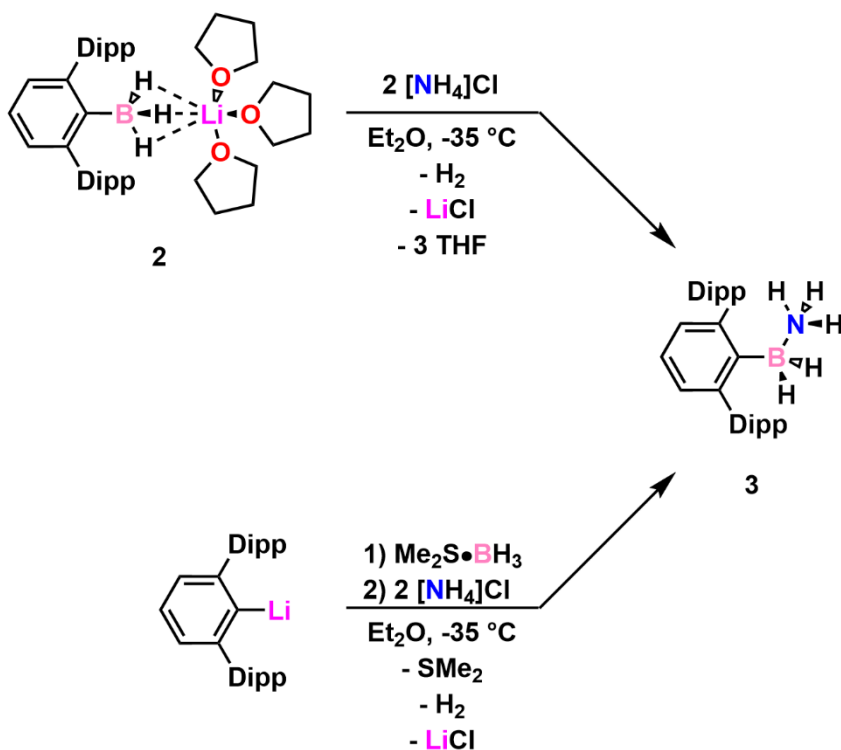


Figure 5.2. Molecular structure of $[\text{Ar}^{\text{Dipp}}\text{BH}_3]\text{Li}(\text{THF})_3$ (**2**) with thermal ellipsoids plotted at 50 % probability. All hydrogen atoms (except the borohydrides) are omitted for clarity. The THF solvent molecule is not shown. Only one of the disordered tetrahydrofuran groups is shown. Selected bond lengths [\AA]: C1–B1 1.608(4), O1–Li1 1.973(9), O2–Li1 1.990(5).

Combining compound **2** with a two-fold excess $[\text{NH}_4]\text{Cl}$ at $-35\text{ }^\circ\text{C}$ in Et_2O and upon recrystallization from toluene afforded $\text{Ar}^{\text{Dipp}}\text{BH}_2\cdot\text{NH}_3$ (**3**) in an isolated yield of 39 % (Scheme 5.2) as a colorless solid; X-ray quality crystals were grown from a saturated toluene solution stored at $-35\text{ }^\circ\text{C}$ for one week. Examination of the ^1H NMR spectrum of **3** in C_6D_6 showed the expected resonance for the $-\text{NH}_3$ unit at 1.66 ppm. The BH_2 fragment was found to have a very broad signal centered at 1.88 ppm. The $^{11}\text{B}\{^1\text{H}\}$ NMR spectrum of **3** revealed a singlet at -14.6 ppm, which is shifted downfield when compared to the ^{11}B NMR resonance for the BH_2 fragment in the frustrated Lewis pair (FLP)-chelated $\text{PB}\{\text{H}_2\text{BNH}_2\}$ ($\text{PB} = \text{Pr}_2\text{P}(\text{C}_6\text{H}_4)\text{BCy}_2$) at -24.6 ppm in C_6D_6 .¹¹ An alternative, and higher-yielding synthetic route

to **3** was envisioned that involved the *in situ* generation of $[\text{Ar}^{\text{Dipp}}\text{BH}_3]\text{Li}$ (**2'**) in Et_2O and subsequent addition of $[\text{NH}_4]\text{Cl}$ in one pot; this procedure afforded **3** as a spectroscopically pure white solid in a yield of 90 % after filtration of the reaction mixture and removal of the volatiles from the filtrate (Scheme 5.2). This method avoids the potential of solubilized LiCl , in the form of $[\text{Li}(\text{THF})_4]\text{Cl}$, which requires removal from **3** by fractional recrystallization.



Scheme 5.2. Synthetic routes to $\text{Ar}^{\text{Dipp}}\text{BH}_2\cdot\text{NH}_3$ (**3**).

The molecular structure of **3** is depicted in Figure 5.3 and features a B1–N1 bond length of 1.545(8) Å, which is the same within error as the B–N single bond in $\text{PB}\{\text{H}_2\text{BNH}_2\}$ [1.573(2) Å]¹¹ yet is marginally shorter than the B–N bond in $\text{H}_3\text{B}\cdot\text{NH}_3$ [1.599(8) Å].¹⁷ Density functional (DFT) computations (M06-2X/cc-pVTZ) on **3** gave a Wiberg bond index (WBI) of 0.69 for the B–N bond indicating the presence of a long single bond, while a WBI

value of 0.91 was obtained for the adjacent B–C, typical of a single bond. The H atoms bonded to boron and nitrogen could not be located in the difference Fourier maps and are placed in idealized positions (Figure 5.3).

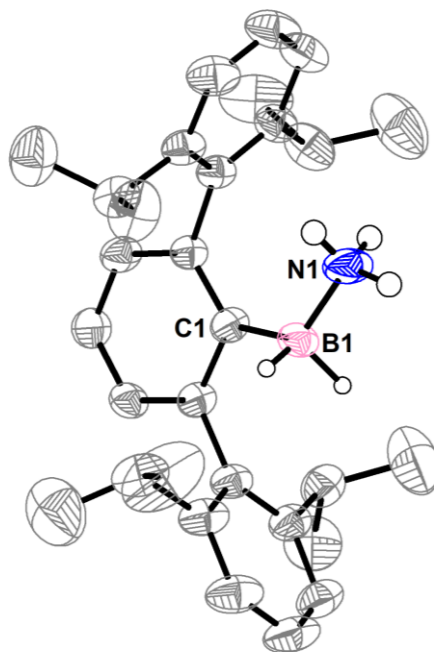
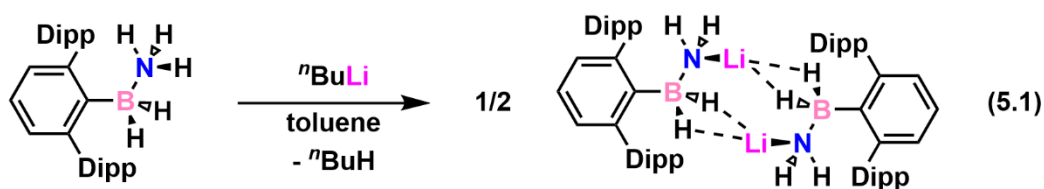


Figure 5.3. Molecular structure of $\text{Ar}^{\text{Dipp}}\text{BH}_2\cdot\text{NH}_3$ (**3**) with thermal ellipsoids plotted at 50 % probability. All carbon-bound hydrogen atoms are omitted for clarity. Only the major orientation of the disordered BH_2NH_3 and isopropyl groups are shown for clarity. Selected bond lengths [\AA] and angles [$^\circ$]: C1–B1 1.624(4), B1–N1 1.545(8); C1–B1–N1 119.0(4).

With analytically pure compound **3** in hand, I turned my attention towards possible routes towards the $\text{Ar}^{\text{Dipp}}\text{B}(\text{H})=\text{NH}_2$ (**5**), which would be an inorganic analogue to styrene. Initial attempts to prepare **5** first involved the lithiation of the datively bound NH_3 fragment to afford $[\text{Ar}^{\text{Dipp}}\text{BH}_2\cdot\text{NH}_2\text{Li}]_2$ (**4**), which was achieved by the addition of $^t\text{BuLi}$ to $\text{Ar}^{\text{Dipp}}\text{BH}_2\cdot\text{NH}_3$ (**3**) in toluene to afford **4** as a white solid in a yield of 84 % (Equation 5.1). Examination of the $^{11}\text{B}\{^1\text{H}\}$ NMR spectrum of **4** in C_6D_6 gave a singlet at -13.0 ppm for the

BH₂ unit, which is slightly shifted when compared to the corresponding BH₂-group in **3** [-14.6 ppm in C₆D₆]; the ¹¹B-¹H coupled spectrum for the BH₂ fragment in **4** yields a triplet at -13.0 ppm (¹J_{BH} = 71 Hz). The ⁷Li{¹H} NMR spectrum of compound **4** gives a singlet resonance at -2.4 ppm, which falls in the range of known lithium amides (*e.g.*, -2.5 ppm for LiTMP; TMP = 2,2,6,6-tetramethylpiperidide).¹⁸



Crystals suitable for X-ray crystallographic analysis were grown from a concentrated hexanes solution of **4** stored at -35 °C (Figure 5.4), and revealed a centrosymmetric dimeric arrangement in the solid state with discernable coordinative interactions between the nitrogen and lithium centers, as well as close contacts between the boron-based hydrides and lithium. The B1–N1 distance in **4** [1.555(3) Å] (Figure 5.4) is identical to the B–N bond length in Ar^{Dipp}BH₂•NH₃ (**3**) [1.545(8) Å *vide supra*]. The N1–Li1 distance 1.923(4) Å is shorter than that of reported in other lithium amides (*e.g.*, 2.00(2) Å in dimeric [Li{N(SiMe₃)₂}]₂)¹⁹ and in dimeric [PB{NLi}]₂ [*avg.* 1.996(7) Å].¹¹

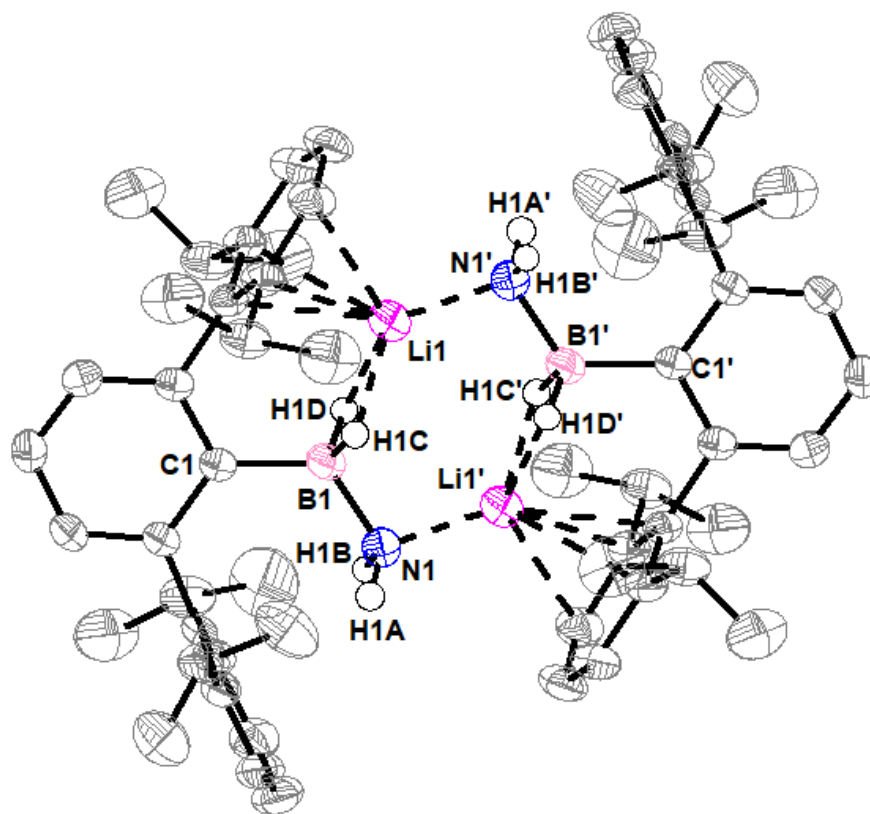
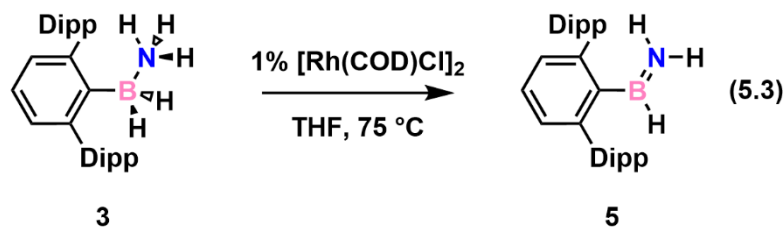


Figure 5.4. Molecular structure of $[\text{Ar}^{\text{Dipp}}\text{BH}_2 \cdot \text{NH}_2\text{Li}]_2$ (**4**) with thermal ellipsoids plotted at 50 % probability. All carbon-bound hydrogen atoms are omitted for clarity. H atoms bound to boron and nitrogen were located in the difference Fourier maps and refined isotropically. The trace amount (~2%) of co-crystallized $\text{Ar}^{\text{Dipp}}\text{I}$ is not shown for clarity. Selected bond lengths [\AA] and angles [$^\circ$]: C1–B1 1.622(3), B1–N1 1.555(3), N1–Li1 1.923(4), B1–Li1' 2.361(4), B1–H1C 1.159(17), B1–H1D 1.157(18), N1–H1A 0.93(3), N1–H1B 0.97(3); C1–B1–N1 121.85(16), B1–N1–Li1 103.70(17), N1–B1–Li1' 123.88(18), C1–B1–Li1' 114.27(18).

From $[\text{Ar}^{\text{Dipp}}\text{BH}_2 \cdot \text{NH}_2\text{Li}]_2$ (**4**) it was envisioned that $\text{Ar}^{\text{Dipp}}\text{B}(\text{H})=\text{NH}_2$ (**5**) could be prepared *via* an overall protocol involving salt-metathesis and hydride abstraction. Initial attempts involved combining ClSiMe_3 and **4** in toluene, which led to only partial conversion to $\text{Ar}^{\text{Dipp}}\text{B}(\text{H})=\text{NH}_2$ (**5**); even heating the reaction mixture to 80 $^\circ\text{C}$ for two days resulted in only 50 % conversion to **5**. It was found that combining **4** with ClCPh_3 or $\text{Ph}_3\text{COTf}^{20}$ ($\text{OTf} =$

O_3SCF_3^-) in toluene led to full conversion to $\text{Ar}^{\text{Dipp}}\text{B}(\text{H})=\text{NH}_2$ (**5**) (Equation 5.2). However, difficulties arose with the separation of compound **5** from the coproduct HCPH_3 due to their similar solubilities, as such, this method for the preparation of pure **5** was abandoned.



Dehydrogenation of amine-boranes with transition metal catalysts is a well-established method for the synthesis of B-N oligomers and polymers.²¹ Combining $\text{Ar}^{\text{Dipp}}\text{BH}_2\text{NH}_3$ (**3**) with the known dehydrogenation pre-catalyst $[\text{Rh}(\text{COD})\text{Cl}_2]$ (COD = 1,5-cyclooctadiene) and heating the reaction mixture to 75 °C in THF for 24 hours led to clean conversion to $\text{Ar}^{\text{Dipp}}\text{B}(\text{H})=\text{NH}_2$ (**5**), which was isolated as a white solid in a yield of 83 % (Equation 5.3). The $^{11}\text{B}\{^1\text{H}\}$ NMR spectrum of **5** in C_6D_6 consisted of a singlet at 39.1 ppm, which is shifted upfield compared to $\text{PB}\{\text{NBH}_2\}$ [45.9 ppm in C_6D_6].¹¹ The NH_2 fragment in **5** appears as two broad singlets at 3.31 and 3.16, respectively, in the ^1H NMR spectrum indicating possible hindered rotation about the B–N array, in line with a B–N double bond. The IR spectrum of **5** showed two stretches for the NH_2 fragment (ν_{sym} and ν_{asym}) at 3486 cm^{-1} and 3405 cm^{-1} , which match well with the DFT calculated IR spectrum. The BH unit appeared at 2506 cm^{-1} (^{10}B H stretch) and 2456 cm^{-1} (^{11}B H stretch), while the B=N stretch was located at 1606 cm^{-1} . Unfortunately, all attempts to grow crystals suitable for X-ray crystallographic analysis have been unsuccessful so far.

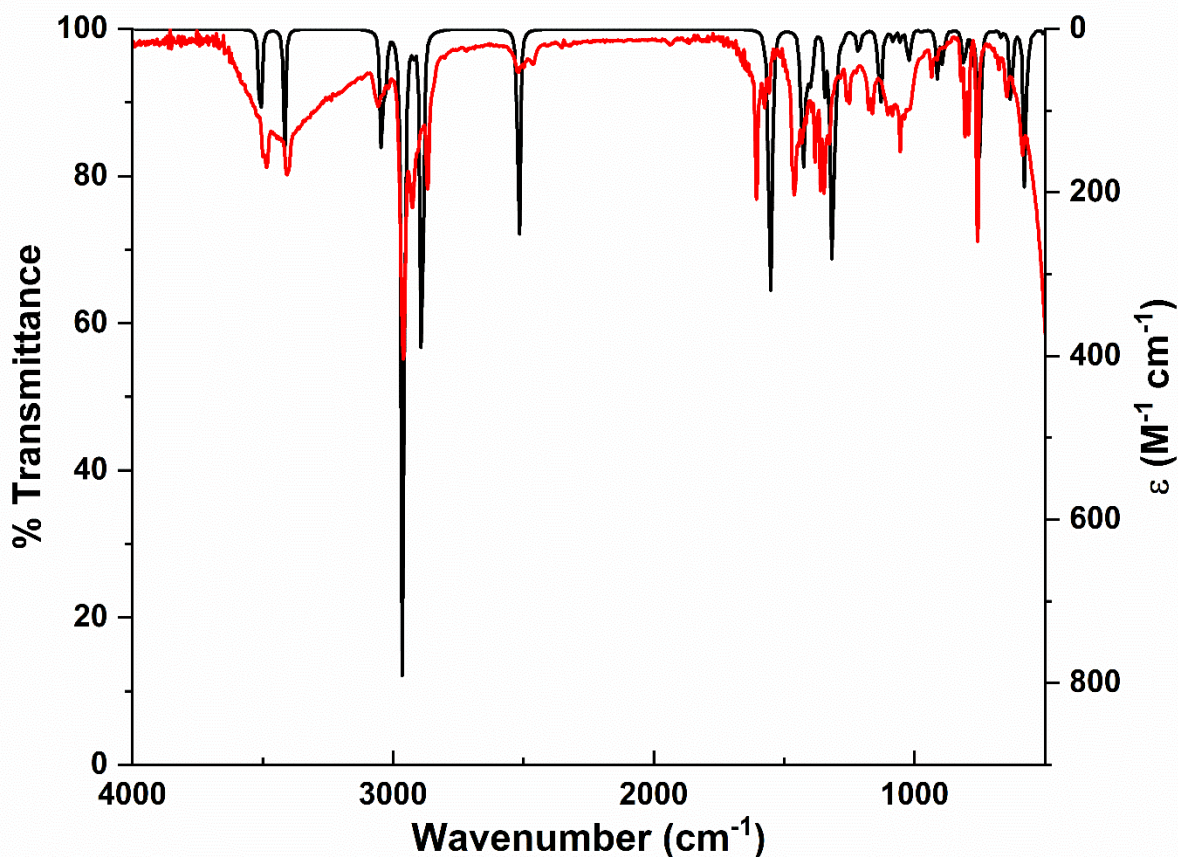
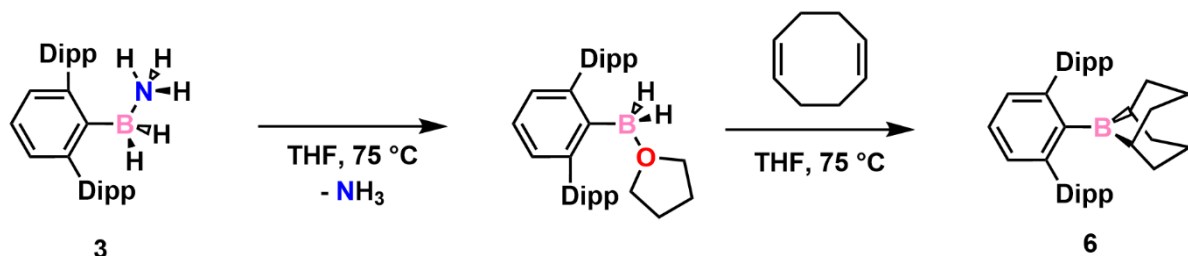


Figure 5.5. Computed (black trace; M06-2x/cc-pVTZ) and measured (red trace) IR spectra (drop-cast from benzene, KBr plate) of $\text{Ar}^{\text{Dipp}}\text{B}(\text{H})=\text{NH}_2$ (**5**).

In one instance during one of many attempts to grow crystals of **5**, a few crystals suitable for X-ray analysis were grown from a mixture of hexamethyldisiloxane/THF (1:1) and its structure determined to be the cycloadduct $\text{Ar}^{\text{Dipp}}\text{B}(\text{C}_8\text{H}_{14})$ (**6**) (Figure 5.6). This species was not observed by ^1H or $^{11}\text{B}\{^1\text{H}\}$ NMR spectroscopy, and as such **6** is likely to be a very minor trace impurity. It is known that $[\text{Rh}(\text{COD})\text{Cl}]_2$ under heating will form Rh-nanoparticles, which partake in dehydrogenation reactions.²² Under such conditions, it may be possible that the NH_3 fragment in $\text{Ar}^{\text{Dipp}}\text{BH}_2\cdot\text{NH}_3$ (**3**) may dissociate from the BH_2 center, possibly forming

the intermediate $\text{Ar}^{\text{Dipp}}\text{BH}_2(\text{THF})$, allowing for COD to undergo double hydroboration leading to the formation of $\text{Ar}^{\text{Dipp}}\text{B}(\text{C}_8\text{H}_{14})$ (**6**) (Scheme 5.3).²³



Scheme 5.3. Proposed synthetic route to $\text{Ar}^{\text{Dipp}}\text{B}(\text{C}_8\text{H}_{14})$.

As a more direct way to determine if I had prepared $\text{Ar}^{\text{Dipp}}\text{B}(\text{H})=\text{NH}_2$ (**5**), I set out to make the deuterated derivatives $\text{Ar}^{\text{Dipp}}\text{BH}_2\cdot\text{ND}_3$ (**7**) and $\text{Ar}^{\text{Dipp}}\text{B}(\text{H})=\text{ND}_2$ (**8**). Compound **7** was prepared in a similar fashion as **3** by combining $\text{Ar}^{\text{Dipp}}\text{Li}$ with $\text{Me}_2\text{S}\cdot\text{BH}_3$, followed by the addition of $[\text{ND}_4]\text{Cl}$, affording $\text{Ar}^{\text{Dipp}}\text{BH}_2\cdot\text{ND}_3$ (**7**) in an isolated yield of 84 % as a spectroscopically pure white solid (Equation 5.4). Analysis of the ^1H NMR spectrum of **7** in C_6D_6 revealed that the resonance for NH_3 fragment was no longer present at 1.66 ppm, while the $^{11}\text{B}\{^1\text{H}\}$ NMR spectrum of **7** afforded a peak at -14.8 ppm, identical to that of **3**. The ^2H NMR spectrum of **7** in C_6H_6 consists of a broad resonance at 1.51 ppm for the ND_3 moiety (Figure 5.7).

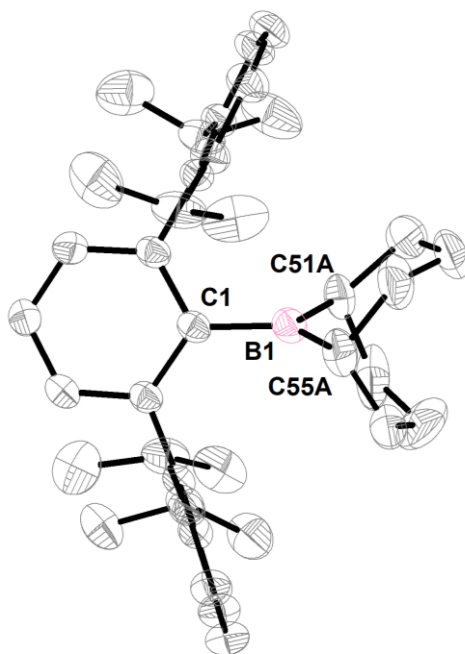
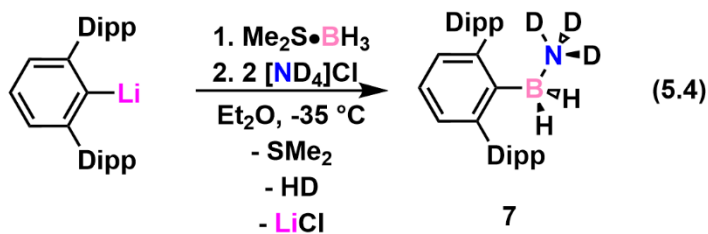


Figure 5.6. Molecular structure of $\text{Ar}^{\text{Dipp}}\text{B}(\text{C}_8\text{H}_{14})$ (**6**) with thermal ellipsoids plotted at 50 % probability. All hydrogen atoms are omitted for clarity. Only the major orientation of the disordered borabicyclo[3.3.1]nonane group is shown for clarity. Selected bond lengths [\AA] and angles [$^\circ$]: C1–B1 1.587(2), B1–C51A 1.51(2), B1–C55A 1.51(2); C1–B1–C51A 119.9(4), C1–B1–C55A 127.1(4), C51A–B1–C55A 113.0(6).



The subsequent dehydrogenation of $\text{Ar}^{\text{Dipp}}\text{BH}_2\cdot\text{ND}_3$ (**7**) with $[\text{Rh}(\text{COD})\text{Cl}]_2$ (Equation 5.5) which afforded $\text{Ar}^{\text{Dipp}}\text{B}(\text{H})=\text{ND}_2$ (**8**) as a white solid in a yield of 81 %. Analysis of the ^1H NMR spectrum of **7** in C_6D_6 revealed that the two broad singlets for the NH_2 fragment at

1.66 and 1.51 ppm were no longer present. The ^2H NMR spectrum of **7** in C_6H_6 revealed two singlets at 3.26 and 3.10 ppm, which indicates the two deuterons are magnetically inequivalent, which would arise due to restricted rotation about the B–N bond and possible π -bonding in this unit B–N double bond. The IR spectrum showed two vibrations at 2607 cm^{-1} and 2494 cm^{-1} for the ND_2 fragment.

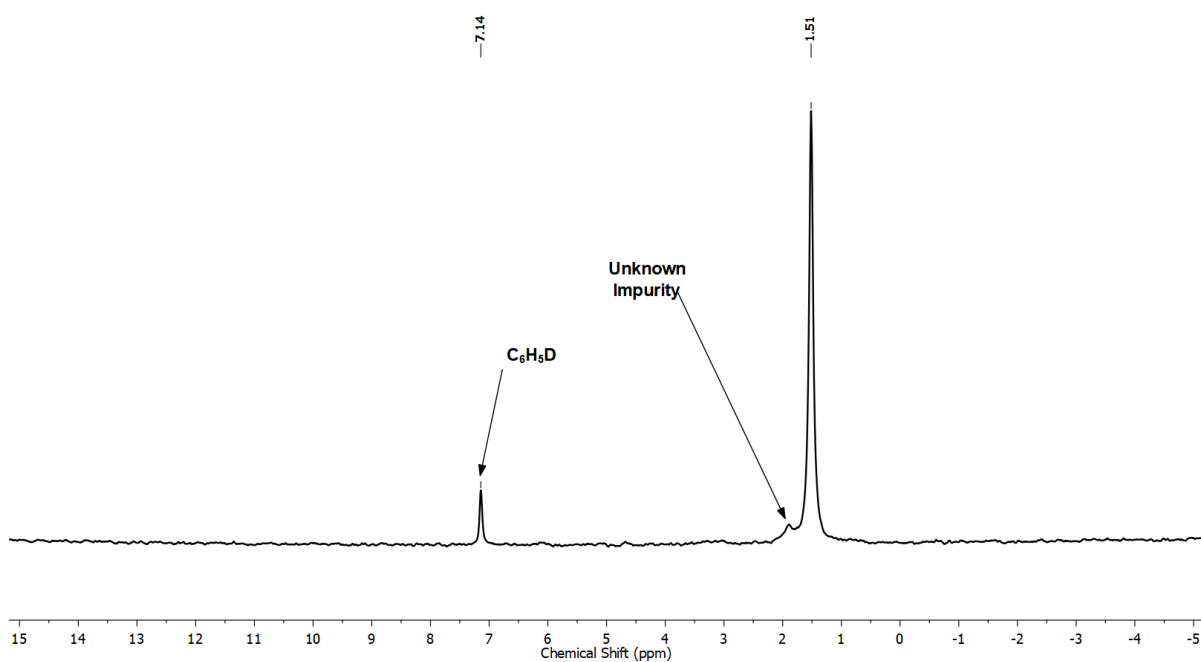
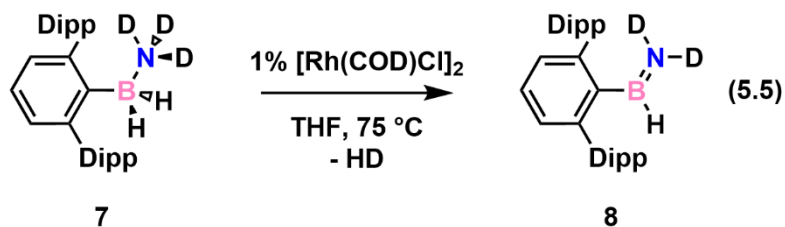


Figure 5.7. ^2H NMR spectrum of $\text{Ar}^{\text{Dipp}}\text{BH}_2\cdot\text{ND}_3$ (**6**) in C_6H_6 .



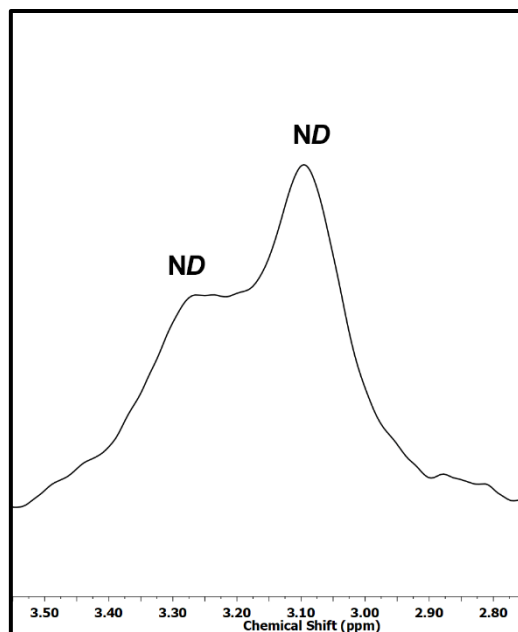


Figure 5.8. Excerpt from the ^2H NMR spectrum of $\text{Ar}^{\text{Dipp}}\text{B}(\text{H})=\text{ND}_2$ (**8**) in C_6H_6 showing two magnetically-inequivalent ND resonances.

Density functional theory (DFT) computations on the idealized gas-phase geometry of $\text{Ar}^{\text{Dipp}}\text{B}(\text{H})=\text{NH}_2$ (**5**) at the M06-2X/cc-pVTZ level of theory revealed that there is π -bonding character in the BN fragment (HOMO-9 Figure 5.9). The B-N array in the computed structure of **5** has a bond length of 1.394 Å, and compares well with the exocyclic B-N distance in $\text{PB}\{\text{NBH}_2\}$ [1.396(6) Å] but is slightly longer than the core B-N distance in $\text{PB}\{\text{HBNH}\}$ [1.347(3) Å], two species that contain B-N double bonds.¹¹ Natural Bond Order (NBO) analysis revealed that there is effectively little to no mixing between the lone-pair on nitrogen and the empty p-orbital on boron (Figure 5.10), similar to $\text{PB}\{\text{NBH}_2\}$. The charges within the B-N array in **5** indicate a polarized double bond with B having a natural charge (Q_{NPA}) of 0.59 and N a Q_{NPA} of -1.03 (Figure 5.11); it should be noted that similar charges are found in $\text{PB}\{\text{NBH}_2\}$ [B $Q_{\text{NPA}} = 0.48$; N $Q_{\text{NPA}} = -1.26$].¹¹ With all being said, it is likely that $\text{Ar}^{\text{Dipp}}\text{B}(\text{H})=\text{NH}_2$ (**5**) contains a polar B-N double bond.

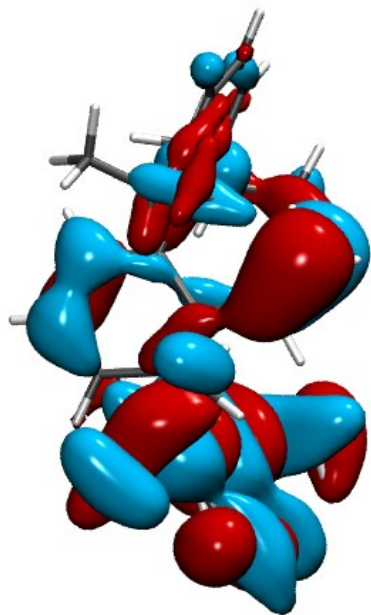


Figure 5.9. Computed HOMO-9 of $\text{Ar}^{\text{Dipp}}\text{B}(\text{H})=\text{NH}_2$ (**5**) at the M06-2X/cc-pVTZ level of theory.

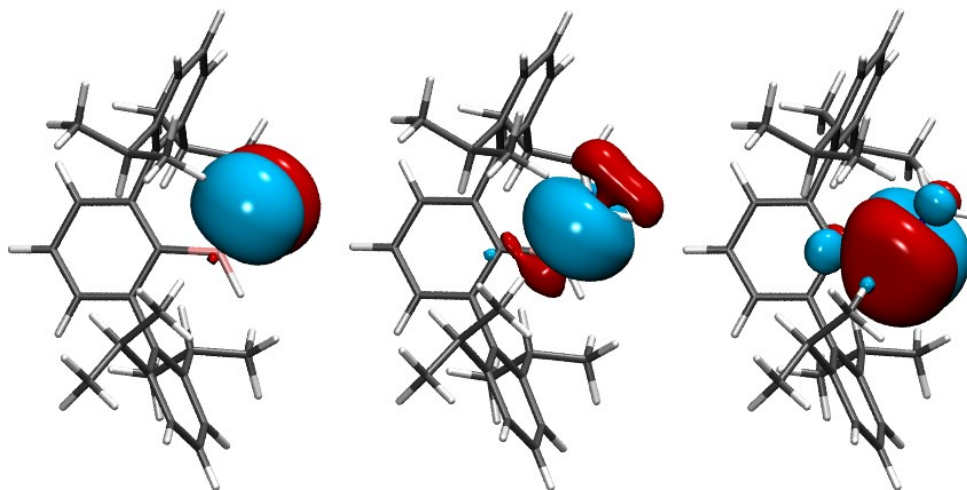
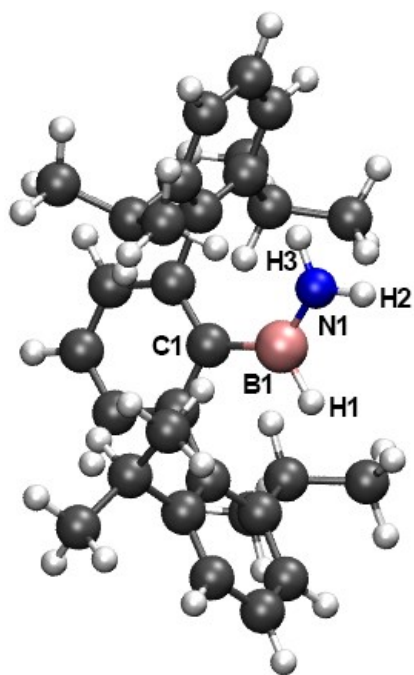


Figure 5.10. NBOs of $\text{Ar}^{\text{Dipp}}\text{B}(\text{H})=\text{NH}_2$ (**5**) depicting (with e^- occupancy): the lone pair of N [$1.7 e^-$] (left); the B-N σ orbital [$2.0 e^-$] (middle); the partially-occupied p-orbital of B [$0.3 e^-$] (right). Computed at the M06-2X/cc-pVTZ level of theory.

So far, attempts to dehydrogenate $\text{Ar}^{\text{Dipp}}\text{B}(\text{H})=\text{NH}_2$ (**5**) further to afford the iminoborane dimer $[\text{Ar}^{\text{Dipp}}\text{BNH}]_2$ (**9**) with 1 mol % of $[\text{Rh}(\text{COD})\text{Cl}]_2$ heated to 75 °C for two days, 5 mol % of $[\text{CpFe}(\text{CO})]_2/h\nu$ ($\text{Cp} = \eta^5\text{-C}_5\text{H}_5$)²¹ and 10 mol % of $\text{Pt}(\text{PCy}_3)_2$ ²⁴ (at room temperature for two days and heating to 75 °C in THF for one week) have proven unsuccessful. Attempts to dehydrogenate **5** with $[\text{CpFe}(\text{CO})]_2/h\nu$ in THF, when monitored by $^{11}\text{B}\{^1\text{H}\}$ NMR spectroscopy, led to the formation of a new species at 29.9 ppm, possibly **9**, only after seven days of irradiation with a 125 W Hg lamp but only in small quantities (*ca.* <5%) and this species could not be isolated from the reaction mixture. Similarly, attempts to induce H/I exchange at boron with $\text{Me}_2\text{S}\cdot\text{BI}_3$ ^{10,25} to prepare $\text{Ar}^{\text{Dipp}}\text{B}(\text{I})=\text{NH}_2$ (**11**), which could then potentially be dehydrohalogenated to afford $[\text{Ar}^{\text{Dipp}}\text{BNH}]_2$ (**9**), have also been unsuccessful due to no reaction being observed between **5** and $\text{Me}_2\text{S}\cdot\text{BI}_3$. The apparent lack of reactivity observed may be attributed, at least partially, to the nearly neutral character of the boron-bound hydride in $\text{Ar}^{\text{Dipp}}\text{B}(\text{H})=\text{NH}_2$ (**5**) with a computed natural charge (Q_{NPA}) of -0.06 (Figure 5.11), a value that is similar to the boron hydride bond in $\text{PB}\{\text{HBNH}\}$ ($Q_{\text{NPA}} = -0.04$),¹¹ a species which was also found to not undergo transition metal-mediated dehydrogenation.^{11,26} It is theorized that a key step in the catalytic dehydrogenation of amine-boranes by transition metals is the scission of B–H bonds,²⁷ thus, the effectively non-polar character the B–H unit in $\text{Ar}^{\text{Dipp}}\text{B}(\text{H})=\text{NH}_2$ (**5**) may be suppressing such metal activation.



(a)

Bond	Calculated
C1–B1	1.581
B1–N1	1.394

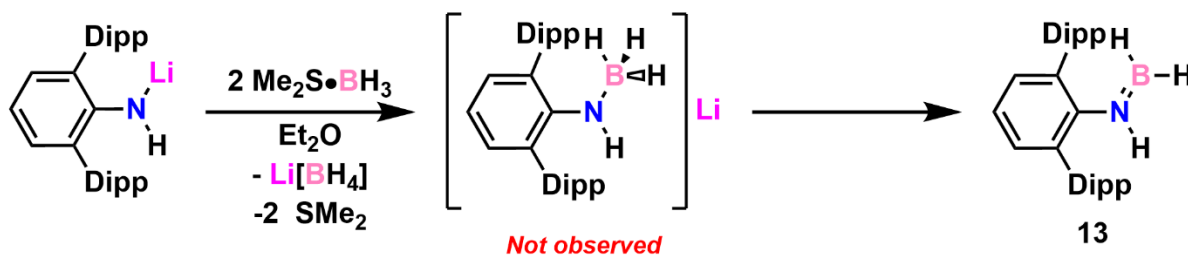
(b)

Bond	WBI	Atom	Q _{NPA}
C1–B1	1.101	C1	-0.36
B1–N1	0.951	B1	0.59
-	-	N1	-1.03
-	-	H1	-0.06
-	-	H2	0.41
-	-	H3	0.39

Figure 5.11. Optimized gas phase geometry of Ar^{Dipp}B(H)=NH₂ (**5**) computed at the M06-2X/cc-pVTZ level of theory with a) calculated bond lengths [Å], and b) Wiberg bond indices (WBI) and natural charges (Q_{NPA}).

I also explored potential synthetic routes for the preparation of the structural isomer of **5**, Ar^{Dipp}N(H)=BH₂ (**13**). Previously, the Rivard group described the synthesis of **PB**{NBH₂} *via* the addition of two equivalents of Me₂S•BH₃ to the FLP chelated lithium amide dimer [PB{NLi}]₂.¹¹ Following this method, two equivalents of Me₂S•BH₃ were combined with the bulky terphenyl amide Ar^{Dipp}N(H)Li²⁸ in Et₂O which resulted in the formation of a precipitate after ten minutes (possibly Li[BH₄]) (Scheme 5.4). Removal of the volatiles from the reaction mixture *in vacuo* and examination of the resulting residue by ¹H NMR spectroscopy in C₆D₆ revealed that the major solubilized species was Ar^{Dipp}NH₂ and a second unidentified species (*ca.* 25 % by integration), potentially the desired product Ar^{Dipp}N(H)=BH₂ (**13**). Close examination of the ¹H NMR spectrum revealed two broad resonances at 5.86 and 5.84 ppm,

possibly indicating two magnetically inequivalent boron bound-hydrides, which would arise due to restricted rotation due to the presence of a N=B double bond. It should be noted that in the ^1H NMR spectrum of $\text{PB}\{\text{NBH}_2\}$ there are two broad resonances at 5.66 and 5.31 ppm, for the BH_2 moiety, which arise due to restricted rotation about the N=B array.¹¹ The $^{11}\text{B}\{^1\text{H}\}$ NMR spectrum of the above-mentioned product mixture (in C_6D_6) showed two broad resonances at 44.6 and 39.6 ppm. The resonance centered at 44.6 ppm may belong to $\text{Ar}^{\text{Dipp}}\text{N}(\text{H})=\text{BH}_2$ (**13**) and would match well with the chemical shift of the terminal BH_2 fragment in $\text{PB}\{\text{NBH}_2\}$ [45.9 ppm in C_6D_6].¹¹ B–H coupling was not observed for the resonances at 44.6 and 39.6 ppm in the ^{11}B NMR spectrum due to the large peak widths. It is also worth noting that the possible intermediate $[\text{Ar}^{\text{Dipp}}\text{N}(\text{H})\text{BH}_3]\text{Li}$ was not observed by $^{11}\text{B}\{^1\text{H}\}$ or $^7\text{Li}\{^1\text{H}\}$ NMR spectroscopy in C_6D_6 . Attempts so far to isolate $\text{Ar}^{\text{Dipp}}\text{N}(\text{H})=\text{BH}_2$ (**13**) by recrystallization from hexamethyldisiloxane, toluene, pentane or hexanes has only afforded $\text{Ar}^{\text{Dipp}}\text{NH}_2$.



Scheme 5.4. Attempted synthesis of $\text{Ar}^{\text{Dipp}}\text{N}(\text{H})=\text{BH}_2$ (**13**).

Density functional theory (DFT) computations on the idealized gas-phase geometry of $\text{Ar}^{\text{Dipp}}\text{N}(\text{H})=\text{BH}_2$ (**13**) at the M06-2X/cc-pVTZ level of theory revealed that the HOMO has some B–N π -bonding character (Figure 5.12) and that the LUMO has significant empty p-

orbital character centered on the terminal boron. The computed structure has a N–B bond length of 1.399 Å, which matches well with the computed bond length in $\text{Ar}^{\text{Dipp}}\text{B}(\text{H})=\text{NH}_2$ (**5**) and with the experimentally-determined N–B bond length of $\text{PB}\{\text{NBH}_2\}$ [1.396(3) Å]¹¹ indicating the presence of a possible N=B double bond.

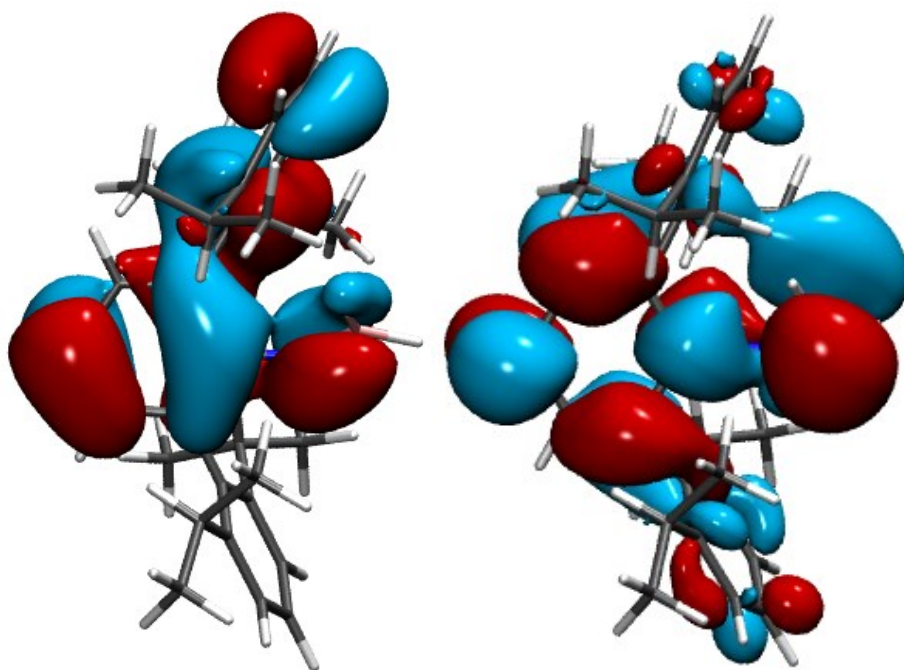


Figure 5.12. Computed HOMO (left) and LUMO (right) of $\text{Ar}^{\text{Dipp}}\text{N}(\text{H})=\text{BH}_2$ (**13**) at the M06-2X/cc-pVTZ level of theory.

I also explored the possibility of preparing $\text{Ar}^{\text{Dipp}}\text{NH}_2\cdot\text{BH}_3$ (**14**), the structural isomer to $\text{Ar}^{\text{Dipp}}\text{BH}_2\cdot\text{NH}_3$ (**3**), with the aim of dehydrogenating **14** with $[\text{Rh}(\text{COD})\text{Cl}]_2$ to give $\text{Ar}^{\text{Dipp}}\text{N}(\text{H})=\text{BH}_2$ (**13**). Interestingly, the addition of $\text{Me}_2\text{S}\cdot\text{BH}_3$ to $\text{Ar}^{\text{Dipp}}\text{NH}_2$ ²⁹ did not give any sign of reaction when the reaction progress was monitored by ^1H and $^{11}\text{B}\{^1\text{H}\}$ NMR spectroscopy in C_6D_6 . This is likely due to the $\text{Ar}^{\text{Dipp}}\text{NH}_2$ being a poor Lewis base.

5.3 Conclusions

This Chapter explores the preparation of the aminoborane, $\text{Ar}^{\text{Dipp}}\text{B}(\text{H})=\text{NH}_2$ (**5**), an inorganic analogue to styrene, which was achieved through successive dehydrogenations from the borohydride complex $[\text{Ar}^{\text{Dipp}}\text{BH}_3]\text{Li}(\text{THF})_3$ (**2**) and transition metal-mediated dehydrogenation of $\text{Ar}^{\text{Dipp}}\text{BH}_2\cdot\text{NH}_3$ (**3**). While the connectivity of $\text{Ar}^{\text{Dipp}}\text{B}(\text{H})=\text{NH}_2$ (**5**) could not be determined by X-ray crystallographic studies, through density functional theory (DFT) and deuterium labelling studies, it is likely that the B–N array consists of a BN double bond. Similar to previously reported FLP-chelated iminoborane adducts from the Rivard group,¹¹ the low degree of hydridic character of the B–H bonds in $\text{Ar}^{\text{Dipp}}\text{B}(\text{H})=\text{NH}_2$ (**5**) may be suppressing further transition metal-mediated dehydrogenation. Future work will focus on using the related terphenyl ligand, Ar^{Mes} ($\text{Ar}^{\text{Mes}} = 2,6\text{-Mes}_2\text{C}_6\text{H}_3$; $\text{Mes} = 2,4,6\text{-Me}_3\text{C}_6\text{H}_2$), to prepare the aminoborane $\text{Ar}^{\text{Mes}}\text{B}(\text{H})=\text{NH}_2$ as a close structural analogue to $\text{Ar}^{\text{Dipp}}\text{B}(\text{H})=\text{NH}_2$ (**5**), which may improve efforts to grow crystals suitable for X-ray crystallographic studies.

5.4 Experimental Details

5.4.1 General Considerations

All reactions were performed using Schlenk and glovebox (Innovative Technology, Inc.) techniques under a nitrogen atmosphere. All solvents (except pentane and hexamethyldisiloxane) were purified using a Grubbs-type solvent purification system³⁰ manufactured by Innovative Technology, Inc., degassed (freeze–pump–thaw method), and stored under an atmosphere of nitrogen prior to use. Pentane and hexamethyldisiloxane were degassed *via* three freeze–pump–thaw cycles and dried over 4 Å molecular sieves. $\text{B}(\text{OMe})_3$

was purchased from Oakwood Chemical and used as received. $[\text{Rh}(\text{COD})\text{Cl}]_2$, $n\text{BuLi}$ (2.5 M solution in hexanes), $\text{Li}[\text{AlH}_4]$ (4.0 M solution in Et_2O), $\text{Me}_2\text{S}\cdot\text{BH}_3$, $[\text{NH}_4]\text{Cl}$, and $[\text{ND}_4]\text{Cl}$ were purchased from Sigma-Aldrich and used as received. $\text{Ar}^{\text{Dipp}}\text{Li}^{14}$ was prepared according to literature procedures. ^1H , $^{13}\text{C}\{^1\text{H}\}$, $^{11}\text{B}\{^1\text{H}\}$, and $^7\text{Li}\{^1\text{H}\}$ NMR spectra were recorded on 400, 500, 600 or 700 MHz Varian Inova instruments and were referenced externally to SiMe_4 (^1H , $^{13}\text{C}\{^1\text{H}\}$), 15 % $\text{F}_3\text{B}\cdot\text{OEt}_2$ (^{11}B), and 9.7 M solution of LiCl in D_2O (^7Li). Elemental analyses were performed by the Analytical and Instrumentation Laboratory at the University of Alberta using a Thermo Flash 2000 Elemental Analyzer. Melting points were measured in sealed glass capillaries under nitrogen with a MelTemp apparatus and are uncorrected. Infrared (IR) spectra were recorded as drop-cast films from benzene solutions on KBr plates with a Nicolet IR100 FTIR spectrometer.

5.4.2 Synthetic Procedures

Synthesis of $\text{Ar}^{\text{Dipp}}\text{B}(\text{OMe})_2$ (1): To a solution of $\text{Ar}^{\text{Dipp}}\text{Li}$ (0.539 g, 1.33 mmol) dissolved in 5 mL of Et_2O was added $\text{B}(\text{OMe})_3$ (149 μL , 1.34 mmol) in one portion. After one minute a flocculent white precipitate formed. After a further 16 hours of stirring the volatiles were removed *in vacuo* affording a white sticky residue that was extracted with 10 mL of pentane and filtered through a plug of diatomaceous earth affording a colorless filtrate. The volatiles were removed from that filtrate *in vacuo* affording $\text{Ar}^{\text{Dipp}}\text{B}(\text{OMe})_2$ (1) as a colorless oil (0.466 g, 74 %). ^1H NMR (700 MHz, C_6D_6): δ 7.24–7.30 (overlapping multiplets, 5H, ArH), 7.20 (d, 4H, $^3J_{\text{HH}} = 7.0$ Hz, *m*- ArH), 3.16 (s, 6H, $\text{B}(\text{OCH}_3)_2$), 3.01 (sept, 4H, $^3J_{\text{HH}} = 7.0$ Hz, $\text{CH}(\text{CH}_3)_2$), 1.26 (d, 12H, $^3J_{\text{HH}} = 7.0$ Hz, $\text{CH}(\text{CH}_3)_2$), 1.09 (d, 12H, $^3J_{\text{HH}} = 7.0$ Hz, $\text{CH}(\text{CH}_3)_2$). $^{13}\text{C}\{^1\text{H}\}$

NMR (176 MHz, C₆D₆): δ 147.5 (ArC), 144.1 (ArC), 140.2 (ArC), 128.7 (ArC), 128.5 (ArC), 128.3 (ArC), 127.4 (ArC), 122.7 (ArC), 51.5 (B(OCH₃)₂), 31.0 (CH(CH₃)₂), 26.5 (CH(CH₃)₂), 22.6 (CH(CH₃)₂). ¹¹B{¹H} NMR (160 MHz, C₆D₆): δ 29.5 (br). Anal. Calcd. for C₃₂H₄₃BO₂ (%): C 81.69, H 9.21; Found: C 79.61, H 9.04. *The experimentally determined elemental analysis values deviate from the calculated values likely due to incompletely combustion of the sample.*

Synthesis of [Ar^{Dipp}BH₃]Li(THF)₃ (2): Route A. A solution of Ar^{Dipp}Li (0.587 g, 1.45 mmol) dissolved in 5 mL of Et₂O was cooled to -35 °C and then added dropwise to a solution of Me₂S•BH₃ (138 μ L, 1.46 mmol) in 5 mL of Et₂O that was pre-cooled to -35 °C. The reaction mixture was allowed to warm to room temperature slowly over the course of 1 hour after which the volatiles were removed *in vacuo*. To the resulting white residue was added 2 mL of hexanes and 2 mL of THF and the solution placed in a -35 °C freezer for 16 hours after to give [Ar^{Dipp}BH₃]Li(THF)₃ (2) as a colorless crystalline solid (0.824 g, 89 %). X-ray quality crystals of 2 were grown from a 1:1 mixture of hexanes and THF stored in a -35 °C for 16 hours. ¹H (700 MHz, C₆D₆): δ 7.31 (t, 1H, ³J_{HH} = 7.0 Hz, *p*-ArH), 7.29–7.25 (overlapping multiplets, 6H, ArH), 7.23 (d, 2H, ³J_{HH} = 7.0 Hz, *m*-ArH), 3.48 (t, 12H, ³J_{HH} = 7.0 Hz, O(CH₂CH₂)₂), 3.28 (sept, 4H, ³J_{HH} = 7.0 Hz, CH(CH₃)₂), 1.42 (d, 12H, ³J_{HH} = 7.0 Hz, CH(CH₃)₂), 1.38 (t, 12H, ³J_{HH} = 7.0 Hz, O(CH₂CH₂)₂), 1.28 (d, 12H, ³J_{HH} = 7.0 Hz, CH(CH₃)₂), 0.59 (q, 3H, ¹J_{HB} = 77 Hz, BH₃). ¹³C{¹H} NMR (176 MHz, C₆D₆): δ 146.9 (ArC), 146.4 (ArC), 146.0 (ArC), 128.3 (ArC), 127.3 (ArC), 126.0 (ArC), 122.9 (ArC), 121.9 (ArC), 68.2 (O(CH₂CH₂)₂), 30.7 (CH(CH₃)₂), 25.5 (O(CH₂CH₂)₂), 25.3 (CH(CH₃)₂), 23.9 (CH(CH₃)₂). ¹¹B{¹H} NMR (160 MHz, C₆D₆): δ -30.2 (s). ¹¹B (160 MHz, C₆D₆): δ -30.1 (q, ¹J_{BH} = 80 Hz). ⁷Li{¹H} NMR (194

MHz, C₆D₆): -0.3 (s). M.p. 127 °C (decomposes). *[Ar^{Dipp}BH₃]Li(THF)₃ is thermally unstable and decomposes even in a -35 °C freezer as a solid into Li[BH₄] and other unidentified products. As such, samples are routinely contaminated with 5 to 15 % Li[BH₄] even when used within 24 hours of preparation.*

Route B. To a solution of Ar^{Dipp}B(OMe)₂ (**1**) (0.492 g, 1.05 mmol) in 15 mL of Et₂O was added Li[AlH₄] (0.30 mL, 4.0 M solution in Et₂O, 1.2 mmol) and the reaction mixture allowed to stir at room temperature for five hours. The reaction mixture was then filtered through a plug of diatomaceous earth and the volatiles removed from the filtrate *in vacuo* affording a white-oily residue to which 2 mL of hexanes and 2 mL of THF were added, and the solution stored in a -35 °C freezer for 16 hours affording **2** as a colorless crystalline solid (0.372 g, 84 %).

Synthesis of Ar^{Dipp}BH₂•NH₃ (3**): Route A.** A solution of [Ar^{Dipp}BH₃]Li(THF)₃ (**2**) (0.824 g, 1.30 mmol) in 10 mL of Et₂O was cooled to -35 °C and then added to a suspension of [NH₄]Cl (0.143 g, 2.67 mmol) in 5 mL of Et₂O. After 16 hours of stirring the reaction mixture was filtered through a plug of diatomaceous earth and the volatiles removed from the filtrate *in vacuo* affording a white solid. This solid was dissolved in 3 mL of toluene and placed in a -35 °C freezer for 16 hours to give Ar^{Dipp}BH₂•NH₃ (**3**) as a colorless solid (0.217 g, 39 %). X-ray quality crystals of **3** were grown from a saturated toluene solution stored at -35 °C for one week. ¹H NMR (700 MHz, C₆D₆): δ 7.22 (t, 2H, ³J_{HH} = 7.0 Hz, *p*-ArH), 7.20 (t, 1H, ³J_{HH} = 7.0 Hz, *p*-ArH), 7.12 (d, 4H, ³J_{HH} = 7.0 Hz, *m*-ArH), 7.07 (d, 2H, ³J_{HH} = 7.0 Hz, *m*-ArH), 2.94 (sept, 4H, ³J_{HH} = 7.0 Hz, CH(CH₃)₂), 1.88 (br s, 2H, BH₂), 1.66 (br s, NH₃), 1.18 (d, 12H, ³J_{HH} = 7.0 Hz, CH(CH₃)₂), 1.11 (d, 12H, ³J_{HH} = 7.0 Hz, CH(CH₃)₂). ¹³C{¹H} NMR (176 MHz,

C₆D₆): δ 146.9 (ArC), 143.8 (ArC), 143.5 (ArC), 128.3 (ArC), 127.9 (ArC), 127.6 (ArC), 124.4 (ArC), 122.6 (ArC), 30.6 (CH(CH₃)₂), 25.1 (CH(CH₃)₂), 23.3 (CH(CH₃)₂). ¹¹B{¹H} NMR (128 MHz, C₆D₆): -14.6 (s). ¹¹B NMR (128 MHz, C₆D₆): -14.6 (br s). Anal. Calcd. for C₃₀H₄₀B (%): C 84.29, H 9.90, N 3.28; Found: C 74.97, H 8.73, N 2.92. M.p. 176 °C (decomposed). *The experimentally determined elemental analysis values deviate from the calculated values likely due to incompletely combustion of the sample.* Selected IR bands (C₆H₆ drop-cast onto KBr plate, cm⁻¹): 3360 (m, ν N–H), 3322 (m, ν N–H), 3238 (m, ν N–H), 2348 (w, ν B–H).

Route B. A solution of Ar^{Dipp}Li (0.531 g, 1.31 mmol) dissolved in 5 mL of Et₂O and cooled to -35 °C, then Me₂S•BH₃ (125 μ L, 1.32 mmol) was added and the mixture was allowed to warm to room temperature. After two hours of stirring at room temperature the reaction mixture was cooled to -35 °C and then added to a suspension of [NH₄]Cl (0.140 g, 2.63 mmol) in 5 mL of Et₂O. After 16 hours of stirring, the reaction mixture was filtered through a plug of diatomaceous earth and the volatiles removed from the filtrate *in vacuo* affording Ar^{Dipp}BH₂•NH₃ (**3**) as a colorless solid (0.503 g, 90 %).

Synthesis of [Ar^{Dipp}BH₂•NH₂Li]₂ (4**):** To a solution of Ar^{Dipp}BH₂•NH₃ (**3**) (0.163 g, 0.381 mmol) in 3 mL of toluene was added ⁿBuLi (153 μ L, 2.5 M solution in hexanes, 0.383 mmol). Upon addition of ⁿBuLi a white precipitate formed. After a further 60 minutes of stirring the volatiles were removed *in vacuo* affording [Ar^{Dipp}BH₂•NH₂Li]₂ (**4**) as a white solid (0.143 g, 87 %). X-ray quality crystals of **4** were grown from a saturated hexanes solution stored in a -35 °C for one week. ¹H NMR (700 MHz, C₆D₆): δ 7.28 (t, 2H, ³J_{HH} = 7.7 Hz, *p*-ArH), 7.20 (t, 4H, ³J_{HH} = 7.7 Hz, *p*-ArH), 7.17 (d, 6H, ³J_{HH} = 7.7 Hz, *m*-ArH), 7.12 (d, 4H, ³J_{HH} = 7.7 Hz,

m-ArH), 7.01 (d, 2H, $^3J_{\text{HH}} = 7.7$ Hz, *m*-ArH), 2.95 (sept, 8H, $^3J_{\text{HH}} = 7.0$ Hz, CH(CH₃)₂), 1.28 (d, 12H, $^3J_{\text{HH}} = 7.0$ Hz, CH(CH₃)₂), 1.19 (d, 2H, $^3J_{\text{HH}} = 7.0$ Hz, CH(CH₃)₂), 1.09 (d, 2H, $^3J_{\text{HH}} = 7.0$ Hz, CH(CH₃)₂), 1.07 (d, 2H, $^3J_{\text{HH}} = 7.0$ Hz, CH(CH₃)₂). $^{13}\text{C}\{^1\text{H}\}$ NMR (176 MHz, C₆D₆): δ 146.8 (ArC), 146.8 (ArC), 143.4 (ArC), 143.0 (ArC), 142.6 (ArC), 141.3 (ArC), 128.8 (ArC), 122.9 (ArC), 122.7 (ArC), 30.9 (CH(CH₃)₂), 30.6 (CH(CH₃)₂), 26.1 (CH(CH₃)₂), 24.9 (CH(CH₃)₃), 23.4 (CH(CH₃)₃), 22.7 (CH(CH₃)₃). $^{11}\text{B}\{^1\text{H}\}$ NMR (128 MHz, C₆D₆): δ -13.0 (s). ^{11}B NMR (128 MHz, C₆D₆): δ -13.0 (t, $^1J_{\text{BH}} = 71$ Hz). $^7\text{Li}\{^1\text{H}\}$ NMR (194 MHz, C₆D₆): δ -2.4 (s). Anal. Calcd. for C₆₀H₈₂B₂Li₂N₂ (%): C 83.14, H 9.54, N 3.23; Found: C 61.86, H 7.39, N 2.20. M.p. 168 °C (decomposed). *The experimentally determined elemental analysis values deviate from the calculated values likely due to incompletely combustion of the sample.*

Synthesis of Ar^{Dipp}B(H)=NH₂ (5): Route A. A solution of Ar^{Dipp}BH₂•NH₃ (**3**) (0.503 g, 1.18 mmol) in 3 mL of THF which was added to a solution of [Rh(COD)Cl]₂ (0.010 g, 0.020 mmol) in 1 mL of THF. The reaction mixture was then heated to 75 °C for 24 hours, after which the reaction mixture was filtered through a plug of diatomaceous earth, and the volatiles removed from the filtrate *in vacuo* affording Ar^{Dipp}B(H)=NH₂ (**5**) as a colorless solid (0.417 g, 83 %). ^1H NMR (700 MHz, C₆D₆): δ 7.31 (t, 2H, $^3J_{\text{HH}} = 7.7$ Hz, *p*-ArH), 7.16–7.25 (overlapping multiplets, 5H, ArH), 7.11 (d, 2H, $^3J_{\text{HH}} = 7.7$ Hz, *m*-ArH), 3.31 (br s, 1H, NH₂), 3.16 (br s, 1H, NH₂), 2.90 (sept, 4H, $^3J_{\text{HH}} = 7.0$ Hz, CH(CH₃)₂), 1.21 (d, 12H, $^3J_{\text{HH}} = 14.0$ Hz, CH(CH₃)₂), 1.14 (d, 12H, $^3J_{\text{HH}} = 7.0$ Hz, CH(CH₃)₂). $^{13}\text{C}\{^1\text{H}\}$ NMR (176 MHz, C₆D₆): δ 147.4 (ArC), 146.5 (ArC), 141.2 (ArC), 129.1 (ArC), 128.7 (ArC), 128.3 (ArC), 128.2 (ArC), 122.9 (ArC), 30.9 (CH(CH₃)₂), 24.8 (CH(CH₃)₂), 23.5 (CH(CH₃)₂). $^{11}\text{B}\{^1\text{H}\}$ NMR (160 MHz, C₆D₆): δ 39.1 (s). ^{11}B NMR (160 MHz, C₆D₆): δ 39.1 (br s). Anal. Calcd. for C₃₀H₄₀B (%): C 84.29, H 9.90,

N 3.28; Found: C 81.01, H 9.18, N 2.94. M.p. 122–124 °C. *The experimentally determined elemental analysis values deviate from the calculated values likely due to incompletely combustion of the sample.* Selected IR bands (C₆H₆ drop-cast KBr plate, cm⁻¹): 3509 (m, νN–H), 3417 (m, νN–H), 2518 (w, νB–H), 1606 (m, νB–N).

Synthesis of Ar^{Dipp}BH₂•ND₃ (6): A solution of Ar^{Dipp}Li (0.580 g, 1.43 mmol) dissolved in 5 mL of Et₂O and cooled to -35 °C to which Me₂S•BH₃ (136 μL, 1.43 mmol) was added, and allowed to warm to room temperature. After two hours of stirring at room temperature the reaction mixture was cooled to -35 °C and then added to a suspension of [ND₄]Cl (0.166 g, 2.89 mmol) in 5 mL of Et₂O. After 16 hours of stirring the reaction mixture was filtered through a plug of diatomaceous earth, and the volatiles removed from the filtrate *in vacuo* affording Ar^{Dipp}BH₂•ND₃ (6) as a colorless solid (0.517 g, 84 %). ¹H NMR (700 MHz, C₆D₆): δ 7.25 (t, 2H, ³J_{HH} = 7.7 Hz, *p*-ArH), 7.21 (t, 1H, ³J_{HH} = 7.7 Hz, *p*-ArH), 7.15 (d, 4H, ³J_{HH} = 7.7 Hz, *m*-ArH), 7.09 (d, 2H, ³J_{HH} = 7.7 Hz, *m*-ArH), 2.97 (sept, ³J_{HH} = 7.0 Hz, CH(CH₃)₂), 1.21 (d, 12H, ³J_{HH} = 7.0 Hz, CH(CH₃)₂), 1.12 (d, 12H, ³J_{HH} = 7.0 Hz, CH(CH₃)₂). ²H NMR (61 MHz, C₆H₆): δ 1.51 (s). ¹³C {¹H} NMR (176 MHz, C₆D₆): δ 146.8 (ArC), 144.1 (ArC), 143.5 (ArC), 128.3 (ArC), 127.5 (ArC), 122.6 (ArC), 30.7 (CH(CH₃)₂), 25.2 (CH(CH₃)₂), 23.3 (CH(CH₃)₂). ¹¹B {¹H} NMR (160 MHz, C₆D₆): δ -14.8 (s). ¹¹B NMR (160 MHz, C₆D₆): δ -14.8 (br s). Selected IR bands (C₆H₆ dropcast onto KBr plate, cm⁻¹): 2469 (w, νN–D), 2366 (w, νN–D), 2513 (w, νN–D). *The BH stretches were not located possibly due to it being obscured by the ND stretches.*

Synthesis of Ar^{Dipp}B(H)=ND₂ (8): A solution of Ar^{Dipp}BH₂•ND₃ (7) (0.251 g, 0.583 mmol) in 3 mL of THF which was added to a solution of [Rh(COD)Cl]₂ (0.010 g, 0.020 mmol) in 1 mL of THF. This reaction mixture was then heated to 75 °C for 24 hours, after which the reaction mixture was filtered through a plug of diatomaceous earth, and the volatiles removed from the filtrate *in vacuo* affording Ar^{Dipp}B(H)=ND₂ (8) as a colorless solid (0.221 g, 88 %). ¹H NMR (700 MHz, C₆D₆): δ 7.31 (t, 2H, ³J_{HH} = 7.7 Hz, *p*-ArH), 7.18–7.25 (overlapping multiplets, 5H, ArH), 7.11 (d, 2H, ³J_{HH} = 7.7 Hz, *m*-ArH), 2.90 (sept, 4H, ³J_{HH} = 7.0 Hz, CH(CH₃)₂), 1.21 (d, 12H, ³J_{HH} = 7.0 Hz, CH(CH₃)₂), 1.40 (d, 12H, ³J_{HH} = 7.0 Hz, CH(CH₃)₂). ²H NMR (61 MHz, C₆H₆): δ 3.26 (s), 3.10 (s). ¹³C{¹H} NMR (178 MHz, C₆D₆): δ 147.4 (ArC), 146.5 (ArC), 143.0 (ArC), 141.2 (ArC), 129.0 (ArC), 128.6 (ArC), 128.3 (ArC), 122.9 (ArC), 30.9 (CH(CH₃)₂), 24.8 (CH(CH₃)₂), 23.5 (CH(CH₃)₂). ¹¹B{¹H} NMR (160 MHz, C₆D₆): δ 39.1 (br s). ¹¹B NMR (160 MHz, C₆D₆): δ 39.1 (br s). Selected IR bands (C₆H₆ drop-cast onto KBr plate, cm⁻¹): 2606 (m, νN–D), 2533 (w, νB–H), 2494 (m, νN–D).

5.4.3 X-Ray Crystallography

Appropriate X-ray quality crystals were coated with a small amount of hydrocarbon oil (Paratone-N) and removed from the glovebox in a vial. Crystals were mounted quickly onto a glass fiber and placed in a low temperature stream of nitrogen on the X-ray diffractometer. All data were collected using a Bruker D8 Venture/PHOTON III, Bruker D8 Bruker APEX II CCD detector/D8 or PLATFORM diffractometer using Mo Kα (0.71073 Å) or Cu Kα (1.54178 Å) radiation, with the crystals cooled to -80 °C or -100 °C. The data were corrected for absorption through Gaussian integration from the indexing of crystal faces.³¹ Crystal structures

were solved using intrinsic phasing (SHELXT)³² and refined using SHELXL-2014.³³ The assignment of hydrogen atom positions is based on the sp²- or sp³- hybridization geometries of their attached carbon atoms and were given thermal parameters 20 % greater than those of their parent atoms.

Table 5.1. X-ray crystallographic data details for [Ar^{Dipp}BH₃Li(THF)₃] (2).*A. Crystal Data*

formula	C ₄₆ H ₇₀ BLiO ₄
formula weight	704.77
crystal color and habit ^a	colorless fragment
crystal dimensions (mm)	0.14 × 0.12 × 0.06
crystal system	orthorhombic
space group	<i>Cmc</i> 2 ₁ (No. 36)
unit cell parameters ^b	
<i>a</i> (Å)	18.3644(8)
<i>b</i> (Å)	17.3198(7)
<i>c</i> (Å)	14.1700(6)
<i>V</i> (Å ³)	4507.0(3)
<i>Z</i>	4
ρ_{calcd} (g cm ⁻³)	1.039
μ (mm ⁻¹)	0.483

B. Data Collection and Refinement Conditions

diffractometer	Bruker D8 Venture/PHOTON III ^c
radiation (λ [Å])	Cu K α (1.54178) (microfocus source)
temperature (°C)	-100
scan type	ω and ϕ scans (1.0°) (θ -dep. exp. from 10-40 s)
data collection 2θ limit (deg)	144.71
total data collected	27667 ($-22 \leq h \leq 22$, $-21 \leq k \leq 19$, $-17 \leq l \leq 17$)
independent reflections	4570 ($R_{\text{int}} = 0.0489$)
number of observed reflections (<i>NO</i>)	3994 [$F_o^2 \geq 2\sigma(F_o^2)$]
structure solution method	intrinsic phasing (<i>SHELXT-2014</i> ^d)
refinement method	full-matrix least-squares on F^2 (<i>SHELXL-2018</i> ^{e,f})
absorption correction method	Gaussian integration (face-indexed)
range of transmission factors	0.9916–0.8181
data/restraints/parameters	4570 / 275 <i>g</i> / 286
Flack absolute structure parameter ^h	-0.04(11)
goodness-of-fit (<i>S</i>) ⁱ [all data]	1.046
final <i>R</i> indices ^j	
<i>R</i> ₁ [$F_o^2 \geq 2\sigma(F_o^2)$]	0.0544
<i>wR</i> ₂ [all data]	0.1699
largest difference peak and hole	0.186 and -0.218 e Å ⁻³

^aObtained by recrystallization from a tetrahydrofuran/pentane solution.

^bObtained from least-squares refinement of 9937 reflections with $7.02^\circ < 2\theta < 144.16^\circ$.

^cPrograms for diffractometer operation, data collection, data reduction and absorption

correction were those supplied by Bruker.

^dG. M. Sheldrick, *Acta Crystallogr.* **2015**, *A71*, 3–8. (*SHELXT-2014*)

^eG. M. Sheldrick, *Acta Crystallogr.* **2015**, *C71*, 3–8. (*SHELXL-2018/3*)

^fAttempts to refine peaks of residual electron density as disordered or partial-occupancy solvent tetrahydrofuran oxygen or carbon atoms were unsuccessful. The data were corrected for disordered electron density through use of the SQUEEZE procedure as implemented in *PLATON* (A. L. Spek, *Acta Crystallogr.* **2015**, *C71*, 9–18. *PLATON* - a multipurpose crystallographic tool. Utrecht University, Utrecht, The Netherlands). A total solvent-accessible void volume of 567 Å³ with a total electron count of 151 (consistent with 4 molecules of solvent tetrahydrofuran, or 1 molecule per formula unit of the target molecule) was found in the unit cell.

^gThe following sets of atoms from the disordered tetrahydrofuran ligands had the *SHELXL SADI* (same distance) restraints: O1–C31, O1–C34; C31–C32, C32–C33, C33–C34; O2–C41, O2–C41A O2–C44, O2–C44A; C41–C42, C41A–C42A, C42–C43, C42A–C43A, C43–C44, C43A–C44A; O2···C42, O2···C42A, O2···C43, O2···C43A; C41···C43, C41A···C43A, C42···C44, C42A···C44A. Additionally, the *SHELXL RIGU* restraint was applied to all atoms to improve the quality of the anisotropic displacement parameters.

^hH. D. Flack, *Acta Crystallogr.* **1983**, *A39*, 876–881; H. D. Flack, G., Bernardinelli, *Acta Crystallogr.* **1999**, *A55*, 908–915; H. D. Flack, G. Bernardinelli, *J. Appl. Cryst.* **2000**, *33*, 1143–1148. The Flack parameter will refine to a value near zero if the structure is in the correct configuration and will refine to a value near one for the inverted configuration. The low anomalous scattering power of the atoms in this structure (none heavier than oxygen) implies that the data cannot be used for absolute structure assignment, thus the Flack parameter is provided for informational purposes only.

ⁱ $S = [\sum w(F_o^2 - F_c^2)^2 / (n - p)]^{1/2}$ (n = number of data; p = number of parameters varied; $w = [\sigma^2(F_o^2) + (0.1144P)^2 + 0.4698P]^{-1}$ where $P = [\text{Max}(F_o^2, 0) + 2F_c^2] / 3$).

^j $R_1 = \sum ||F_o| - |F_c|| / \sum |F_o|$; $wR_2 = [\sum w(F_o^2 - F_c^2)^2 / \sum w(F_o^4)]^{1/2}$.

Table 5.2. X-ray crystallographic data details for Ar^{Dipp}BH₂•NH₃ (**3**).*A. Crystal Data*

formula	C ₃₀ H ₄₂ BN
formula weight	427.45
crystal color and habit ^a	colorless block
crystal dimensions (mm)	0.16 × 0.12 × 0.07
crystal system	orthorhombic
space group	<i>Pccn</i> (No. 56)
unit cell parameters ^b	
<i>a</i> (Å)	20.5804(5)
<i>b</i> (Å)	15.7187(4)
<i>c</i> (Å)	16.9269(5)
<i>V</i> (Å ³)	5475.8(3)
<i>Z</i>	8
ρ_{calcd} (g cm ⁻³)	1.037
μ (mm ⁻¹)	0.429

B. Data Collection and Refinement Conditions

diffractometer	Bruker D8 Venture/PHOTON III ^c
radiation (λ [Å])	Cu K α (1.54178) (microfocus source)
temperature (°C)	–100
scan type	ω and ϕ scans (1.0°) (5 s exposures)
data collection 2θ limit (deg)	144.62
total data collected	75333 ($-25 \leq h \leq 25$, $-19 \leq k \leq 19$, $-20 \leq l \leq 20$)
independent reflections	5397 ($R_{\text{int}} = 0.0569$)
number of observed reflections (<i>NO</i>)	4212 [$F_o^2 \geq 2\sigma(F_o^2)$]
structure solution method	intrinsic phasing (<i>SHELXT-2014</i> ^d)
refinement method	full-matrix least-squares on F^2 (<i>SHELXL-2018</i> ^e)
absorption correction method	multi-scan (<i>SADABS</i>)
range of transmission factors	0.7536–0.6247
data/restraints/parameters	5397 / 40 ^f / 340
extinction coefficient (<i>x</i>) ^g	0.00052(11)
goodness-of-fit (<i>S</i>) ^h [all data]	1.065
final <i>R</i> indices ⁱ	
<i>R</i> ₁ [$F_o^2 \geq 2\sigma(F_o^2)$]	0.0512
<i>wR</i> ₂ [all data]	0.1571
largest difference peak and hole	0.226 and –0.211 e Å ⁻³

^aObtained by recrystallization from a toluene solution.

^bObtained from least-squares refinement of 9010 reflections with $8.60^\circ < 2\theta < 143.26^\circ$.

^dG. M. Sheldrick, *Acta Crystallogr.* **2015**, *A71*, 3–8. (*SHELXT-2014*)

^eG. M. Sheldrick, *Acta Crystallogr.* **2015**, *C71*, 3–8. (*SHELXL-2018/3*)

^fThe N–B and the C–B distances within the disordered BH₂NH₃ fragment were restrained to be approximately the same by use of the *SHELXL SADI* instruction. The C–C distances within the disordered isopropyl group were similarly restrained. Finally, the anisotropic displacement parameters of all disordered atoms were restrained by use of the *SHELXL RIGU* instruction.

^g $F_c^* = kF_c[1 + x\{0.001F_c^2\lambda^3/\sin(2\theta)\}]^{-1/4}$ where k is the overall scale factor.

^h $S = [\sum w(F_o^2 - F_c^2)^2/(n - p)]^{1/2}$ (n = number of data; p = number of parameters varied; $w = [\sigma^2(F_o^2) + (0.0742P)^2 + 1.6821P]^{-1}$ where $P = [\text{Max}(F_o^2, 0) + 2F_c^2]/3$).

ⁱ $R_1 = \sum ||F_o| - |F_c||/\sum |F_o|$; $wR_2 = [\sum w(F_o^2 - F_c^2)^2/\sum w(F_o^4)]^{1/2}$.

Table 5.3. X-ray crystallographic data details for $[\text{Ar}^{\text{Dipp}}\text{BH}_2\cdot\text{NH}_2\text{Li}]_2$ (**4**) and $\sim 2\%$ Ar^{Dipp} .*A. Crystal Data*

formula	$\text{C}_{66}\text{H}_{95.82}\text{B}_{1.96}\text{I}_{0.04}\text{Li}_{1.96}\text{N}_{1.96}$
formula weight	956.57
crystal color and habit ^a	colorless fragment
crystal dimensions (mm)	$0.35 \times 0.32 \times 0.13$
crystal system	monoclinic
space group	$P2_1/n$ (an alternate setting of $P2_1/c$ [No. 14])
unit cell parameters ^b	
<i>a</i> (Å)	12.0005(11)
<i>b</i> (Å)	20.870(2)
<i>c</i> (Å)	12.7164(12)
β (deg)	99.0479(17)
<i>V</i> (Å ³)	3145.2(5)
<i>Z</i>	2
ρ_{calcd} (g cm ⁻³)	1.010
μ (mm ⁻¹)	0.075

B. Data Collection and Refinement Conditions

diffractometer	Bruker PLATFORM/APEX II CCD ^c
radiation (λ [Å])	graphite-monochromated Mo K α (0.71073)
temperature (°C)	-80
scan type	ω scans (0.3°) (45 s exposures)
data collection 2θ limit (deg)	51.44
total data collected	25818 ($-14 \leq h \leq 14$, $-25 \leq k \leq 25$, $-15 \leq l \leq 15$)
independent reflections	5979 ($R_{\text{int}} = 0.0467$)
number of observed reflections (<i>NO</i>)	4066 [$F_o^2 \geq 2\sigma(F_o^2)$]
structure solution method	intrinsic phasing (<i>SHELXT-2014</i> ^d)
refinement method	full-matrix least-squares on F^2 (<i>SHELXL-2018</i> ^e)
absorption correction method	Gaussian integration (face-indexed)
range of transmission factors	1.0000–0.9081
data/restraints/parameters	5979 / 283 ^f / 436
goodness-of-fit (<i>S</i>) ^g [all data]	1.047
final <i>R</i> indices ^h	
<i>R</i> ₁ [$F_o^2 \geq 2\sigma(F_o^2)$]	0.0547
<i>wR</i> ₂ [all data]	0.1674
largest difference peak and hole	0.277 and -0.162 e Å ⁻³

^aObtained by recrystallization from a hexanes solution.

^bObtained from least-squares refinement of 3680 reflections with $5.08^\circ < 2\theta < 46.16^\circ$.

^cPrograms for diffractometer operation, data collection, data reduction and absorption correction were those supplied by Bruker.

^dG. M. Sheldrick, *Acta Crystallogr.* **2015**, *A71*, 3–8. (*SHELXT-2014*)

^eG. M. Sheldrick, *Acta Crystallogr.* **2015**, *C71*, 3–8. (*SHELXL-2018/3*)

^fThe solvent hexane molecule was found to be disordered across an inversion center. The C–C and C···C distances were restrained by use of the *SHELXL SADI* instruction (total of 73 restraints). Additionally, the anisotropic displacement parameters of the carbon atoms were improved by using a combination of **RIGU** (total of 54 restraints) and **SIMU** (total of 156 restraints).

^g $S = [\sum w(F_o^2 - F_c^2)^2 / (n - p)]^{1/2}$ (n = number of data; p = number of parameters varied; $w = [\sigma^2(F_o^2) + (0.0861P)^2 + 0.3985P]^{-1}$ where $P = [\text{Max}(F_o^2, 0) + 2F_c^2] / 3$).

^h $R_1 = \sum ||F_o| - |F_c|| / \sum |F_o|$; $wR_2 = [\sum w(F_o^2 - F_c^2)^2 / \sum w(F_o^4)]^{1/2}$.

Table 5.4. X-ray crystallographic data details for Ar^{Dipp}B(C₈H₁₄) (**4**).*A. Crystal Data*

formula	C ₃₈ H ₅₁ B
formula weight	518.59
crystal color and habit ^a	colorless block
crystal dimensions (mm)	0.33 × 0.28 × 0.21
crystal system	monoclinic
space group	<i>P</i> 2 ₁ / <i>c</i> (No. 14)
unit cell parameters ^b	
<i>a</i> (Å)	17.7216(13)
<i>b</i> (Å)	9.8674(7)
<i>c</i> (Å)	19.5159(12)
β (deg)	112.740(4)
<i>V</i> (Å ³)	3147.4(4)
<i>Z</i>	4
ρ _{calcd} (g cm ⁻³)	1.094
μ (mm ⁻¹)	0.444

B. Data Collection and Refinement Conditions

diffractometer	Bruker D8/APEX II CCD ^c
radiation (λ [Å])	Cu Kα (1.54178) (microfocus source)
temperature (°C)	-100
scan type	ω and φ scans (1.0°) (5 s exposures)
data collection 2θ limit (deg)	147.32
total data collected	69084 (-20 ≤ <i>h</i> ≤ 21, -12 ≤ <i>k</i> ≤ 12, -24 ≤ <i>l</i> ≤ 24)
independent reflections	6277 (<i>R</i> _{int} = 0.0733)
number of observed reflections (<i>NO</i>)	5204 [<i>F</i> _o ² ≥ 2σ(<i>F</i> _o ²)]
structure solution method	intrinsic phasing (<i>SHELXT-2014</i> ^d)
refinement method	full-matrix least-squares on <i>F</i> ² (<i>SHELXL-2018</i> ^e)
absorption correction method	Gaussian integration (face-indexed)
range of transmission factors	0.9891–0.8483
data/restraints/parameters	6277 / 697 ^f / 489
goodness-of-fit (<i>S</i>) ^g [all data]	1.033
final <i>R</i> indices ^h	
<i>R</i> ₁ [<i>F</i> _o ² ≥ 2σ(<i>F</i> _o ²)]	0.0511
<i>wR</i> ₂ [all data]	0.1451
largest difference peak and hole	0.203 and -0.185 e Å ⁻³

^aObtained by recrystallization from a hexamethyldisiloxane/THF solution.

^bObtained from least-squares refinement of 9824 reflections with $5.40^\circ < 2\theta < 146.14^\circ$.

^cPrograms for diffractometer operation, data collection, data reduction and absorption correction were those supplied by Bruker.

^dG. M. Sheldrick, *Acta Crystallogr.* **2015**, *A71*, 3–8. (*SHELXT-2014*)

^eG. M. Sheldrick, *Acta Crystallogr.* **2015**, *C71*, 3–8. (*SHELXL-2018/3*)

^fThe disordered borabicyclo[3.3.1]nonane group had distance restraints applied by use of the *SHELXL SADI* instruction to the following sets of atoms: B1–C51 & B1–C55; B1···C52, B1···C54, B1···C56, B1···C58; C51–C58, C51–C52, C58–C57, C55–C54, C55–C56, C52–C53, C54–C53, C56–C57; C51···C53, C51···C57, C58···C52, C58···C56, C55···C53, C55···C57, C52···C54, C54···C56 [total number of **SADI** restraints: 552]. The anisotropic displacement parameters (ADPs) of the carbon atoms of the borabicyclo[3.3.1]nonane group were restrained by use of the **SIMU** instruction [total number of **SIMU** restraints: 144]. Finally, the following pairs of atoms were constrained to have the same ADPs by use of the **EADP** instruction: C51_1 & C51_2; C54_1 & C54_2; C55_1 & C55_2.

^g $S = [\sum w(F_o^2 - F_c^2)^2 / (n - p)]^{1/2}$ (n = number of data; p = number of parameters varied; $w = [\sigma^2(F_o^2) + (0.0665P)^2 + 0.9880P]^{-1}$ where $P = [\text{Max}(F_o^2, 0) + 2F_c^2]/3$).

^h $R_1 = \sum ||F_o| - |F_c|| / \sum |F_o|$; $wR_2 = [\sum w(F_o^2 - F_c^2)^2 / \sum w(F_o^4)]^{1/2}$.

5.4.4 Density Functional Theory (DFT) Computations

All computations were performed with Gaussian16.³⁴ Gas-phase geometries were optimized using density functional theory (DFT) with the M06-2X functional³⁵ and the cc-pTVZ basis set.³⁶ Frequency analysis confirmed all obtained structures to be local minima on the potential energy surfaces. Optimized geometries and orbitals were visualized with Visual Molecular Dynamics (VMD).³⁷ Natural Bond Order (NBO) analyses were performed with NBO 6.0.³⁸ IR frequencies were correct by a scaling factor of 0.946.³⁹

5.5 References

1. a) P. J. Frazen, J. S. Beck, A. T. Lynch, E. E. Remsen, L. G. Sneddon, *Chem. Mater.* **1990**, *2*, 96–97; b) D. J. Heldebrant, A. Karkamkar, N. J. Hess, M. Bowden, W. Rassat, F. Zheng, K. Rappe, T. Autrey, *Chem. Mater.* **2008**, *20*, 5332–5336; c) S. Frueh, R. Kellet, C. Mallery, T. Molter, W. S. Willis, C. King' ondu, S. L. Suib, *Inorg. Chem.* **2011**, *50*, 783–792.
2. R. Kumar, A. Karkamkar, M. Bowden, T. Autrey, *Chem. Soc. Rev.* **2019**, *48*, 5350–5380.
3. a) P. Paetzold, *Pure Appl. Chem.* **1991**, *63*, 345–350; b) Z. X. Giustra, S.-Y. Liu, *J. Am. Chem. Soc.* **2018**, *140*, 1184–1194.
4. L. Winner, G. Bélanger-Chabot, M. A. Celik, M. Schäfer, H. Braunschweig, *Chem. Commun.* **2018**, *54*, 9349–9351.
5. P. Paetzold, C. von Plotho, G. Schmid, R. Boese, B. Schrader, D. Bougeard, U. Pfeiffer, R. Gleiter, W. Schäfer, *Chem. Ber.* **1984**, *117*, 1089–1102.
6. B. Kröckert, K–H. van Bonn, P. Paetzold, *Z. Anorg. Allg. Chem.* **2005**, *631*, 866–868.
7. a) H. Braunschweig, K. Radacki, D. Rais, K. Uttinger, *Angew. Chem. Int. Ed.* **2005**, *45*, 162–165; b) H. Braunschweig, K. Radacki, D. Rais, A. Schneider, F. Seeler, *J. Am. Chem. Soc.* **2007**, *129*, 10350–10351.
8. K. Ota, R. Kinjo, *J. Am. Chem. Soc.* **2021**, *143*, 11152–11159.
9. Y. Fan, J. Cui, L. Kong, *Eur. J. Org. Chem.* **2022**, e202201086.
10. A. K. Swarnakar, C. Hering-Junghans, K. Nagata, M. J. Ferguson, R. McDonald, N. Tokitoh, E. Rivard, *Angew. Chem. Int. Ed.* **2015**, *54*, 10666–10669.

11. B. L. Frenette, A. A. Omaña, M. J. Ferguson, Y. Zhou, E. Rivard, *Chem. Commun.* **2021**, 57, 10895–10898.
12. R. Guo, T. Li, R. Wei, X. Zhang, Q. Li, L. L. Liu, C-H. Tung, L. Kong, *J. Am. Chem. Soc.* **2021**, *143*, 13483–13488.
13. a) R. J. Wright, A. D. Phillips, T. L. Allen, W. H. Fink, P. P. Power, *J. Am. Chem. Soc.* **2003**, *125*, 1694–1695; b) J. D. Queen, S. Irvankoski, J. C. Fettinger, H. M. Tuononen, P. P. Power, *J. Am. Chem. Soc.* **2021**, *143*, 6351–6356.
14. B. R. Barnett, C. C. Mokhtarzadeh, J. S. Figueroa, *Inorg. Synth.* **2018**, *37*, 85–122.
15. N. Kuhn, G. Henkel, T. Kratz, J. Kreutzberg, R. Boese, A. H. Maulitz, *Chem. Ber.* **1993**, *126*, 2041–2045.
16. Y. Wang, B. Quillian, P. Wei, C. S. Wannere, Y. Xie, R. B. King, H. F. Schaefer, P. v R. Schleyer, G. H. Robinson, *J. Am. Chem. Soc.* **2007**, *129*, 12412–12413.
17. M. E. Bowden, G. J. Gainsford, W. T. Robinson, *Aust. J. Chem.* **2007**, *60*, 149–153.
18. S. Morisako, R. Shang, Y. Yamamoto, *Inorg. Chem.* **2016**, *55*, 10767–10773.
19. M. F. Lappert, M. J. Slade, A. Singh, J. L. Atwood, R. D. Rogers, R. Shakir, *J. Am. Chem. Soc.* **1983**, *105*, 302–304.
20. D. A. Strauss, C. Zhang, T. D. Tilley, *J. Organomet. Chem.* **1989**, *369*, C13–C17.
21. A. Staubitz, A. P. M. Robertson, M. E. Sloan, I. Manners, *Chem. Rev.* **2010**, *110*, 4023–4078.
22. S. Karahan, M. Zahmakiran, S. Özkar, *Chem. Commun.* **2012**, *48*, 1180–1182.

23. J. A. Soderquist, H. C. Brown, *J. Org. Chem.* **1981**, *46*, 4599–4600.
24. Platinum complexes have been shown to dehydrogenate silanes, see: M. Tanaka, Y. Uchimaru, H.-J. Lautenschlager, *Organometallics* **1991**, *10*, 16–18.
25. For similar hydride-halide exchanges at boron, see: a) P. Bag, A. Porzelt, P. J. Altmann, S. Inoue, *J. Am. Chem. Soc.* **2017**, *139*, 14384–14387; b) J. H. Muessig, M. Thaler, R. D. Dewhurst, V. Paprocki, J. Seufert, J. D. Mattock, A. Vargas, H. Braunschweig, *Angew. Chem. Int. Ed.* **2019**, *58*, 4405–4409.
26. A. A. Omaña, R. Watt, Y. Zhou, M. J. Ferguson, E. Rivard, *Inorg. Chem.* **2022**, *61*, 16430–16440.
27. D. E. Ryan, K. Andrea, J. J. Race, T. M. Boyd, G. C. Lloyd-Jones, A. S. Weller, *ACS. Catal.* **2020**, *10*, 7443–7448.
28. J. Li, H. Song, C. Cui, J.-P. Cheng, *Inorg. Chem.* **2008**, *47*, 3468–3470.
29. T. B. Ditri, B. J. Fox, C. E. Moor, A. L. Rheingold, J. S. Figueroa, *Inorg. Chem.* **2009**, *48*, 8362–8375.
30. A. B. Pangborn, M. A. Giardello, R. H. Grubbs, R. K. Rosen, F. J. Timmers, *Organometallics* **1996**, *15*, 1518–1520.
31. H. Hope, *Prog. Inorg. Chem.* **1994**, *41*, 1–19.
32. G. M. Sheldrick, *Acta Crystallogr. Sect. A* **2015**, *71*, 3–8.
33. G. M. Sheldrick, *Acta Crystallogr. Sect. C* **2015**, *71*, 3–8.

34. M. J. Frisch, G. W. Trucks, H. B. Schlegel, G. E. Scuseria, M. A. Robb, J. R. Cheeseman, G. Scalmani, V. Barone, G. A. Petersson, H. Nakatsuji, X. Li, M. Caricato, A. V. Marenich, J. Bloino, B. G. Janesko, R. Gomperts, B. Mennucci, H. P. Hratchian, J. V. Ortiz, A. F. Izmaylov, J. L. Sonnenberg, D. Williams-Young, F. Ding, F. Lipparini, F. Egidi, J. Goings, B. Peng, A. Petrone, T. Henderson, D. Ranasinghe, V. G. Zakrzewski, J. Gao, N. Rega, G. Zheng, W. Liang, M. Hada, M. Ehara, K. Toyota, R. Fukuda, J. Hasegawa, M. Ishida, T. Nakajima, Y. Honda, O. Kitao, H. Nakai, T. Vreven, K. Throssell, J. A. Montgomery, Jr., J. E. Peralta, F. Ogliaro, M. J. Bearpark, J. J. Heyd, E. N. Brothers, K. N. Kudin, V. N. Staroverov, T. A. Keith, R. Kobayashi, J. Normand, K. Raghavachari, A. P. Rendell, J. C. Burant, S. S. Iyengar, J. Tomasi, M. Cossi, J. M. Millam, M. Klene, C. Adamo, R. Cammi, J. W. Ochterski, R. L. Martin, K. Morokuma, O. Farkas, J. B. Foresman, D. J. Fox, Gaussian 16, Revision A. 03, Gaussian Inc., Wallingford CT, 2016.
35. Y. Zhao, D. G. Truhlar, *Theo. Chem. Acc.* **2008**, *120*, 215–241.
36. T. H. Dunning, *J. Chem. Phys.* **1989**, *90*, 1007–1023.
37. W. Humphrey, A. Dalke, K. Schulten *J. Molec. Graphics* **1996**, *14*, 33–38.
38. E. D. Glendening, J. K. Badenhoop, A. E. Reed, J. E. Carpenter, J. A. Bohmann, C. M. Morales, C. R. Landis, F. Weinhold, NBO 6.0, Theoretical Chemistry Institute, University of Wisconsin, Madison WI, 2013.
39. I. M. Alecu, J. Zheng, Y. Zhao, D. G. Truhlar, *J. Chem. Theory Comput.* **2010**, *6*, 2872–2887.

Chapter 6 – The Synthesis of The World’s Bulkiest *N*-Heterocyclic Carbene

6.1 Introduction

Carbenes are defined as neutral compounds containing a divalent carbon atom with a six-electron valence shell. Due to their incomplete octet configuration at carbon, carbenes were long considered to be too reactive to isolate.¹ In 1988, Bertrand and coworkers reported a stable phosphinocarbene, (ⁱPr₂N)₂PC(SiMe₃), wherein the carbene center is stabilized by flanking phosphorus- and silicon-based substituents.² This was followed in 1991 by Arduengo’s landmark report on the isolation of the first *N*-heterocyclic carbene (NHC), IAd (IAd = (HCNAd)₂C: ; Ad = adamantyl).³ Some key features of NHCs are their strong donor ability, ease of preparation, and structural diversity.⁴ As such, NHCs have cemented their place as an important class of compounds/ligands in transition metal-mediated catalysis, organocatalysis, and in the stabilization of low-valent main group species.⁵

The isolation of low-coordinate species with new bonding motifs⁶ or species previously thought to be too reactive to be isolated (*e.g.*, one-coordinate Bi(I))^{6a} has required the development of new ligands, typically, of ever-increasing steric bulk. The Rivard group has previously reported the World’s bulkiest carbene at the time, ITr (ITr = (HCNCPH₃)₂C:), with an impressive percent buried volume (%V_{bur}) of 57.3 %, due to the incorporation of flanking trityl groups (CPh₃) at the heterocyclic nitrogen atoms on the NHC (Figure 6.1). Utilizing ITr, the Rivard group was able to prepare a thermally-stable Tl(I) complex [ITrTl]OTf (OTf = O₃SCF₃⁻) as a versatile transmetalation/ligation reagent,⁷ and a weakly associated Ag(I) dimer [(ITr)Ag]₂[BAR^F₄]₂ (Ar^F = 3,5-(F₃C)₂C₆H₃).⁸ In an effort to prepare an

even more sterically-demanding NHC based on the ITr framework, I envisioned that the incorporation of methyl groups in the backbone would increase the steric bulk of the carbene by forcing the nitrogen-bound trityl groups forward.⁴ If the steric bulk of this carbene is sufficient, it may be able to support monocoordinate, low-valent transition metals such as Pd⁰ and other Group 10 metals. Monocoordinate Pd⁰ complexes, such as (Ph₃P)Pd, are of particular interest as they are suspected to be important intermediates in the oxidative addition of chloroarenes.⁹ To the best of my knowledge, a monocoordinate Pd⁰ complex has not yet been reported and may display interesting reactivity. This Chapter explores the development of a new bulky NHC and initial attempts to form Group 10 NHC-metal complexes.

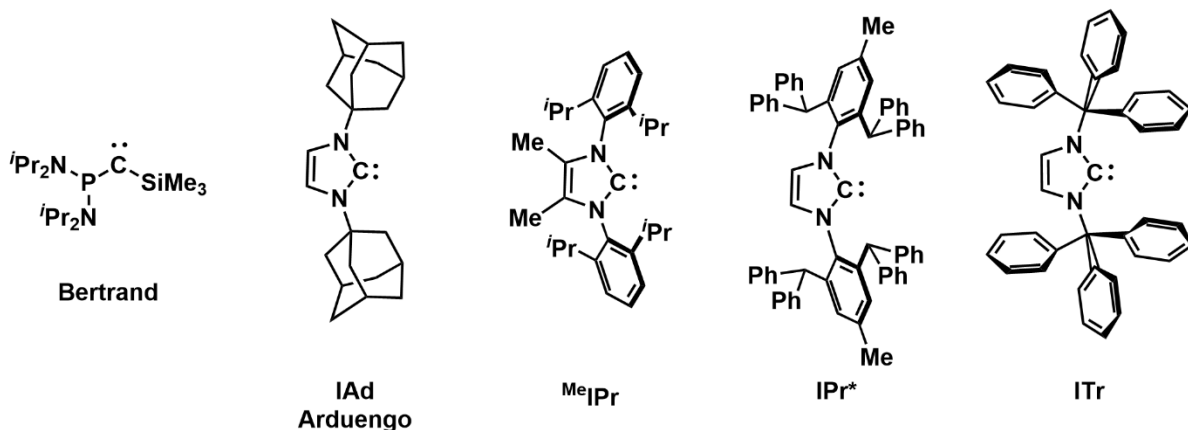
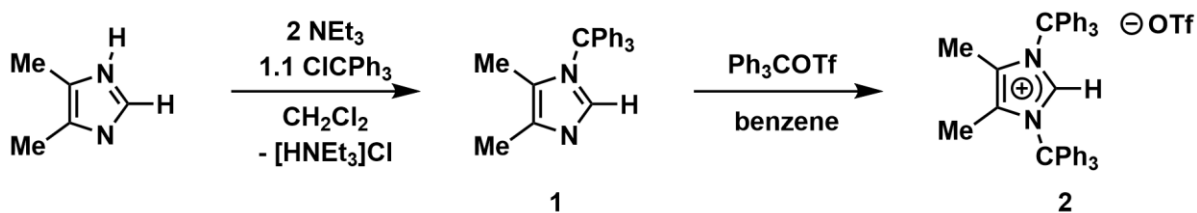


Figure 6.1. Bertrand's phosphinocarbene and select sterically-demanding NHCs.

6.2 Results and Discussion

The starting point of this project involved the preparation of the precursor 2-trityl-4,5-dimethylimidazole (**1**), which has been previously reported but not characterized fully.¹⁰ Combining 4,5-dimethylimidazole¹¹ with a slight excess of ClCPh₃ afforded **1** in an isolated

yield of 42 % after recrystallization from EtOH. The addition of $\text{Ph}_3\text{COTf}^{\text{f}2}$ to **1** in benzene gave the desired imidazolium salt precursor $[\text{Me}^{\text{c}}\text{ITrH}]\text{OTf}$ (**2**) ($[\text{Me}^{\text{c}}\text{ITrH}] = [(\text{MeCNCPh}_3)_2\text{C}-\text{H}]^+$) in a yield of 78 % (Scheme 6.1), and could be prepared on a multigram scale (*ca.* 7 g). Analysis of the ^1H NMR spectrum of **2** in CDCl_3 showed a resonance at 7.58 ppm for the imidazolium proton, which is very similar to the resonance of the imidazolium proton in $[\text{ITrH}]\text{OTf}$ [7.92 ppm in CDCl_3].⁷ X-ray quality crystals of **2** were grown from a concentrated solution of PhF stored at -35 °C. The solid-state structure shows that the triflate anion is not coordinating to the imidazolium cation (Figure 6.2). Interestingly, the N-C-N bond angle in **2** is $110.4(2)^\circ$, about 3° larger than the N-C-N bond angle in $[\text{ITrH}]\text{OTf}$ [$107.92(16)^\circ$].⁷



Scheme 6.1. The synthesis of 2-trityl-4,5-dimethylimidazole (**1**) and $[\text{Me}^{\text{c}}\text{ITrH}]\text{OTf}$ (**2**).

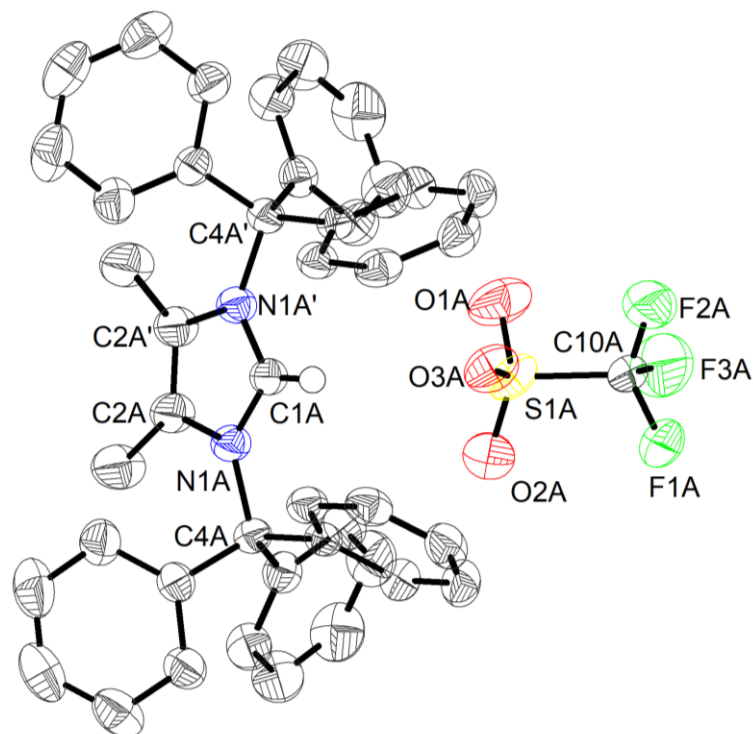
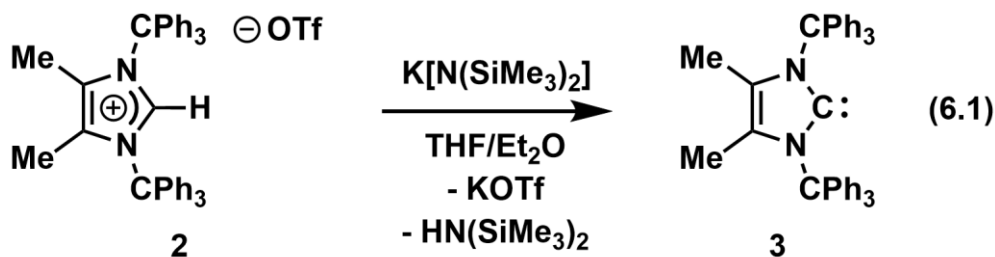


Figure 6.2. Molecular structure of $[\text{MeITrH}]\text{OTf}$ (**2**) plotted with thermal ellipsoids at 50 % probability. All hydrogen atoms (except for the imidazolium proton at C1A) are omitted for clarity. The PhF solvent molecules are not shown. Only one of the two crystallographically-independent $[\text{MeITrH}]\text{OTf}$ (**3**) molecules is shown for clarity. Only one orientation of the disordered triflate counter anion is shown for clarity. Selected bond lengths [\AA] and angles [$^\circ$] with values associated with the second molecule in the asymmetric unit shown in square brackets: N1A–C1A 1.329(2) [N1B–C1B 1.331(2)], N1A–C2A 1.401(3) [N1B–C2B 1.398(3)], N1A–C4A 1.519(3) [N1B–C4B 1.507(2)], C2A–C2A' 1.362(5) [C2B–C2B' 1.360(4)], S1A–O1A 1.441(10) [S1B–O1B 1.453(13)], S1A–O2A 1.435(10) [S1B–O2B 1.432(13)], S1A–O3A 1.412(5) [S1B–O3A 1.464(11)]; N1A–C1A–N1A' 110.4(2) [N1B–C1B–N2B' 109.1(2)], C2A–N1A–C4A 126.24(18) [C2B–N1B–C4B 127.01(16)].

Deprotonation of $[\text{MeITrH}]\text{OTf}$ (**2**) with $\text{K}[\text{N}(\text{SiMe}_3)_2]$ in a 1:1 mixture of THF/Et₂O afforded $^{\text{Me}}\text{ITr}$ (**3**) (Equation 6.1) in a yield of 50 % after filtration and removal of the volatiles from the filtrate *in vacuo*. Typical of NHCs, a highly deshielded carbene resonance is found at 220.2 ppm in the $^{13}\text{C}\{^1\text{H}\}$ NMR spectrum in C_6D_6 , which compares well with the related ITr carbene shift [225.8 ppm in C_6D_6].⁷ X-ray quality crystals of **3** were grown from a mixture of

THF/hexanes stored at -35 °C for one week. The average $C_{\text{carbene}}\text{-N-C}_{\text{trityl}}$ bond angle of 121.2(4)° and average $C_{\text{backbone}}\text{-N-C}_{\text{trityl}}$ angle of 125.7(3)° in **3** are remarkably similar to the corresponding angles in ITr [$C_{\text{carbene}}\text{-N-C}_{\text{trityl}}$ 120.2(1)° (*avg.*); $C_{\text{backbone}}\text{-N-C}_{\text{trityl}}$ 127.1(1)° (*avg.*)]⁷ indicating that the methyl backbone is not forcing the flanking trityl groups forward compared to in ITr. However, the most striking feature of **3** is that the trityl groups have rotated about the N–C bond so that one aryl ring is sitting above and below the carbene center (Figure 6.3), with the remaining aryl rings of the trityl groups pointing backwards towards the methyl groups. The effect of this configuration results in a very protected carbene center as evident by the space-filling model in Figure 6.4. The percent buried volume (% V_{bur}) of **3** was determined to be an incredible 72.6 % when **3** was coordinated to a gold dummy atom at a distance of 2 Å from the carbene center, as this procedure is standard when a specific gold-NHC complex has not been prepared yet,¹³ making **3** the most sterically demanding NHC to date. For comparison, the % V_{bur} of the ITrAuCl complex is 57.3 %.⁷ For added comparison, the % V_{Bur} of the AuCl complexes of $^{\text{Me}}\text{IPr}$ ($^{\text{Me}}\text{IPr} = (\text{MeCNDipp})_2\text{C};$ Dipp = 2,6-*i*Pr₂C₆H₃) and IPr* (IPr* = (HCNDipp*)₂C;; Dipp* = 2,6-CHPh₂-3-Me-C₆H₂) are 44.4 and 50.4 % respectively (Figure 6.1).⁴ The computed HOMO (B3YLP/def2-TZVP) of **3** shows significant s-character centered on the carbene center with the LUMO (of largely C-C π^* parentage) being located on the aryl rings of the flanking trityl groups (Figure 6.5).



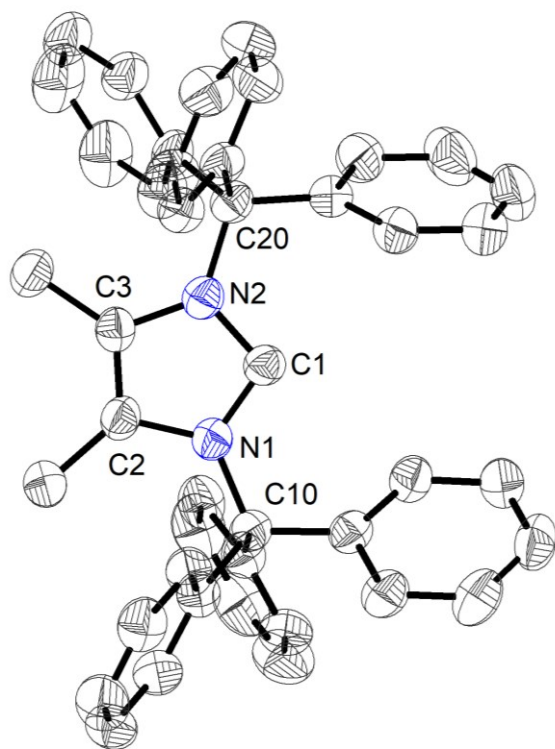


Figure 6.3. Molecular structure of ^{Me}ITr (**3**) plotted with thermal ellipsoids at 50 % probability. All hydrogen atoms are omitted for clarity. The THF solvent molecule is not shown for clarity. Selected bond lengths [Å] and angles [°]: C1–N1 1.365(6), C1–N2 1.399(6), C2–N1 1.410(6), C3–N2 1.399(6), N1–C10 1.505(6), N2–C20 1.503(3); N1–C1–N2 102.3(4), C1–N1–C10 121.6(3), C1–N2–C20 120.8(4), C2–N1–C10 125.5(3), C3–N2–C20 126.8(3).

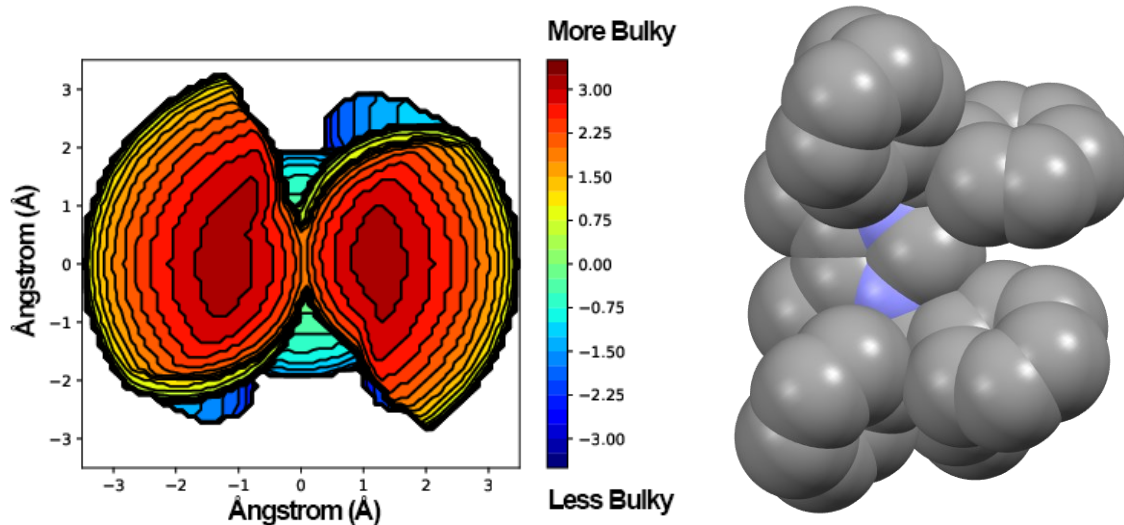


Figure 6.4. Computed steric map generated during the %V_{Bur} calculation¹³ and space-filling model of ^{Me}ITr (**3**) extracted from X-ray crystallographic data.

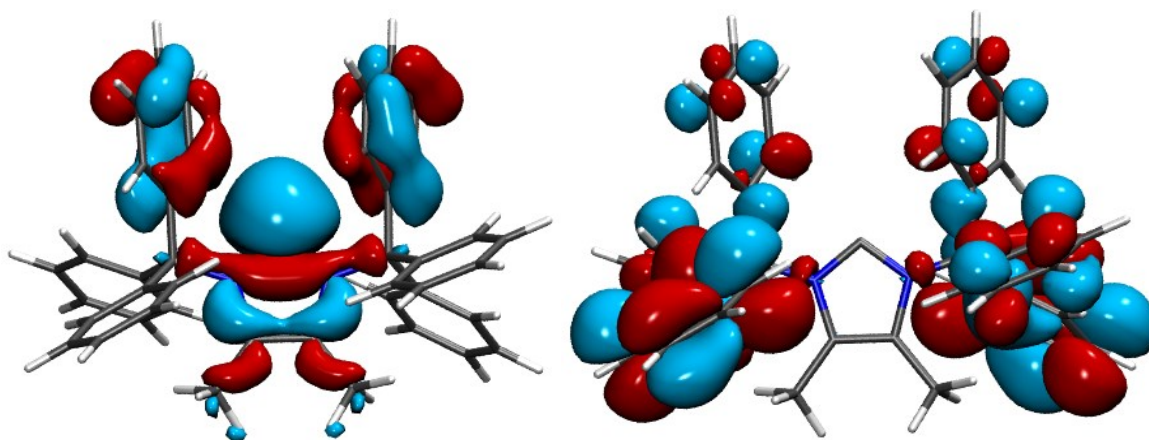


Figure 6.5. Computed HOMO (right) and LUMO (left) of ^{Me}ITr (**3**) at the B3LYP/def2-TZVP level of theory.

With ^{Me}ITr (**3**) in hand, I turned my attention to the coordinating ability of **3** with Group 10 elements (M = Ni, Pd). Unfortunately, attempts to prepare a Ni⁰ or Pd⁰ complex with Ni(COD)₂ (COD = 1,5-cyclooctadiene), and Pd(P^tBu₃)₂ in benzene, THF or PhF did not afford

any discernable $^{\text{Me}}\text{ITr}\cdot\text{M}$ complexes. Heating the reaction mixtures to 80 °C for 24 hours led exclusively to decomposition of the $\text{Ni}(\text{COD})_2$ and no reaction was found in the case of $\text{Pd}(\text{P}^t\text{Bu}_3)_2$. Attempts to prepare a Pd^0 complex with $\text{Pd}_2(\text{dba})_3$ (dba = dibenzylideneacetone), a common source of Pd^0 for NHC complexes,¹⁴ at room temperature in toluene or PhF led to no observable reaction. Attempts to prepare $^{\text{Me}}\text{ITr}\cdot\text{Pd}$ from $\text{Pd}_2(\text{dba})_3$ in THF at room temperature over the course of 16 hours led exclusively to decomposition of **3**, likely due to hydrolysis as Ph_3COH was observed in the ^1H NMR spectrum. This apparent lack of reactivity of $^{\text{Me}}\text{ITr}$ (**3**) may be due to the highly-protected carbene center by the flanking trityl groups preventing the metal centers within the precursor complexes from interacting with the carbene center in **3**.

I was concerned that the steric bulk of $^{\text{Me}}\text{ITr}$ (**3**) may prevent coordination to transition metals, as such, the structure of $^{\text{Me}}\text{ITr}\cdot\text{Pd}$ was computed (Figure 6.6) at the B3LYP/def2-TZVP level of theory. The computed structure of $^{\text{Me}}\text{ITr}\cdot\text{Pd}$ indicates a computed Pd–C bond length of 2.131 Å, typical of related mixed NHC-phosphine Pd^0 complexes,¹⁵ and close η^1 -arene interactions between single carbon atoms on the flanking trityl rings with a shortest computed distance of 2.154 Å. Previously, an η^1 -arene interaction in the related species $(\text{dcpBiph})_2\text{Pd}$ complex (dcpBiph = 2-(dicyclohexylphosphino)-biphenyl) was reported to be 2.676(5) Å.¹⁶ Such close arene interactions in $^{\text{Me}}\text{ITr}\cdot\text{Pd}$ may be required to stabilize the coordinatively unsaturated Pd center. While it appears that $^{\text{Me}}\text{ITr}\cdot\text{Pd}$ is stable, at least in the gas phase, it may be difficult to find an appropriate Pd-source to introduce this metal into the sterically crowded coordination pocket of the $^{\text{Me}}\text{ITr}$ ligand.

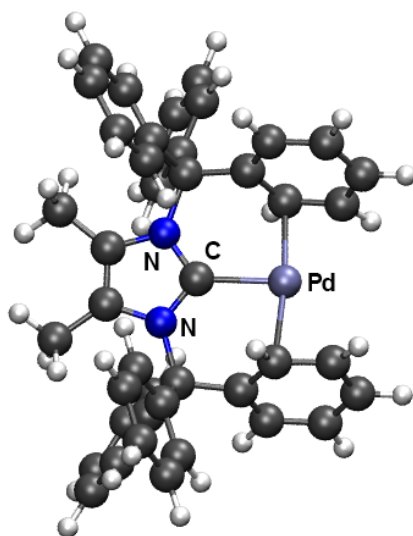


Figure 6.6. Computed structure of $^{\text{Me}}\text{ITr}\cdot\text{Pd}$ at the B3LYP/def2-TZVP level of theory.

Carbene-metal complexes are commonly prepared from the corresponding imidazolium salt by *in situ* deprotonation and subsequent coordination to the metal center. With this in mind, I attempted to prepare the Ni(II) complex $[\text{MeITrNiCp}]\text{OTf}$ ($\text{Cp} = \eta^5\text{-C}_5\text{H}_5^-$) by combining Cp_2Ni and $[\text{MeITrH}]\text{OTf}$ (**2**) in THF or toluene and heating to 80 °C for 24 hours.¹⁷ ^1H NMR spectroscopic analysis of the reaction mixtures in CDCl_3 revealed complete consumption of **2** and the presence of significantly broadened chemical resonances indicating possible paramagnetic species. Crystals suitable for X-ray crystallographic analysis have not yet been obtained.

6.3 Conclusions

This Chapter explores the efficient multigram-scale synthesis of [^{Me}ITrH]OTf (**2**) and its subsequent deprotonation to afford the World's most sterically demanding NHC, ^{Me}ITr (**3**), with an impressive estimated %V_{bur} of 72.6 %. Initial exploratory attempts to prepare ^{Me}ITr•M complexes from Ni(COD)₂ and Pd₂(dba)₃ were unsuccessful, likely due to the sterically-demanding trityl groups preventing interaction between the metal centers in the precursor complexes investigated and the carbene. Future work will focus on alternative soluble metal sources utilizing smaller and more labile ligands such as dimethylsulfide (SMe₂) (e.g., PdCl₂(SMe₂)₂) which has been used previously to prepare Pd-NHC complexes,¹⁸ or (TMEDA)PdMe₂ (TMEDA = tetramethylethylenediamine) which has been demonstrated to form Pd⁰-phosphine complexes *via* reductive elimination of ethylene and loss of TMEDA.¹⁶

6.4 Experimental Details

6.4.1 General Considerations

All reactions were performed using Schlenk and glovebox (Innovative Technologies, Inc.) techniques under a nitrogen atmosphere. Fluorobenzene (PhF) was dried by refluxing over CaH₂, then distilled, degassed (freeze-pump-thaw method) and stored over molecular sieves under a nitrogen atmosphere prior to use. All other solvents were purified using a Grubbs-type solvent purification system¹⁹ provided by Innovative Technologies, Inc., degassed (freeze-pump-thaw method), and stored under an atmosphere of nitrogen prior to use. K[N(SiMe₃)₂] was purchased from Sigma-Aldrich and recrystallized from toluene at -35 °C prior to use. Trityl chloride was purchased from TCI America and used as received. 4,5-

Dimethylimidazole¹¹ and Ph₃COTf¹² were prepared according to literature procedures. ¹H, ¹³C {¹H}, and ¹⁹F {¹H} NMR spectra were recorded on 400, 500, 600 or 700 MHz Varian Inova instruments and were referenced externally to SiMe₄ (¹H, ¹³C {¹H}), and CFC₃ (¹⁹F {¹H}). Elemental analyses were performed with a Thermo Flash 2000 Elemental Analyzer by the Analytical and Instrumentation Laboratory at the University of Alberta. Melting points were measured in sealed glass capillaries under nitrogen by using a MelTemp apparatus and are uncorrected.

6.4.2 Synthetic Procedures

Synthesis of 2-trityl-3,4-dimethylimidazole (1): 3,4-Dimethylimidazole (1.185 g, 12.33 mmol) and trityl chloride (3.501 g, 12.55 mmol) were dissolved in 20 mL of dichloromethane. To this mixture was added 3 mL of Et₃N, followed by stirring for 16 hours, and then 20 mL of distilled water was added. The two phases were separated, and the aqueous phase was washed with 3 × 20 mL of dichloromethane. The combined organic fractions were dried over MgSO₄, filtered, and the volatiles were removed from the filtrate *in vacuo* to give 2-trityl-3,4-dimethylimidazole (**1**) (1.748 g, 42 %) as an off-white solid. ¹H NMR (700 MHz, CDCl₃): δ 7.28–7.29 (overlapping m, 9H, ArH), 7.17 (s, 1H, NCHN), 7.13–7.14 (overlapping m, 6H, ArH), 2.13 (s, 3H, NC(CH₃)), 1.36 (s, 3H, NC(CH₃)). ¹³C {¹H} NMR (178 MHz, CDCl₃): δ 142.1 (NC(CH₃)), 137.0 (NCHN), 136.1 (ArC), 130.1 (ArC), 127.9 (ArC), 127.7 (ArC), 124.4 (NC(CH₃)), 74.7 (CPh₃), 13.1 (NC(CH₃)), 11.7 (NC(CH₃)). Anal. Calcd. for C₂₄H₂₂N₂ (%): C 85.17, H 6.55, N 8.28; Found: C 85.09, H 6.60, N 7.94. M.p. 228–230 °C.

Synthesis of [MeITrH]OTf (2): A solution of [Ph₃C][OTf] (4.415 g, 13.05 mmol) in 5 mL of benzene was added dropwise to a solution of 2-trityl-3,4-dimethylimidazole (1) (5.093 g, 12.98 mmol) in 5 mL of benzene; after one minute of stirring the formation of a white precipitate was noted. The reaction mixture was allowed to stir for a further 16 hours, the precipitate was then allowed to settle, and the mother liquor was decanted away and discarded. The remaining solid was dried *in vacuo* to afford [MeITrH]OTf (2) as a yellow solid (6.938 g, 73 %). X-ray quality crystals were grown from a concentrated solution of PhF stored in a -35 °C freezer for 48 hours. ¹H NMR (700 MHz, CDCl₃): δ 7.58 (s, 1H, NCHN), 7.42–7.43 (overlapping multiplets, 18 H, ArH), 7.13–7.15 (overlapping multiplets, 12H, ArH), 1.64 (s, 6H, NC(CH₃)). ¹³C {¹H} NMR (178 MHz, CDCl₃): δ 138.4 (NC(CH₃), 136.3 (NCHN), 133.1 (ArC), 129.6 (ArC), 129.2 (ArC), 129.0 (ArC), 128.3 (ArC), 79.4 (CPh₃), 12.2 (NC(CH₃)). ¹⁹F {¹H} NMR (376 MHz, CDCl₃): δ -78.0 (s). Anal. Calcd. for C₄₄H₃₇F₃N₂O₃S (%): C 72.31, H 5.10, N 3.83, S 4.39; Found: C 72.63, H 5.27, N 3.05, S 4.64. M.p. 108–110 °C.

Synthesis of MeITr (3): To a suspension of [MeITrH]OTf (2) (0.220 g, 0.301 mmol) in 6 mL of toluene was added dropwise to a solution of K[N(SiMe₃)₂] (0.060 g, 0.30 mmol) dissolved in 3 mL of toluene, resulting in the formation of a white precipitate. The resulting mixture was allowed to stir for a further 16 hours, then the mixture was filtered through a plug of Celite to give an orange solution. The volatiles were removed from the filtrate *in vacuo* to give a dark orange oil which was triturated with 5 mL of hexanes; the resulting solid was dried *in vacuo* to afford MeITr (3) as a beige solid (0.088 g, 50 %). X-ray quality crystals were grown from a solution of THF/hexanes (1:1, *ca.* 1 mL) stored in a -35 °C freezer for 48 hours. ¹H NMR (700 MHz, C₆D₆): δ 7.42 (d, 12H, ³J_{HH} = 7.7 Hz, *o*-ArH), 7.05 (t, 12 H, ³J_{HH} = 7.7 Hz, *m*-ArH),

7.00 (t, 6H, $^3J_{\text{HH}} = 7.7$ Hz, *p*-ArH), 1.32 (s, 6H, NC(CH₃)). $^{13}\text{C}\{^1\text{H}\}$ NMR (178 MHz, C₆D₆): δ 220.2 (NCN), 145.4 (NC(CH₃)), 131.3 (ArC), 127.2 (ArC), 126.7 (ArC), 77.1 (CPh₃), 12.7 (NC(CH₃)). Anal. Calcd. for C₄₃H₃₆N₂ (%): C 88.93, H 6.25, N 4.82; Found: C 84.34, H 6.01, N 4.45. M.p. 130–132 °C. *Repeated attempts at elemental analysis consistently resulted in carbon values lower than the calculated, possibly due to incomplete combustion.*

6.4.3 X-Ray Crystallography

Appropriate X-ray quality crystals were coated with a small amount of hydrocarbon oil (Paratone-N) and removed from the glovebox in a vial. Crystals were mounted quickly onto a glass fiber and placed in a low temperature stream of nitrogen on the X-ray diffractometer. All data were collected using a Bruker D8 Venture/PHOTON III, Bruker APEX II CCD detector/D8 or PLATFORM diffractometer using Mo K α (0.71073 Å) or Cu K α (1.54178 Å) radiation, with the crystals cooled to -80 °C or -100 °C. The data were corrected for absorption through Gaussian integration from the indexing of crystal faces.²⁰ Molecular structures were solved using intrinsic phasing (SHELXT)²¹ and refined using SHELXL-2014.²² The assignment of hydrogen atom positions is based on the sp²- or sp³- hybridization geometries of their attached carbon atoms and were given thermal parameters 20 % greater than those of their parent atoms.

Table 6.1. X-ray crystallographic details for [Me^eITrH]OTf (2)•1.5 PhF*A. Crystal Data*

formula	C ₅₃ H _{44.50} F _{4.50} N ₂ O ₃ S
formula weight	874.96
crystal color and habit ^a	colorless fragment
crystal dimensions (mm)	0.28 × 0.21 × 0.10
crystal system	monoclinic
space group	<i>P</i> 2 ₁ / <i>m</i> (No. 11)
unit cell parameters ^b	
<i>a</i> (Å)	12.0147(5)
<i>b</i> (Å)	19.0074(8)
<i>c</i> (Å)	19.8081(9)
β (deg)	92.640(2)
<i>V</i> (Å ³)	4518.7(3)
<i>Z</i>	4
ρ _{calcd} (g cm ⁻³)	1.286
μ (mm ⁻¹)	1.174

B. Data Collection and Refinement Conditions

diffractometer	Bruker D8 Venture/PHOTON III ^c
radiation (λ [Å])	Cu Kα (1.54178) (microfocus source)
temperature (°C)	-100
scan type	ω and φ scans (1.0°) (5 s exposures)
data collection 2θ limit (deg)	144.87
total data collected	99834 (-14 ≤ <i>h</i> ≤ 14, -23 ≤ <i>k</i> ≤ 23, -24 ≤ <i>l</i> ≤ 24)
independent reflections	9204 (<i>R</i> _{int} = 0.0681)
number of observed reflections (<i>NO</i>)	7843 [<i>F</i> _o ² ≥ 2σ(<i>F</i> _o ²)]
structure solution method	intrinsic phasing (<i>SHELXT-2018/2</i> ^d)
refinement method	full-matrix least-squares on <i>F</i> ² (<i>SHELXL-2019/1</i> ^{e,f})
absorption correction method	Gaussian integration (face-indexed)
range of transmission factors	1.0000–0.7122
data/restraints/parameters	9204 / 501 <i>g</i> / 731
goodness-of-fit (<i>S</i>) ^h [all data]	1.046
final <i>R</i> indices ⁱ	
<i>R</i> ₁ [<i>F</i> _o ² ≥ 2σ(<i>F</i> _o ²)]	0.0733
<i>wR</i> ₂ [all data]	0.2222
largest difference peak and hole	0.985 and -0.551 e Å ⁻³

^aObtained by recrystallization from a fluorobenzene solution.

^bObtained from least-squares refinement of 9314 reflections with 0.1175° < 2θ < 3.2719°.

^cPrograms for diffractometer operation, data collection, data reduction and absorption correction were those supplied by Bruker.

^dG. M. Sheldrick, *Acta Crystallogr.* **2015**, *A71*, 3–8. (*SHELXT-2018/2*)

^eG. M. Sheldrick, *Acta Crystallogr.* **2015**, *C71*, 3–8. (*SHELXL-2019/1*)

^fAttempts to refine peaks of residual electron density as disordered or partial-occupancy solvent fluorobenzene fluorine or carbon atoms were unsuccessful. The data were corrected for disordered electron density through use of the SQUEEZE procedure as implemented in *PLATON* (A. L. Spek, *Acta Crystallogr.* **2015**, *C71*, 9–18. *PLATON* - a multipurpose crystallographic tool. Utrecht University, Utrecht, The Netherlands). A total solvent-accessible void volume of 825 Å³ with a total electron count of 216 (consistent with ~4 molecules of solvent fluorobenzene, or 1 molecule per formula unit of the target molecule) was found in the unit cell.

^gThe interatomic distances for the following sets of atoms were restrained to be approximately the same by use of the *SHELXL* same distance (**SADI**) restraint: S1A–C10A, S1B–C10B, S2A–C20A, S2B–C20B; S1A–O1A, S1A–O2A, S1A–O3A, S1B–O1B, S1B–O2B, S1B–O3B, S2A–O4A, S2A–O5A, S2A–O6A, S2B–O4B, S2B–O5B, S2B–O6B; F1A–C10A, F2A–C10A, F3A–C10A, F1B–C10B, F2B–C10B, F3B–C10B, F4A–C20A, F5A–C20A, F6A–C20A, F4B–C20B, F5B–C20B, F6B–C20B. Similarly, the following non-bonded contacts were restrained: O1A···O2A, O1A···O3A, O2A···O3A, O1B···O2B, O1B···O3B, O2B···O3B, O4A···O5A, O4A···O6A, O5A···O6A, O4B···O5B, O4B···O6B, O5B···O6B; F1A···F2A, F1A···F3A, F2A···F3A, F1B···F2B, F1B···F3B, F2B···F3B, F4A···F5A, F4A···F6A, F5A···F6A, F4B···F5B, F4B···F6B, F5B···F6B. All of the anisotropic displacement parameters for the triflate ion atoms were restrained by use of the *SHELXL* **RIGU** instruction. The following pairs of atoms had an additional restraint (**SIMU**) applied to their ADPs: O1A & O1B; O2A & O2B, O4A & O5B. Furthermore, the ADPs for the following pairs of atoms were constrained to be the same by use of the **EADP** instruction: O1A & O1B; O4A & O5B. Finally (and unrelated to the triflates), the F1S···C2S and F1S···C6S nonbonded contacts of the solvent fluorobenzene molecule were restrained to be approximately the same distance by use of the **SADI** instruction.

$$^hS = [\sum w(F_o^2 - F_c^2)^2 / (n - p)]^{1/2} \quad (n = \text{number of data}; p = \text{number of parameters varied}; w = [\sigma^2(F_o^2) + (0.1175P)^2 + 3.2719P]^{-1} \text{ where } P = [\text{Max}(F_o^2, 0) + 2F_c^2] / 3).$$

$$^iR_1 = \sum ||F_o| - |F_c|| / \sum |F_o|; wR_2 = [\sum w(F_o^2 - F_c^2)^2 / \sum w(F_o^4)]^{1/2}.$$

Table 6.2. X-ray crystallographic details for $\text{MeITr (3)} \cdot \text{THF}$ *A. Crystal Data*

formula	$\text{C}_{47}\text{H}_{44}\text{N}_2\text{O}$
formula weight	652.84
crystal color and habit ^a	colorless plate
crystal dimensions (mm)	$0.11 \times 0.05 \times 0.02$
crystal system	orthorhombic
space group	$Pna2_1$ (No. 33)
unit cell parameters ^b	
<i>a</i> (Å)	17.8284(15)
<i>b</i> (Å)	9.7528(8)
<i>c</i> (Å)	20.8684(18)
<i>V</i> (Å ³)	3628.5(5)
<i>Z</i>	4
ρ_{calcd} (g cm ⁻³)	1.195
μ (mm ⁻¹)	0.541

B. Data Collection and Refinement Conditions

diffractometer	Bruker D8 Venture/PHOTON III ^c
radiation (λ [Å])	$\text{Cu K}\alpha$ (1.54178) (microfocus source)
temperature (°C)	-100
scan type	ω and ϕ scans (1.0°) (θ -dep. exp. from 15-60 s)
data collection 2θ limit (deg)	145.52
total data collected	36070 ($-22 \leq h \leq 21$, $-11 \leq k \leq 11$, $-25 \leq l \leq 25$)
independent reflections	6991 ($R_{\text{int}} = 0.1604$)
number of observed reflections (<i>NO</i>)	4573 [$F_o^2 \geq 2\sigma(F_o^2)$]
structure solution method	intrinsic phasing (<i>SHELXT-2018/2</i> ^d)
refinement method	full-matrix least-squares on F^2 (<i>SHELXL-2019/1</i> ^{e,f})
absorption correction method	Gaussian integration (face-indexed)
range of transmission factors	1.0000–0.7356
data/restraints/parameters	6991 / 0 / 409
extinction coefficient (<i>x</i>) ^g	0.0027(5)
goodness-of-fit (<i>S</i>) ^h [all data]	0.984
final <i>R</i> indices ⁱ	
R_1 [$F_o^2 \geq 2\sigma(F_o^2)$]	0.0600
wR_2 [all data]	0.1679
largest difference peak and hole	0.236 and $-0.214 \text{ e } \text{Å}^{-3}$

^aObtained by recrystallization from a tetrahydrofuran/hexanes solution.

^bObtained from least-squares refinement of 2458 reflections with $8.48^\circ < 2\theta < 114.78^\circ$.

^cPrograms for diffractometer operation, data collection, data reduction and absorption correction were those supplied by Bruker.

^dG. M. Sheldrick, *Acta Crystallogr.* **2015**, *A71*, 3–8. (*SHELXT-2018/2*)

^eG. M. Sheldrick, *Acta Crystallogr.* **2015**, *C71*, 3–8. (*SHELXL-2019/1*)

^fAttempts to refine peaks of residual electron density as disordered or partial-occupancy solvent tetrahydrofuran oxygen or carbon atoms were unsuccessful. The data were corrected for disordered electron density through use of the SQUEEZE procedure as implemented in *PLATON* (A. L. Spek, *Acta Crystallogr.* **2015**, *C71*, 9–18. *PLATON* - a multipurpose crystallographic tool. Utrecht University, Utrecht, The Netherlands). A total solvent-accessible void volume of 631 Å³ with a total electron count of 171 (consistent with 4 molecules of solvent tetrahydrofuran, or 1 molecule per formula unit of the target molecule) was found in the unit cell.

^g $F_c^* = kF_c[1 + x\{0.001F_c^2\lambda^3/\sin(2\theta)\}]^{-1/4}$ where k is the overall scale factor.

^h $S = [\sum w(F_o^2 - F_c^2)^2/(n - p)]^{1/2}$ (n = number of data; p = number of parameters varied; $w = [\sigma^2(F_o^2) + (0.0770P)^2]^{-1}$ where $P = [\text{Max}(F_o^2, 0) + 2F_c^2]/3$).

ⁱ $R_1 = \sum||F_o| - |F_c||/\sum|F_o|$; $wR_2 = [\sum w(F_o^2 - F_c^2)^2/\sum w(F_o^4)]^{1/2}$.

6.4.4 Density Functional Theory (DFT) Computations

All computations were performed with Gaussian16.²³ Gas-phase geometries were optimized using density functional theory (DFT) with the B3LYP functional²⁴ and the def2-TZVP basis set.²⁵ Optimized geometries and orbitals were visualized with Visual Molecular Dynamics (VMD).²⁶ The percent buried volume and steric map of ^MeITr (**3**) were calculated with the SambVca 2.1 web tool.¹³

6.5 References

1. M. H. Hopkinson, C. Richter, M. Schedler, F. Glorius, *Nature* **2014**, *510*, 485–496.
2. A. Igau, H. Gruztmacher, A. Baceiredo, G. Bertrand, *J. Am. Chem. Soc.* **1988**, *110*, 6463–6466.
3. A. J. Arduengo III, R. L. Harlow, M. Kline, *J. Am. Chem. Soc.* **1991**, *113*, 361–363.
4. A. Gómez-Suárez, D. J. Nelson, S. P. Nolan, *Chem. Commun.* **2017**, *53*, 2650–2660.
5. For select reviews, see: a) M. M. D. Roy, A. A. Omaña, A. S. S. Wilson, M. S. Hill, S. Aldridge, E. Rivard, *Chem. Rev.* **2021**, *121*, 12784–12965; b) P. Belloti, M. Koy, M. N. Hopkinson, F. Glorius, *Nat. Rev. Chem.* **2021**, *5*, 711–725; c) M. Fèvre, J. Pinaud, Y. Gnanou, J. Vignolle, D. Taton, *Chem. Soc. Rev.* **2013**, *42*, 2142–2172; d) S. Díez-González, N. Marion, S. P. Nolan, *Chem. Rev.* **2009**, *109*, 3612–3676; e) V. Nesterov, D. Reiter, P. Bag, P. Frisch, R. Holzner, A. Porzelt, S. Inoue, *Chem. Rev.* **2018**, *118*, 9678–9842.
6. For select articles and reviews, see: a) Y. Pang, N. Nöthling, M. Leutzsch, L. Kang, E. Bill, M. van Gastel, E. Reijerse, R. Goddard, L. Wagner, D. SantaLucia, S. DeBeer, F. Neese, J.

- Cornella, *Science* **2023**, *380*, 1043–1048; b) R. C. Fisher, P. P. Power, *Chem. Rev.* **2010**, *110*, 3877–3923; c) H. Chen, W. Chen, D. Wang, Y. Chen, Z. Liu, S. Ye, G. Tan, S. Gao, *Angew. Chem. Int. Ed.* **2024**, *63*, e202402093; d) D. Wang, W. Chen, C. Zhai, L. Zhao, S. Ye, G. Tan, *J. Am. Chem. Soc.* **2023**, *145*, 6914–6920; d) M. Wu, H. Li, W. Chen, D. Wang, Y. He, L. Xu, S. Ye, G. Tan, *Chem.* **2023**, *9*, 2573–2584; e) T. Ochiai, D. Franz, S. Inoue, *Chem. Soc. Rev.* **2016**, *45*, 6327–6344.
7. M. M. D. Roy, P. A. Lummis, M. J. Ferguson, R. McDonald, E. Rivard, *Chem. Eur. J.* **2017**, *23*, 11249–11252.
8. M. M. D. Roy, M. J. Ferguson, R. McDonald, E. Rivard, *Chem. Commun.* **2018**, *54*, 483–486.
9. a) C. L. McMullin, N. Fey, J. N. Harvey, *Dalton Trans.* **2014**, *43*, 13545–13556; b) M. Ahlquist, P. Fristrup, D. Tanner, P.-O. Norrby, *Organometallics* **2006**, *25*, 2066–2073; c) A. H. Roy, J. F. Hartwig, *J. Am. Chem. Soc.* **2001**, *123*, 1232–1233.
10. H. Giesemann, G. Hälschke, *Chem. Ber.* **1959**, *92*, 92–98.
11. M. A. Bernd, F. Dyckhoff, B. J. Hoffman, A. D. Böth, J. F. Schlagintweit, J. Oberkofler, R. M. Reich, F. E. Kühn, *J. Catal.* **2020**, *391*, 548–561.
12. D. A. Strauss, C. Zhang, T. D. Tilley, *J. Organomet. Chem.* **1989**, *369*, C13–C17.
13. The percent buried volume was calculated with the SambVca 2.1 web tool with bondi radii scaled by 1.17, a sphere radius of 3.5 Å, a M-C_{NHC} length of 2.0 Å, a mesh spacing of 0.10 Å and H atoms omitted from the calculation, see: L. Falivene, Z. Cao, A. Petta, L. Serra, A. Poater, R. Oliva, V. Scarano, L. Cavallo, *Nat. Chem.* **2019**, *11*, 872–879.
14. S. S. Zaleskiy, V. P. Ananikov, *Organometallics* **2012**, *31*, 2302–2309.
15. S. Fantasia, S. P. Nolan, *Chem. Eur. J.* **2008**, *14*, 6987–6993.

16. S. M. Reid, R. C. Boyle, J. T. Mague, M. J. Fink, *J. Am. Chem. Soc.* **2003**, *125*, 7816–7817.
17. NHC-NiCpCl complexes can be prepared from Cp₂Ni and the corresponding imidazolium salt with loss of CpH, see: R. A. Kelly, N. M. Scott, S. Díez-González, E. D. Stevens, S. P. Nolan, *Organometallics* **2005**, *24*, 3442–3447.
18. Y. Liu, V. A. Voloshkin, T. Scattloin, M. Peng, K. Van Hecke, S. P. Nolan, C. S. J. Cazin, *Eur. J. Org. Chem.* **2022**, e202200309.
19. A. B. Pangborn, M. A. Giardello, R. H. Grubbs, R. K. Rosen, F. J. Timmers, *Organometallics* **1996**, *15*, 1518–1520.
20. H. Hope, *Prog. Inorg. Chem.* **1994**, *41*, 1–19.
21. G. M. Sheldrick, *Acta Crystallogr. Sect. A* **2015**, *71*, 3–8.
22. G. M. Sheldrick, *Acta Crystallogr. Sect. C* **2015**, *71*, 3–8.
23. M. J. Frisch, G. W. Trucks, H. B. Schlegel, G. E. Scuseria, M. A. Robb, J. R. Cheeseman, G. Scalmani, V. Barone, G. A. Petersson, H. Nakatsuji, X. Li, M. Caricato, A. V. Marenich, J. Bloino, B. G. Janesko, R. Gomperts, B. Mennucci, H. P. Hratchian, J. V. Ortiz, A. F. Izmaylov, J. L. Sonnenberg, D. Williams-Young, F. Ding, F. Lipparini, F. Egidi, J. Goings, B. Peng, A. Petrone, T. Henderson, D. Ranasinghe, V. G. Zakrzewski, J. Gao, N. Rega, G. Zheng, W. Liang, M. Hada, M. Ehara, K. Toyota, R. Fukuda, J. Hasegawa, M. Ishida, T. Nakajima, Y. Honda, O. Kitao, H. Nakai, T. Vreven, K. Throssell, J. A. Montgomery, Jr., J. E. Peralta, F. Ogliaro, M. J. Bearpark, J. J. Heyd, E. N. Brothers, K. N. Kudin, V. N. Staroverov, T. A. Keith, R. Kobayashi, J. Normand, K. Raghavachari, A. P. Rendell, J. C. Burant, S. S. Iyengar, J. Tomasi, M. Cossi, J. M. Millam, M. Klene, C. Adamo, R. Cammi, J. W. Ochterski, R. L.

Martin, K. Morokuma, O. Farkas, J. B. Foresman, D. J. Fox, Gaussian 16, Revision A. 03, Gaussian Inc., Wallingford CT, 2016.

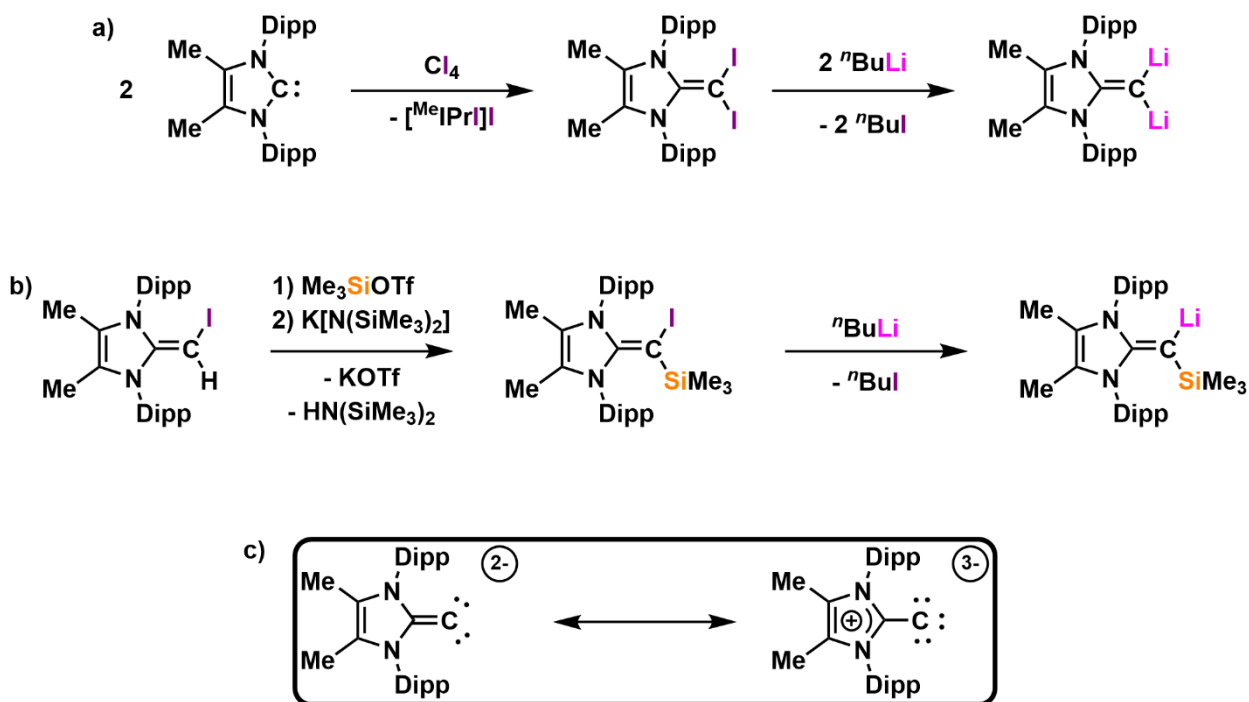
24. a) C. Lee, W. Yang, R. G. Parr, *Phys. Rev. B* **1988**, *37*, 785–789; b) A. D. Becke, *Phys. Rev. A* **1988**, *38*, 3098–3100; c) P. J. Stephens, F. J. Devlin, C. F. Chabalowski, M. J. Frisch, *J. Phys. Chem.* **1994**, *98*, 11623–11627.

25. a) F. Weigend, R. Ahlrichs, *Phys. Chem. Chem. Phys.* **2005**, *7*, 3297–3305; b) F. Weigend, *Phys. Chem. Chem. Phys.* **2006**, *8*, 1057–1065.

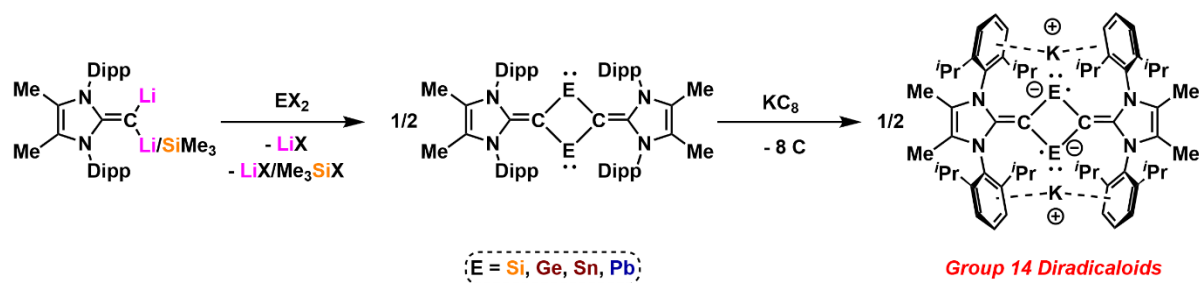
26. W. Humphrey, A. Dalke, K. Schulten, *J. Molec. Graphics* **1996**, *14*, 33–38.

Chapter 7 – Summary and Future Directions

Starting with Chapter 2, the synthesis of a new anionic *N*-heterocyclic olefin (aNHO), $[(^{\text{Me}}\text{IPrCH})\text{Li}]_2$ ($^{\text{Me}}\text{IPr} = (\text{MeCNDipp})_2\text{C}$; Dipp = 2,6-*i*-Pr₂C₆H₃), was described and utilized to prepare a complete homoleptic acyclic divinyltetrelene series $(^{\text{Me}}\text{IPrCH})_2\text{E}$: (E = Si, Sn, Ge, Pb). A key step in this project was the development of a new aNHO synthon, $[(^{\text{Me}}\text{IPrCH})\text{Li}]_2$, which involved the preparation of the iodinated *N*-heterocyclic olefin (NHO) $^{\text{Me}}\text{IPrCH}(\text{I})$, which was achieved by the addition of I₂ to $^{\text{Me}}\text{IPrCH}_2$ and subsequent deprotonation with the strong base K[N(SiMe₃)₂]. The aNHO synthon, $[(^{\text{Me}}\text{IPrCH})\text{Li}]_2$, may be modified structurally to include a dianionic NHO (*i.e.*, $[(^{\text{Me}}\text{IPr}=\text{C})^{2-}]$) unit as a potential 6-electron donor. As shown in Scheme 7.1, the combination of two equivalents of $^{\text{Me}}\text{IPr}$ with an equivalent of carbon tetraiodide (CI₄) may give the doubly iodinated NHO, $^{\text{Me}}\text{IPrCI}_2$, which could undergo double lithium-halogen exchange to afford $[(^{\text{Me}}\text{IPrC})\text{Li}]_2$. It is worthy to note that Arduengo and coworkers reported the doubly-chlorinated NHOs SIMesCCl₂ (SIMes = (H₂CNMe₃)₂C; Mes = 2,4,6-Me₃C₆H₂) and ^{Cl}IMesCCl₂ (^{Cl}IMes = (ClCNMe₃)₂C) by combining two equivalents of the appropriate NHC with carbon tetrachloride (CCl₄).¹ Alternatively, the addition of Me₃SiOTf (OTf = O₃SCF₃⁻) to $^{\text{Me}}\text{IPrCH}(\text{I})$ followed by deprotonation of the *in situ* formed $[(^{\text{Me}}\text{IPrCH}(\text{I})\text{SiMe}_3)\text{OTf}]$ with a strong base (such as K[N(SiMe₃)₂]) will likely give the precursor $^{\text{Me}}\text{IPrC}(\text{I})\text{SiMe}_3$ which should be able to undergo lithium-halogen exchange to give $[(^{\text{Me}}\text{IPrC}(\text{SiMe}_3)\text{Li}]$. The addition of either $[(^{\text{Me}}\text{IPrC})\text{Li}]_2$ or $[(^{\text{Me}}\text{IPrC}(\text{SiMe}_3)\text{Li}]$ to Group 14 EX₂ species (E = Si, Ge, Sn, Pb; X = halide) may produce a cyclic-divinylditetrelene series in the form of four-membered rings (C₂E₂), which could be potentially reduced further with a strong reducing agent (*i.e.*, KC₈) to afford Group 14 diradicaloids (Scheme 7.2).²



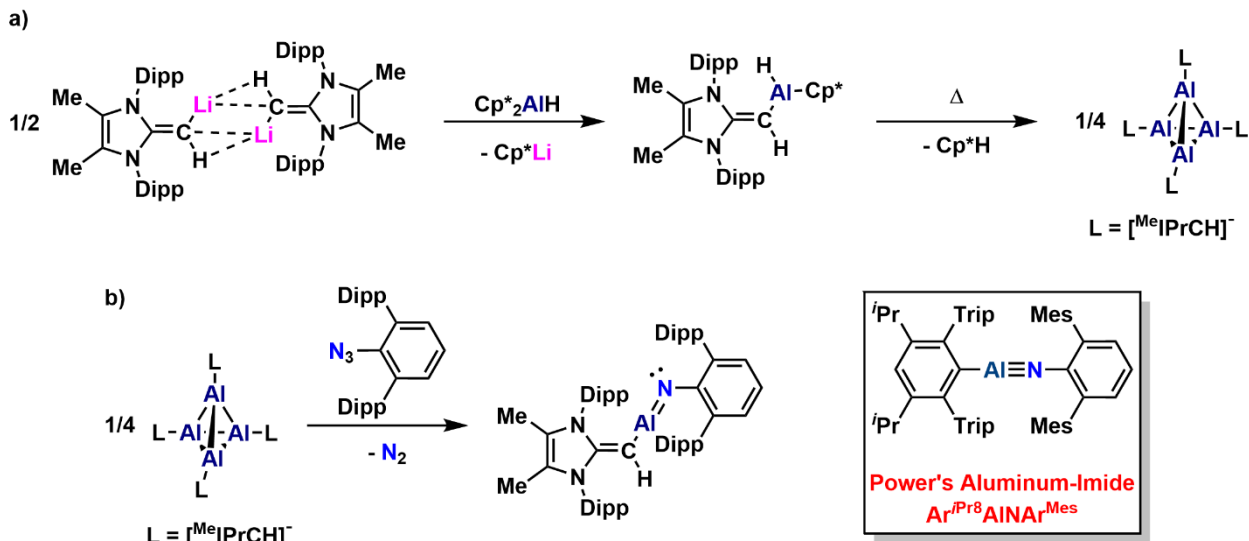
Scheme 7.1. a) Proposed synthetic route to the dianionic NHO synthon $[(^{\text{Me}}\text{IPrC})\text{Li}]_2$; b) Proposed synthetic route to silylated aNHO $[(^{\text{Me}}\text{IPrC}(\text{SiMe}_3)\text{Li}]_2$; c) Resonance forms of a dianionic NHO.



Scheme 7.2. Proposed synthesis of cyclic divinylditetrelenes and cyclic Group 14 diradicaloids.

In Chapter 3, $[(^{\text{Me}}\text{IPrCH})\text{Li}]_2$ was combined with CpIn ($\text{Cp} = \eta^5\text{-C}_5\text{H}_5$) to prepare the indium(I) tetramer $[(^{\text{Me}}\text{IPrCH})\text{In}]_4$, which activated strong H–B bonds in boranes, and was used to prepare $(^{\text{Me}}\text{IPrCH})\text{InNAr}^{\text{Dipp}}$ ($\text{Ar}^{\text{Dipp}} = 2,6\text{-Dipp}_2\text{C}_6\text{H}_3$), a two-coordinate indium-imide. Given that examples of two-coordinate Group 13-imides (RENr ; $\text{E} = \text{Ga}, \text{In}$)³ are

exceedingly rare, and that a stable two-coordinate aluminium-imide, $\text{Ar}^{i\text{Pr}8}\text{AlNAr}^{\text{Mes}}$ ($\text{Ar}^{i\text{Pr}8} = 2,6\text{-Trip-3,5-}^i\text{Pr}_2\text{C}_6\text{H}$; $\text{Trip} = 2,4,6\text{-}^i\text{Pr}_3\text{C}_6\text{H}_2$; $\text{Ar}^{\text{Mes}} = 2,6\text{-Mes}_2\text{C}_6\text{H}_3$; $\text{Mes} = 2,4,6\text{-Me}_3\text{C}_6\text{H}_2$), was only reported in 2021 by Power and coworkers,⁴ I envision the preparation an aNHO-stabilized aluminum-imide (*i.e.*, $(^{\text{Me}}\text{IPrCH})\text{AlNAr}^{\text{Dipp}}$) to expand upon known examples and potentially probe its reactivity towards small molecules (*e.g.*, CO_2). It was established in Chapter 3, and by others,⁵ that Cp-derivatives are excellent leaving groups particularly for Group 13 elements. The obvious precursor then to prepare an Al(I) species supported by aNHOs is $[\text{Cp}^*\text{Al}]_4$. However, recent work by the Aldridge group has shown that heating (*ca.* 80 °C) is required when adding anionic ligands (*e.g.*, $[(\text{HCNDipp})_2\text{BO}]\text{K}$) to $[\text{Cp}^*\text{Al}]_4$,⁶ likely to increase the solubility of the rather insoluble $[\text{Cp}^*\text{Al}]_4$ and to cause the tetramer to dissociate into monomeric Cp^*Al . Due to the thermal instability of $[(^{\text{Me}}\text{IPrCH})\text{Li}]_2$ heating a solution of $[\text{Cp}^*\text{Al}]_4$ and $[(^{\text{Me}}\text{IPrCH})\text{Li}]_2$ may not be a viable synthetic route. An alternative pathway, inspired by the synthesis of $[\text{Cp}^*\text{Al}]_4$,⁷ could involve the addition of $[(^{\text{Me}}\text{IPrCH})\text{Li}]_2$ to Cp^*_2AlH giving the target species $(^{\text{Me}}\text{IPrCH})\text{Al}(\text{H})\text{Cp}^*$ and Cp^*Li as a by-product. Heating $(^{\text{Me}}\text{IPrCH})\text{Al}(\text{H})\text{Cp}^*$ may induce reductive elimination of Cp^*H to give $[(^{\text{Me}}\text{IPrCH})\text{Al}]_4$. The addition of the terphenyl azide $\text{Ar}^{\text{Dipp}}\text{N}_3$ to $[(^{\text{Me}}\text{IPrCH})\text{Al}]_4$ would likely eliminate N_2 gas and afford $(^{\text{Me}}\text{IPrCH})\text{AlNAr}^{\text{Dipp}}$ in the same manner of preparation as $(^{\text{Me}}\text{IPrCH})\text{InNAr}^{\text{Dipp}}$. I speculate that $(^{\text{Me}}\text{IPrCH})\text{AlNAr}^{\text{Dipp}}$ may be more stable than Power's aluminum-imide due to the electron-donating aNHO moiety offering electronic stabilization in conjunction with the steric protect provide by the flanking NHO and terphenyl fragments; it should be noted that $\text{Ar}^{i\text{Pr}8}\text{AlNAr}^{\text{Mes}}$ decomposes over the course of 12 hours in solution, likely through ligand activation.⁴



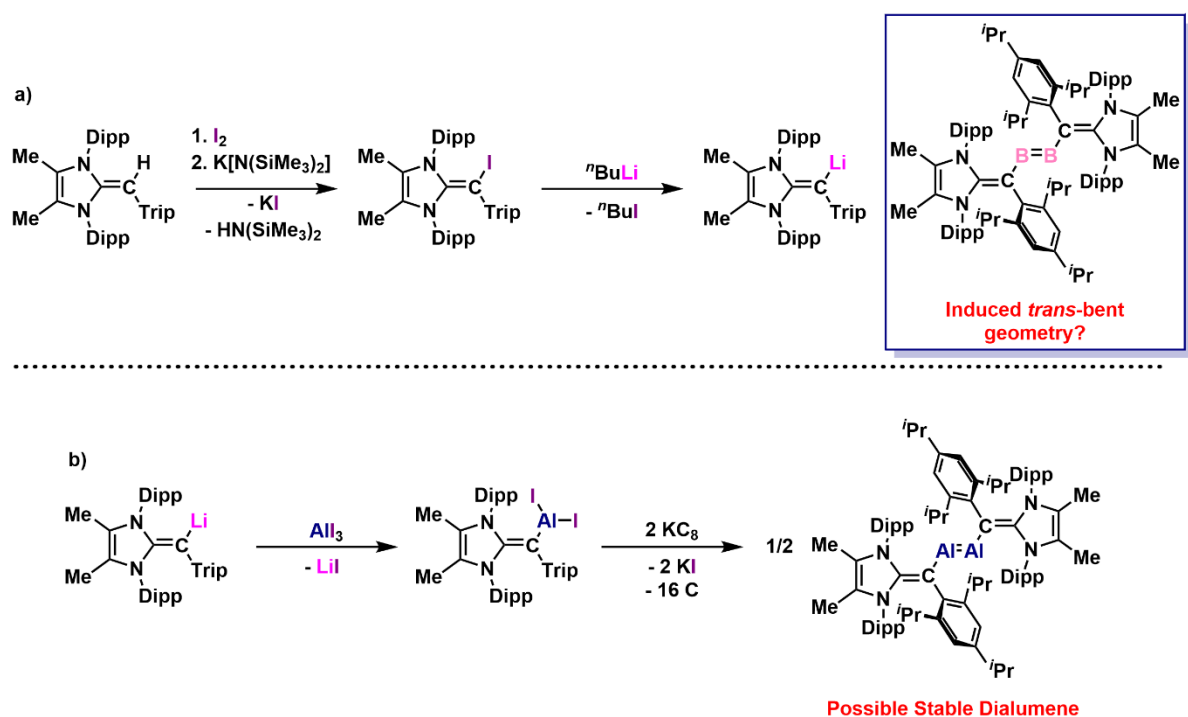
Scheme 7.3. a) Proposed synthetic route to the Al(I) tetramer $[({}^{\text{Me}}\text{iPrCH})\text{Al}]_4$; b) Proposed synthesis of the aluminum-imide $({}^{\text{Me}}\text{iPrCH})\text{AlNAr}^{\text{Dipp}}$ and Power's aluminum-imide $\text{Ar}^{\text{iPr}_8}\text{AlNAr}^{\text{Mes}}$.

Continuing to Chapter 4, the aNHO synthon $[(\text{SiPrCH})\text{Li}]_2$, first described in Chapter 3, was utilized to prepare $(\text{SiPrCH})\text{ClB-BCl}(\text{CHSiPr})$, a potential precursor to the diborene $(\text{SiPrCH})\text{B}=\text{B}(\text{CHSiPr})$. Attempts to reduce $(\text{SiPrCH})\text{ClB-BCl}(\text{CHSiPr})$ with sodium naphthalene ($\text{Na}[\text{C}_{10}\text{H}_8]$) in THF led exclusively to the formation free ligand (*i.e.*, SiPrCH_2), and in one instance a ligand-activated product was isolated. The target diborene $(\text{SiPrCH})\text{B}=\text{B}(\text{CHSiPr})$ was found computationally to have a triplet ground state, and when computed in the gas phase, a linear geometry was found. Currently, a series of NHOs with increasing steric bulk situated on the exocyclic carbon (*e.g.*, ${}^{\text{Me}}\text{iPrC}(\text{H})\text{Trip}$) are being investigated computationally to see if they can induce a *trans*-bending in the C–B–B–C array of an aNHO supported diborene in an effort to break the degeneracy of the B–B π -bonding orbitals and promote a singlet ground state.⁸

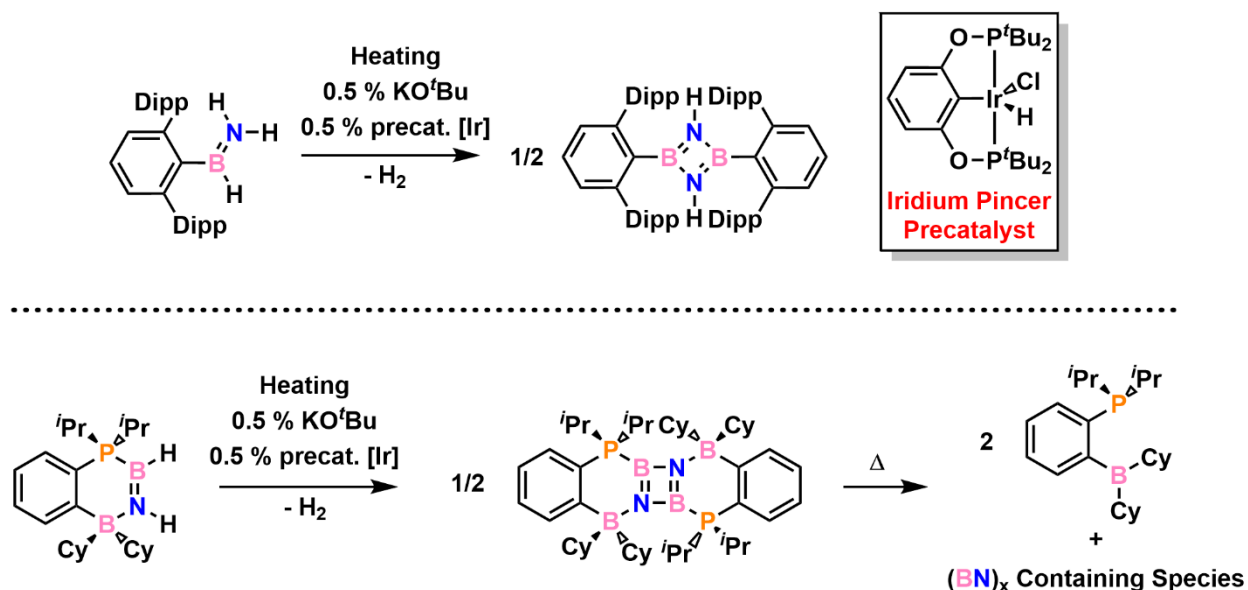
The Rivard group has recently developed an unpublished synthetic route to $^{\text{Me}}\text{IPrC(H)Trip}$. The addition of the Trip moiety should increase the steric parameters around exocyclic carbon. If this NHO can be converted to an aNHO synthon (*e.g.*, $[(^{\text{Me}}\text{IPrCTrip})\text{Li}]$), using a similar synthetic method used to prepare $[(^{\text{Me}}\text{IPrCH})\text{Li}]_2$, it may be able to induce *trans*-bending in the C–B–B–C core of the diborene $(^{\text{Me}}\text{IPrCTrip})\text{B}=\text{B}(\text{CTrip}^{\text{Me}}\text{IPr})$. The aNHO $[(^{\text{Me}}\text{IPrCTrip})]^-$ may also be an ideal ligand for the isolation of a stable dialumene ($\text{RAl}=\text{AlR}$), of which none are known,⁸ by providing a sterically shielded pocket for the Al–Al multiple bonded core, preventing activation of aromatic solvents (*e.g.*, toluene),⁹ while also stabilizing the Al(I) atoms *via* donation of π -electron density from the exocyclic carbon atom to aluminum.¹⁰ The dialumene $(^{\text{Me}}\text{IPrCTrip})\text{Al}=\text{Al}(\text{CTrip}^{\text{Me}}\text{IPr})$ might be prepared by reduction of the precursor $(^{\text{Me}}\text{IPrCTrip})\text{AlI}_2$ with KC_8 , as shown in Scheme 7.4b.

Chapter 5 describes the use of the bulky terphenyl ligand, Ar^{Dipp} , to prepare the aminoborane $\text{Ar}^{\text{Dipp}}\text{B(H)}=\text{NH}_2$, an inorganic analogue of styrene, through successive dehydrogenations. It was hoped that this aminoborane could be dehydrogenated further by using transition metals catalysts or through halogen/hydride exchange followed by dehydrohalogenation to give the iminoborane dimer $[\text{Ar}^{\text{Dipp}}\text{BNH}]_2$. Unfortunately, these attempts were unsuccessful. Computationally, it was found that the B–H and N–H linkages in $\text{Ar}^{\text{Dipp}}\text{B(H)}=\text{NH}_2$ have little hydridic and protic character respectively which may explain the aforementioned failed dehydrogenation attempts. This is in line with the previous reports from the Rivard group that described the frustrated Lewis pair FLP-chelated amino- and iminoborane adducts $\text{PB}\{\text{H}_2\text{BNH}_2\}$ and $\text{PB}\{\text{HBNH}\}$ ($\text{PB} = {}^i\text{Pr}_2\text{P}(\text{C}_6\text{H}_4)\text{BCy}_2$; Cy = cyclohexyl), which were found to not undergo catalytic dehydrogenations.¹¹ Pincer iridium complexes, such as $[\text{IrHCl}\{2,6-({}^t\text{BuPO})_2\text{C}_6\text{H}_3\}]$, have been shown to be highly efficient

catalysts in the dehydrogenation of alkanes even at extremely low catalytic loadings (*ca.* 0.033 mmol %).¹² The dehydrogenation of $\text{Ar}^{\text{Dipp}}\text{B}(\text{H})=\text{NH}_2$ may be possible with such pincer complexes to give $[\text{Ar}^{\text{Dipp}}\text{BNH}]_2$. It may be possible to extend this approach to the dehydrogenation of $\text{PB}\{\text{HBNH}\}$ to form the dimer $\text{PB}\{\text{BN}\}_2\text{PB}$, a potentially useful boron-nitride (BN) precursor for solution deposition of $(\text{BN})_x$ at relatively low temperatures (Scheme 7.5).¹³



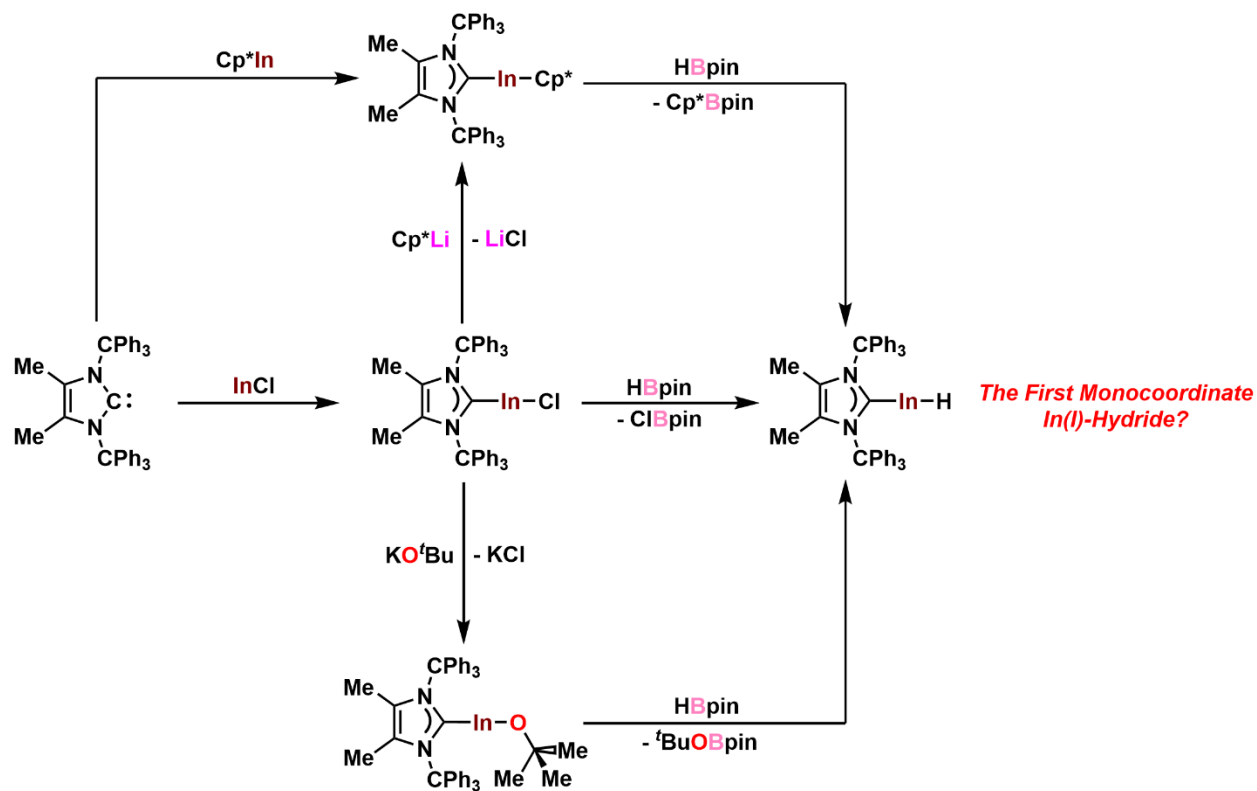
Scheme 7.4. a) Proposed synthetic route to $[(^{\text{Me}}\text{IPrC}(\text{Trip})\text{Li}]$ and the possibly *trans*-bent diborene $(^{\text{Me}}\text{IPrC}(\text{Trip})\text{B}=\text{B}(\text{CTrip}^{\text{Me}}\text{IPr}))$; b) Postulated synthetic pathway to the dialumene $(^{\text{Me}}\text{IPrC}(\text{Trip})\text{Al}=\text{Al}(\text{CTrip}^{\text{Me}}\text{IPr}))$.



Scheme 7.5. Proposed dehydrogenation of $\text{Ar}^{\text{Dipp}}\text{B}(\text{H})=\text{NH}_2$ with an iridium catalyst to give $[\text{Ar}^{\text{Dipp}}\text{BNH}]_2$ (top) and dehydrogenation of $\text{PB}\{\text{HBNH}\}$ to give $\text{PB}\{\text{BN}\}_2\text{PB}$ and subsequent deposition of $(\text{BN})_x$.

Finally, Chapter 6 described the synthesis of the world's bulkiest *N*-heterocyclic carbene (NHC) $^{\text{Me}}\text{ITr}$ ($^{\text{Me}}\text{ITr} = (\text{MeCNCPh}_3)_2\text{C}$), which has an impressive percent buried volume ($\%V_{\text{Bur}}$) of 72.6%. While current efforts are focused on the preparation of low-coordinate transition metal complexes (*i.e.*, with $\text{Pd}(0)$), $^{\text{Me}}\text{ITr}$ may find applications in the stabilization of main group hydrides. For example, while NHC stabilized $\text{In}(\text{III})$ hydrides are known (*e.g.*, $\text{ImMe}_2^i\text{Pr}_2 \cdot \text{InH}_3$),¹⁴ a one-coordinate $\text{In}(\text{I})$ hydride has not been reported to the best of my knowledge. It is thought that known $\text{In}(\text{I})$ -hydrides (*e.g.*, $\{\text{HC}(\text{NDipp})_2\}_2\text{InH}$)¹⁵ are, at least in part, stabilized by sterically-encapsulating the $\text{In}-\text{H}$ moiety as this prevents $\text{In}-\text{H}-\text{In}$ bridging from occurring. The preparation of the precursor $^{\text{Me}}\text{ITr} \cdot \text{InCl}$ should be relatively straightforward and achievable by simply combining $^{\text{Me}}\text{ITr}$ and InCl in Et_2O . With $^{\text{Me}}\text{ITr} \cdot \text{InCl}$ in hand one may be able to prepare $^{\text{Me}}\text{ITr} \cdot \text{InH}$ by simple hydride/heteroatom metathesis with

HBpin (pin = pinacolate). Two alternative methods to prepare $^{\text{Me}}\text{ITr}\cdot\text{InH}$ could involve treating $^{\text{Me}}\text{ITr}\cdot\text{InO}^t\text{Bu}$ or $^{\text{Me}}\text{ITr}\cdot\text{InCp}$, with HBpin,^{14,16} as shown in Scheme 7.6.



Scheme 7.6. Proposed synthetic routes to $^{\text{Me}}\text{ITr}\cdot\text{InH}$, a monocoordinated In(I)-hydride.

7.1 References

1. A. J. Arduengo III, F. Davidson, H. V. Rasika Dias, J. R. Goerlich, D. Khasnis, W. J. Marshall, T. K. Prakasha, *J. Am. Chem. Soc.* **1997**, *119*, 12742–12749.
2. For select examples of cyclic Group 14 and Group 15 diradicaloid species supported by organic fragments, see: a) M. K. Sharma, D. Rottschäfer, T. Glodde, B. Neumann, H.-G. Stammler, R. S. Ghadwal, *Angew. Chem. Int. Ed.* **2021**, *60*, 6414–6418; b) H. Steffenfauseweh, Y. V. Vishnevsky, B. Neumann, H.-G. Stammler, D. M. Andrada, R. S. Ghadwal, *Angew. Chem. Int. Ed.* **2022**, *61*, e202207415; c) M. K. Sharma, F. Ebeler, T. Glodde, B. Neumann, H.-G. Stammler, R. S. Ghadwal, *J. Am. Chem. Soc.* **2021**, *143*, 121–125; d) D. Rottschäfer, B. Neumann, H.-G. Stammler, R. S. Ghadwal, *Chem. Eur. J.* **2017**, *23*, 9044–9047; e) Z. Li, X. Chen, D. M. Andrada, G. Frenking, Z. Benkö, Y. Li, J. R. Harmer, C.-Y. Su, H. Grützmacher, *Angew. Chem. Int. Ed.* **2017**, *56*, 5744–5749.
3. a) R. J. Wright, A. D. Phillips, T. L. Allen, W. H. Fink, P. P. Power, *J. Am. Chem. Soc.* **2002**, *125*, 1694–1695; b) R. J. Wright, M. Brynda, J. C. Fettinger, A. R. Betzer, P. P. Power, *J. Am. Chem. Soc.* **2006**, *128*, 12498–12509.
4. J. D. Queen, S. Irvankoski, J. C. Fettinger, H. M. Tuononen, P. P. Power, *J. Am. Chem. Soc.* **2021**, *143*, 6351–6356.
5. a) C. Dohmeier, E. Baum, A. Ecker, R. Köppe, H. Schnöckel, *Organometallics* **1996**, *15*, 4702–4706; b) L. Denker, B. Trzaskowski, R. Frank, *Chem. Commun.* **2021**, *57*, 2816–2819; c) P. Dabringhaus, J. Willrett, I. Krossing, *Nat. Chem.* **2022**, *14*, 1151–1157; d) I.-A. Bischoff, S. Danés, P. Thoni, B. Morgenstern, D. M. Andrada, C. Müller, J. Lambert, E. C. J. Gielßelmann, M. Zimmer, A. Schäfer, *Nat. Chem.* **2024**, 10.1038/s41557-024-01531-y.

6. a) D. Sarkar, P. Vasko, A. F. Roper, A. E. Crumpton, M. M. D. Roy, L. P. Griffin, C. Bogle, S. Aldridge, *J. Am. Chem. Soc.* **2024**, *146*, 11792–11800; b) D. Sarkar, P. Vasko, T. Gluharev, L. P. Griffin, C. Bogle, J. Struijs, J. Tang, A. F. Roper, A. E. Crumpton, S. Aldridge, *Angew. Chem. Int. Ed.* **2024**, e202407427.
7. C. Ganesamoorthy, S. Loerke, C. Gemel, P. Jerabek, M. Winter, G. Frenking, R. A. Fischer, *Chem. Commun.* **2013**, *49*, 2858–2860.
8. C. A. Caputo, P. P. Power, *Organometallics* **2013**, *32*, 2278–2286.
9. a) R. J. Wright, A. D. Phillips, P. P. Power, *J. Am. Chem. Soc.* **2003**, *125*, 36, 10784–10785; b) T. Agou, K. Nagata, N. Tokitoh, *Angew. Chem. Int. Ed.* **2013**, *52*, 10818–10821.
10. M. M. D. Roy, E. Rivard, *Acc. Chem. Res.* **2017**, *50*, 2017–2025.
11. a) A. A. Omaña, R. Watt, Y. Zhou, M. J. Ferguson, E. Rivard, *Inorg. Chem.* **2022**, *61*, 16430–16440; b) B. L. Frenette, A. A. Omaña, M. J. Ferguson, Y. Zhou, E. Rivard, *Chem. Commun.* **2021**, *57*, 10895–10898.
12. a) M. Gupta, C. Hagen, R. J. Flesher, W. C. Kaska, C. M. Jensen, *Chem. Commun.* **1996**, 2083–2084; b) I. Göttker-Schnetmann, P. White, M. Brookhart, *J. Am. Chem. Soc.* **2004**, *126*, 1804–1811.
13. For an example of **PB** depositing Si and Ge films in solution, see: A. A. Omaña, R. K. Green, R. Kobayashi, Y. He, E. R. Antoniuk, M. J. Ferguson, Y. Zhou, J. G. C. Veinot, T. Iwamoto, A. Brown, E. Rivard, *Angew. Chem. Int. Ed.* **2021**, *60*, 228–231.
14. M. M. D. Roy, A. A. Omaña, A. S. S. Wilson, M. S. Hill, S. Aldridge, E. Rivard, *Chem. Rev.* **2021**, *121*, 12784–12965.

15. R. J. Baker, C. Jones, P. C. Junk, M. Kloth, *Angew. Chem. Int. Ed.* **2004**, *43*, 3852–3855.
16. J. Bykowski, J. Sinclair, J. Trach, M. J. Ferguson, E. Rivard, *Dalton Trans.* **2023**, *52*, 1602–1607.

Complete Bibliography

Chapter 1

1. W. C. Zeise, *Annalen der Physik* **1831**, *4*, 497–451.
2. a) M. Black, R. H. B. Mais, P. G. Owston, *Acta. Cryst.* **1969**, *B25*, 1753–1759; b) J. A. J. Jarvis, B. T. Kilbourn, P. G. Owston, *Acta. Cryst.* **1971**, *B27*, 366–372.
3. T. J. Kealy, P. L. Pauson, *Nature* **1951**, *168*, 1039–1040.
4. J. A. Osborn, F. H. Jardine, J. F. Young, G. Wilkinson, *J. Chem. Soc. A.* **1966**, 1711–1732.
5. a) L. Vaska, J. W. DiLuzio, *J. Am. Chem. Soc.* **1961**, *83*, 2784–2785; b) L. Vaska, J. W. DiLuzio, *J. Am. Chem. Soc.* **1962**, *84*, 679–680.
6. a) A. H. Janowicz, R. G. Bergman, *J. Am. Chem. Soc.* **1982**, *104*, 352–354; b) J. K. Hoyano, W. A. G. Graham, *J. Am. Chem. Soc.* **1982**, *104*, 3723–3725.
7. D. Seyferth, *Organometallics* **2001**, *20*, 1488–1498.
8. A. Stock, A. Brandt, H. Fischer, *Ber. Deut. Chemie. Ges. B.* **1925**, *58*, 643–657.
9. a) R. West, *Polyhedron* **2002**, *21*, 467–472; b) T. J. Hadlington, M. Driess, C. Jones, *Chem. Soc. Rev.* **2018**, *47*, 4176–4197.
10. P. P. Power, *Nature* **2010**, *436*, 171–177.
11. a) P. J. Davidson, M. F. Lappert, *J. Chem. Soc., Chem. Commun.* **1973**, 317a; b) D. E. Goldberg, D. E. Harris, M. F. Lappert, K. M. Thomas, *J. Chem. Soc., Chem. Commun.* **1976**, 261–262; c) P. J. Davidson, D. H. Harris, M. F. Lappert, *J. Chem. Soc., Dalton Trans.* **1976**,

2268–2274; d) P. B. Hitchcock, M. F. Lappert, S. J. Miles, A. J. Thorne, *J. Chem. Soc., Chem. Commun.* **1984**, 480–482.

12. R. West, M. J. Fink, J. Michl, *Science* **1981**, *214*, 1343–1344.

13. M. Yoshifuji, I. Shima, N. Inamoto, K. Hirotsu, T. Higuchi, *J. Am. Chem. Soc.* **1981**, *103*, 4587–4589.

14. G. H. Spikes, J. C. Fettinger, P. P. Power, *J. Am. Chem. Soc.* **2005**, *127*, 12232–12233.

15. G. C. Welch, R. R. San Juan, J. D. Masuda, D. W. Stephan, *Science* **2006**, *314*, 1124–1126.

16. D. J. Liptrot, P. P. Power, *Nat. Chem. Rev.* **2017**, *1*, 0004.

17. R. D. Miller, J. Michl, *Chem. Rev.* **1989**, *89*, 1359–1410.

18. F. S. Kipping, J. E. Sands, *J. Chem. Soc., Trans.* **1921**, *119*, 830–847.

19. T. J. Drahnak, J. Michl, R. West, *J. Am. Chem. Soc.* **1979**, *101*, 5427–5428.

20. a) A. G. Moiseev, W. J. Leigh, *Organometallics* **2007**, *26*, 6268–6276; b) A. G. Moiseev, W. J. Leigh, *Organometallics* **2007**, *26*, 6277–6289.

21. C. Dohmeier, C. Robl, M. Tacke, H. Schnöckel, *Angew. Chem. Int. Ed. Engl.* **1991**, *30*, 564–565.

22. D. Loos, E. Baum, A. Ecker, H. Schnöckel, A. J. Downs, *Angew. Chem. Int. Ed.* **1997**, *36*, 860–862.

23. a) R. D. Schluter, A. H. Cowley, D. A. Atwood, R. A. Jones, J. L. Atwood, *J. Coord. Chem.* **1993**, *30*, 25–28; b) W. Uhl, R. Graupner, M. Pohlmann, S. Pohl, W. Saak, *Chem. Ber.* **1996**,

- 129, 143–146; c) M. Bühler, G. Linti, *Z. Anorg. Allg. Chem.* **2006**, 632, 2453–2460; d) A. Seifert, G. Linti, *Eur. J. Inorg. Chem.* **2007**, 5080–5086.
24. a) E. O. Fischer, H. P. Hofmann, *Angew. Chem.* **1957**, 69, 639–640; b) O. T. Beachley, J. C. Pazik, T. E. Glassman, M. R. Churchill, J. C. Fettingner, R. Blom, *Organometallics* **1988**, 7, 1051–1059
25. For related work on $[\text{Tl}(\text{C}(\text{SiMe}_3)_3)_4]$, see: W. Uhl, S. U. Keimling, K. W. Klinkhammer, D. Schwarz, *Angew. Chem. Int. Ed.* **1997**, 36, 64–65.
26. S. T. Haubrich, P. P. Power, *J. Am. Chem. Soc.* **1998**, 120, 2202–2203.
27. M. Niemeyer, P. P. Power, *Angew. Chem. Int. Ed.* **1998**, 37, 1277–1279.
28. Z. Zhu, R. C. Fischer, B. D. Ellis, E. Rivard, W. A. Merrill, M. M. Olmstead, P. P. Power, J. D. Guo, S. Nagase, L. Pu, *Chem. Eur. J.* **2009**, 15, 5263–5272.
29. J. D. Queen, A. Lehmann, J. C. Fettingner, H. M. Tuononen, P. P. Power, *J. Am. Chem. Soc.* **2020**, 142, 20554–20559.
30. a) R. J. Wright, A. D. Phillips, N. J. Hardman, P. P. Power, *J. Am. Chem. Soc.* **2002**, 124, 8538–8539; b) N. J. Hardman, A. D. Phillips, P. P. Power, *J. Am. Chem. Soc.* **2003**, 125, 2667–2679; c) R. J. Wright, A. D. Phillips, S. Hino, P. P. Power, *J. Am. Chem. Soc.* **2005**, 127, 4794–4799.
31. a) C. A. Caputo, P. P. Power, *Organometallics* **2013**, 32, 2278–2286; b) H. B. Wedler, P. Wendelboe, P. P. Power, *Organometallics* **2018**, 37, 2929–2936; c) E. Rivard, *Chem. Soc. Rev.* **2016**, 45, 989–1003.

32. Z. Zhu, X. Wang, Y. Peng, H. Lei, J. C. Fettinger, E. Rivard, P. P. Power, *Angew. Chem. Int. Ed.* **2009**, *48*, 2031–2034.
33. a) R. J. Wright, A. D. Phillips, P. P. Power, *J. Am. Chem. Soc.* **2003**, *125*, 10784–10785; b) T. Agou, K. Nagata, N. Tokitoh, *Angew. Chem. Int. Ed.* **2013**, *52*, 10818–10821; c) For an example of a dialumene being trapped with an alkyne, see: C. Cui, X. Li, C. Wang, J. Zhang, J. Cheng, X. Zhu, *Angew. Chem. Int. Ed.* **2006**, *45*, 2245–2247.
34. T. Mennekes, P. Paetzold, R. Boese, D. Bläser, *Angew. Chem. Int. Ed. Engl.* **1991**, *30*, 173–175.
35. C.-J. Maier, H. Pritzkow, W. Siebert, *Angew. Chem. Int. Ed.* **1999**, *38*, 1666–1667.
36. W. J. Grigsby, P. P. Power, *J. Am. Chem. Soc.* **1996**, *118*, 7981–7988.
37. P. Schwerdtfeger, G. A. Heath, M. Dolg, M. A. Bennet, *J. Am. Chem. Soc.* **1992**, *114*, 7518–7527.
38. A. Sekiguchi, R. Kinjo, M. Ichinohe, *Science* **2004**, *305*, 1755–1757.
39. a) L. Pu, B. Twamley, P. P. Power, *J. Am. Chem. Soc.* **2000**, *122*, 3524–3525; b) A. D. Phillips, R. J. Wright, M. M. Olmstead, P. P. Power, *J. Am. Chem. Soc.* **2002**, *124*, 5930–5931; c) M. Stender, A. D. Phillips, R. J. Wright, P. P. Power, *Angew. Chem. Int. Ed.* **2002**, *41*, 1785–1787.
40. P. P. Power, *Organometallics* **2007**, *26*, 4362–4372.
41. M. Stürmann, M. Weidenbruch, K. W. Klinkhammer, F. Lissner, H. Marsmann, *Organometallics* **1998**, *17*, 4425–4428.
42. C. Shan, S. Yao, M. Driess, *Chem. Soc. Rev.* **2020**, *49*, 6733–6754.

43. M. J. S. Gynane, D. H. Harris, M. F. Lappert, P. P. Power, P. Rivère, M. Rivière-Baudet, *J. Chem. Soc., Dalton Trans.* **1977**, 2004–2009.
44. P. Jutzi, U. Holtmann, D. Kanna, C. Krüger, R. Blom, R. Gleiter, I. Hyla-Kyrspin, *Chem. Ber.* **1989**, *122*, 1629–1639.
45. M. Denk, R. Lennon, R. Hayashi, R. West, A. V. Belyakov, H. P. Verne, A. Haaland, M. Wagner, N. Metzler, *J. Am. Chem. Soc.* **1994**, *116*, 2691–2692.
46. M. Kira, S. Ishida, T. Iwamoto, C. Kabuto, *J. Am. Chem. Soc.* **1999**, *121*, 9722–9723.
47. a) P. Paetzold, *Pure Appl. Chem.* **1991**, *63*, 345–350; b) Z. X. Giustra, S.-Y. Liu, *J. Am. Chem. Soc.* **2018**, *140*, 1184–1194.
48. E. J. Little, M. M. Jones, *J. Chem. Educ.* **1960**, *37*, 231–233.
49. G. D. Piero, M. Cesari, G. Perego, S. Cucinella, E. Cernia, *J. Organomet. Chem.* **1977**, *129*, 289–298.
50. P. Paetzold, C. von Plotho, G. Schmid, R. Boese, B. Schrader, D. Bougeard, U. Pfeiffer, R. Gleiter, W. Schäfer, *Chem. Ber.* **1984**, *117*, 1089–1102.
51. R. J. Wright, A. D. Phillips, T. L. Allen, W. H. Fink, P. P. Power, *J. Am. Chem. Soc.* **2003**, *125*, 1694–1695.
52. J. D. Queen, S. Irvankoski, J. C. Fettinger, H. M. Tuononen, P. P. Power, *J. Am. Chem. Soc.* **2021**, *143*, 6351–6356.
53. M. N. Hopkinson, C. Richter, M. Schedler, F. Glorius, *Nature* **2014**, *510*, 485–496.
54. A. J. Arduengo III, R. L. Harlow, M. Kline, *J. Am. Chem. Soc.* **1991**, *113*, 361–363.

55. a) V. Nesterov, D. Reiter, P. Bag, P. Frisch, R. Holtzner, A. Porzelt, S. Inoue, *Chem. Rev.* **2018**, *118*, 9678–9842; b) M. Melaimi, R. Jazzar, M. Soleihavoup, G. Bertrand, *Angew. Chem. Int. Ed.* **2017**, *56*, 10046–10068.
56. A. A. D. Tulloch, A. A. Danopoulos, S. Kleinhenz, M. E. Light, M. B. Hursthouse, G. Eastham, *Organometallics* **2001**, *20*, 2027–2031.
57. V. Lavallo, Y. Canac, C. Präsang, B. Donnadiou, G. Bertrand, *Angew. Chem. Int. Ed.* **2005**, *44*, 5705–5709.
58. A. Gómez-Suárez, D. J. Nelson, S. P. Nolan, *Chem. Commun.* **2017**, *53*, 2650–2660.
59. a) H. Clavier, S. P. Nolan, *Chem. Commun.* **2010**, *46*, 841–861; b) L. Falivene, Z. Cao, A. Petta, L. Serra, A. Poater, R. Oliva, V. Scarano, L. Cavallo, *Nat. Chem.* **2019**, *11*, 872–879; c) A. Poater, B. Cosenza, A. Correa, S. Giudice, F. Ragone, V. Scarano, L. Cavallo, *Eur. J. Inorg. Chem.* **2009**, 1759–1766.
60. Y. Wang, B. Quillian, P. Wei, C. S. Wannere, Y. Xie, R. B. King, H. F. Schaefer III, P. v R. Schleyer, G. H. Robinson, *J. Am. Chem. Soc.* **2007**, *129*, 12412–12413.
61. H. Braunschweig, R. D. Dewhurst, K. Hammond, J. Mies, K. Radacki, A. Vargas, *Science* **2012**, *336*, 1420–1422.
62. A. C. Filippou, O. Chernov, G. Schnakenburg, *Angew. Chem. Int. Ed.* **2009**, *48*, 5687–5690.
63. M. M. D. Roy, E. Rivard, *Acc. Chem. Res.* **2017**, *50*, 2017–2025.
64. S. Ling-Chung, K. D. Sales, J. H. P. Utley, *J. Chem. Soc., Chem. Commun.* **1990**, 622–664.
65. M. Pareek, Y. Reddi, R. B. Sunoj, *Chem. Sci.* **2021**, *12*, 7973–7992.

66. S. M. I. Al-Rafia, A. C. Malcolm, S. K. Liew, M. J. Ferguson, R. McDonald, E. Rivard, *Chem. Commun.* **2011**, *47*, 6987–6989.
67. H. Böhme, F. Soldan, *Chem. Ber.* **1961**, *94*, 3109–3119.
68. P. P. Ponti, J. C. Baldwin, W. C. Kaska, *Inorg. Chem.* **1979**, *18*, 873–875.
69. U. Gruseck, M. Heuschmann, *Chem. Ber.* **1987**, *120*, 2053–2064.
70. a) N. Kuhn, H. Bohnen, J. Kreuzberg, D. Bläser, R. Boese, *J. Chem. Soc., Chem. Commun.* **1993**, 1136–1137; b) N. Kuhn, H. Bohnen, D. Bläser, R. Boese, *Chem. Ber.* **1994**, *127*, 1405–1407; c) N. Kuhn, H. Bohnen, G. Henkel, J. Kreuzberg, *Z. Naturforsch.* **1996**, *51b*, 1267–1278.
71. A. Dumrath, X-F. Wu, H. Neumann, A. Spannenberg, R. Jackstell, M. Beller, *Angew. Chem. Int. Ed.* **2010**, *49*, 8988–8992.
72. For select articles from the Rivard group on this topic, see: a) I. C. Watson, Y. Zhou, M. J. Ferguson, E. Rivard, *Z. Anorg. Allg. Chem.* **2022**, *68*, e202200082; b) I. C. Watson, M. J. Ferguson, E. Rivard, *Inorg. Chem.* **2021**, *60*, 18347–18359; c) N. Paisley, M. Lui, R. McDonald, M. J. Ferguson, E. Rivard, *Dalton Trans.* **2016**, *45*, 9860–9870; d) M. W. Lui, O. Shynkaruk, M. S. Oakley, R. Sinelnikov, R. McDonald, M. J. Ferguson, A. Meldrum, M. Klobukowski, E. Rivard, *Dalton Trans.* **2017**, *46*, 5946–5954.
73. For select reviews and articles, see: a) R. S. Ghadwal, *Acc. Chem. Res.* **2022**, *55*, 457–470; b) P. Varava, Z. Dong, R. Scopelliti, F. Fadaei-Tirani, K. Severin, *Nat. Chem.* **2021**, *13*, 1055–1060; c) L. Y. M. Eymann, P. Varava, A. M. Shved, B. F. E. Curchod, Y. Liu, O. M. Planes, A. Sienkiewicz, R. Scopelliti, F. F. Tirani, K. Severin, *J. Am. Chem. Soc.* **2019**, *141*, 17112–

17116; d) M. K. Sharma, S. Blomeyer, B. Neumann, H.-G. Stammler, M. van Gastel, A. Hinz, R. S. Ghadwal, *Angew. Chem. Int. Ed.* **2019**, *58*, 17599–17603.

74. For select reviews and articles, see: a) M. G. S. Deepika, R. Dandela, V. Dhayalan, *Chem. Eur. J.* **2023**, *29*, e202302106; b) C. Hering-Junghans, I. C. Watson, M. J. Ferguson, R. McDonald, E. Rivard, *Dalton Trans.* **2017**, *46*, 7150–7153; c) I. C. Watson, Y. Zhou, M. J. Ferguson, M. Kranzlein, B. Rieger, E. Rivard, *Z. Anorg. Allen. Chem.* **2020**, *646*, 547–551; d) C. Czysch, T. Dinh, Y. Fröder, L. Bixenmann, P. Komforth, A. Balint, H.-J. Räder, S. Naumann, L. Nuhn, *ACS Polym. Au* **2022**, *2*, 371–379.

75. K. Powers, C. Hering-Junghans, R. McDonald, M. J. Ferguson, E. Rivard, *Polyhedron* **2016**, *108*, 8–14.

76. Y. Wang, M. Y. Abraham, R. J. Gillard, D. R. Sexton, P. Wei, G. H. Robinson, *Organometallics* **2013**, *32*, 6639–6642.

77. M. M. Hansmann, P. W. Antoni, H. Pescht, *Angew. Chem. Int. Ed.* **2020**, *59*, 5782–5787.

78. D. Enders, K. Breuer, G. Raabe, J. Runsink, J. H. Teles, J.-P. Melder, K. Ebel, S. Brode, *Angew. Chem. Int. Ed. Engl.* **1995**, *34*, 1021–1023.

79. For related work by Matusoka and coworkers wherein they combined Enders' carbene with methyl methacrylate (MMA) to give a functionalized triazole NHO, see: S. Matsuoka, Y. Tochigi, K. Takagi, M. Suzuki, *Tetrahedron* **2012**, *68*, 9836–9841.

80. Z. Li, P. Ji, J.-P. Cheng, *J. Org. Chem.* **2021**, *86*, 2974–2985.

81. a) C. A. Tolman, *Chem. Rev.* **1977**, *77*, 313–348; b) T. Dröge, F. Glorius, *Angew. Chem. Int. Ed.* **2010**, *49*, 6940–6952.

82. For earlier reports on NHO–rhodium complexes; see: a) A. Fürstner, M. Alcarazo, R. Goddard, C. W. Lehmann, *Angew. Chem. Int. Ed.* **2008**, *47*, 3210–3214; b) S. Kronig, P. G. Jones, M. Tamm, *Eur. J. Inorg. Chem.* **2013**, 2301–2314.
83. A. Eitzinger, J. Reitz, P. W. Antoni, H. Mayr, A. R. Ofial, M. M. Hansmann, *Angew. Chem. Int. Ed.* **2023**, *62*, e202309790.
84. A. El-Hellani, J. Monot, R. Guillot, C. Bour, V. Gandon, *Inorg. Chem.* **2013**, *52*, 506–514.
85. S. M. I. Al-Rafia, M. R. Momeni, M. J. Ferguson, R. McDonald, A. Brown, E. Rivard, *Organometallics* **2013**, *32*, 6658–6665.
86. Y. W. Wang, M. Y. Abraham, R. J. Gilliard, D. R. Sexton, P. Wei, G. H. Robinson, *Organometallics* **2013**, *32*, 6639–6642.
87. R. J. Ghadwal, C. J. Schürmann, F. Engelhardt, C. Steinmetzger, *Eur. J. Inorg. Chem.* **2014**, 4921–4926.
88. M. W. Lui, C. Merten, M. J. Ferguson, R. McDonald, Y. Xu, E. Rivard, *Inorg. Chem.* **2015**, *54*, 2040–2049.
89. C. Hering-Junghans, P. Andreiuk, M. J. Ferguson, R. McDonald, E. Rivard, *Angew. Chem. Int. Ed.* **2017**, *56*, 6272–6275.
90. M. M. D. Roy, M. J. Ferguson, R. McDonald, Y. Zhou, E. Rivard, *Chem. Sci.* **2019**, *10*, 6476–9481.
91. D. Rottschäfer, M. K. Sharma, B. Neumann, H.-G. Stammer, D. M. Andrada, R. S. Ghadwal, *Chem. Eur. J.* **2019**, *25*, 8127–8134.
92. L. L. Liu, L. L. Cao, J. Zhang, D. W. Stephan, *Angew. Chem. Int. Ed.* **2019**, *58*, 273–277.

Chapter 2

1. a) P. J. Davidson, M. F. Lappert, *J. Chem. Soc., Chem. Commun.* **1973**, 317a; b) D. E. Goldberg, D. E. Harris, M. F. Lappert, K. M. Thomas, *J. Chem. Soc., Chem. Commun.* **1976**, 261–262; c) P. J. Davidson, D. H. Harris, M. F. Lappert, *J. Chem. Soc., Dalton Trans.* **1976**, 2268–2274; d) P. B. Hitchcock, M. F. Lappert, S. J. Miles, A. J. Thorne, *J. Chem. Soc., Chem. Commun.* **1984**, 480–482.

2. For select reviews and articles, see: a) R. C. Fischer, P. P. Power, *Chem. Rev.* **2010**, *110*, 3877–3923; b) Y. Wang, G. H. Robinson, *Inorg. Chem.* **2011**, *50*, 12326–12337; c) R. S. Ghadwal, R. Azhakar, H. W. Roesky, *Acc. Chem. Res.* **2013**, *46*, 444–456; d) J. Brand, H. Braunschweig, S. S. Sen, *Acc. Chem. Res.* **2014**, *47*, 180–191; e) G. He, O. Shynkaruk, M. W. Lui, E. Rivard, *Chem. Rev.* **2014**, *114*, 7815–7880; f) A. V. Protchenko, M. P. Blake, A. D. Schwarz, C. Jones, P. Mountford, S. Aldridge, *Organometallics* **2015**, *34*, 2126–2129; g) C. Präsang, D. Scheschkewitz, *Chem. Soc. Rev.* **2016**, *45*, 900–921; h) E. Rivard, *Chem. Soc. Rev.* **2016**, *45*, 989–1003; i) T. Ochiai, D. Franz, S. Inoue, *Chem. Soc. Rev.* **2016**, *45*, 6327–6344; j) M. Melaimi, R. Jazzar, M. Soleilhavoup, G. Bertrand, *Angew. Chem. Int. Ed.* **2017**, *56*, 10046–10068; k) J. Schneider, C. P. Sindlinger, K. Eichele, H. Schubert, L. Wesemann, *J. Am. Chem. Soc.* **2017**, *139*, 6542–6545; l) S. Yao, Y. Xiong, M. Driess, *Acc. Chem. Res.* **2017**, *50*, 2026–2037; m) V. Nesterov, D. Reiter, P. Bag, P. Frisch, R. Holzner, A. Porzelt, S. Inoue, *Chem. Rev.* **2018**, *118*, 9678–9842; n) M.-A. Légaré, M. Rang, G. Bélanger-Chabot, J. I. Schweizer, I. Krummenacher, R. Bertermann, M. Arrowsmith, M. C. Holthausen, H. Braunschweig, *Science* **2019**, *363*, 1329–1332; o) Y. Wang, A. Kostenko, T. J. Hadlington, M.-P. Luecke, S. Yao, M. Driess, *J. Am. Chem. Soc.* **2019**, *141*, 626–634.

3. a) N. Tokitoh, K. Manmaru, R. Okazaki, *Organometallics* **1994**, *13*, 167–171; b) N. Tokitoh, M. Saito, R. Okazaki, *J. Am. Chem. Soc.* **1993**, *115*, 2065–2066; c) S. Brooker, J.-K. Buijink, F. T. Edelman, *Organometallics* **1991**, *10*, 25–26.

4. For example: a) K. A. Miller, T. W. Watson, J. E. Bender, M. M. Banaszak Holl, J. W. Kampf, *J. Am. Chem. Soc.* **2001**, *123*, 982–983; b) Y. Peng, B. D. Ellis, X. Wang, P. P. Power, *J. Am. Chem. Soc.* **2008**, *130*, 12268–12269; c) S. K. Mandal, H. W. Roesky, *Acc. Chem. Rev.* **2011**, *45*, 298–307; d) K. Inomata, T. Watanabe, Y. Miyazaki, H. Tobita, *J. Am. Chem. Soc.* **2015**, *137*, 11935–11937; e) A. V. Protchenko, J. I. Bates, L. M. A. Saleh, M. P. Blake, A. D. Schwarz, E. L. Kolychev, A. L. Thompson, C. Jones, P. Mountford, S. Aldridge, *J. Am. Chem. Soc.* **2016**, *138*, 4555–4564; f) M. M. D. Roy, S. Fujimori, M. J. Ferguson, R. McDonald, N. Tokitoh, E. Rivard, *Chem. Eur. J.* **2018**, *24*, 14392–14399; g) T. J. Hadlington, M. Driess, C. Jones, *Chem. Soc. Rev.* **2018**, *47*, 4176–4197; h) B.-X. Leong, J. Lee, Y. Li, M.-C. Yang, C.-K. Siu, M.-D. Su, C.-W. So, *J. Am. Chem. Soc.* **2019**, *141*, 17629–17636.

5. For related acyclic silylenes, see: a) A. V. Protchenko, K. H. Birj Kumar, D. Dange, A. D. Schwarz, D. Vidovic, C. Jones, N. Kaltsoyannis, P. Mountford, S. Aldridge, *J. Am. Chem. Soc.* **2012**, *134*, 6500–6503; b) B. D. Reken, T. M. Brown, J. C. Fettinger, H. M. Tuononen, P. P. Power, *J. Am. Chem. Soc.* **2012**, *134*, 6504–6507; c) Cyclic diorganosilylenes are also known: M. Kira, S. Ishida, T. Iwamoto, C. Kabuto, *J. Am. Chem. Soc.* **1999**, *121*, 9722–9723; d) M. Asay, S. Inoue, M. Driess, *Angew. Chem. Int. Ed.* **2011**, *50*, 9589–9592.

6. a) D. Seyferth, *Organometallics* **2001**, *40*, 4978–4992; b) For a recent example of generating $[\text{Me}_2\text{Si}]_n$ from an isolable complex of SiMe_2 , see: A. A. Omaña, R. K. Green, R. Kobayashi, Y. He, E. R. Antoniuk, M. J. Ferguson, Y. Zhou, J. G. C. Veinot, T. Iwamoto, A. Brown, E.

Rivard, *Angew. Chem. Int. Ed.* **2021**, *60*, 228–231; c) T. J. Drahnak, J. Michl, R. West, *J. Am. Chem. Soc.* **1979**, *101*, 5427–5428.

7. P. Jutzi, U. Holtmann, D. Kanne, C. Krüger, R. Blom, R. Gleiter, I. Hyla-Kryspin, *Chem. Ber.* **1989**, *122*, 1629–1939.

8. a) A. V. Protchenko, A. D. Schwarz, M. P. Blake, C. Jones, N. Kaltsoyannis, P. Mountford, S. Aldridge, *Angew. Chem. Int. Ed.* **2012**, *52*, 568–571; b) T. J. Hadlington, J. A. B. Adballa, R. Tirfoin, S. Aldridge, C. Jones, *Chem. Commun.* **2016**, *52*, 1717–1720; c) D. Wendel, A. Porzelt, F. A. D. Herz, D. Sarkar, C. Jandl, S. Inoue, B. Rieger, *J. Am. Chem. Soc.* **2017**, *139*, 8134–8137; d) D. Wendel, D. Reiter, A. Porzelt, P. J. Altmann, S. Inoue, B. Rieger, *J. Am. Chem. Soc.* **2017**, *139*, 17193–17198; e) Y. K. Loh, L. Ying, M. Á. Fuentes, D. C. H. Do, S. Aldridge, *Angew. Chem. Int. Ed.* **2019**, *58*, 4847–4851; f) M. M. D. Roy, M. J. Ferguson, R. McDonald, Y. Zhou, E. Rivard, *Chem. Sci.* **2019**, *10*, 6476–6481; g) S. Fujimori, S. Inoue, *Eur. J. Inorg. Chem.* **2020**, 3131–3142; h) C. Shan, S. Yao, M. Driess, *Chem. Soc. Rev.* **2020**, *49*, 6733–6754; h) C. Ganesamoorthy, J. Schoening, C. Wölper, L. Song, P. R. Schreiner, S. Schulz, *Nat. Chem.* **2020**, *12*, 608–614; j) D. Reiter, R. Holzner, A. Porzelt, P. Frisch, S. Inoue, *Nat. Chem.* **2020**, *12*, 1131–1135.

9. a) M. M. D. Roy, E. Rivard, *Acc. Chem. Rev.* **2017**, *50*, 2017–2025; b) S. M. I. Al-Rafia, M. J. Ferguson, E. Rivard, *Inorg. Chem.* **2011**, *50*, 10543–10545; c) C. Hering-Junghans, P. Andreiuk, M. J. Ferguson, R. McDonald, E. Rivard, *Angew. Chem. Int. Ed.* **2017**, *56*, 6272–6275.

10. a) N. Kuhn, M. Göhner, M. Siemann, *Z. Anorg. Allg. Chem.* **2002**, *628*, 1108–1115; b) R. S. Ghadwal, *Acc. Chem. Res.* **2022**, *55*, 457–470; c) L. Y. M. Eymann, P. Varava, A. M. Shved,

B. F. E. Curchod, Y. Liu, O. M. Planes, A. Sienkiewicz, R. Scopelliti, F. F. Tirani, K. Severin, *J. Am. Chem. Soc.* **2019**, *141*, 17112–17116; d) A. Causero, H. Elsen, J. Pahl, S. Harder, *Angew. Chem. Int. Ed.* **2017**, *56*, 6906–6910.

11. For related work on *N*-heterocyclic imines, see: a) T. Ochiai, D. Franz, S. Inoue, *Chem. Soc. Rev.* **2016**, *45*, 6327–6344; b) M. W. Lui, C. Merten, M. J. Ferguson, R. McDonald, Y. Xu, E. Rivard, *Inorg. Chem.* **2015**, *54*, 2040–2049.

12. a) R. S. Ghawdal, S. O. Reichmann, F. Engelhardt, D. M. Andrada, G. Frenking, *Chem. Commun.* **2013**, *49*, 9440–9442; b) K. Powers, C. Hering-Junghans, R. McDonald, M. J. Ferguson, E. Rivard, *Polyhedron* **2016**, *108*, 8–18; c) R. S. Ghawdal, *Dalton Trans.* **2016**, *45*, 16081–16095; d) R. D. Crocker, T. B. Nguyen, *Chem. Eur. J.* **2016**, *22*, 2208–2213; e) M. A. Wünsche, T. Witteler, F. Dielmann, *Angew. Chem. Int. Ed.* **2018**, *57*, 7234–7239; f) M. K. Sharma, S. Blomeyer, B. Neumann, N.-G. Stammer, M. von Gastel, A. Hinz, R. S. Ghadwal, *Angew. Chem. Int. Ed.* **2019**, *58*, 17599–17603; g) S. Naumann, *Chem. Commun.* **2019**, *55*, 11658–11670; h) P. Gupta, J.-E. Siewart, T. Wellnitz, M. Fischer, W. Baumann, T. Beweries, C. Hering-Junghans, *Dalton Trans.* **2021**, *50*, 1838–1844.

13. T. X. Gentner, G. Ballmann, J. Pahl, H. Elsen, S. Harder, *Organometallics* **2018**, *37*, 4473–4480.

14. NHOs are known to react with I₂ to form [(NHO)I]₃ salts: N. Kuhn, H. Bohnen, G. Henkel, J. Kreutzberg, *Z. Naturforsch.* **1996**, *51b*, 1267–1278.

15. S. Evjen, A. Fiksdahl, *Synth. Commun.* **2017**, *47*, 1392–1399.

16. R. S. Ghadwal, H. W. Roesky, S. Merkel, J. Henn, D. Stalke, *Angew. Chem. Int. Ed.* **2009**, *48*, 5683–5686.

17. A. C. Filippou, O. Chernov, G. Schnakenburg, *Angew. Chem. Int. Ed.* **2009**, *48*, 5687–5690.
18. J. I. Schweizer, A. G. Sturm, T. Porsch, M. Berger, M. Bolte, N. Auner, M. C. Holtausen, *Z. Anorg. Allg. Chem.* **2018**, *114*, 982–988.
19. C. Marschner, *Eur. J. Inorg. Chem.* **1998**, 221–226.
20. A. B. Pangborn, M. A. Giardello, R. H. Grubbs, R. K. Rosen, F. J. Timmers, *Organometallics* **1996**, *15*, 1518–1520.
21. S. J. Ryan, S. D. Schimler, D. C. Bland, M. S. Sanford, *Org. Lett.* **2017**, *17*, 1866–1869.
22. G. Blankson, A. K. Parhi, M. Kaul, D. S. Pilch, E. J. LaVoie, *Eur. J. Med. Chem.* **2019**, *178*, 30–38.
23. H. Hope, *Prog. Inorg. Chem.* **1994**, *41*, 1–19.
24. G. M. Sheldrick, *Acta Crystallogr.* **2015**, *A71*, 3–8.
25. G. M. Sheldrick, *Acta Crystallogr.* **2015**, *C71*, 3–8.

Chapter 3

1. E. O. Fischer, H. P. Hofmann, *Angew. Chem.* **1957**, *69*, 639–640.
2. a) O. T. Beachley, J. C. Pazik, T. E. Glassman, M. R. Churchill, J. C. Fettinger, R. Blom, *Organometallics* **1988**, *7*, 1051–1059; b) O. T. Beachley, R. Blom, M. R. Churchill, K. Kaegri, J. C. Fettinger, J. C. Pazik, L. Victoriano, *Organometallics* **1989**, *8*, 346–356.
3. O. T. Beachley, M. R. Churchill, J. C. Fettinger, J. C. Pazik, L. Victoriano, *J. Am. Chem. Soc.* **1986**, *108*, 4666–4668.

4. M. S. Hill, P. B. Hitchcock, R. Pongtavornpinyo, *Science* **2006**, *311*, 1904–1907.
5. R. J. Wright, A. D. Phillips, N. J. Hardman, P. P. Power, *J. Am. Chem. Soc.* **2002**, *124*, 8538–8539.
6. S. T. Haubrich, P. P. Power, *J. Am. Chem. Soc.* **1998**, *120*, 2202–2203.
7. a) R. D. Schluter, A. H. Cowley, D. A. Atwood, R. A. Jones, J. L. Atwood, *J. Coord. Chem.* **1993**, *30*, 25–28; b) W. Uhl, R. Graupner, M. Pohlmann, S. Pohl, W. Saak, *Chem. Ber.* **1996**, *129*, 143–146; c) M. Bühler, G. Linti, *Z. Anorg. Allg. Chem.* **2006**, *632*, 2453–2460; d) For a novel cyclic $[\text{RIn}]_4^{2-}$ species, see: A. Protchenko, J. Urbano, J. A. B. Abdalla, J. Campos, D. Vidovic, A. D. Schwarz, M. P. Blake, P. Mountford, C. Jones, S. Aldridge, *Angew. Chem. Int. Ed.* **2017**, *56*, 15098–15102; e) See also: O. Kysliak, S. H. F. Schreiner, N. Grabicki, P. Liebing, F. Weigend, O. Dumele, R. Kretschmer, *Angew. Chem. Int. Ed.* **2022**, *61*, e202206963.
8. a) M. M. D. Roy, E. Rivard, *Acc. Chem. Rev.* **2017**, *50*, 2017–2025; b) S. M. I. Al-Rafia, M. J. Ferguson, E. Rivard, *Inorg. Chem.* **2011**, *50*, 10543–10545; c) C. Hering-Junghans, P. Andreiuk, M. J. Ferguson, R. McDonald, E. Rivard, *Angew. Chem. Int. Ed.* **2017**, *56*, 6272–6275.
9. a) N. Kuhn, M. Göhner, M. Siemann, *Z. Anorg. Allg. Chem.* **2002**, *628*, 1108–1115; b) R. S. Ghadwal, *Acc. Chem. Res.* **2022**, *55*, 457–470; c) L. Y. M. Eymann, P. Varava, A. M. Shved, B. F. E. Curchod, Y. Liu, O. M. Planes, A. Sienkiewicz, R. Scopelliti, F. F. Tirani, K. Severin, *J. Am. Chem. Soc.* **2019**, *141*, 17112–17116; d) A. Causero, H. Elsen, J. Pahl, S. Harder, *Angew. Chem. Int. Ed.* **2017**, *56*, 6906–6910.

10. For related work on formally dianionic NHOs, see: a) Z. Li, X. Chen, D. M. Andrada, G. Frenking, Z. Benkő, Y. Li, J. R. Harmer, C.-Y. Su, H. Grützmacher, *Angew. Chem. Int. Ed.* **2017**, *56*, 5744–5749; b) H. Steffenfausewach, Y. V. Vishnevskiy, B. Neumann, H.-G. Stammer, D. M. Andrada, R. S. Ghadwal, *Angew. Chem. Int. Ed.* **2022**, *61*, e202207415.
11. For related work on *N*-heterocyclic imines, see: a) T. Ochiai, D. Franz, S. Inoue, *Chem. Soc. Rev.* **2016**, *45*, 6327–6344; b) M. W. Lui, C. Merten, M. J. Ferguson, R. McDonald, Y. Xu, E. Rivard, *Inorg. Chem.* **2015**, *54*, 2040–2049.
12. M. M. D. Roy, S. R. Baird, E. Dornsiepen, L. A. Paul, L. Miao, M. J. Ferguson, Y. Zhou, I. Siewart, E. Rivard, *Chem. Eur. J.* **2021**, *27*, 8572–8579.
13. H. W. Moon, J. Cornella, *ACS Catal.* **2022**, *12*, 1382–1393.
14. a) M. M. D. Roy, A. A. Omaña, A. S. S. Wilson, M. S. Hill, S. Aldridge, E. Rivard, *Chem. Rev.* **2021**, *121*, 12784–12965; b) T. Chu, G. I. Nikonov, *Chem. Rev.* **2018**, *118*, 3608–3680.
15. For examples of aNHOs bound to transition metals, see: a) I. C. Watson, M. J. Ferguson, E. Rivard, *Inorg. Chem.* **2021**, *60*, 18347–18359; b) I. C. Watson, Y. Zhou, M. J. Ferguson, E. Rivard, *Z. Anorg. Allg. Chem.* **2022**, *648*, e202200082.
16. For similar reactions involving the substitution of Cp (and derivatives), see: a) C. Dohmeier, E. Baum, A. Ecker, R. Köppe, H. Schnöckel, *Organometallics* **1996**, *15*, 4702–4706; b) L. Denker, B. Trzaskowski, R. Frank, *Chem. Commun.* **2021**, *57*, 2816–2819; c) P. Dabringhaus, J. Willrett, I. Krossing, *Nat. Chem.* **2022**, *14*, 1151–1157.
17. K. Powers, C. Hering-Junghans, R. McDonald, M. J. Ferguson, E. Rivard, *Polyhedron* **2016**, *108*, 8–14.

18. For related work on [RGa]₄ tetramers, see: A. Seifert, G. Linti, *Eur. J. Inorg. Chem.* **2007**, 5080–5086.
19. A. V. Protchneko, D. Dange, J. R. Harmer, C. Y. Tang, A. D. Schwarz, M. J. Kelly, N. Phillips, R. Tirfoin, K. Hassomal Birjkumar, C. Jones, N. Kaltsoyannis, P. Mountford, S. Aldridge, *Nat. Chem.* **2014**, *6*, 315–319.
20. a) R. J. Wright, A. D. Phillips, T. L. Allen, W. H. Fink, P. P. Power, *J. Am. Chem. Soc.* **2003**, *125*, 1694–1695; b) R. C. Fischer, P. P. Power, *Chem. Rev.* **2010**, *110*, 3877–3923.
21. T. B. Ditri, B. J. Fox, C. E. Moore, A. L. Rheingold, J. S. Figueroa, *Inorg. Chem.* **2009**, *48*, 8362–8375.
22. M. D. Anker, M. Lein, M. P. Coles, *Chem. Sci.* **2019**, *10* 1212–1218.
23. A. B. Pangborn, M. A. Giardello, R. H. Grubbs, R. K. Rosen, F. J. Timmers, *Organometallics* **1996**, *15*, 1518–1520.
24. I. C. Watson, A. Schumann, H. Yu, E. C. Davy, R. McDonald, M. J. Ferguson, C. Hering-Junghans, E. Rivard, *Chem. Eur. J.* **2019**, *25*, 9678–9690.
25. O. T. Beachley, J. C. Pazik, T. E. Glassman, M. R. Churchill, J. C. Fettinger, R. Blom, *Organometallics* **1988**, *7*, 1051–1059.
26. H. Hope, *Prog. Inorg. Chem.* **1994**, *41*, 1–19.
27. G. M. Sheldrick, *Acta Crystallogr.* **2015**, *A71*, 3–8.
28. G. M. Sheldrick, *Acta Crystallogr.* **2015**, *C71*, 3–8.

29. M. J. Frisch, G. W. Trucks, H. B. Schlegel, G. E. Scuseria, M. A. Robb, J. R. Cheeseman, G. Scalmani, V. Barone, G. A. Petersson, H. Nakatsuji, X. Li, M. Caricato, A. V. Marenich, J. Bloino, B. G. Janesko, R. Gomperts, B. Mennucci, H. P. Hratchian, J. V. Ortiz, A. F. Izmaylov, J. L. Sonnenberg, D. Williams-Young, F. Ding, F. Lipparini, F. Egidi, J. Goings, B. Peng, A. Petrone, T. Henderson, D. Ranasinghe, V. G. Zakrzewski, J. Gao, N. Rega, G. Zheng, W. Liang, M. Hada, M. Ehara, K. Toyota, R. Fukuda, J. Hasegawa, M. Ishida, T. Nakajima, Y. Honda, O. Kitao, H. Nakai, T. Vreven, K. Throssell, J. A. Montgomery, Jr., J. E. Peralta, F. Ogliaro, M. J. Bearpark, J. J. Heyd, E. N. Brothers, K. N. Kudin, V. N. Staroverov, T. A. Keith, R. Kobayashi, J. Normand, K. Raghavachari, A. P. Rendell, J. C. Burant, S. S. Iyengar, J. Tomasi, M. Cossi, J. M. Millam, M. Klene, C. Adamo, R. Cammi, J. W. Ochterski, R. L. Martin, K. Morokuma, O. Farkas, J. B. Foresman, D. J. Fox, Gaussian 16, Revision A. 03, Gaussian Inc., Wallingford CT, 2016.

30. a) C. Lee, W. Yang, R. G. Parr, *Phys. Rev. B* **1988**, *37*, 785–789.; b) A. D. Becke, *Phys. Rev. A* **1988**, *38*, 3098–3100; c) P. J. Stephens, F. J. Devlin, C. F. Chabalowski, M. J. Frisch, *J. Phys. Chem.* **1994**, *98*, 11623–11627.

31. T. H. Dunning, *J. Chem. Phys.* **1989**, *90*, 1007–1023.

32. K. A. Peterson, *J. Chem. Phys.* **2003**, *119*, 11099–11123.

33. a) B. P. Pritchard, D. Altarawy, B. Didier, T. D. Gibson, T. L. Windus, *J. Chem. Inf. Model.* **2019**, *59*, 4814–4820; b) D. J. Feller *J. Comput. Chem.* **1996**, *17*, 1571–1586; c) K. L. Schuchardt, B. T. Didier, T. Elsethagen, L. Sun, V. Gurumoorthi, J. Chase, J. Li, T. L. Windus, *J. Chem. Inf. Model.* **2007**, *47*, 1045–1052.

34. W. Humphrey, A. Dalke, and K. Schulten, *J. Molec. Graphics* **1996**, *14*, 33–38.

35. E. D. Glendening, J. K. Badenhoop, A. E. Reed, J. E. Carpenter, J. A. Bohmann, C. M. Morales, C. R. Landis, F. Weinhold, NBO 6.0, Theoretical Chemistry Institute, University of Wisconsin, Madison WI, 2013.
36. R. W. F. Bader, *Atoms in Molecules. A Quantum Theory*, Cambridge University Press: Oxford U. K., 1991.
37. T. A. Keith, AIMAll (Version 15.09.27), TK Gristmill Software, Overland Park KS, USA, 2015 (aim.tkgristmill.com).
38. J. Contreras-García, E. Johnson, S. Keinan, R. Chaudret, J.-P. Piquemal, D. Beratan, W. Yang, *J. Chem. Theory Comput.* **2011**, *7*, 625–632.

Chapter 4

1. A. Stock, A. Brandt, H. Fischer, *Ber. Deutsch. Chemie Ges. B* **1925**, *58*, 643–657.
2. E. C. Neeve, S. J. Geier, I. A. I. Mkhaliid, S. A. Westcott, T. B. Marder, *Chem. Rev.* **2016**, *116*, 9091–9161.
3. a) W. Biffar, H. Nöth, H. Pommerening, *Angew. Chem. Int. Ed. Engl.* **1980**, *19*, 56–57; b) K. Schlüter, A. Berndt, *Angew. Chem. Int. Ed. Engl.* **1980**, *19*, 57–58.
4. a) A. Moezzi, M. M. Olmstead, P. P. Power, *J. Am. Chem. Soc.* **1992**, *114*, 2715–2717; b) W. J. Grigsby, P. P. Power, *Chem. Commun.* **1996**, 2235–2236; c) H. Braunschweig, R. D. Dewhurst, J. O. C. Jiménez-Halla, E. Matito, J. H. Muessig, *Angew. Chem, Int. Ed.* **2018**, *57*, 412–416; d) S. Akiyama, S. Ikemoto, S. Muratsugu, M. Tada, M. Yamashita, *Organometallics* **2020**, *39*, 500–504.
5. a) T. J. Tague, L. Andrews, *J. Am. Chem. Soc.* **1994**, *116*, 4970–4976; b) L. B. Knight, K. Kerr, P. K. Miller, C. A. Arrington, *J. Phys. Chem.* **1995**, *99*, 16482–16484.

6. Y. Wang, B. Quillian, P. Wei, C. S. Wannere, Y. Xie, R. B. King, H. F. Schaefer III, P. v R. Schleyer, G. H. Robinson, *J. Am. Chem. Soc.* **2007**, *129*, 12412–12413.
7. For select reviews on boron-boron multiple-bonded species, see: a) H. Braunschweig, R. D. Dewhurst, *Angew. Chem. Int. Ed.* **2013**, *52*, 3574–3583; b) M. Arrowsmith, H. Braunschweig, T. E. Stennett, *Angew. Chem. Int. Ed.* **2017**, *56*, 96–115; c) R. Borthakur, K. Saha, S. Kar, S. Ghosh, *Coord. Chem. Rev.* **2019**, *399*, 213021.
8. a) S. R. Baird, E. Hupf, I. C. Watson, M. J. Ferguson, E. Rivard, *Chem. Commun.* **2023**, *59*, 2903–2906; b) I. C. Watson, Y. Zhou, M. J. Ferguson, E. Rivard, *Z. Anorg. Allg. Chem.* **2022**, *68*, e202200082; c) I. C. Watson, M. J. Ferguson, E. Rivard, *Inorg. Chem.* **2021**, *60*, 18347–18359; d) M. M. D. Roy, S. R. Baird, E. Dornsiepen, L. A. Paul, L. Miao, M. J. Ferguson, Y. Zhou, I. Siewert, E. Rivard, *Chem. Eur. J.* **2021**, *27*, 8572–8579.
9. a) T. Eisner, A. Kostenko, F. J. Kiefer, S. Inoue, *Chem. Commun.* **2024**, *60*, 558–561; b) H. Steffenfauseweh, Y. V. Vishnevskiy, B. Neumann, H.-G. Stammler, D. M. Andrada, R. S. Ghadwal, *Angew. Chem. Int. Ed.* **2022**, *61*, e202207415; c) M. K. Sharma, S. Blomeyer, T. Glodde, B. Neumann, H.-G. Stammler, A. Hinz, M. van Gastel, R. S. Ghadwal, *Chem. Sci.* **2020**, *11*, 1975–1984; d) M. K. Sharma, S. Blomeyer, B. Neumann, H.-G. Stammler, M. van Gastel, A. Hinz, R. S. Ghadwal, *Angew. Chem. Int. Ed.* **2019**, *58*, 17599–17603; e) R. S. Ghadwal, *Acc. Chem. Res.* **2022**, *55*, 457–470.
10. M. M. D. Roy, E. Rivard, *Acc. Chem. Res.* **2017**, *50*, 2017–2025.
11. K. Powers, C. Hering-Junghans, R. McDonald, M. J. Ferguson, M. J. Ferguson, E. Rivard, *Polyhedron* **2016**, *108*, 8–14.

12. Y. Wang, M. Y. Abraham, R. J. Gilliard, D. R. Sexton, P. Wei, G. H. Robinson, *Organometallics* **2013**, *32*, 6639–6642.
13. S. Muthaiah, D. C. Do, R. Ganguly, D. Vidović, *Organometallics* **2013**, *32*, 6718–6724.
14. M. Arrowsmith, J. Böhnke, H. Braunschweig, A. Deißberger, R. D. Dewhurst, W. C. Ewing, C. Hörl, J. Mies, J. H. Muessig, *Chem. Commun.* **2017**, *53*, 8265–8267.
15. Ligand activation of lithium amides, and lithium β -diketiminato ligands upon the addition to some element chlorides ECl_n ($E = Si, Ge, P$) is known, see: a) D. Dhara, T. Vijayakanth, M. K. Nayak, P. Kalita, R. Boomishankar, C. B. Yildiz, V. Chandrasekhar, A. Jana, *Dalton. Trans.* **2018**, *47*, 14411–14415. b) P. B. Hitchcock, M. F. Lappert, J. E. Nycz, *Chem. Commun.* **2003**, 1142–1143. c) B. Räge, F. Zülch, Y. Ding, J. Prust, H. W. Roesky, M. Notlemeyer, H.-G. Schmidt, *Z. Anorg. Allg. Chem.* **2001**, *627*, 836–840.
16. The formation of $Ar^{Dipp}PCl$ ($Ar^{Dipp} = 2,6-Dipp_2C_6H_3$) has been observed during the synthesis of $Ar^{Dipp}PCl_2$, see: B. Buster, A. A. Diaz, T. Graham, R. Khan, M. A. Khan, D. R. Powell, R. J. Wehmschulte, *Inorg. Chim. Acta* **2009**, *362*, 3465–3474.
17. a) S. Kumar, T. A. Shah, T. Punniyamurthy, *Org. Chem. Front.* **2021**, *8*, 4288–4314; b) R. Appel, *Angew. Chem. Int. Ed. Engl.* **1975**, *12*, 801–811.
18. S. C. Rasmussen, *ChemTexts* **2021**, *7*, 1–8.
19. C. Hering-Junghans, P. Andreiuk, M. J. Ferguson, R. McDonald, E. Rivard, *Angew. Chem. Int. Ed.* **2017**, *56*, 6272–6275.
20. C. Li, S. K. Møllerup, X. Wang, S. Wang, *Organometallics* **2018**, *37*, 3360–3367.
21. J. T. Goettel, H. Gao, S. Dotzauer, H. Braunschweig, *Chem. Eur. J.* **2020**, *26*, 1136–1143.

22. H. Braunschweig, S. Demeshko, W. C. Ewing, I. Krummenacher, B. B. Macha, J. D. Mattock, F. Meyer, J. Mies, M. Schäfer, A. Vargas, *Angew. Chem. Int. Ed.* **2016**, *55*, 7708–7711.
23. M. M. D. Roy, M. J. Ferguson, R. McDonald, Y. Zhou, E. Rivard, *Chem. Sci.* **2019**, *10*, 6476–6481.
24. H. Tsurugi, K. Mashima, *Acc. Chem. Res.* **2019**, *52*, 769–779.
25. H. Braunschweig, R. D. Dewhurst, K. Hammond, J. Mies, K. Radacki, A. Vargas, *Science* **2012**, *336*, 1420–1422.
26. E. E. Nahon, G. R. Nelmes, P. J. Brothers, J. Hicks, *Chem. Commun.* **2023**, *59*, 14281–14284.
27. I. C. Watson, A. Schumann, H. Yu, E. C. Davy, R. McDonald, M. J. Ferguson, C. Hering-Junghans, E. Rivard, *Chem. Eur. J.* **2019**, *25*, 9678–9690.
28. H. Braunschweig, A. Damme, R. D. Dewhurst, A. Vargas, *Nat. Chem.* **2013**, *5*, 115–121.
29. A. B. Pangborn, M. A. Giardello, R. H. Grubbs, R. K. Rosen, F. J. Timmers, *Organometallics* **1996**, *15*, 1518–1520.
30. H. Hope, *Prog. Inorg. Chem.* **1994**, *41*, 1–19.
31. G. M. Sheldrick, *Acta Crystallogr. Sect. A* **2015**, *71*, 3–8.
32. G. M. Sheldrick, *Acta Crystallogr. Sect. C* **2015**, *71*, 3–8.
33. M. J. Frisch, G. W. Trucks, H. B. Schlegel, G. E. Scuseria, M. A. Robb, J. R. Cheeseman, G. Scalmani, V. Barone, G. A. Petersson, H. Nakatsuji, X. Li, M. Caricato, A. V. Marenich, J.

Bloino, B. G. Janesko, R. Gomperts, B. Mennucci, H. P. Hratchian, J. V. Ortiz, A. F. Izmaylov, J. L. Sonnenberg, D. Williams-Young, F. Ding, F. Lipparini, F. Egidi, J. Goings, B. Peng, A. Petrone, T. Henderson, D. Ranasinghe, V. G. Zakrzewski, J. Gao, N. Rega, G. Zheng, W. Liang, M. Hada, M. Ehara, K. Toyota, R. Fukuda, J. Hasegawa, M. Ishida, T. Nakajima, Y. Honda, O. Kitao, H. Nakai, T. Vreven, K. Throssell, J. A. Montgomery, Jr., J. E. Peralta, F. Ogliaro, M. J. Bearpark, J. J. Heyd, E. N. Brothers, K. N. Kudin, V. N. Staroverov, T. A. Keith, R. Kobayashi, J. Normand, K. Raghavachari, A. P. Rendell, J. C. Burant, S. S. Iyengar, J. Tomasi, M. Cossi, J. M. Millam, M. Klene, C. Adamo, R. Cammi, J. W. Ochterski, R. L. Martin, K. Morokuma, O. Farkas, J. B. Foresman, D. J. Fox, Gaussian 16, Revision A. 03, Gaussian Inc., Wallingford CT, 2016.

34. a) C. Lee, W. Yang, R. G. Parr, *Phys. Rev. B* **1988**, *37*, 785–789; b) A. D. Becke, *Phys. Rev. A* **1988**, *38*, 3098–3100; c) P. J. Stephens, F. J. Devlin, C. F. Chabalowski, M. J. Frisch, *J. Phys. Chem.* **1994**, *98*, 11623–11627.

35. T. H. Dunning, *J. Chem. Phys.* **1989**, *90*, 1007–1023.

36. W. Humphrey, A. Dalke, K. Schulten, *J. Molec. Graphics* **1996**, *14*, 33–38.

Chapter 5

1. a) P. J. Frazen, J. S. Beck, A. T. Lynch, E. E. Remsen, L. G. Sneddon, *Chem. Mater.* **1990**, *2*, 96–97; b) D. J. Heldebrant, A. Karkamkar, N. J. Hess, M. Bowden, W. Rassat, F. Zheng, K. Rappe, T. Autrey, *Chem. Mater.* **2008**, *20*, 5332–5336; c) S. Frueh, R. Kellet, C. Mallery, T. Molter, W. S. Willis, C. King'ondeu, S. L. Suib, *Inorg. Chem.* **2011**, *50*, 783–792.

2. R. Kumar, A. Karkamkar, M. Bowden, T. Autrey, *Chem. Soc. Rev.* **2019**, *48*, 5350–5380.

3. a) P. Paetzold, *Pure Appl. Chem.* **1991**, *63*, 345–350; b) Z. X. Giustra, S.-Y. Liu, *J. Am. Chem. Soc.* **2018**, *140*, 1184–1194.
4. L. Winner, G. Bélanger-Chabot, M. A. Celik, M. Schäfer, H. Braunschweig, *Chem. Commun.* **2018**, *54*, 9349–9351.
5. P. Paetzold, C. von Plotho, G. Schmid, R. Boese, B. Schrader, D. Bougeard, U. Pfeiffer, R. Gleiter, W. Schäfer, *Chem. Ber.* **1984**, *117*, 1089–1102.
6. B. Kröckert, K–H. van Bonn, P. Paetzold, *Z. Anorg. Allg. Chem.* **2005**, *631*, 866–868.
7. a) H. Braunschweig, K. Radacki, D. Rais, K. Uttinger, *Angew. Chem. Int. Ed.* **2005**, *45*, 162–165; b) H. Braunschweig, K. Radacki, D. Rais, A. Schneider, F. Seeler, *J. Am. Chem. Soc.* **2007**, *129*, 10350–10351.
8. K. Ota, R. Kinjo, *J. Am. Chem. Soc.* **2021**, *143*, 11152–11159.
9. Y. Fan, J. Cui, L. Kong, *Eur. J. Org. Chem.* **2022**, e202201086.
10. A. K. Swarnakar, C. Hering-Junghans, K. Nagata, M. J. Ferguson, R. McDonald, N. Tokitoh, E. Rivard, *Angew. Chem. Int. Ed.* **2015**, *54*, 10666–10669.
11. B. L. Frenette, A. A. Omaña, M. J. Ferguson, Y. Zhou, E. Rivard, *Chem. Commun.* **2021**, *57*, 10895–10898.
12. R. Guo, T. Li, R. Wei, X. Zhang, Q. Li, L. L. Liu, C-H. Tung, L. Kong, *J. Am. Chem. Soc.* **2021**, *143*, 13483–13488.
13. a) R. J. Wright, A. D. Phillips, T. L. Allen, W. H. Fink, P. P. Power, *J. Am. Chem. Soc.* **2003**, *125*, 1694–1695; b) J. D. Queen, S. Irvankoski, J. C. Fettinger, H. M. Tuononen, P. P. Power, *J. Am. Chem. Soc.* **2021**, *143*, 6351–6356.

14. B. R. Barnett, C. C. Mokhtarzadeh, J. S. Figueroa, *Inorg. Synth.* **2018**, *37*, 85–122.
15. N. Kuhn, G. Henkel, T. Kratz, J. Kreutzberg, R. Boese, A. H. Maulitz, *Chem. Ber.* **1993**, *126*, 2041–2045.
16. Y. Wang, B. Quillian, P. Wei, C. S. Wannere, Y. Xie, R. B. King, H. F. Schaefer, P. v R. Schleyer, G. H. Robinson, *J. Am. Chem. Soc.* **2007**, *129*, 12412–12413.
17. M. E. Bowden, G. J. Gainsford, W. T. Robinson, *Aust. J. Chem.* **2007**, *60*, 149–153.
18. S. Morisako, R. Shang, Y. Yamamoto, *Inorg. Chem.* **2016**, *55*, 10767–10773.
19. M. F. Lappert, M. J. Slade, A. Singh, J. L. Atwood, R. D. Rogers, R. Shakir, *J. Am. Chem. Soc.* **1983**, *105*, 302–304.
20. D. A. Strauss, C. Zhang, T. D. Tilley, *J. Organomet. Chem.* **1989**, *369*, C13–C17.
21. A. Staubitz, A. P. M. Robertson, M. E. Sloan, I. Manners, *Chem. Rev.* **2010**, *110*, 4023–4078.
22. S. Karahan, M. Zahmakiran, S. Özkar, *Chem. Commun.* **2012**, *48*, 1180–1182.
23. J. A. Soderquist, H. C. Brown, *J. Org. Chem.* **1981**, *46*, 4599–4600.
24. Platinum complexes have been shown to dehydrogenate silanes, see: M. Tanaka, Y. Uchimaru, H.-J. Lautenschlager, *Organometallics* **1991**, *10*, 16–18.
25. For similar hydride-halide exchanges at boron, see: a) P. Bag, A. Porzelt, P. J. Altmann, S. Inoue, *J. Am. Chem. Soc.* **2017**, *139*, 14384–14387; b) J. H. Muessig, M. Thaler, R. D. Dewhurst, V. Paprocki, J. Seufert, J. D. Mattock, A. Vargas, H. Braunschweig, *Angew. Chem. Int. Ed.* **2019**, *58*, 4405–4409.

26. A. A. Omaña, R. Watt, Y. Zhou, M. J. Ferguson, E. Rivard, *Inorg. Chem.* **2022**, *61*, 16430–16440.
27. D. E. Ryan, K. Andrea, J. J. Race, T. M. Boyd, G. C. Lloyd-Jones, A. S. Weller, *ACS. Catal.* **2020**, *10*, 7443–7448.
28. J. Li, H. Song, C. Cui, J.-P. Cheng, *Inorg. Chem.* **2008**, *47*, 3468–3470.
29. T. B. Ditri, B. J. Fox, C. E. Moor, A. L. Rheingold, J. S. Figueroa, *Inorg. Chem.* **2009**, *48*, 8362–8375.
30. A. B. Pangborn, M. A. Giardello, R. H. Grubbs, R. K. Rosen, F. J. Timmers, *Organometallics* **1996**, *15*, 1518–1520.
31. H. Hope, *Prog. Inorg. Chem.* **1994**, *41*, 1–19.
32. G. M. Sheldrick, *Acta Crystallogr. Sect. A* **2015**, *71*, 3–8.
33. G. M. Sheldrick, *Acta Crystallogr. Sect. C* **2015**, *71*, 3–8.
34. M. J. Frisch, G. W. Trucks, H. B. Schlegel, G. E. Scuseria, M. A. Robb, J. R. Cheeseman, G. Scalmani, V. Barone, G. A. Petersson, H. Nakatsuji, X. Li, M. Caricato, A. V. Marenich, J. Bloino, B. G. Janesko, R. Gomperts, B. Mennucci, H. P. Hratchian, J. V. Ortiz, A. F. Izmaylov, J. L. Sonnenberg, D. Williams-Young, F. Ding, F. Lipparini, F. Egidi, J. Goings, B. Peng, A. Petrone, T. Henderson, D. Ranasinghe, V. G. Zakrzewski, J. Gao, N. Rega, G. Zheng, W. Liang, M. Hada, M. Ehara, K. Toyota, R. Fukuda, J. Hasegawa, M. Ishida, T. Nakajima, Y. Honda, O. Kitao, H. Nakai, T. Vreven, K. Throssell, J. A. Montgomery, Jr., J. E. Peralta, F. Ogliaro, M. J. Bearpark, J. J. Heyd, E. N. Brothers, K. N. Kudin, V. N. Staroverov, T. A. Keith, R. Kobayashi, J. Normand, K. Raghavachari, A. P. Rendell, J. C. Burant, S. S. Iyengar, J.

Tomasi, M. Cossi, J. M. Millam, M. Klene, C. Adamo, R. Cammi, J. W. Ochterski, R. L. Martin, K. Morokuma, O. Farkas, J. B. Foresman, D. J. Fox, Gaussian 16, Revision A. 03, Gaussian Inc., Wallingford CT, 2016.

35. Y. Zhao, D. G. Truhlar, *Theo. Chem. Acc.* **2008**, *120*, 215–241.

36. T. H. Dunning, *J. Chem. Phys.* **1989**, *90*, 1007–1023.

37. W. Humphrey, A. Dalke, K. Schulten *J. Molec. Graphics* **1996**, *14*, 33–38.

38. E. D. Glendening, J. K. Badenhoop, A. E. Reed, J. E. Carpenter, J. A. Bohmann, C. M. Morales, C. R. Landis, F. Weinhold, NBO 6.0, Theoretical Chemistry Institute, University of Wisconsin, Madison WI, 2013.

39. I. M. Alecu, J. Zheng, Y. Zhao, D. G. Truhlar, *J. Chem. Theory Comput.* **2010**, *6*, 2872–2887.

Chapter 6

1. M. H. Hopkinson, C. Richter, M. Schedler, F. Glorius, *Nature* **2014**, *510*, 485–496.

2. A. Igau, H. Gruztmacher, A. Baceiredo, G. Bertrand, *J. Am. Chem. Soc.* **1988**, *110*, 6463–6466.

3. A. J. Arduengo III, R. L. Harlow, M. Kline, *J. Am. Chem. Soc.* **1991**, *113*, 361–363.

4. A. Gómez-Suárez, D. J. Nelson, S. P. Nolan, *Chem. Commun.* **2017**, *53*, 2650–2660.

5. For select reviews, see: a) M. M. D. Roy, A. A. Omaña, A. S. S. Wilson, M. S. Hill, S. Aldridge, E. Rivard, *Chem. Rev.* **2021**, *121*, 12784–12965; b) P. Belloti, M. Koy, M. N. Hopkinson, F. Glorius, *Nat. Rev. Chem.* **2021**, *5*, 711–725; c) M. Fèvre, J. Pinaud, Y. Gnanou, J. Vignolle, D. Taton, *Chem. Soc. Rev.* **2013**, *42*, 2142–2172; d) S. Díez-González, N. Marion,

S. P. Nolan, *Chem. Rev.* **2009**, *109*, 3612–3676; e) V. Nesterov, D. Reiter, P. Bag, P. Frisch, R. Holzner, A. Porzelt, S. Inoue, *Chem. Rev.* **2018**, *118*, 9678–9842.

6. For select articles and reviews, see: a) Y. Pang, N. Nöthling, M. Leutzsch, L. Kang, E. Bill, M. van Gastel, E. Reijerse, R. Goddard, L. Wagner, D. SantaLucia, S. DeBeer, F. Neese, J. Cornella, *Science* **2023**, *380*, 1043–1048; b) R. C. Fisher, P. P. Power, *Chem. Rev.* **2010**, *110*, 3877–3923; c) H. Chen, W. Chen, D. Wang, Y. Chen, Z. Liu, S. Ye, G. Tan, S. Gao, *Angew. Chem. Int. Ed.* **2024**, *63*, e202402093; d) D. Wang, W. Chen, C. Zhai, L. Zhao, S. Ye, G. Tan, *J. Am. Chem. Soc.* **2023**, *145*, 6914–6920; d) M. Wu, H. Li, W. Chen, D. Wang, Y. He, L. Xu, S. Ye, G. Tan, *Chem.* **2023**, *9*, 2573–2584; e) T. Ochiai, D. Franz, S. Inoue, *Chem. Soc. Rev.* **2016**, *45*, 6327–6344.

7. M. M. D. Roy, P. A. Lummis, M. J. Ferguson, R. McDonald, E. Rivard, *Chem. Eur. J.* **2017**, *23*, 11249–11252.

8. M. M. D. Roy, M. J. Ferguson, R. McDonald, E. Rivard, *Chem. Commun.* **2018**, *54*, 483–486.

9. a) C. L. McMullin, N. Fey, J. N. Harvey, *Dalton Trans.* **2014**, *43*, 13545–13556; b) M. Ahlquist, P. Fristrup, D. Tanner, P.-O. Norrby, *Organometallics* **2006**, *25*, 2066–2073; c) A. H. Roy, J. F. Hartwig, *J. Am. Chem. Soc.* **2001**, *123*, 1232–1233.

10. H. Giesemann, G. Hälschke, *Chem. Ber.* **1959**, *92*, 92–98.

11. M. A. Bernd, F. Dyckhoff, B. J. Hoffman, A. D. Böth, J. F. Schlagintweit, J. Oberkofler, R. M. Reich, F. E. Kühn, *J. Catal.* **2020**, *391*, 548–561.

12. D. A. Strauss, C. Zhang, T. D. Tilley, *J. Organomet. Chem.* **1989**, *369*, C13–C17.

13. The percent buried volume was calculated with the SambVca 2.1 web tool with bondi radii scaled by 1.17, a sphere radius of 3.5 Å, a M-C_{NHC} length of 2.0 Å, a mesh spacing of 0.10 Å

- and H atoms omitted from the calculation, see: L. Falivene, Z. Cao, A. Petta, L. Serra, A. Poater, R. Oliva, V. Scarano, L. Cavallo, *Nat. Chem.* **2019**, *11*, 872–879.
14. S. S. Zaleskiy, V. P. Ananikov, *Organometallics* **2012**, *31*, 2302–2309.
15. S. Fantasia, S. P. Nolan, *Chem. Eur. J.* **2008**, *14*, 6987–6993.
16. S. M. Reid, R. C. Boyle, J. T. Mague, M. J. Fink, *J. Am. Chem. Soc.* **2003**, *125*, 7816–7817.
17. NHC-NiCpCl complexes can be prepared from Cp₂Ni and the corresponding imidazolium salt with loss of CpH, see: R. A. Kelly, N. M. Scott, S. Díez-González, E. D. Stevens, S. P. Nolan, *Organometallics* **2005**, *24*, 3442–3447.
18. Y. Liu, V. A. Voloshkin, T. Scattloin, M. Peng, K. Van Hecke, S. P. Nolan, C. S. J. Cazin, *Eur. J. Org. Chem.* **2022**, e202200309.
19. A. B. Pangborn, M. A. Giardello, R. H. Grubbs, R. K. Rosen, F. J. Timmers, *Organometallics* **1996**, *15*, 1518–1520.
20. H. Hope, *Prog. Inorg. Chem.* **1994**, *41*, 1–19.
21. G. M. Sheldrick, *Acta Crystallogr. Sect. A* **2015**, *71*, 3–8.
22. G. M. Sheldrick, *Acta Crystallogr. Sect. C* **2015**, *71*, 3–8.
23. M. J. Frisch, G. W. Trucks, H. B. Schlegel, G. E. Scuseria, M. A. Robb, J. R. Cheeseman, G. Scalmani, V. Barone, G. A. Petersson, H. Nakatsuji, X. Li, M. Caricato, A. V. Marenich, J. Bloino, B. G. Janesko, R. Gomperts, B. Mennucci, H. P. Hratchian, J. V. Ortiz, A. F. Izmaylov, J. L. Sonnenberg, D. Williams-Young, F. Ding, F. Lipparini, F. Egidi, J. Goings, B. Peng, A. Petrone, T. Henderson, D. Ranasinghe, V. G. Zakrzewski, J. Gao, N. Rega, G. Zheng, W. Liang, M. Hada, M. Ehara, K. Toyota, R. Fukuda, J. Hasegawa, M. Ishida, T. Nakajima, Y. Honda, O. Kitao, H. Nakai, T. Vreven, K. Throssell, J. A. Montgomery, Jr., J. E. Peralta, F.

Ogliaro, M. J. Bearpark, J. J. Heyd, E. N. Brothers, K. N. Kudin, V. N. Staroverov, T. A. Keith, R. Kobayashi, J. Normand, K. Raghavachari, A. P. Rendell, J. C. Burant, S. S. Iyengar, J. Tomasi, M. Cossi, J. M. Millam, M. Klene, C. Adamo, R. Cammi, J. W. Ochterski, R. L. Martin, K. Morokuma, O. Farkas, J. B. Foresman, D. J. Fox, Gaussian 16, Revision A. 03, Gaussian Inc., Wallingford CT, 2016.

24. a) C. Lee, W. Yang, R. G. Parr, *Phys. Rev. B* **1988**, *37*, 785–789; b) A. D. Becke, *Phys. Rev. A* **1988**, *38*, 3098–3100; c) P. J. Stephens, F. J. Devlin, C. F. Chabalowski, M. J. Frisch, *J. Phys. Chem.* **1994**, *98*, 11623–11627.

25. a) F. Weigend, R. Ahlrichs, *Phys. Chem. Chem. Phys.* **2005**, *7*, 3297–3305; b) F. Weigend, *Phys. Chem. Chem. Phys.* **2006**, *8*, 1057–1065.

26. W. Humphrey, A. Dalke, K. Schulten, *J. Molec. Graphics* **1996**, *14*, 33–38.

Chapter 7

1. A. J. Arduengo III, F. Davidson, H. V. Rasika Dias, J. R. Goerlich, D. Khasnis, W. J. Marshall, T. K. Prakasha, *J. Am. Chem. Soc.* **1997**, *119*, 12742–12749.

2. For select examples of cyclic Group 14 and Group 15 diradicaloid species supported by organic fragments, see: a) M. K. Sharma, D. Rottschäfer, T. Glodde, B. Neumann, H.-G. Stammler, R. S. Ghadwal, *Angew. Chem. Int. Ed.* **2021**, *60*, 6414–6418; b) H. Steffenfauseweh, Y. V. Vishnevsky, B. Neumann, H.-G. Stammler, D. M. Andrada, R. S. Ghadwal, *Angew. Chem. Int. Ed.* **2022**, *61*, e202207415; c) M. K. Sharma, F. Ebeler, T. Glodde, B. Neumann, H.-G. Stammler, R. S. Ghadwal, *J. Am. Chem. Soc.* **2021**, *143*, 121–125; d) D. Rottschäfer, B. Neumann, H.-G. Stammler, R. S. Ghadwal, *Chem. Eur. J.* **2017**, *23*, 9044–9047; e) Z. Li, X. Chen, D. M. Andrada, G. Frenking, Z. Benkö, Y. Li, J. R. Harmer, C.-Y. Su, H. Grützmacher, *Angew. Chem. Int. Ed.* **2017**, *56*, 5744–5749.

3. a) R. J. Wright, A. D. Phillips, T. L. Allen, W. H. Fink, P. P. Power, *J. Am. Chem. Soc.* **2002**, *125*, 1694–1695; b) R. J. Wright, M. Brynda, J. C. Fettinger, A. R. Betzer, P. P. Power, *J. Am. Chem. Soc.* **2006**, *128*, 12498–12509.
4. J. D. Queen, S. Irvankoski, J. C. Fettinger, H. M. Tuononen, P. P. Power, *J. Am. Chem. Soc.* **2021**, *143*, 6351–6356.
5. a) C. Dohmeier, E. Baum, A. Ecker, R. Köppe, H. Schnöckel, *Organometallics* **1996**, *15*, 4702–4706; b) L. Denker, B. Trzaskowski, R. Frank, *Chem. Commun.* **2021**, *57*, 2816–2819; c) P. Dabringhaus, J. Willrett, I. Krossing, *Nat. Chem.* **2022**, *14*, 1151–1157; d) I.-A. Bischoff, S. Danés, P. Thoni, B. Morgenstern, D. M. Andrada, C. Müller, J. Lambert, E. C. J. Gielßelmann, M. Zimmer, A. Schäfer, *Nat. Chem.* **2024**, 10.1038/s41557-024-01531-y.
6. a) D. Sarkar, P. Vasko, A. F. Roper, A. E. Crumpton, M. M. D. Roy, L. P. Griffin, C. Bogle, S. Aldridge, *J. Am. Chem. Soc.* **2024**, *146*, 11792–11800; b) D. Sarkar, P. Vasko, T. Gluharev, L. P. Griffin, C. Bogle, J. Struijs, J. Tang, A. F. Roper, A. E. Crumpton, S. Aldridge, *Angew. Chem. Int. Ed.* **2024**, e202407427.
7. C. Ganesamoorthy, S. Loerke, C. Gemel, P. Jerabek, M. Winter, G. Frenking, R. A. Fischer, *Chem. Commun.* **2013**, *49*, 2858–2860.
8. C. A. Caputo, P. P. Power, *Organometallics* **2013**, *32*, 2278–2286.
9. a) R. J. Wright, A. D. Phillips, P. P. Power, *J. Am. Chem. Soc.* **2003**, *125*, 36, 10784–10785; b) T. Agou, K. Nagata, N. Tokitoh, *Angew. Chem. Int. Ed.* **2013**, *52*, 10818–10821.
10. M. M. D. Roy, E. Rivard, *Acc. Chem. Res.* **2017**, *50*, 2017–2025.

11. a) A. A. Omaña, R. Watt, Y. Zhou, M. J. Ferguson, E. Rivard, *Inorg. Chem.* **2022**, *61*, 16430–16440; b) B. L. Frenette, A. A. Omaña, M. J. Ferguson, Y. Zhou, E. Rivard, *Chem. Commun.* **2021**, *57*, 10895–10898.
12. a) M. Gupta, C. Hagen, R. J. Flesher, W. C. Kaska, C. M. Jensen, *Chem. Commun.* **1996**, 2083–2084; b) I. Göttker-Schnetmann, P. White, M. Brookhart, *J. Am. Chem. Soc.* **2004**, *126*, 1804–1811.
13. For an example of **PB** depositing Si and Ge films in solution, see: A. A. Omaña, R. K. Green, R. Kobayashi, Y. He, E. R. Antoniuk, M. J. Ferguson, Y. Zhou, J. G. C. Veinot, T. Iwamoto, A. Brown, E. Rivard, *Angew. Chem. Int. Ed.* **2021**, *60*, 228–231.
14. M. M. D. Roy, A. A. Omaña, A. S. S. Wilson, M. S. Hill, S. Aldridge, E. Rivard, *Chem. Rev.* **2021**, *121*, 12784–12965.
15. R. J. Baker, C. Jones, P. C. Junk, M. Kloth, *Angew. Chem. Int. Ed.* **2004**, *43*, 3852–3855.
16. J. Bykowski, J. Sinclair, J. Trach, M. J. Ferguson, E. Rivard, *Dalton Trans.* **2023**, *52*, 1602–1607.